

Polypyrrole modified with sulfated β -cyclodextrin: characterization and application in the sensing of viologens



NUI MAYNOOTH

Ollscoil na hÉireann Má Nuad

Valeria Annibaldi, Laurea in CTF

**Department of Chemistry
National University of Ireland Maynooth**

February 2010

**Thesis submitted to the National University of Ireland in fulfilment of the
requirements for the Degree of Doctor of Philosophy**

Supervisors: Prof. Carmel B. Breslin and Dr. Denise A. Rooney

Head of Department: Prof. John Lowry

Declaration

I hereby certify that this thesis, which I now submit for assessment on the programme of study leading to the award of PhD has not been submitted, in whole or part, to this or any other University for any degree and is, except where otherwise stated the original work of the author.

Signed : _____

Acknowledgements

I would like to express my sincere gratitude to my supervisors Prof. Carmel Breslin and Dr. Denise Rooney for their continuous support during my PhD. Thank you for your enthusiasm, encouragement and guidance. You were always there to discuss my work and to help me think through my problems. Thank you for all that you have taught me. You were also very understanding of my personal needs as a foreign student and I greatly appreciated that.

I would like to acknowledge SFI for funding my PhD, the Tyndall Institute and the National Access Programme (NAP) for the SEM data shown in this thesis.

A heart felt thank you to the academic and technical staff of the chemistry department, in particular to Ria and Ken, for their help and support over these years. A special thanks to Noel. He was the only one able to deal with my static-superhuman powers.

A special thank to my mates in the “Matrix lab” aka “Little Italy” Enrico, Adelaide and Sinead. I am honored to be your friend. Thank you Aidy for your patience and for helping me to win the war against the computer technology. Enrico, you are an excellent electrochemist and I have learnt a lot from you. Your support was invaluable. Sinead, I could not imagine a better friend to share these last months with. Thanks for all the foolish chats at 10 p.m. I would also like to thank Gillian (Dr. Hendy), Claire (Dr. Harley) and Catherine, especially for all the help they gave me during my first months in Maynooth. Likewise, thank you to all my lab colleagues of the electrochemistry groups, in particular Johnny (Dr. Colleran), Eimear and Richard.

To all my fellow postdoc and postgraduate students, both past and present, with a special mention to Declan, John, Owen, Roisin, Linda, Rob, Conor and Denis – thank you for the laughs and the great nights out.

Un grazie affettuoso agli amici italiani in Italia e a quelli di Maynooth e Dublino, in particolare a Patrizia e Davide per l'affetto e la generosità che hanno avuto nei miei confronti e alle piccole amiche Elena e Greta per tutti i momenti spensierati insieme a loro. Emanuele, senza di te il mio dottorato non sarebbe stato possibile e per questo ti ringrazio. Un pensiero speciale per la Prof. Maria Jole Carafa, per avermi trasmesso la passione per questo lavoro e soprattutto per avermi insegnato che l'ottimo è nemico del buono.

Il ringraziamento più grande ai miei genitori, a mio fratello e a tutta la mia famiglia, per l'amore e il sostegno che mi hanno sempre dimostrato, per le telefonate che ricevo ogni sera e per la calda atmosfera che respiro ogni volta che torno a casa.

Ai miei genitori, a mio fratello e a Giulia
Con l'amore di sempre

Nil satis nisi optimum

*I have not failed, I've just found 10,000 ways
that won't work.*

*I am not discouraged, because every wrong
attempt discarded is another step forward.*

Thomas A. Edison

Abstract

In this thesis a conducting polypyrrole (ppy) matrix doped with the anionic sulfated β -cyclodextrin ($s\beta$ -CD) was electrosynthesized and characterized. This modified polymer, ppys β -CD, was used as a sensor for the detection of three compounds, methyl, ethyl and benzyl viologen. Methyl viologen is commonly known as paraquat and it is one of the most commonly used herbicides worldwide.

The $s\beta$ -CD was permanently immobilized within the ppy backbone during the potentiostatic growth of the polymer. The incorporation of the macrocycle was confirmed by means of cyclic voltammetry (CV), quartz crystal microbalance (QCM) and differential scanning calorimetry (DSC). The large dopant was found not to significantly alter certain properties of the polymer such as diffusion of a probe analyte to the surface and charge transfer rate constant. The cyclodextrin modified polymer was shown to have cation exchange properties and this characteristic was used towards the sensing of the three electroactive viologen compounds. The three viologens were detected by means of differential pulse voltammetry (DPV), while for methyl viologen constant potential amperometry (CPA) experiments were also performed. These techniques gave a good linear response for the current measured at the polymer surface, as a function of the viologen concentration. Detection limits of 1.00×10^{-4} M for ethyl viologen (DPV), 2.50×10^{-5} M for benzyl viologen (DPV) and 1.56×10^{-5} M for methyl viologen (CPA) were measured experimentally.

A detailed analysis was performed on the interaction of the $s\beta$ -CD with methyl, ethyl and benzyl viologen, using both electrochemistry (CV and RDV) and spectroscopy (UV-Vis, ^1H NMR). It was established that a 1:1 interaction occurs between the $s\beta$ -CD and each of the viologens. The formation of inclusion complexes was verified not to occur. The generation of association complexes was instead suggested. These complexes result from an ion pairing interaction between the $s\beta$ -CD and the viologens, either in their dication state or in their radical state.

Table of Contents

Chapter 1 - Introduction and literature review	1
1.1 Introduction.....	2
1.2 Conducting Polymers	3
1.2.1 Synthesis of Conducting Polymers	7
1.2.2 Polypyrrole.....	9
1.2.3 Synthesis of Polypyrrole.....	10
1.2.4 Parameters affecting Electropolymerization	14
1.2.5 Redox Properties of Polypyrrole	17
1.3 Cyclodextrins.....	19
1.3.1 Overview	19
1.3.2 Derivatization of cyclodextrins	21
1.3.3 Applications of cyclodextrins.....	25
1.3.4 Inclusion complex formation and driving forces controlling complexation	29
1.4 Viologens.....	32
1.4.1 Applications of the viologens	33
1.4.2 Paraquat	35
1.5 Development of a sensor for viologens	36
1.6 References	37
Chapter 2 - Experimental	44
2.1 Introduction.....	45
2.2 Chemicals	45
2.2.1 Purification of the β -CD.....	45
2.3 Electrochemical set-up.....	49

Table of contents

2.3.1	Electrochemical apparatus.....	49
2.3.2	The electrochemical cell.....	49
2.3.3	Electrode materials and preparation.....	50
2.4	Polymer electrosynthesis.....	52
2.5	Experimental techniques.....	53
2.5.1	EQCM measurements.....	53
2.5.2	UV-Vis spectroscopy.....	54
2.5.3	Spectroelectrochemical technique.....	55
2.5.4	Cyclic voltammetry.....	56
2.5.5	Rotating disc voltammetry.....	58
2.5.6	Differential pulse voltammetry (DPV).....	61
2.5.7	Electrochemical Impedance Spectroscopy.....	63
2.5.8	Nuclear magnetic resonance spectroscopy.....	68
2.5.9	Differential Scanning Calorimetry (DSC).....	69
2.5.10	Optical and scanning electron microscopy.....	70
2.5.11	Solution properties.....	70
2.6	Theory of experimental techniques and equations used.....	70
2.6.1	Complexation studies.....	71
2.6.1.1	Job's method.....	71
2.6.1.2	Formation constants.....	72
2.7	References.....	75
Chapter 3 - Synthesis and characterization of the polymer.....		77
3.1	Introduction.....	78
3.2	Electrosynthesis of the polymer.....	78
3.2.1	Polymer growth.....	79
3.2.2	Reproducibility of the electrosynthesis.....	82
3.2.3	Influence of the substrate.....	84

3.2.4	Influence of the dopant	86
3.3	Diffusion coefficient and rate constant of ferricyanide	88
3.3.1	Diffusion coefficient and rate constant by means of cyclic voltammetry (CV).....	88
3.3.2	Diffusion coefficient and rate constant by means of RDV	95
3.3.3	Reversibility.....	102
3.4	Redox properties of the polymer: cyclic voltammetry.....	107
3.5	Doping levels and redox properties of the polymer: Electrochemical Quartz Crystal Microbalance (EQCM).....	110
3.5.1	Doping level	110
3.5.2	Ionic exchange	114
3.6	Differential Scanning Calorimetry	122
3.7	Capacitance study	127
3.7.1	Cyclic Voltammetry	127
3.7.2	Electrochemical Impedance Spectroscopy	130
3.8	Morphology.....	138
3.9	Preliminary study on polypyrrole doped with carboxy methyl β -cyclodextrin (ppyCM β -CD).....	141
3.9.1	Introduction.....	141
3.9.2	Electrosynthesis	142
3.9.3	Diffusion and Rate Constant	143
3.9.4	Capacitance measurement (by CV)	146
3.9.5	Cyclic Voltammetry and Quartz Crystal Microbalance	147
3.9.6	Morphology.....	150
3.10	Summary of results.....	150
3.11	References.....	154
Chapter 4 - Conducting ppysβ-CD as a sensor for viologens		157

Table of contents

4.1	Introduction.....	158
4.2	Electrochemistry of the viologens	160
4.3	The detection of methyl, ethyl and benzyl viologens by means of cyclic voltammetry (CV).....	164
4.3.1	Influence of the substrate	165
4.3.2	Redox behavior of viologens at ppys β -CD investigated by CV and QCM	166
4.3.3	Comparison of the s β -CD to a small anionic dopant.....	174
4.3.4	Influence of the electrochemical window	177
4.3.5	Calibration curves.....	178
4.4	Optimization of the experimental parameters	180
4.4.1	Electrosynthesis potential.....	181
4.4.2	Polymer thickness	182
4.4.3	Supporting electrolyte.....	183
4.5	Differential pulse voltammetry (DPV).....	186
4.6	Constant potential amperometry (CPA).....	191
4.7	Summary of results and conclusions.....	195
4.8	References	196
	Chapter 5 - Interaction of sβ-CD with viologens: electrochemical study	198
5.1	Introduction.....	199
5.2	Interaction of methyl viologen with β -CD and s β -CD investigated by means of CV and RDV	201
5.2.1	Methyl viologen (MV) and β -cyclodextrin (β -CD).....	201
5.2.2	Methyl viologen (MV) and sulfated β -cyclodextrin (s β -CD).....	208
5.2.3	Influence of oxygen	220
5.3	Interaction of ethyl viologen with β -CD and s β -CD investigated by means of CV and RDV.....	228

Table of contents

5.3.1	Ethyl viologen and β -CD	228
5.3.2	Ethyl viologen and $s\beta$ -CD	233
5.3.3	Influence of oxygen	242
5.4	Interaction of benzyl viologen with β -CD and $s\beta$ -CD investigated by means of CV and RDV	246
5.4.1	Benzyl viologen and β -CD	246
5.4.2	Benzyl viologen and $s\beta$ -CD	249
5.4.3	Influence of oxygen	254
5.5	Conclusions and summary of results.....	256
5.6	References	260
Chapter 6 - Interaction of $s\beta$-CD with viologens: spectroscopic study.....		262
6.1	Introduction.....	263
6.2	Determination of the stoichiometry of the complex between $s\beta$ -CD and the viologens.....	264
6.3	UV-Vis spectroscopic study on the interaction of the viologen dications with $s\beta$ -CD.....	270
6.4	UV-Vis spectroscopy study on the interaction of the radical species with $s\beta$ -CD	272
6.5	^1H NMR spectroscopic study on the interaction of the viologen dications with $s\beta$ -CD.....	283
6.6	Summary of results	289
6.7	References	291
Chapter 7 - Conclusions.....		294
7.1	Conclusions	295
7.2	Conference presentations	300
7.2.1	Poster presentations	300
7.2.2	Oral presentations:.....	301
7.3	References	301

Chapter 1

Introduction and literature review

1.1 Introduction

The aim of this thesis was to characterize and study potential applications of a modified sensor, composed of a conducting polypyrrole (ppy) matrix doped with large macrocyclic species such as sulfated β -cyclodextrin anions. In previous work in Professor Breslin's group, results have been obtained on the application of polypyrrole modified with sulfated β -cyclodextrin to sense the neurotransmitter dopamine.^{1,2} These promising studies prompted a more in depth investigation into cyclodextrin-modified polypyrrole and to apply this new system to detect other cationic electroactive molecules. In particular, in the present thesis, ppy doped with sulfated β -cyclodextrin (s β -CD) has been used to detect three molecules belonging to the class of viologen compounds: methyl, ethyl and benzyl viologen. Methyl viologen is commonly known as paraquat and it is one of the most used herbicides world wide.³

In Chapter 3, the growth of ppy films in the presence of a large anionic cyclodextrin (CD), sulfated β -cyclodextrin (s β -CD) is explored. Although s β -CD doped ppy films have been reported in the recent literature, there has been very little work devoted to the characterization of these films.⁴ On the other hand, ppy doped with small anions, such as chloride anions has been extensively characterized⁵⁻⁸ and for this reason it has been used in this work for comparison. An extensive section is devoted to the unique redox properties of the s β -CD doped ppy films. In addition, the properties and characteristics of the CD modified polymer are outlined in Chapter 3.

In Chapter 4 detection properties of the polymer towards three different viologen compounds, methyl, ethyl and benzyl viologen are presented. It is shown that the viologen compounds interact differently with a cyclodextrin modified polypyrrole surface compared to a metal electrode surface. In order to comprehend how the polymer of interest interacts with the viologens and affects their electrochemistry, the well-known supramolecular complexation properties of cyclodextrins were considered. However, to the best of our knowledge there are no reports on the complexation of viologens with anionic

cyclodextrins and consequently this was studied in detail. Solutions containing the desired viologen and β -CD or a neutral β -CD, in different molar ratios were examined using a variety of techniques, both spectroscopic and electrochemical. These findings are presented in Chapter 5 and Chapter 6.

In this introductory chapter, the concept of conducting polymers is introduced and polypyrrole electrochemistry and its applications are described in detail. This is then followed with information on cyclodextrins and on the current state of art of their applications. Finally, the chapter ends with a section on the electrochemistry of viologen compounds and a short introduction to the work in this thesis.

1.2 Conducting Polymers

The term 'polymer' derives from the Greek 'poly', meaning many and 'mer', meaning part. They are built up, in fact, from simple molecules called 'monomers', single parts. In everyday life the concept of a polymer is often associated with plastic materials or more in general to substances having insulating properties which are widely used in the production of packaging and of electrical and electronic devices.⁹ Conducting polymers (CPs) differ from the materials described above since they are intrinsically conducting. Three scientists, A.J. Heeger, A.G. MacDiarmid and H. Shirakawa, are credited for the advancement and development of electrically conducting polymers and they were awarded the Noble Prize in Chemistry in 2000. CPs are constituted of carbon, hydrogen and simple heteroatoms, such as nitrogen or sulfur, and contain π -conjugation across the polymer backbone. Typical π -conjugated conducting polymers include polyaniline (PANi), polypyrrole (ppy) and polythiophene, Figure 1.1. These and a number of other conducting polymers have been used in a variety of applications ranging from corrosion protection of materials, sensors to many biomedical applications, such as tissue engineering, nerve cell regeneration and drug delivery.¹⁰⁻¹²

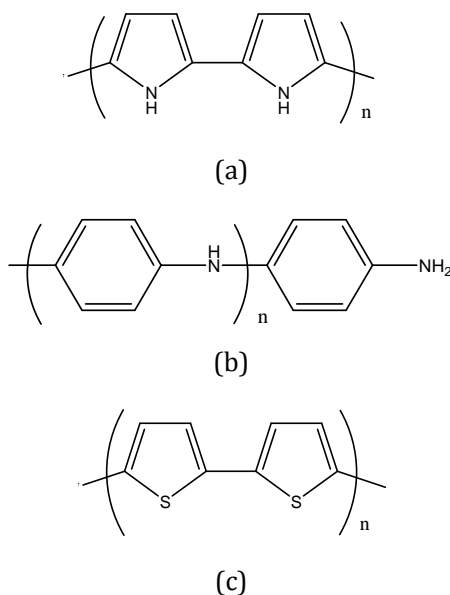


Figure 1.1: Structure of (a) polypyrrole (ppy), (b) polyaniline (PANi) and (c) polythiophene in the dedoped state.

Bredas and Street¹³ gave one of the first explanation of the conductivity exhibited by conducting polymers. The authors used the band theory of solids to determine the conductivity classification of conducting polymers. In general, materials can be classified into three categories depending on their electrical conductivity: insulators, semiconductors and conductors. The highest occupied molecular orbital is equivalent to the valence band, while the lowest unoccupied molecular orbital may be equated to the conduction band. The difference between each band is known as the band gap energy, E_g , and it is this energy gap that establishes the electrical properties of a material, as shown in Figure 1.2. In insulators the electrons in the valence band are separated from the conduction band by a large band gap, $E_g > 10$ eV. This high energy barrier is hard to overcome. Consequently, it is difficult to excite the electrons from the valence band into the conduction band. In semiconductors, E_g is about 1.0 eV and the electrons can be excited from the valence band into the conduction band at room temperature. In the case of conductors, the valence band overlaps the conduction band and hence the conduction band is now partially filled with electrons. Bredas and Street categorized conducting polymers as semiconductors since they calculated for these polymers an energy gap close to

1.0 eV.¹³ However, the band theory model in itself is not enough to explain the conductivity associated with conducting polymers.

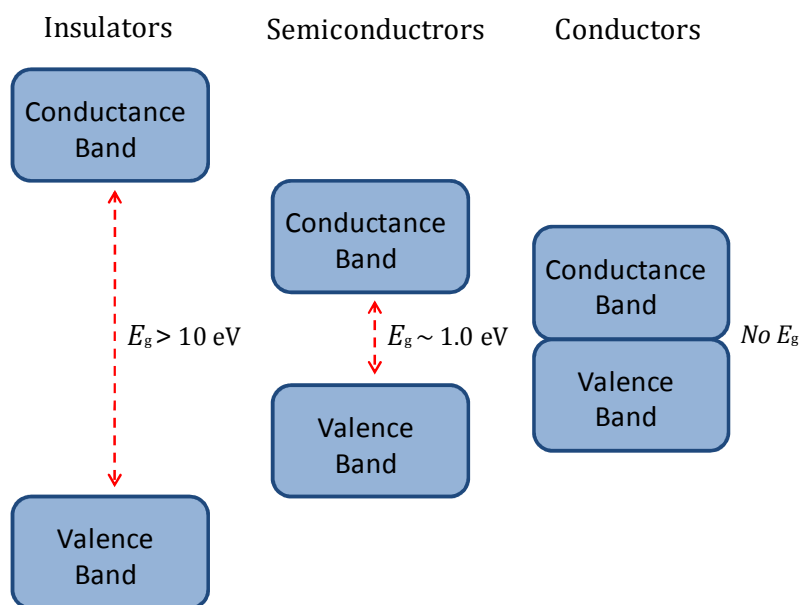
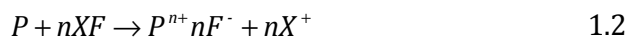
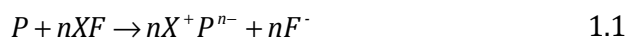


Figure 1.2: The difference in the band gap, E_g , for insulators, semiconductors and conductors.

As pointed out by Bredas and Street¹³, the conductivity observed upon doping of the CPs was originally thought to be from the formation of unfilled electronic bands. However this idea was quickly dissipated upon experimental analysis of ppy and polyacetylene and now scientists agree that the conductivity is due to the formation of polarons and bipolarons, which are more energetically favoured.^{13,14} The π -bonded system of CPs, formed by the alternation of single and double bonds, enables the delocalization of electrons along the polymer backbone and this peculiarity is connected with the conductivity of the system. More precisely, the conductivity of these polymers arises from a state of relative oxidation or reduction. When the polymer is oxidized or reduced it loses or gains an electron. Usually, in such processes one electron for every four monomer units is involved.¹⁵ In the oxidation state the polymer is electronically charged and requires the incorporation of counter ions, generally known as dopants to compensate the polymer backbone charge and hence establish again

the electroneutrality of the system. The oxidation of the polymer in which an electron is removed from a π -bond, leads to a new energy state, which leaves the remaining electron in a non-bonding orbital. This energy level is higher than the valence band and behaves like a heavily doped semiconductor.¹⁵ The extent of doping can be controlled during the polymerization of the polymers. The maximum doping level varies for different conducting polymers and for different dopants. For example, the doping level for ppy ranges from 20% to 50% depending on the dopant used.¹⁶ The mechanism of cationic and anionic doping are described in Equations 1.1 and 1.2, respectively:



where P indicates the polymer in the neutral state, P^{n+} is the polymer in its oxidized state, P^{n-} is the polymer in its reduced state, X is any cation, F is any anion and n is the moles of the salt. Both the anionic and cationic doping processes enhance the conductive properties of the conducting polymer. This is because the conductivity increases as the doping level increases due to the creation of more mobile charges.¹⁷

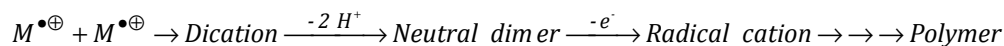
The electrical properties of conducting polymers together with the fact that they retain the mechanical properties of traditional polymers have made them very useful in a wide variety of areas. These include sensors, corrosion resistance materials, batteries, optics, electronics and biomedical/biological applications.¹⁸ In particular, the exchange properties of conducting polymers have been utilized to develop such applications. For example, conducting polymers doped with small mobile anions have anion exchange properties, whereas conducting polymers doped with large immobile anions generally have cation exchange properties.¹⁹ This has resulted in the formation of actuators²⁰⁻²², drug delivery systems²³, selective sensors²⁴ and metal ion transporters²⁵ to name a few.

In the recent literature, papers describing the electrochemical synthesis and applications of conducting polymers doped with cyclodextrins have been published. Incorporation of cyclodextrins within a polymer matrix is a possible method to overcome the problem of lack of stability of CD monolayers directly attached on the electrode surface.²⁶ Lagrost *et al.*,²⁷ for example, polymerized under potentiostatic conditions bithiophene in the presence of hydroxypropyl- β -cyclodextrin. Bouchta and coworkers²⁶ were the first to synthesize a poly-3-methylthiophene modified with γ -cyclodextrin. This system was successfully employed to detect the neuroleptic drug chlorpromazine. Lepretre and coworkers²⁸ have used a pyrrole-derivatized CD to electrosynthesize a conducting polymer which exhibited molecular recognition for phenothiazine and naphthalene disulfonate.

Conducting polymers have also been extensively used for various electrochromic and optoelectronic devices.²⁹⁻³² This is because the introduction of dopants into the polymer changes the optical properties of the polymer in the ultraviolet-visible (UV-Vis) and the near infrared (NIR) regions, as well as increasing the electrical properties.³³

1.2.1 Synthesis of Conducting Polymers

The synthesis of conducting polymers can be achieved either chemically or electrochemically. In both cases, the initial step of polymerization involves the oxidation of the monomer to its radical cation, $M^{\bullet+}$. Once formed, the radical cations react with each other in the case of electrochemical polymerization, or with other monomers, M , in the case of chemical polymerization. In the electrochemical synthesis, the radical-radical coupling generates a dication. In the following step, the dication loses two protons to form a neutral dimer. The dimer can then be oxidized again to a radical cation, which reacts further to form the polymer, Scheme 1.1. By contrast, during chemical polymerization the formation of the polymer occurs straight from a dimer radical cation¹⁷ as shown in Scheme 1.2.



Scheme 1.1: Electrochemical polymerization.



Scheme 1.2: Chemical polymerization.

Chemical synthesis is achieved when the monomer is exposed to relatively strong oxidizing agents, such as ammonium peroxydisulfate, potassium dichromate or ferric chloride.³⁴ This can be carried out in solution or directly onto a surface. The chemical deposition of a conducting polymer directly onto a surface involves coating the desired surface with the monomer solution and then subsequently treating the surface with the solution or vapor of the oxidizing agent. This results in the polymer film being polymerized exclusively on the surface of preference. In solution, the polymer is precipitated from an acidic monomer solution upon the addition of the oxidizing agent which normally results in bulk polymerization. However, this bulk polymerization can be impeded to some degree so that the conducting polymer can be deposited on a surface. This is achieved by varying several reaction conditions such as the concentration and ratio of oxidant and monomer, the reaction temperature and appropriate treatment of the surface to be coated by the polymer.³⁵

The electrochemical deposition is a simple and reproducible technique where the electrolyte solution has the double function to ensure conductivity of the solution and to provide dopants for the polymer. The monomer and the supporting electrolyte are both dissolved in the desired solvent and they constitute the polymerization solution where either current or potential is applied. Electrosynthesis is generally performed in a conventional three electrode cell set up, depicted in Chapter 2. The CP is deposited at the positively charged working electrode or anode.¹⁰ Polymerization is initiated through the oxidation of the monomer which forms a radical cation. This can then react with another radical to form a dication. The propagation of these steps lead to the

formation of the insoluble polymer chain and deposition of the polymer onto the working electrode.³⁶

Galvanostatic (constant current), potentiostatic (constant potential) and potential sweeping techniques, such as cyclic voltammetry, are the methods generally employed for electropolymerization. Electrochemical polymerization, in particular galvanostatic and potentiostatic modes, has several advantages over chemical polymerization. An adherent polymer film can be grafted directly onto an electrode surface in one simple step. Reproducible films can be obtained as the film thickness can be controlled by monitoring the charge passed during deposition and the polymer films formed have fewer impurities as harsh oxidizing agents are not used. In addition, it is also possible to perform *in situ* characterization of the polymer while it is growing.³⁷ Since CPs were discovered, their electrochemical synthesis and characterization have evolved substantially. A significant majority of the research on CPs is based in the electrochemistry field due to the ease and control of experimental parameters.³⁸

1.2.2 Polypyrrole

Polypyrrole is an organic material simply comprised of C, H and N. It is formed by the repetition of a single monomer, pyrrole. The structure of pyrrole is illustrated in Figure 1.3.

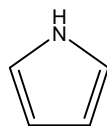


Figure 1.3: Structure of pyrrole.

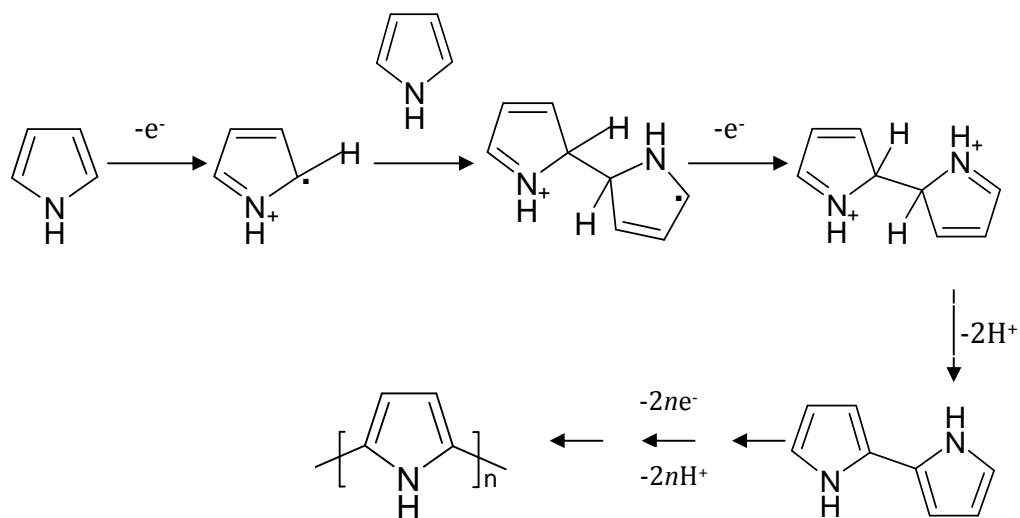
The first chemical synthesis of ppy dates back to 1916, when a report on the oxidation of pyrrole with hydrogen peroxide to give an amorphous black powder was published.³⁴ About five decades later, in 1968, Dall'Olio and coworkers³⁹ were the first scientists who electrochemically synthesized ppy on

a platinum substrate, from an aqueous solution of pyrrole and sulfuric acid. From the pioneering experiments of Dall'Ollio to date, a large variety of ppy films and ppy derivatives have been successfully synthesized on different electrode substrates, using various polymerizing solutions. Consequently ppy has found applications in a wide range of advanced technologies such as chemical sensors,^{40,41} batteries,^{42,43} supercapacitors^{44,45} and corrosion protection^{46,47}. As a matter of fact, today ppy is one of the most extensively employed and studied conducting polymers. The main reasons for the success of this material lies in its ease of preparation, good conductivity, biocompatibility and relative stability.⁴⁸ Another interesting and prominent property of ppy is its ability to switch its redox states. This has resulted in the design of ion-selective electrodes, electrochromic displays, solar cells, drug delivery systems and actuators.⁴⁹⁻⁵³

1.2.3 Synthesis of Polypyrrole

Polypyrrole can be synthesized *via* a chemical and electrochemical polymerization. One of the easiest and most common ways of chemically synthesizing ppy is in solution. Chemical synthesis in solution yields a black precipitate when the monomer, pyrrole, is exposed to an oxidizing agent. The oxidizing agent used in chemical synthesis initiates polymerization by oxidising the monomer and also provides dopant anions to balance the positive charge existing on the polymer in its oxidized state. The radical cation formed upon oxidation attacks another monomer molecule generating a dimer radical cation which is further oxidized and, coupled with the loss of hydrogen; the polymer chain grows until termination, as depicted in Scheme 1.3. The most often used oxidizing agents for pyrrole polymerization are salts of transition metal ions, such as Fe^{3+} , Cu^{2+} , Cr^{6+} , Ce^{4+} , Ru^{3+} and Mn^{7+} . Several other oxidizing agents, including organic acids and peroxides have been employed. However, films generated from these oxidants usually exhibit lower conductivity in comparison to films synthesized electrochemically.⁵⁴ One major disadvantage of this method is that the ppy is produced in the bulk of the solution and only some of the polymer will cover the surface of a material that has been introduced into the

solution. This process can be hindered; however it is complicated and dependant on many parameters. Another way of chemically synthesizing ppy is to directly deposit the polymer film onto a surface. One way to achieve this is to use a process known as vapour phase polymerization. Vapour phase polymerization involves applying the oxidant to the surface using a solvent coating process and then exposing the coated surface to the vapour of the monomer. The vapour phase polymerization method was first described by Mohammadi and co-workers.⁵⁵ The authors used FeCl_3 or H_2O_2 as oxidants to generate ppy films. Since then the vapor phase polymerization of pyrrole has been carried out using Fe(III) , *p*-toluenesulfonic acid and a range of other Fe(III) sulfonates as oxidizing agents.^{56,57}



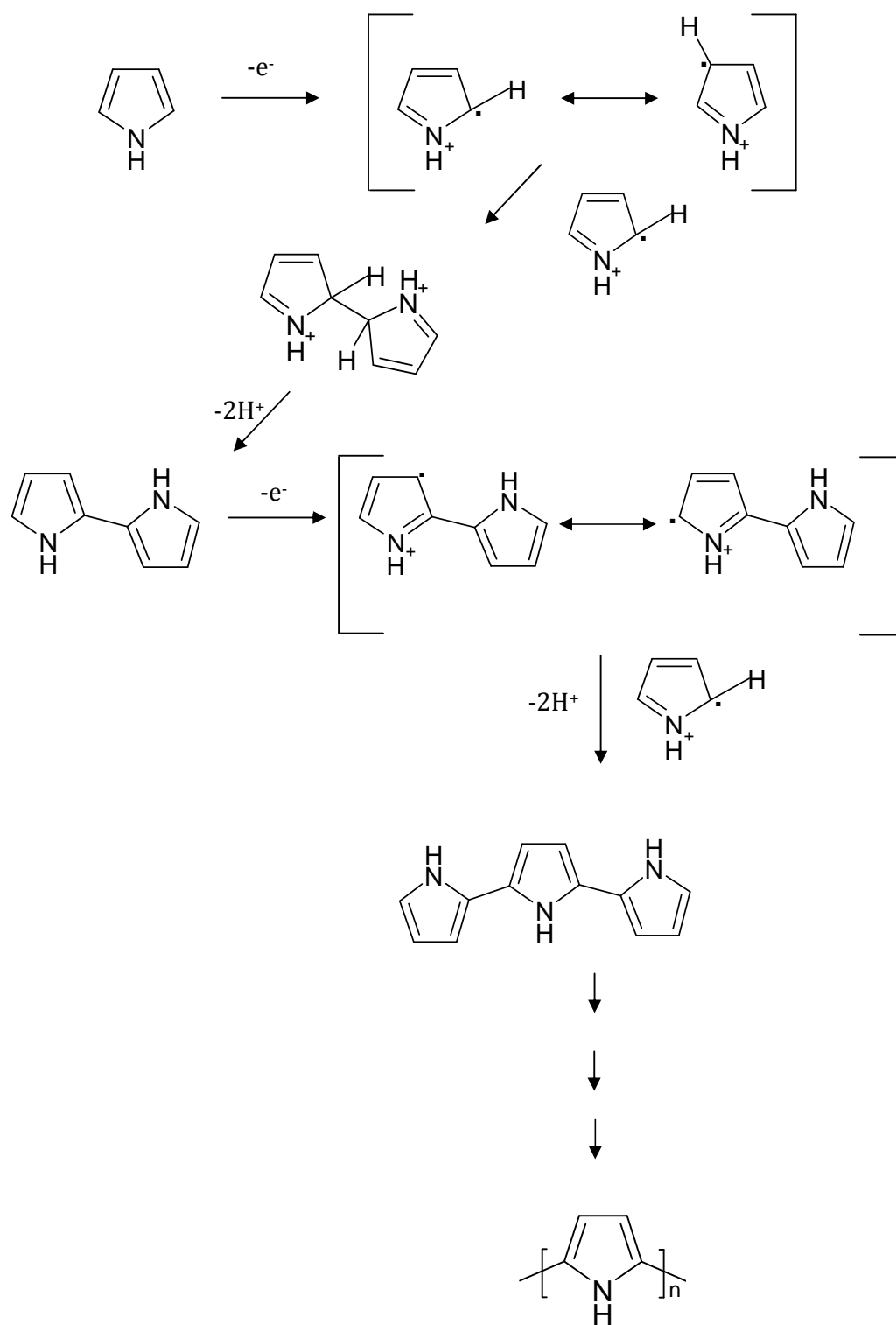
Scheme 1.3: Scheme for the chemical synthesis of polypyrrole.

Regarding the electropolymerization of pyrrole, the mechanism proposed by Diaz and his colleagues⁵⁸ and later used by Baker and Reynolds⁵⁹ is in good agreement with many experimental reports. The mechanism is described in Scheme 1.4. The initial step is the generation of the radical cation. This cation has different resonance forms, as shown in Scheme 1.4. In the chemical case, the radical cation attacks another monomer molecule, generating a dimer radical cation, as shown in Scheme 1.3. In the electrochemical case, the concentration of radical cations is much larger than that of neutral monomers in the vicinity of

the electrode where reactions take place and radical-radical coupling generates a dication. This coupling between the two pyrrole radicals results in the formation of a bond between the two α positions to give the dication, as highlighted in Scheme 1.4. This is then followed by the loss of two protons, generating a neutral dimer. This dimer is then oxidized into a radical cation, where the unpaired electron is delocalized over the dimer. The radical dimer then couples with the radical cation monomer to form a trimer. The polymerization thus progresses in this fashion to completion.

Electrochemical polymerization of pyrrole can be achieved by applying a suitable anodic potential or current to an electrode immersed in the desired electrolyte containing the monomer and the required doping salt. The most common techniques to deposit ppy electrochemically include galvanostatic,⁶⁰ potentiostatic⁶¹ and potentiodynamic⁶² methods. The controversy in the mechanism of electropolymerization is not surprising given that many factors, such as the nature of the electrolyte, ionic strength, pH, temperature and potential are important and can influence the mechanism of the reaction. All these parameters will be further explained in Section 1.2.4.

It would appear from the mechanisms given in Scheme 1.3 and in Scheme 1.4 that the final ppy chain is neutral. This, however, is not the case. The final ppy chain synthesized from both chemical and electrochemical polymerization will actually be in an oxidized/doped state,⁶³ Figure 1.4. This is explained in more detail in Section 1.2.5.



Scheme 1.4: Mechanism for the electrochemical synthesis of ppy.

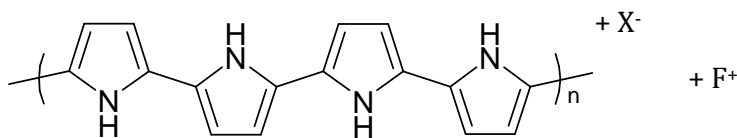


Figure 1.4: The final doped polymer, where X⁻ and F⁺ are the anion and cation from a simple XF salt, which was dissolved in a suitable solvent with the monomer.

1.2.4 Parameters affecting Electropolymerization

The electrochemical polymerization of pyrrole is affected by a number of conditions used to synthesize the polymer. First of all the material of the electrode substrate must be considered. In addition, the supporting electrolyte is a crucial parameter. Moreover the solvent, potential, temperature and pH also play an important role in the polymerization process.

The nature of the electrode is a critical parameter for the synthesis of ppy films. The substrate used must be inert towards oxidation, otherwise it would compete with the oxidation of the pyrrole monomer. For this reason, most studies have focused on the electrodeposition of ppy at inert anodes such as, platinum, glassy carbon or gold.⁶⁴⁻⁶⁶ However, a range of active metals which form oxides have also been used like iron, titanium and aluminium.⁶⁷⁻⁶⁹ In these circumstances, the potential of pyrrole oxidation usually increases and the current density generally decreases.¹⁴ Apart from metals, pyrrole has also been electropolymerized on various other materials including indium tin oxide glass (ITO)⁷⁰ and silicon.⁷¹

The supporting electrolyte also plays a major role in the electropolymerization process. Usually, the electrolyte provides the doping anions that will then be incorporated in the polymer matrix to neutralize the positive charge generated during pyrrole oxidation. The size of the anions can influence various characteristics such as redox properties of the film or its porosity.⁶³ A wide variety of dopants have been used to electrosynthesize ppy. These include small anions such as Cl⁻, Br⁻, ClO₄⁻, NO₃⁻, BF₄⁻, PF₆⁻ or medium to large anions, such as benzenesulfonate, dodecylsulfonate and polyvinylsulfonate.⁷²

The solvent used affects the electropolymerization of pyrrole. A good ionic conductivity is the most important characteristic for a good solvent. Obviously, a good electrochemical resistance against decomposition at the monomer oxidation potentials is required as well.³⁴ A variety of aqueous, organic and ionic liquids have been used to electropolymerize pyrrole.⁷³⁻⁷⁵ Aqueous solutions usually require a reasonably high amount of supporting electrolyte to achieve the desired conductivity. Likewise, organic solutions generally need a suitable organic salt. Carquigny *et al.*⁷⁶ investigated the characteristics of ppy grown from aqueous, non aqueous and mixed solutions. Thin ppy films were deposited from the pure acetonitrile/LiClO₄ solutions while films grown from the water/LiClO₄ solution and the mixed solution of acetonitrile/water/LiClO₄ were thicker, but more porous. This result is consistent with other publications. For example Ko *et al.*⁷⁷ also found that the ppy films prepared in acetonitrile/tetraethylammonium perchlorate solution had superior electron transfer characteristics and conductivities to those prepared in an aqueous medium.

The potential at which ppy is electrosynthesized is also significant in the preparation of these polymer films. Oxidation of pyrrole occurs between 0.65 V vs. SCE and 0.90 V vs. SCE.⁷⁸ At higher potentials the ppy generated is less conductive because such a potential irreversibly overoxidizes the polymer. Over-oxidation occurs gradually with increasing potential. The mechanism for this process still remains unclear. The most accepted mechanism to explain it is the nucleophilic attack of ppy by strong aqueous nucleophiles such as OH⁻, Br⁻ and H₂O.⁷⁹ The nucleophilic attack leads to the formation of carbonyl groups on the α -carbons of the pyrrole ring which interrupt the conjugation of the polymeric chain.⁸⁰

Several scientists investigated the electrodeposition of ppy films from acidic, neutral and basic aqueous solutions and they found that polymerization is favoured in a neutral or weakly acidic pH.^{78,81} A major disadvantage associated with the polymerization of pyrrole from acidic solutions is that the conductivity of the film deteriorates. This is because an acid catalyzed non-conjugated trimer

is formed and its further reaction forms only partly conjugated ppy.⁶³ Alkaline solutions tend to inhibit the polymerization as it causes the cation radicals to deprotonate to neutral radicals. This interferes with the radical-radical coupling reaction and results in non-conducting films.⁸² There are various exceptions to these statements and it is important to highlight that the effect of the pH is dependent on a number of other variables, such as the buffer species, the supporting electrolyte and the substrate anode material.⁸²

Polymerization carried out at low temperature also affects the growth of ppy films. In general, the rate of polymerization will increase with increasing temperature because the kinetics of the synthesis reaction are accelerated. Unfortunately, this usually corresponds to a decrease in the conductivity and redox properties of the polymer. For example, films prepared in propylene carbonate solution at -20 °C are much more conductive than those prepared at 20 °C. However, films produced at low temperatures have a rugged appearance and poor adhesion to the electrode substrate.⁶³

Finally, the electrochemical technique employed to deposit the polymer will also exert an effect on the polymerization of pyrrole. The ppy films are most commonly electrosynthesized by means of galvanostatic, potentiostatic and potentiodynamic methods. Films generated by applying a constant current (galvanostatic) or constant potential (potentiostatic) mode of polymerization are usually more porous and rough. By contrast, films obtained using cyclic voltammetry are generally more smooth and compact.⁸³ However, recent studies have shown that potentiostatic methods also give rise to smooth surfaces.⁸⁴ Atomic force microscopy (AFM) was utilized to investigate the surface morphology of ppy films prepared at platinum electrodes by potentiostatic and voltammetric methods with the conclusion that the potentiostatic method resulted in thin films with a smoother surface morphology. In addition, the growth of the ppy film was easier to control using this technique.⁸⁴

1.2.5 Redox Properties of Polypyrrole

One of the main features that makes ppy such an interesting system is its redox behavior. Polypyrrole can be easily switched between the neutral, partially oxidized and fully oxidized states, as described in Figure 1.5. In its neutral state ppy exists as an insulator where the conduction band is empty as all the electrons remain in the valence band. Upon oxidation, an electron is removed from a π -bond valence band and a polaron is formed. The separation of the positive charge and the unpaired electron decreases during continual oxidation as the number of polarons increases. This in turn leads to the formation of a bipolaron, as depicted in Figure 1.5 (c), and the polymer is now in its fully oxidized state. During ppy oxidation, anions are incorporated into the polymer to neutralize the positive charges formed, Figure 1.6 (a). On the other hand, when ppy is reduced to its neutral state, dopant anions are consequently expelled from the polymer matrix, Figure 1.6 (b).

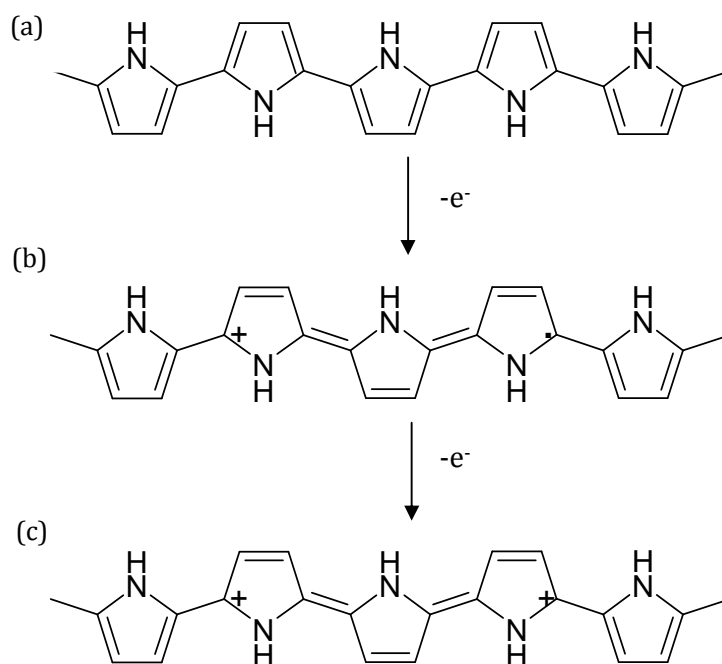


Figure 1.5: Formation of a polaron and bipolaron where, (a) is the neutral ppy, (b) is the partially oxidised ppy (polaron) and (c) is the fully oxidised ppy (bipolaron).

This behavior is especially true for small mobile anions such as chlorides. However, larger anions such as *p*-dodecylbenzene sulfonate⁸⁵ and poly(styrenesulfonate)⁸⁶ are permanently anchored into the polymer matrix. In this situation, the electroneutrality during the reduction of the polymer is maintained by the influx of mobile cations from the electrolyte solution into the polymer, Figure 1.7 (b). Medium sized anions on the other hand generally exhibit both anionic and cationic exchange, as confirmed by several works published in the literature.⁸⁵

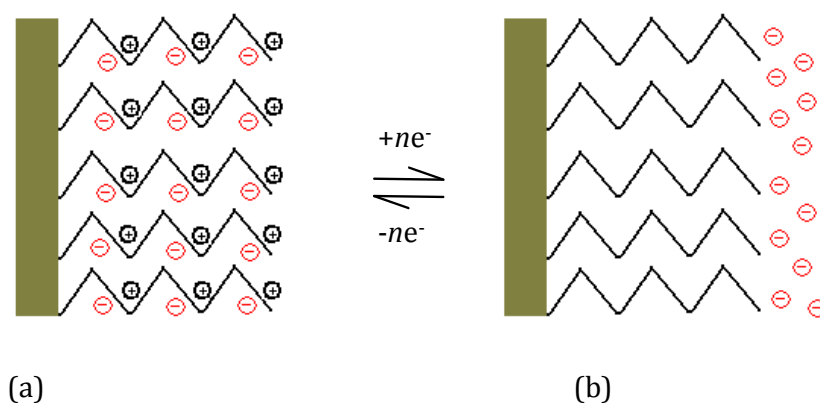


Figure 1.6: (a) Incorporation of anions into ppy film and (b) release of anions from ppy film where + is the charge on the ppy and - is the charge of the anions.

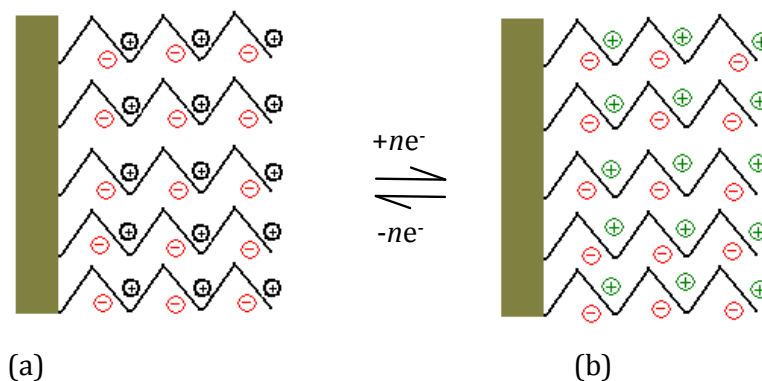


Figure 1.7: (a) Cation expulsion from ppy film and (b) cation incorporation into ppy film where + is the charge on the ppy, - is the charge of the anions and + is the charge of the cations.

1.3 Cyclodextrins

1.3.1 Overview

Cyclodextrins (CDs) are macrocyclic, non reducing oligosaccharides composed of α -D-glucopyranoside units linked by α -(1,4) glycosidic bonds. They were first discovered by Villiers in 1891⁸⁷ and twelve years later, Schardinger⁸⁸ further developed the cyclic structures, hence CDs are sometimes referred to as Schardinger dextrins. In the following years Pringsheim and his group^{89,90} played the leading role in cyclodextrin research. Their research led to the discovery of the ability of the CDs to form complexes with various organic compounds.⁹¹ However, it was only until the mid 1970s that the structure and chemical properties of natural cyclodextrins were fully characterized.⁹²

CDs are naturally occurring water-soluble glucans. They are produced through enzymatic degradation of starch in the presence of a glycosyl transferase, a type of amylase.⁹³ Many organisms contain glycosyl transferase, however, in general it is obtained from *Bacillus megaterium*, *Bacillus circulans*, *Bacillus stercorophilus*, *Klebsiella oxyoca* and *Bacillus macerans*.^{91,93} Those microorganisms produce a mixture of different CDs that can be separated using, for example, chromatography or crystallization.⁹⁴

CDs are generally made up of glucopyranoside units of 4C_1 chair conformation which leads to a truncated cone shape encasing a cavity, as depicted in Figure 1.8 and in Figure 1.9.⁹⁵ In Figure 1.10, the structures of the most common CD members; α -, β - and γ -CD, which include 6, 7 and 8 repeating glucopyranoside units, respectively, are represented. These units are orientated in a cyclic manner offering a typical conical or truncated cone structure with a relatively hydrophobic interior and hydrophilic exterior, due to the presence of hydroxyl groups in positions 2, 3 and 6 of the glucopyranose units.^{91,96}

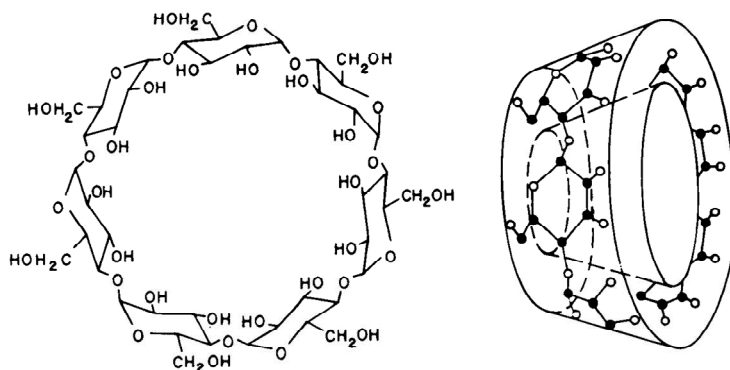


Figure 1.8: Schematic of a β -CD showing the chair conformation of glucose moieties.

The structural features described above give cyclodextrins good water solubility and the ability to hold appropriately sized guests through non covalent interactions such as hydrogen bonding, hydrophobic interactions, and electrostatic interactions.⁹⁷ Despite the fact that CDs with 6 to 12 glucose units have been separated, only those with six, seven and eight units (with the Greek names α -, β -, and γ -CD, respectively) are commonly used. The physical properties of the three native CDs are quite different, e.g. width of the cavity, solubility, molecular mass etc.; however they possess the same depth.⁹⁴ In Table 1.1, the approximate geometries and characteristics of the most common CDs are reported.⁹⁶

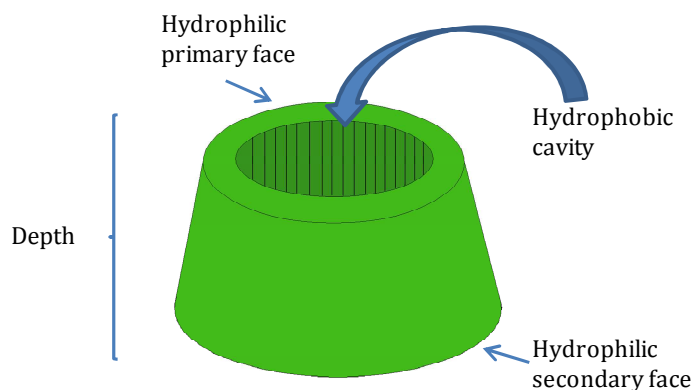


Figure 1.9: Schematic of a cyclodextrin.

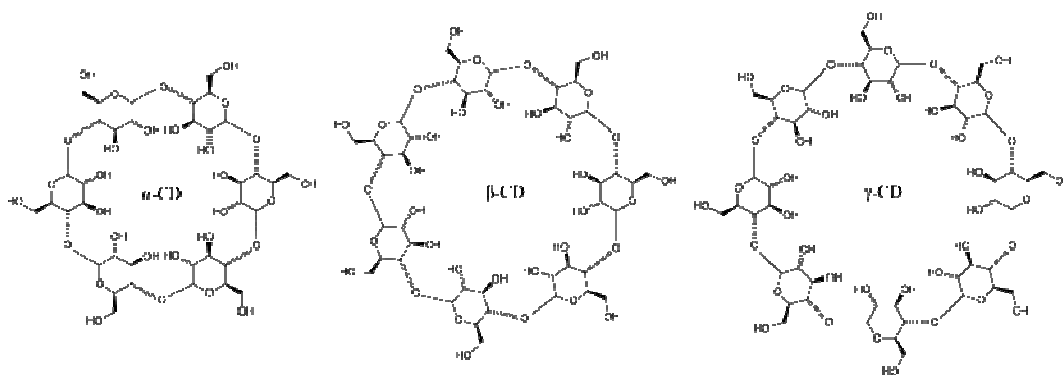


Figure 1.10: Chemical structures of α -, β - and γ -cyclodextrins.

Table 1.1: The main characteristics of native cyclodextrins.

CDs	α	β	γ
Glucose units	6	7	8
Molecular mass / g	972	1135	1237
Inner diameter / nm	0.57	0.78	0.95
Outer diameter / nm	1.37	1.53	1.69
Cavity volumes / nm ³	0.174	0.262	0.472
Depth / nm	0.78	0.78	0.78
Solubility in water / g/100 ml	14.50	1.85	23.20
pK _a	12.33	12.20	12.08

1.3.2 Derivatization of cyclodextrins

Cyclodextrins can be chemically modified by replacing the hydroxyl groups either in the primary or secondary rims of the CDs, with a variety of appropriate neutral or charged groups. It has been reported that this can improve binding affinity.⁹⁵ The modified CDs can exhibit different properties than their native counterparts, such as increased solubility or differences in the hydrophobicity of the cavity.⁹⁶ For example, the solubility of the β -CD in water is very low compared to that of the other CDs, as listed in Table 1.1. The lower solubility of

the β -CD is due to the formation of intramolecular hydrogen bonds among secondary hydroxyl groups (Figure 1.11) and hence hydrogen bonding with water molecules is avoided. The substitution of the hydroxyl groups involved in the intramolecular hydrogen bonding with methoxy or hydroxypropyl groups is accompanied by a drastic enhancement of the CD solubility.^{98,99} Furthermore, the formation of intramolecular hydrogen bonds makes the CD ring rigid.

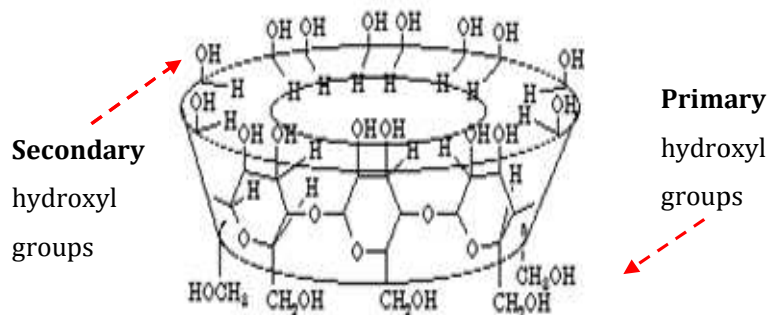


Figure 1.11: Representation of the primary and secondary hydroxyl groups of a β -CD.

In the research work developed in the present thesis, a negatively charged cyclodextrin with a number of sulfated groups present on the outer rims was used, sulfated β -cyclodextrin ($s\beta$ -CD). The $s\beta$ -CD is obtained by substitution of either the primary or secondary hydroxyl groups with sulfate groups. The $s\beta$ -CD utilized in the experiments has an average from 7 to 11 substituents per CD molecule therefore, it has between 7 and 11 negative charges associated with it, which are counterbalanced with sodium ions, as illustrated in Figure 1.12.¹⁰⁰ It is fundamental to highlight that β -CD and $s\beta$ -CD have the same ring structure, differing only in the substituent located on the rims of the CD ring.¹⁰¹

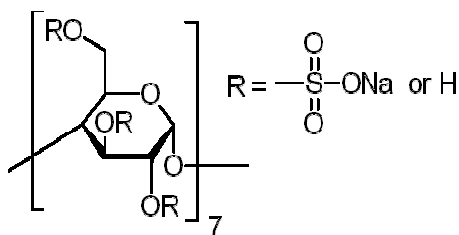


Figure 1.12: Representation of a sulfated β -cyclodextrin.

Although β -CD has the same ring structure as other derivatized CDs, the presence of the substituents on the ring contributes to its chiral discrimination properties.¹⁰¹ As a matter of fact, a major area in which sulfated CDs are being utilized is chromatography and capillary electrophoresis.^{96,102,103} In enantiomeric separation, neutral CDs are not useful for neutral racemates because a neutral inclusion complex has no electrophoretic mobility. By using a charged CD, such as the β -CD, uncharged enantiomers can be moved to the detector as charged analytes due to the formation of an inclusion complex with the modified anionic CD.⁹⁶

The sulfated β -cyclodextrin has been characterized by several research groups.^{102,104} Figure 1.13 illustrates a single glucose unit of a β -CD (comprised of 7 units). On the primary rim there are 7 primary hydroxyls, covalently linked to the C-6 positions and hence 7 potential substitution sites, while, on the secondary rim there are 14 secondary hydroxyl groups. Amini *et al.*¹⁰⁴ found that substitution of these CDs is predominantly at the C-2 and C-6 positions. Those data are consistent with the studies of Chen *et al.*¹⁰² They confirmed nearly complete sulfation at the C-6 position of the primary hydroxyl groups and partial sulfation at the C-2 secondary hydroxyl groups. However, they reported no substitution at the C-3 positions. Considering the results published by Amini and Chen, it is reasonable to state that for most molecules all the hydroxyl groups on the primary rim are derivatized with sulfate groups while only a partial substitution occurs on the secondary rim. Even if the exact number of sulfate groups per cyclodextrin molecule cannot be determined, the predominant aspect of this derivatization is the introduction of negative charges on the CD surface which make this material a suitable dopant for conducting polymers.

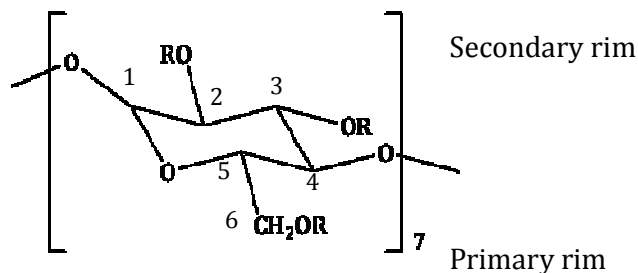


Figure 1.13: Single unit of glucose (R=H) of a cyclodextrin, showing IUPAC numbering of the carbon atoms.

Another β -CD derivative considered in the present thesis is the carboxymethyl β -cyclodextrin (CM β -CD). This cyclodextrin has been investigated as possible tool in the development of new drug delivery systems. Cserhati¹⁰⁵ studied the interactions of some anticancer drugs with carboxymethyl β -CD, while Shuang *et al.*¹⁰⁶ investigated the ability of CM β -CD to include basic drugs, such as procaine hydrochloride. In the CM β -CD, hydroxyl groups are replaced with carboxymethyl substituents, as illustrated in Figure 1.14. The average degree of substitution is 3 carboxymethyl groups per cyclodextrin molecule. Even for this CD the negative charges, originating from the carboxylated groups, are counterbalanced with sodium cations. While the $s\beta$ -CD is a cyclodextrin with a high negative charge density, the CM β -CD possesses only three negative charges per molecule and therefore has a lower negative charge density. Preliminary experiments of pyrrole electropolymerization have been carried out using CM β -CD as a dopant and these results have been compared to measurements recorded when $s\beta$ -CD was used as the dopant.

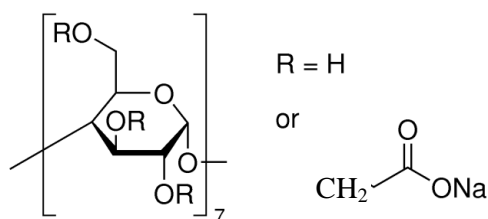


Figure 1.14: Structure of the carboxymethyl β -cyclodextrin.

Apart from the two modified CDs employed in this work, a variety of other derivatized CDs have been extensively investigated. Among the neutral derivatives the most relevant are the methylated-, hydroxyethylated, hydroxypropylated and acetylated CDs. On the other hand, methylamino-, sulphobutylether- and phosphate CDs can be mentioned to summarize the more prominent charged modified cyclodextrins.

1.3.3 Applications of cyclodextrins

Due to their exceptional host-guest complexation characteristic, CDs have been used in a variety of fields. As a matter of fact, the price of native CDs and their derivatives has dramatically dropped over the last three decades as a consequence of their large industrial production. About half a dozen of companies are producing cyclodextrins with a total output that exceeds a thousand tons per year.⁹¹ The pie chart illustrated in Figure 1.15 represents a distribution of publications concerning cyclodextrins, which reflects their versatility. In the following section, an overview of the most important applications of the cyclodextrins is provided.

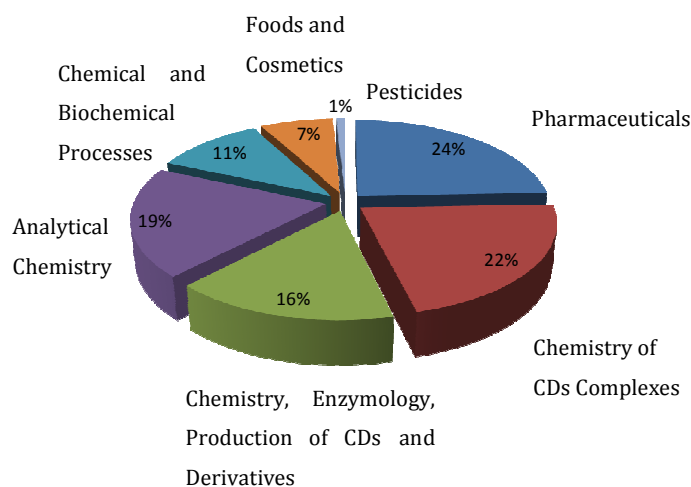


Figure 1.15: Distribution of the most relevant abstracts published by the journal *Cyclodextrin News* (1996).⁹¹

CDs are extensively utilized in the pharmaceutical industry. CDs complexation of an active ingredient can stabilize it, enhance its solubility, bioavailability or diminish its adverse effect.¹⁰⁷ CDs have the ability to alter the physical, chemical and biological properties of guest molecules through the formation of inclusion complexes, for these reasons they are good candidates in the design of new drug delivery system. For example, Bekers *et al.*¹⁰⁸ and Bhardwaj and coworkers¹⁰⁹ studied the effect of cyclodextrins on the chemical stability of mitomycin C, a useful anticancer drug which causes severe dermatological problems upon injection. Complexation of the drug with CDs was reported to reduce skin necrosis. Uekama *et al.*¹¹⁰ published work where the oral absorption of ketoconazole was improved after the complexation of the drug with β -cyclodextrin or hydroxypropyl- β -cyclodextrin. Loftsson *et al.*¹¹¹ published a study where they report the implementation of the bioavailability of the antimicrobial triclosan, after cyclodextrin complexation.

CDs play a role in environmental remediation. Organic contaminants and heavy metals can be complexed and removed from soil, water and atmosphere. Fava *et al.*¹¹² and Luong *et al.*¹¹³ studied the possibility of enhancing intrinsic ex-situ bioremediation of a chronically contaminated soil by using hydroxypropyl- β -cyclodextrin and γ -cyclodextrin. Cyclodextrins have been used to scrub gaseous effluent from organic chemical industries, as reported by Szejtli in 1989.¹¹⁴

Another prominent application of CDs is in catalytic reactions because they have the ability to serve as enzyme mimics. These are generated by modifying naturally occurring CDs. Various functional groups are introduced on the primary or secondary face. The derivatized cyclodextrins bind the substrate in the hydrophobic cavity and the reaction is initiated by the catalytic group linked to the CDs.¹¹⁵ For example Ye *et al.*¹¹⁶ explained the catalytic effect of a β -CD derivative in the conversion of benzyl alcohol to aldehydes. In biocatalytic processes CDs increase the enantioselectivity. After the formation of the host-guest complex with the prochiral guest molecule, the preferential attack by the reagent takes place only from one of the enantiotopic

faces, resulting in higher enantioselectivity. Kamal *et al.*¹¹⁷ published a study where the hydrolysis of racemic arylpropionic esters by the carrier protein, BSA, resulted in a lower enantioselectivity than the corresponding reaction in the presence of β -CD. Finally, CDs affect the catalytic activity by involving the inclusion of the catalyst. This phenomenon can either inhibit completely the reaction, or cause an enhancement in catalytic activity. Granados and de Rossi¹¹⁸ found that cyclodextrins inhibited the intramolecular catalysis of amide hydrolysis as the geometry of the substrate changed due to the interaction of the carboxylic and/or the amide groups with the hydroxides at the rim of the CD.

Cyclodextrins are extensively used in analytical chemistry as well. In particular, they are useful tools in separation chemistry because of their ability to discriminate between positional isomers, functional groups, homologous and enantiomers.¹¹⁹ Hydrophilic CDs have been frequently used in capillary electrophoresis as buffer modifiers to affect chiral separation of drugs.^{96,120} Moreover, cyclodextrins are utilized in high-performance liquid chromatography (HPLC) as stationary phases when they are bonded to a solid support, or as mobile phase additives in HPLC or capillary electrophoresis for the separation of chiral compounds.¹²¹

Rocco and Fanali¹²² employed the heptakis (2,3,6-tri-O-methyl)- β -CD as the chiral mobile phase additive for the enantiomeric resolution of several acidic compounds by means of nano-liquid chromatography on achiral capillary columns.

Another fundamental application of CDs in analytical chemistry includes their use as electrode modifiers. For example, Prime *et al.*¹²³ and Pospisil *et al.*¹²⁴ have worked on the adsorption of CDs on a mercury drop electrode. CDs were found to form a compact layer on the mercury drop and this modified electrode was applied to study the stereoselectivity of the reduction of phenylglyoxalid acid. Another application involves the deposition of CD-modified polymers on metal and carbon electrodes. Koradecki *et al.*¹²⁵ have deposited a polymer of a chemically modified β -cyclodextrin on a carbon electrode and they have

investigated the modified electrode by means of cyclic voltammetry, using ferrocene, as an analytical probe to test the host-guest equilibria of the system. They showed that the system was suitable for membrane-type applications because of its selectivity, chemical inertness and insolubility in solvents.

The food industry is another area in which there is a widespread use of cyclodextrins. CDs form inclusion complexes with a wide range of molecules including fats, flavours and colours.¹⁰⁷ CDs possess the property of removing and masking undesirable components and they can control the release of desired food constituents.¹²⁶ Many natural and artificial flavours are volatile oils and complexation with cyclodextrins provides a valid alternative to conventional encapsulation technologies for the protection of the flavour. CDs behave as encapsulants which protect the flavour against severe food processing such as freezing or microwaving. One of the main applications of CDs in food chemistry is the removal of cholesterol from animal products such as eggs and dairy products. Material treated with CDs can remove up to 80% of cholesterol. Free fatty acids also are removed upon the treatment with CDs, with the advantage of improving the frying property of fat.⁹² Flavonoids and terpenoids are important antioxidative and antimicrobial agents but they cannot be utilized as foodstuff owing to their bitter taste and low aqueous solubility. Sumiyoshi¹²⁷ discussed the enhancement of these plant extract properties upon complexation with CDs. The last example is the use of CDs in chewing gum to retain the flavour for longer duration.¹²⁸

Cosmetic, personal care and toiletries are another set of products in which CDs are being employed. They are mainly used in controlled release of perfumes, room fresheners and detergents from the inclusion compounds.¹⁰⁷ The host-guest interaction results in a higher energy barrier to volatilize the guest, thus producing long lasting fragrances.¹²⁶ Dishwashing and laundry detergents containing a formulation based on CDs can mask odors in washed items.¹²⁹ The CDs complexation of fragrances in skin formulations, such as talcum powder, stabilizes the fragrance against evaporation and oxidation over a long period. The antimicrobial effect of the product is also improved.¹³⁰

The textile industry is another area in which CDs are increasingly attracting attention. Hirose and Yamamoto proved that food-packaging bags manufactured using CDs with an ethylene-tetracyclo-3-dodecane copolymer resulted in no odor and good antifungal properties after one week of storage at room temperature.¹⁰⁷ CDs are also used for dyeing fabrics to increase the dye uptake by the fabric and thus reduce the amount of dye lost in the wastewater. Using the hydrophobic tosyl derivative of β -CD, a 3-fold increase in the binding of fluorescent dye to polyester fibers was attained.⁹²

1.3.4 Inclusion complex formation and driving forces controlling complexation

Cyclodextrins have developed quickly in the past two decades and have become an important branch of host-guest chemistry, specifically due to their ability to be involved in several practical applications.^{91,107,129} The main interest in cyclodextrins lies in their ability to form inclusion complexes with a variety of compounds. Host-guest chemistry is the study of these inclusion phenomena, where the 'host' molecules are capable of including smaller 'guest' molecules through non-covalent interactions. The lipophilic cavity of CDs offers a microenvironment into which non-polar moieties or non polar molecules of appropriate size can enter to form inclusion complexes.⁹¹ The main driving force in this kind of host-guest interaction is the release of water molecules from the CD cavity. They are displaced by the more hydrophobic molecules of the guest, in order to attain an apolar-apolar association which leads to a decrease of the cyclodextrin ring strain and to a lower energy state of the complex.⁹¹ In addition, water molecules included in the CD cavity cannot satisfy their hydrogen bonding potential and hence when they are released into the bulk solution they increase the number of hydrogen bonding with other water molecules, resulting in a decrease of enthalpy and in a lower energy of the system.^{97,129} Another factor that promotes complexation is the reduction of repulsive interactions between the hydrophobic guest and the water environment once the complex is formed.¹²⁹ As CDs are known to have large dipole moments it is logical that van de Waals forces are important too in

complexation. Once inside the CD cavity, the guest molecule undergoes conformational adjustments to gain maximum advantage of the weak van de Waals interactions.¹²⁹

Binding strength depends on how well the guest fits in the host. Considering the size of α -CDs, they can include low molecular weight compounds with aliphatic side chain, while β -CDs can host aromatics and heterocycles. Larger molecules such as steroids can be accommodated within the cavity of γ -CDs.¹²⁹

The complexation process is not a static process but it is a dynamic equilibrium and complexes can be formed either in solution or in the crystalline state.¹²⁹ Inclusion in cyclodextrins induces a modification of the physicochemical properties of the guest while it is temporarily caged within the host cavity. For example, the solubility of insoluble guests is enhanced upon complexation.¹⁰⁷ Labile guests are stabilized against visible light, UV light or heat.¹⁰⁷ Complexation can also have an effect on controlling the volatility of guests.¹⁰⁷ Finally, the formation of an inclusion complex is a useful tool in chromatographic separation.¹²⁹

During the formation of an inclusion complex the change in the chemical and physical properties of the guest molecule can be monitored using a number of techniques. Various spectroscopic and electrochemical techniques can be used to confirm complexation, including UV-visible spectroscopy (UV-Vis), nuclear magnetic resonance (NMR) spectroscopy and electrochemical studies.^{91,129,131} Changes attributed to the complexation can be used to evaluate the apparent binding or formation constant (K_f). However, prior to the determination of the K_f value the stoichiometry of the host-guest complex must be established.¹³² This is obtained by the well known continuous variation or Job's method which is described in more detail in Chapter 2.¹³³ Generally, inclusion complexes form a ratio of 1:1, 1:2 and sometimes 2:1 (CD:guest).¹³⁴

NMR spectroscopy is also a useful tool to analyze host-guest interactions and it can provide quantitative and qualitative information. Assuming the guest enters

the cavity, ^1H NMR spectroscopy, can be used to locate the protons which are most affected by the complexation.¹³¹ The chemical shift of these protons can be used to evaluate the apparent binding or formation constant (K_f).¹³¹ Furthermore ^1H NMR spectroscopy measurements can provide indications on the structural interaction between the cyclodextrin and the guest compound. Several groups have studied the complexation properties of neutral β -CD and monitored the changes in the chemical shifts of the ^1H signals for both the CD and the guest. However, ^1H NMR spectral data of the sulfated β -CD, which is the cyclodextrin employed in this research work, are too difficult to differentiate so the chemical shift of the guest is followed.¹³²

If a guest absorbs light in the UV or visible region then the inclusion phenomenon can be evaluated by UV-Vis spectroscopy.⁹³ This technique can be used to confirm complexation and indeed to obtain the formation constant associated with the inclusion complex. Usually a guest that interacts with the cyclodextrin undergoes a shift in its absorption band in the UV-Vis region and a change in the intensity of absorption. These spectral changes can be used to determine the K_f constant. Generally, a Hiedlebrand-Benesi modified equation is used to evaluate the K_f constant.^{135,136}

Electrochemical techniques can also be performed to explore the complexation properties of CDs. If the guest is electroactive the peak current and potential can be followed for the free analyte and compared to results collected for the complexed state. If an inclusion complex is formed, two features are generally observed: a decrease in the peak current, attributed to a decrease in the diffusion of the bulky CD complex with respect to the more mobile free guest and a shift in the peak potential of the complexed species as it is harder to oxidize or reduce the guest located in the cavity. Coutouli-Argyropoulou and his group,¹³⁷ for example reported the effect of complexation on the electrochemical properties of ferrocene derivatives and showed shifts in both the peak current and peak potential, when higher concentrations of a neutral β -CD were added. Once again based on these variations a number of equations can

be used to evaluate the formation constant.^{136,138,139} These equations will be discussed in Chapter 2.

1.4 Viologens

In 1933 Michaelis first reported on the electrochemical characteristics of a class of compounds which he named 'viologens'.¹⁴⁰ This class of molecules are formally known as 1,1'-disubstituted-4,4'-bipyridinium ions.

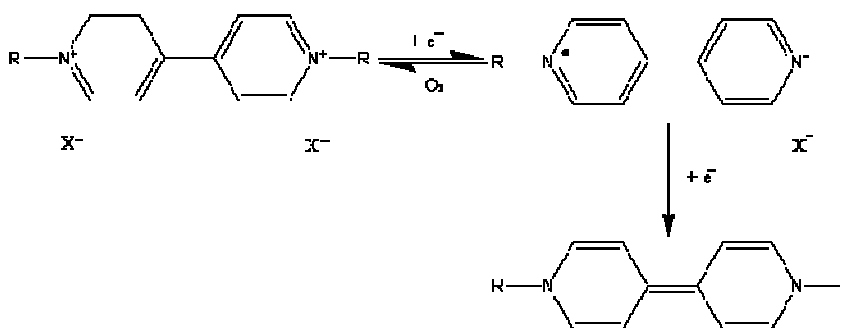


Figure 1.16: Schematic representation of the three oxidation states for the viologen compounds.

They exist in three main oxidation states: dicationic (V²⁺), cationic radical (V^{•+}) and neutral state (V⁰), as illustrated in Figure 1.16. Of the three common viologen redox states, the dication is the most stable.¹⁴¹ The colourless dication can undergo a one-electron reduction, generating a radical cation which may be soluble or can form a deposit on the electrode if large substituents are bound to the pyridinium nitrogen.¹⁴² These radicals exhibit a colour which depends on the substituents. Simple alkyl groups, for example, promote a blue-violet colour whereas aryl groups generally impart a green hue to the radical cation.¹⁴¹ When the molecule undergoes a second stage of reduction, the radical gains an electron to form a yellow to brown neutral species which is frequently insoluble in aqueous media.¹⁴²

Viologens can be reduced electrochemically by applying a suitable potential. The 1,1'-substituents affect the potential of both reduction steps.¹⁴³ In this work three different viologen have been investigated: methyl, ethyl and benzyl viologen and the respective 1,1'-substituents are summarized in Scheme 1.5.

R = CH_3	X = Cl^-	Methyl viologen dichloride (Paraquat)
R = CH_2CH_3	X = ClO_4^-	Ethyl viologen diperchlorate
R = $\text{CH}_2\text{-Ph}$	X = Cl^-	Benzyl viologen dichloride

Scheme 1.5: Summary of the substituents and counterions for methyl, ethyl and benzyl viologen.

The methyl viologen is the simplest molecule of this class of compounds and it is commonly known as paraquat. It was discovered to possess herbicidal activity. Ethyl viologen and benzyl viologen were also selected for study. This latter compound was chosen to point out differences in the interaction with the β -CD when alkyl substituents are replaced by aromatic rings.

1.4.1 Applications of the viologens

Michaelis and his group¹⁴⁰ originally investigated the viologens as redox indicators in biological studies. Since that time the interest in this class of compound has increased. Various examples to elucidate the applications of viologens are discussed in the present section.

Viologens are widely studied as electron transfer mediators in enzymatic reactions. Hale *et al.*¹⁴⁴ published results on the efficiency of several water soluble viologens in mediating electron transfer from reduced glucose oxidase to a carbon paste electrode. The advantage of using viologens is that these molecules have sufficiently anodic redox potentials (more positive than that of flavin adenine dinucleotide) to reoxidize reduced glucose oxidase. These redox potentials are, however, sufficiently cathodic that glucose sensors based on glucose oxidase and its mediators can operate in a potential range where the

oxidation of common interfering species, such as ascorbic acid and uric acid, does not occur. Gomez Moreno and coworkers¹⁴⁵ found that the covalent binding of the viologen N-methyl-N'(aminopropyl)-4,4'-bipyridinium to the flavoprotein ferredoxin-NADP(+) reductase, a photosynthetic enzyme from a cyanobacterium, facilitates the transfer of electrons between the FAD group in the enzyme and oxygen molecules present in the solution. This oxidase activity, which is completely absent in the native protein, indicates that there is an efficient electron transfer between the FAD group in the enzyme and the viologen molecule. These type of studies could give important information on the structural requirements for the electron transfer reaction between redox groups present in biological molecules.

Modification of electrode surfaces in order to establish an electrical connection with enzyme molecules is considered a topic of great interest. The redox centre of enzymes, in fact, is usually deeply located within the protein and the protein shell avoids direct electron transfer between the enzymatic active sites and the electrode surface.¹⁴⁶ Cosnier *et al.*¹⁴⁶ constructed a biosensor composed of ppy functionalized with viologens with the ability to shuttle electrons between the electrode and the reactive centre of an enzyme, a nitrate reductase.

Other successful applications of viologens are as electrochromic materials and nanomaterials.¹⁴⁷ As mentioned above, viologens can change their optical properties and so can be switched between different colours when exposed to chemical perturbations. These materials are called chromogenics. When a reversible optical modification is observed as a consequence of the application of an electric voltage or current, the phenomenon is called electrochromism. Electrochromism results from the generation of different visible region electronic absorption bands on switching between redox states.¹⁴⁷ Such a phenomenon occurs in viologens because the radical cations have a delocalized positive charge and hence their colouration arises from an intramolecular electronic transition. By contrast, the dicationic species are transparent since they do not possess any delocalized charge. Suitable choice of nitrogen substituents to attain the appropriate molecular orbital energy levels can, in principle, allow

colour choice of the radical cation.¹⁴¹ Electrochromic materials are employed in controllable light-reflective or light-transmissive devices for optical information and storage, anti-glare car rear-view mirrors, sunglasses, protective eyewear for the military, controllable aircraft canopies and glare-reduction systems for offices.¹⁴¹

1.4.2 Paraquat

Several viologens exhibit herbicidal activity and such a property gave rise to the most relevant application of this class of compounds. Among the viologens, methyl viologen, commonly known as paraquat is the most effective herbicide, however other members with herbicidal activity include diquat, chlormequat, morfamquat, and difenzoquat.¹⁴⁸ The termination *-quat* indicates that the molecule contains a quaternary nitrogen atom.¹⁴⁹

Paraquat was registered for use in 1965 and since that time has been one of the most widely used herbicides for broadleaf weed control.¹⁵⁰ It is a quick-acting compound that destroys green plant tissue on contact. However it binds tenaciously to soil, especially the clay mineral factor which results in rapid loss of herbicidal activity and hence sprayed fields can be planted within a day or two of paraquat application.¹⁴⁸

Exposure to dangerous levels of paraquat can occur in several ways including inhalation of spray, skin contact, ingestion, and even suicidal hypodermic injections. Acute toxicological effects include skin and eye irritation, lung congestion, which in some cases leads to convulsions, incoordination and death by respiratory failure. Burning of the mouth and throat occur if paraquat is swallowed, followed by gastrointestinal tract irritation, loss of appetite, nausea, abdominal pain, vomiting and diarrhea. Because of its widespread use as a herbicide, the possibility exists of substantial paraquat contamination of food. Drinking water contamination by paraquat has also been observed. The European Union has forbidden the use of paraquat since July 2007 but apart from Sri Lanka, Syria, Ivory Coast, Malaysia and Switzerland where it has also

been banned, this herbicide is still widely used in a considerable number of other countries, including USA and China.¹⁵¹ The above concerns point out that new technologies in pollution remediation are required. In this thesis the possibility to develop a new sensor to detect paraquat and two other viologens has been studied.

1.5 Development of a sensor for viologens

Pyrrole and the β -CD were used as the starting material for the development of a new electrochemical sensor for the pollutant paraquat and for two other compounds of the same class, ethyl and benzyl viologen.

Besides electrochemical methods, several other techniques have been employed to detect paraquat in water samples, including UV-Vis spectroscopy, solid phase extraction (SPE), chromatography and mass spectrometry.¹⁵²⁻¹⁵⁵

One of the major advantages of an electrochemical sensor is that it can be used *in situ*, preventing expensive or time consuming pretreatment of the working solutions. The electrochemical sensor outlined in this thesis also has the advantage of its easy electrosynthesis, from inexpensive starting materials. Finally promising results have already been obtained with polypyrrole modified with β -CD to sense another electroactive molecule, dopamine. The goal of this thesis was to construct a sensor capable of providing a good detection limit for the sensing of three analytes and to trap and remove viologens from solution, by using the well known ability of the cyclodextrins to form inclusion complexes. Despite several studies published on the electrochemical determination of paraquat at different modified electrodes, to the best of our knowledge none of them describes a method to remove the pollutant from solutions.¹⁵⁶⁻¹⁶⁰ For example, Lu and Sun¹⁵⁸ studied the determination of methyl viologen (paraquat) at a nafion film coated glassy carbon electrode by using differential pulse voltammetry (DPV). With this method they obtained a detection limit of $0.5 \mu\text{g L}^{-1}$ ($1.94 \times 10^{-9} \text{ M}$). This value is close to the limit established by the European Union. The maximum concentration limit for methyl viologen in natural waters

is $0.1 \mu\text{g L}^{-1}$. Zen *et al.*¹⁵⁹ and de Oliveira *et al.*¹⁶¹ also employed nafion modified electrodes for the determination of methyl viologen by means of square wave voltammetry (SWV) and DPV, respectively. They reached detection limit values similar to that reported by Lu and Sun.¹⁵⁸ Chang *et al.*¹⁶² modified a gold electrode by electrodepositing a polyviologen film and they used this system to detect methyl viologen, obtaining a detection limit of 1.00×10^{-4} M.

Polypyrrole doped with the anionic CD was electrodeposited on a metal substrate, from a solution containing pyrrole and the β -CD. Firstly, the best metal electrode support was selected among gold, platinum and glassy carbon. To explore the detection properties of the polymer towards the redox chemistry of the viologens, high concentration of the analytes were initially used. Unfortunately, the sensitivity of the polymer evaluated by cyclic voltammetry (CV) was not satisfactory. However, CV was used to study the optimum conditions for using the sensor. The sensitivity of ppy modified with β -CD was improved by means of differential pulse voltammetry (DPV). Finally, constant potential amperometry (CPA) experiments were carried out for the determination of paraquat at the modified polymer.

1.6 References

1. Harley C. C.; The Formation of an Electrochemical Sensor for the Selective Detection of Dopamine, Ph.D thesis, NUIM, Department of Chemistry, 2009.
2. Hendy G. M.; Polypyrrole modified with sulfonated β -cyclodextrin: Controlled release of dopamine and host-guest complexation properties, Ph.D thesis, NUIM, Department of Chemistry, 2009.
3. "R.E.D Facts, Paraquat dichloride," United States Environmental Protection Agency, EPA-738-F-96-018, August 1997.
4. Tamsamani K. R., Mark H. B., Kutner W. and Stalcup A. M.; *Journal of Solid State Electrochemistry*, 6, 2002, 391-395.
5. Kupila E. L. and Kankare J.; *Synthetic Metals*, 55, 1993, 1402-1405.
6. Tamm J., Alumaa A., Hallik A., Silk T. and Sammelselg V.; *Journal of Electroanalytical Chemistry*, 414, 1996, 149-158.
7. Weidlich C., Mangold K. M. and Juttner K.; *Electrochimica Acta*, 47, 2001, 741-745.
8. Weidlich C., Mangold K. M. and Juttner K.; *Electrochimica Acta*, 50, 2005, 1547-1552.

9. Azapagic A. and Emsley A.; *Polymers: the environment and sustainable development*; John Wiley and Sons, 2003.
10. Guimard N. K., Gomez N. and Schmidt C. E.; *Progress in Polymer Science*, 32, 2007, 876-921.
11. Malinauskas A., Malinauskiene J. and Ramanavicius A.; *Nanotechnology*, 16, 2005, R51-R62.
12. Schmidt C. E., Shastri V. R., Vacanti J. P. and Langer R. "Stimulation of neurite outgrowth using an electrically conducting polymer"; *Proceedings of the National Academy of Sciences*, 1997, USA.
13. Bredas J. L. and Street G. B.; *Accounts of Chemical Research*, 18, 1985, 309-315.
14. Wise D. L.; *Electrical and optical polymer systems*; CRC Press, 1998.
15. Alcacer L.; *Conducting Polymers: Special Applications*; Springer, 1986.
16. Briseno A. L., Baca A., Zhou Q. Z., Lai R. and Zhou F. M.; *Analytica Chimica Acta*, 441, 2001, 123-134.
17. Chandrasekhar P.; *Conducting Polymers, Fundamental and Applications*; Kluwer Academic Publishers, 1999.
18. Wallace G. G., Spinks G. M., L. A. P. Kane-Maguire L. A. P. and Teasdale P. R.; *Conductive Electroactive Polymers: Intelligent Materials Systems*; CRC Press, 2003.
19. Bidan G., Ehui B. and Lapkowski M.; *Journal of Physics D-Applied Physics*, 21, 1988, 1043-1054.
20. Han G. Y. and Shi G. Q.; *Sensors and Actuators B-Chemical*, 99, 2004, 525-531.
21. Cho M. S., Seo H. J., Nam J. D., Choi H. R., Koo J. C. and Lee Y.; *Smart Materials and Structures*, 16, 2007, S237-S242.
22. Anquetil P. A., Yu H. H., Madden J. D., Madden P. G., Swager T. M. and Hunter I. W.; *Smart Structures and Materials 2002: Electroactive Polymer Actuators and Devices (Epad)*, 4695, 2002, 424-434.
23. George P. M., LaVan D. A., Burdick J. A., Chen C. Y., Liang E. and Langer R.; *Advanced Materials*, 18, 2006, 577-581.
24. Zanganeh A. R. and Amini M. K.; *Sensors and Actuators B-Chemical*, 135, 2008, 358-365.
25. Reece D. A., Ralph S. F. and Wallace G. G.; *Journal of Membrane Science*, 249, 2005, 9-20.
26. Bouchta D., Izaoumen N., Zejli H., El Kaoutit M. and Temsamani K. R.; *Biosensors & Bioelectronics*, 20, 2005, 2228-2235.
27. Lagrost C., Jouini M., Tanguy J., Aeiyaich S., Lacroix J. C., Chane-Ching K. I. and Lacaze P. C.; *Electrochimica Acta*, 46, 2001, 3985-3992.
28. Lepretre J. C., Saintaman E. and Utile J. P.; *Journal of Electroanalytical Chemistry*, 347, 1993, 465-470.
29. Gurunathan K., Murugan A. V., Marimuthu R., Mulik U. P. and Amalnerkar D. P.; *Materials Chemistry and Physics*, 61, 1999, 173-191.
30. Nicho M. E., Hu H. L., Lopez-Mata C. and Escalante J.; *Solar Energy Materials and Solar Cells*, 82, 2004, 105-118.
31. Mortimer R. J., Dyer A. L. and Reynolds J. R.; *Displays*, 27, 2006, 2-18.
32. Choi M. C., Kim Y. and Ha C. S.; *Progress in Polymer Science*, 33, 2008, 581-630.

33. Lange U., Roznyatouskaya N. V. and Mirsky V. M.; *Analytica Chimica Acta*, 614, 2008, 1-26.
34. Nalwa H. S.; *Advanced Functional Molecules and Polymers: Volume 3: Electronic and Photonic Properties*; Taylor & Francis, 2001.
35. Malinauskas A.; *Polymer*, 42, 2001, 3957-3972.
36. Skotheim T. A. and Reynolds J. R.; *Handbook of Conducting Polymers: Conjugated polymers*; CRC Press, 2007.
37. Nuñez M.; *Progress in electrochemistry research*; Nova Publishers, 2005.
38. Inzelt G.; *Conducting polymers, a new era in electrochemistry*; Springer, 2008.
39. Dall'Olio A., Dascola G., Varacca V. and Bocchi V.; *Comptes Rendus Hebdomadaires Des Seances De L Academie Des Sciences Serie C*, 267, 1968, 433-&.
40. Carquigny S., Sanchez J. B., Berger F., Lakard B. and Lallemand F.; *Talanta*, 78, 2009, 199-206.
41. Waghuley S. A., Yenorkar S. M., Yawale S. S. and Yawale S. P.; *Sensors and Actuators B-Chemical*, 128, 2008, 366-373.
42. Mermilliod N., Tanguy J. and Petiot F.; *Journal of the Electrochemical Society*, 133, 1986, 1073-1079.
43. Song H. K. and Palmore G. T. R.; *Advanced Materials*, 18, 2006, 1764-1768.
44. Muthulakshmi B., Kalpana D., Pitchumani S. and Renganathan N. G.; *Journal of Power Sources*, 158, 2006, 1533-1537.
45. Ingram M. D., Staesche H. and Ryder K. S.; *Solid State Ionics*, 169, 2004, 51-57.
46. Fenelon A. M. and Breslin C. B.; *Electrochimica Acta*, 47, 2002, 4467-4476.
47. Zhu R., Li G. and Huang G.; *Materials and Corrosion-Werkstoffe Und Korrosion*, 60, 2009, 34-39.
48. Geetha S., Rao C. R. K., Vijayan M. and Trivedi D. C.; *Analytica Chimica Acta*, 568, 2006, 119-125.
49. Kwon J. D., Kim P. H., Keum J. H. and Kim J. S.; *Solar Energy Materials and Solar Cells*, 83, 2004, 311-321.
50. Richardson R. T., Thompson B., Moulton S., Newbold C., Lum M. G., Cameron A., Wallace G., Kapsa R., Clark G. and O'Leary S.; *Biomaterials*, 28, 2007, 513-523.
51. Rocco A. M., DePaoli M. A., Zanelli A. and Mastragostino M.; *Electrochimica Acta*, 41, 1996, 2805-2816.
52. Spinks G. M., Xi B. B., Zhou D. Z., Truong V. T. and Wallace G. G.; *Synthetic Metals*, 140, 2004, 273-280.
53. Migdalski J., Blaz T. and Lewenstam A.; *Analytica Chimica Acta*, 322, 1996, 141-149.
54. Ghosh S. K.; *Functional coatings: by polymer microencapsulation*; Wiley-VCH, 2006.
55. Mohammadi A., Hasan M. A., Liedberg B., Lundstrom I. and Salaneck W. R.; *Synthetic Metals*, 14, 1986, 189-197.
56. Subramanian P., Clark N. B., Spiccia L., MacFarlane D. R., Winther-Jensen B. and Forsyth C.; *Synthetic Metals*, 158, 2008, 704-711.
57. Winther-Jensen B., Chen J., West K. and Wallace G.; *Macromolecules*, 37, 2004, 5930-5935.

58. Diaz A. F. and Castillo J. I.; *Journal of the Chemical Society-Chemical Communications*, 1980, 397-398.
59. Baker C. K. and Reynolds J. R.; *Journal of Electroanalytical Chemistry*, 251, 1988, 307-322.
60. Liu A. S. and Oliveira M. A. S.; *Materials Research*, 10, 2007, 205-209
61. Prissanaroon-Ouajai W., Pigram P. J., Jones R. and Sirivat A.; *Sensors and Actuators B-Chemical*, 135, 2008, 366-374.
62. Tietje-Girault J., Ponce de Leon C. and Walsh F. C.; *Surface & Coatings Technology*, 201, 2007, 6025-6034.
63. Sadki S., Schottland P., Brodie N. and Sabouraud G.; *Chemical Society Reviews*, 29, 2000, 283-293.
64. Zhou M. and Heinze J.; *Electrochimica Acta*, 44, 1999, 1733-1748.
65. Korri-Youssoufi H., Desbenoit N., Ricoux R., Mahy J. P. and Lecomte S.; *Materials Science & Engineering C-Biomimetic and Supramolecular Systems*, 28, 2008, 855-860.
66. Ben Fredj H., Helali S., Esseghaier C., Vonna L., Vidal L. and Abdelghani A.; *Talanta*, 75, 2008, 740-747.
67. Bazzaoui M., Martins L., Bazzaoui E. A. and Martins J. I.; *Electrochimica Acta*, 47, 2002, 2953-2962.
68. Earley S. T., Dowling D. P., Lowry J. P. and Breslin C. B.; *Synthetic Metals*, 148, 2005, 111-118.
69. Lehr I. L. and Saidman S. B.; *Materials Chemistry and Physics*, 100, 2006, 262-267.
70. Tian L., Qi Y. J. and Wang B. B.; *Journal of Colloid and Interface Science*, 333, 2009, 249-253.
71. Sharma R. K., Rastogi A. C. and Desu S. B.; *Physica B-Condensed Matter*, 388, 2007, 344-349.
72. Johanson U., Marandi A., Tamm T. and Tamm J.; *Electrochimica Acta*, 50, 2005, 1523-1528.
73. De Giglio E., Guascito M. R., Sabbatini L. and Zambonin G.; *Biomaterials*, 22, 2001, 2609-2616.
74. Wu J. C., Yu X. M., Lord H. and Pawliszyn J.; *Analyst*, 125, 2000, 391-394.
75. Deepa M. and Ahmad S.; *European Polymer Journal*, 44, 2008, 3288-3299.
76. Carquigny S., Segut O., Lakard B., Lallemand F. and Fievet P.; *Synthetic Metals*, 158, 2008, 453-461.
77. Ko J. M., Rhee H. W., Park S. M. and Kim C. Y.; *Journal of the Electrochemical Society*, 137, 1990, 905-909.
78. Asavapiriyant S., Chandler G. K., Gunawardena G. A. and Pletcher D.; *Journal of Electroanalytical Chemistry*, 177, 1984, 229-244.
79. Beck F., Braun P. and Oberst M.; *Berichte Der Bunsen-Gesellschaft-Physical Chemistry Chemical Physics*, 91, 1987, 967-974.
80. Ge H. L., Qi G. J., Kang E. T. and Neoh K. G.; *Polymer*, 35, 1994, 504-508.
81. Zhou M. and Heinze J.; *Journal of Physical Chemistry B*, 103, 1999, 8443-8450.
82. Shimoda S. and Smela E.; *Electrochimica Acta*, 44, 1998, 219-238.
83. Otero T. F. and Delarreta E.; *Synthetic Metals*, 26, 1988, 79-88.
84. Hernandez-Perez T., Morales M., Batina N. and Salmon M.; *Journal of the Electrochemical Society*, 148, 2001, C369-C375.

85. Khalkhali R. A., Price W. E. and Wallace G. G.; *Reactive & Functional Polymers*, 56, 2003, 141-146.
86. Baker C. K., Qiu Y. J. and Reynolds J. R.; *Journal of Physical Chemistry*, 95, 1991, 4446-4452.
87. Villiers A.; *Comptes Rendus de l'Académie des sciences*, 112, 1891, 536-538.
88. Schardinger F.; *Wien Klin Wochenschr.*, 17, 1904, 207-209.
89. Pringsheim H.; *Chemistry of the Saccharides*; Mc Graw-Hill: New York, 1932.
90. Pringsheim H.; *A Comprehensive Survey of Starch Chemistry*; Walton R.P, Chemical Catalogue Co.: New York, 1928.
91. Szejtli J.; *Chemical Reviews*, 98, 1998, 1743-1753.
92. Hedges A. R.; *Chemical Reviews*, 98, 1998, 2035-2044.
93. Saenger W.; *Angewandte Chemie-International Edition in English*, 19, 1980, 344-362.
94. Szejtli J.; *Cyclodextrins and their inclusion complexes* Akademiai Kiado: Budapest, 1982.
95. Dodziuk H.; *Cyclodextrins and their complexes*; Wiley-VCH, 2006.
96. Fanali S.; *Journal of Chromatography A*, 875, 2000, 89-122.
97. Rekharsky M. V. and Inoue Y.; *Chemical Reviews*, 98, 1998, 1875-1917.
98. Aleem O., Kuchekar B., Pore Y. and Late S.; *Journal of Pharmaceutical and Biomedical Analysis*, 47, 2008, 535-540.
99. Shikata T., Takahashi R. and Satokawa Y.; *Journal of Physical Chemistry B*, 111, 2007, 12239-12247.
100. Zia V., Rajewski R. A. and Stella V. J.; *Pharmaceutical Research*, 18, 2001, 667-673.
101. Wang J. J., Zheng G. J., Yang L. and Sun W. R.; *Analyst*, 126, 2001, 438-440.
102. Chen F. T. A., Shen G. and Evangelista R. A.; *Journal of Chromatography A*, 924, 2001, 523-532.
103. Kwatczak A., Duszczak K. and Bielejewska A.; *Analytica Chimica Acta*, 645, 2009, 98-104.
104. Amini A., Rundlof T., Rydberg M. B. G. and Arvidsson T.; *Journal of Separation Science*, 27, 2004, 1102-1108.
105. Cserhati T.; *International Journal of Pharmaceutics*, 124, 1995, 205-211.
106. Shuang S. M., Guo S. Y., Pan J. H., Li L. and Cai M. Y.; *Analytical Letters*, 31, 1998, 879-889.
107. Singh M., Sharma R. and Banerjee U. C.; *Biotechnology Advances*, 20, 2002, 341-359.
108. Bekers O., Beijnen J. H., Tank M., Bult A. and Underberg W. J. M.; *Journal of Pharmaceutical and Biomedical Analysis*, 9, 1991, 1055-1060.
109. Bhardwaj R., Dorr R. T. and Blanchard J.; *Pda Journal of Pharmaceutical Science and Technology*, 54, 2000, 233-239.
110. Uekama K., Hirayama F. and Irie T.; *Chemical Reviews*, 98, 1998, 2045-2076.
111. Loftsson T. and Brewster M. E.; *Journal of Pharmaceutical Sciences*, 85, 1996, 1017-1025.
112. Fava F., Di Gioia D. and Marchetti L.; *Biotechnology and Bioengineering*, 58, 1998, 345-355.

113. Luong J. H., Brown R. S., Male K. B., Cattaneo M. V. and Zhao S.; *Trends in Biotechnology*, 13, 1995, 457-463.
114. Szejtli J.; *Trends in Biotechnology*, 7, 1989, 170-174.
115. Breslow R. and Dong S. D.; *Chemical Reviews*, 98, 1998, 1997-2011.
116. Ye H. P., Tong W. and Dsouza V. T.; *Journal of the American Chemical Society*, 114, 1992, 5470-5472.
117. Kamal A., Ramalingam T. and Venugopal N.; *Tetrahedron-Asymmetry*, 2, 1991, 39-42.
118. Granados A. M. and de Rossi R. H.; *Journal of Organic Chemistry*, 66, 2001, 1548-1552.
119. Han S. M.; *Biomedical Chromatography*, 11, 1997, 259-271.
120. Iwata Y. T., Garcia A., Kanamori T., Inoue H., Kishi T. and Lurie I. S.; *Electrophoresis*, 23, 2002, 1328-1334.
121. Zarzycki P. K., Kulhanek K. M. and Smith R.; *Journal of Chromatography A*, 955, 2002, 71-78.
122. Rocco A. and Fanali S.; *Journal of Separation Science*, 32, 2009, 1696-1703.
123. Prime R., Martre A. M., Mousset G. and Pouillen P.; *Bulletin De La Societe Chimique De France*, 1991, 18-25.
124. Pospisil L. and Svestka M.; *Journal of Electroanalytical Chemistry*, 366, 1994, 295-302.
125. Koradecki D. and Kutner W.; *Journal of Inclusion Phenomena and Molecular Recognition in Chemistry*, 10, 1991, 79-96.
126. Prasad N., Strauss D. and Reichart G.; Cyclodextrins inclusion for food, cosmetics and pharmaceuticals; European Patent 1,084,625; CA 2310790; 1999
127. Sumiyoshi H.; *Journal of Japanese Council for Advanced Food Ingredients Research*, 2, 1999, 109-114.
128. Mabuchi N. and Ngoa M.; Controlled release powdered flavour preparations and confectioneries containing preparations; Japanese Patent, JP 128,638; 2001.
129. Del Valle E. M. M.; *Process Biochemistry*, 39, 2004, 1033-1046.
130. Tatsuya S.; Stabilisation of fragrance in bathing preparations; Japanese Patent 11,209,787; 1999.
131. Schneider H. J., Hacket F., Rudiger V. and Ikeda H.; *Chemical Reviews*, 98, 1998, 1755-1785.
132. Fielding L.; *Tetrahedron*, 56, 2000, 6151-6170.
133. Job P.; *Annales de chimie*, 9, 1928, 113-203.
134. Mosinger J., Tomankova V., Nemcova I. and Zyka J.; *Analytical Letters*, 34, 2001, 1979-2004.
135. Benesi H. A. and Hildebrand J. H.; *Journal of the American Chemical Society*, 71, 1949, 2703-2707.
136. Ibrahim M. S., Shehatta I. S. and Al-Nayeli A. A.; *Journal of Pharmaceutical and Biomedical Analysis*, 28, 2002, 217-225.
137. Coutouli-Argyropoulou E., Kelaidopoulou A., Sideris C. and Kokkinidis G.; *Journal of Electroanalytical Chemistry*, 477, 1999, 130-139.
138. Zhao G. C., Zhu J. J., Zhang J. J. and Chen H. Y.; *Analytica Chimica Acta*, 394, 1999, 337-344.

139. Yanez C., Nunez-Vergara L. J. and Squella J. A.; *Electroanalysis*, 15, 2003, 1771-1777.
140. Michaelis L. and Hill E. S.; *The Journal of General Physiology*, 16, 1933, 859-873.
141. Mortimer R. J.; *Chemical Society Reviews*, 26, 1997, 147-156.
142. Engelman E. E. and Evans D. H.; *Journal of Electroanalytical Chemistry*, 349, 1993, 141-158.
143. Bird C. L. and Kuhn A. T.; *Chemical Society Reviews*, 10, 1981, 49-82.
144. Hale P. D., Boguslavsky L. I., Karan H. I., Lan H. L., Lee H. S., Okamoto Y. and Skotheim T. A.; *Analytica Chimica Acta*, 248, 1991, 155-161.
145. Gomez Moreno C. and Bes M. T.; *Biochimica et Biophysica Acta-Bioenergetics*, 1187, 1994, 236-240.
146. Cosnier S., Galland B. and Innocent C.; *Journal of Electroanalytical Chemistry*, 433, 1997, 113-119.
147. Vidotti M. and de Torresi S. I. C.; *Journal of the Brazilian Chemical Society*, 19, 2008, 1248-1257.
148. Manahan S. E.; *Fundamentals of Environmental Chemistry*; CRC Press LLC: Boca Raton, 2001.
149. Baird C.; *Chimica Ambientale*; Zanichelli, 1997.
150. University of California-Davis, Oregon State University, Michigan State University, Cornell University and University of Idaho. Extension Toxicology Network, <http://extoxnet.orst.edu/>, 1997.
151. <http://www.evb.ch/en/p9451.html>.
152. Masque N., Galia M., Marce R. M. and Borrull F.; *Journal of Chromatography A*, 771, 1997, 55-61.
153. Kuo T. L., Lin D. L., Liu R. H., Moriya F. and Hashimoto Y.; *Forensic Science International*, 121, 2001, 134-139.
154. Ibanez M., Pico Y. and Manes J.; *Journal of Chromatography A*, 728, 1996, 325-331.
155. Shivhare P. and Gupta V. K.; *Analyst*, 116, 1991, 391-393.
156. Luque M., Rios A. and Valcarcel M.; *Analyst*, 123, 1998, 2383-2387.
157. Walcarius A. and Lamberts L.; *Journal of Electroanalytical Chemistry*, 406, 1996, 59-68.
158. Lu T. H. and Sun I. W.; *Talanta*, 53, 2000, 443-451.
159. Zen J. M., Jeng S. H. and Chen H. J.; *Analytical Chemistry*, 68, 1996, 498-502.
160. El Mhammedi M. A., Bakasse M. and Chtaini A.; *Journal of Hazardous Materials*, 145, 2007, 1-7.
161. de Oliveira U. M. F., Lichtig J. and Masini J. C.; *Journal of the Brazilian Chemical Society*, 15, 2004, 735-741.
162. Chang H. C., Cheng T. J. and Chen R. J.; *Electroanalysis*, 10, 1998, 1275-1280.

Chapter 2

Experimental

2.1 Introduction

The materials and methods used for the present study are outlined in this chapter. Firstly, a description of all the chemicals used is provided, followed by an explanation of the techniques and instrumentation employed for all experiments. In particular, the electrochemical cell, the electrochemical set-up and the preparation of the polymers are depicted in detail. Finally, a summary of theories behind the techniques employed and the equations applied to process the experimental data is given.

2.2 Chemicals

Pyrrole was purchased from Aldrich, distilled under vacuum before use and kept refrigerated in the dark to prevent oxidation. Sulfated β -cyclodextrin ($s\beta$ -CD) sodium salt, with a degree of substitution from 7 to 11 moles of sulfate per mole of β -CD, as reported by the vendor, was obtained from Aldrich. The molecular mass of this compound was calculated by assuming an average of 9 sulfated groups. Carboxymethyl β -cyclodextrin ($CM\beta$ -CD) sodium salt was purchased from Cyclolab. The degree of substitution calculated by Cyclolab is 3.5 and the average molecular weight is 1375.1 g/mol. β -cyclodextrin hydrate (β -CD) having a molecular weight of 1134.98 g/mol was purchased from Aldrich. Benzyl, methyl and ethyl viologens were obtained from Aldrich and used without further purification. All other chemicals were of analytical reagent grade and used as received.

2.2.1 Purification of the $s\beta$ -CD

During experimental analysis an impurity was discovered in the $s\beta$ -CD powder. Nuclear magnetic resonance spectroscopy (NMR) and UV-Vis (techniques described later in more detail in Section 2.5.8 and 2.5.2 respectively) were employed to determine the nature of the impurity. The NMR data were obtained using a 300 MHz Bruker instrument, in D_2O . Figure 2.1 shows the 1H NMR spectra of a sample of $s\beta$ -CD in 0.10 mol dm^{-3} NaCl in D_2O . In this figure, the blue region highlighted corresponds to the protons of the impurity. The impurity was confirmed to be pyridine. Figure 2.2 shows the chemical structure of pyridine.

Attempts were made to purify the salt. The powder was washed with volatile solvents *e.g.* diethyl ether and acetone and then dried in oven at 70 °C. However these procedures were not efficient in purifying the sample. A common way of removing pyridine is by dissolving the salt in toluene and rotary evaporating the solvent off. However, s β -CD is insoluble in this solvent system and this purification step was unsuccessful. Pyridine is well known to form an azeotrope with water, the boiling point of which is 92.6 °C.¹ For this reason, a weighed amount of s β -CD was dissolved in a minimal amount of water. The sample was then connected to a Schlenk line, held under vacuum at a pressure of 1×10^{-2} mbar under stirring, and heated at a temperature of 70 °C for twelve hours. UV-Vis measurements, on a sample before and after the purification, reveal a substantial decrease in the absorption of pyridine, as shown in Figure 2.3.

To determine the concentration of pyridine in the s β -CD, before and after purification, a calibration curve of pyridine was firstly constructed. The unknown concentration of pyridine can be determined by measuring the absorbance at a particular wavelength and applying the Beer-Lambert law, Equation 2.1:

$$A = \epsilon bc \quad 2.1$$

where A is the absorbance, b is the path length of the sample in cm, ϵ is the molar absorptivity in $\text{mol dm}^3 \text{ cm}^{-1}$ and c is the concentration of the molecule in solution, expressed in mol dm^{-3} . From the linear relationship between absorbance and concentration, a linear equation can be obtained and used to extrapolate the concentration of unknown samples, from the measured absorbance. Figure 2.4 illustrates the calibration curve for pyridine at the λ_{max} of 257 nm. The slope of this linear plot was $2723.69 \text{ dm}^3 \text{ mol}^{-1}$ and it was used to compute the concentration of pyridine in the s β -CD batch, *prior* to and after purification. These values were $2.34 \times 10^{-4} \text{ M}$ and $5.14 \times 10^{-5} \text{ M}$, respectively, in a $1.00 \times 10^{-3} \text{ M}$ solution of s β -CD. In terms of mass, the impurity of pyridine in the s β -CD batch was calculated to be 0.91 % w/w. After purification it was reduced to 0.19% w/w.

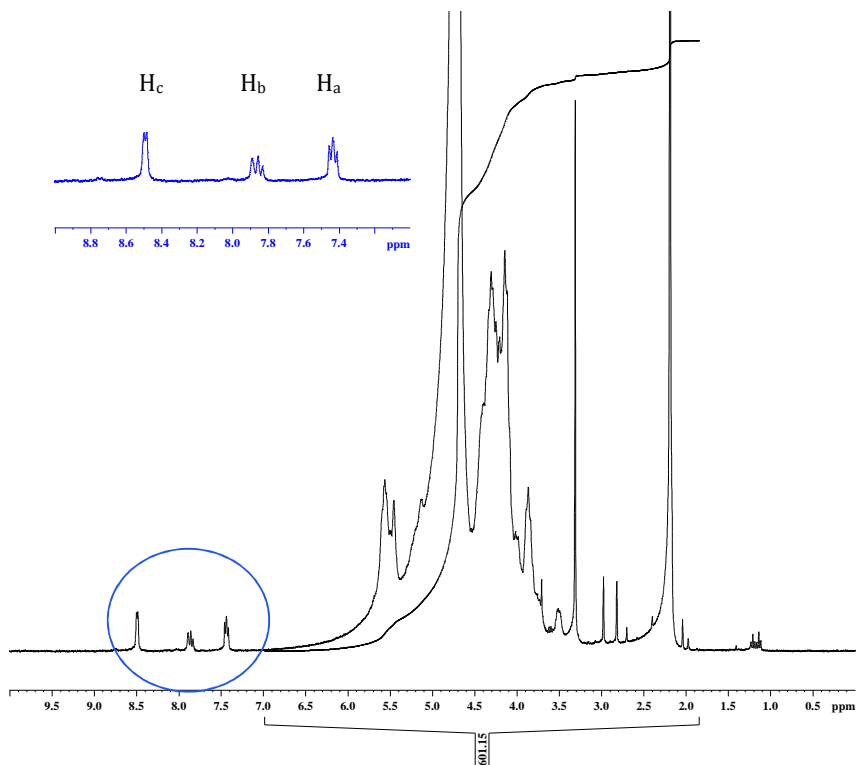


Figure 2.1: ^1H NMR spectra of 1.00×10^{-2} M $s\beta\text{-CD}$ in 0.10 M NaCl in D_2O . Highlighted in blue is the presence of the peaks corresponding to pyridine.

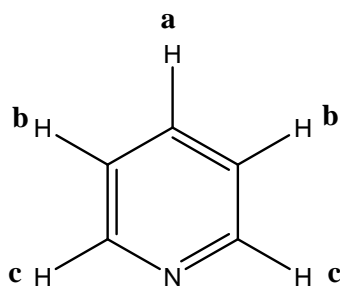


Figure 2.2: Structure of pyridine. (300 MHz, D_2O): δ 7.45 (1H, *m*, a-H), δ 8.49 (2H, *m*, b-H), δ 7.84 (2H, *m*, c-H).

Additional tests to verify the reproducibility of the purification method gave positive results. However no improvements in the purity of the $s\beta\text{-CD}$ were achieved when the purification process was repeated twice on the same sample.

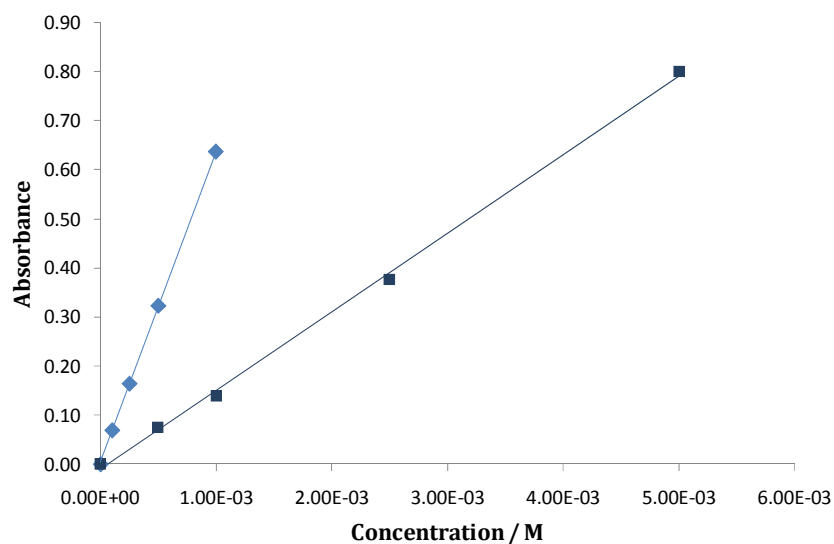


Figure 2.3: Absorbance as a function of the concentration for the pyridine present in the β -CD powder before (—, $R^2=0.999$) and after (—, $R^2=0.998$) purification. $\lambda_{\max}=257$ nm.

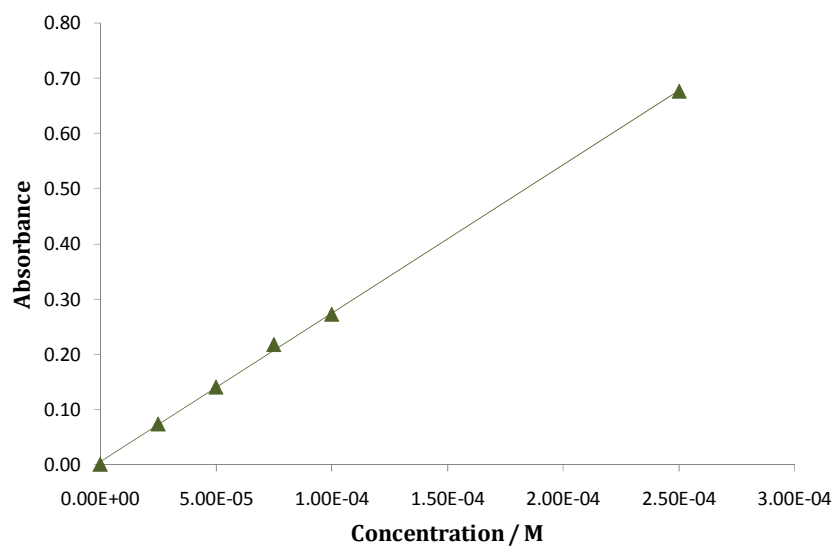


Figure 2.4: Calibration curve for pyridine in water, at 257 nm, $R^2=0.999$.

2.3 Electrochemical set-up

2.3.1 Electrochemical apparatus

Electrochemical experiments, such as potentiostatic, cyclic voltammetry (CV), electrochemical quartz crystal microbalance (EQCM) and differential pulse

voltammetry (DPV) measurements were carried out using a potentiostat CHI440 instrument (Model EA160). Electrochemical impedance spectroscopy analyses were performed using a Solartron potentiostat (Model SI 1285) coupled with a frequency response analyser (Model SI 1250). Each system was controlled by a computer and the various software packages used were CorrWare for Windows™, Version 2.1, Zplot Version 2.1 and CHI440 software, Version 1.0.0.1, respectively. A schematic of the electrochemical equipment is shown in Figure 2.5. In all cases, experiments were carried out using a conventional three-electrode system, as described in Section 2.3.2.

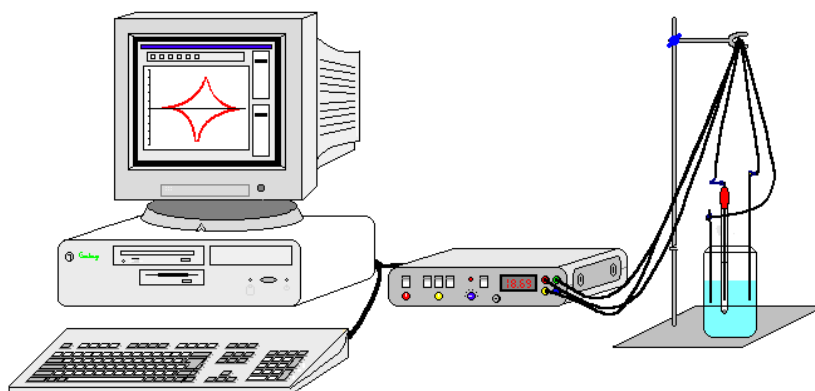


Figure 2.5: Experimental set-up used to record all electrochemical measurements.

2.3.2 *The electrochemical cell*

The electrochemical cell employed was a standard three-electrode cell consisting of a working electrode (WE), an auxiliary or counter electrode (CE) and a reference electrode (RE), as shown in Figure 2.6. A standard saturated calomel electrode (SCE) was utilized as the reference electrode for the majority of this work, except in the case of the Electrochemical Quartz Crystal Microbalance (EQCM) experiments, where a silver/silver chloride (Ag/AgCl) electrode (3.0 mol dm^{-3} KCl filling solution) was used. The working electrode varied from one experiment to the next. For the characterisation of the polymers, a glassy carbon (GC) electrode ($d = 4.0 \text{ mm}$) was used, while for all

the work involving the viologen compounds, including complexation studies and sensing properties, a gold electrode ($d = 3.0$ mm) was found to give a better response. Gold ($d = 5.0$ mm) was the substrate chosen for the EQCM measurements. Platinum was used as a substrate to synthesize polymers for Differential Scanning Calorimetry analysis, because its surface is the most suitable to be scraped with a blade in order to remove the polymer film. A platinum wire of 1.0 mm diameter was used as a counter electrode. The electrodes were connected to the potentiostat using coloured wires and the experiments and the results were computer controlled, as shown in Figure 2.5.

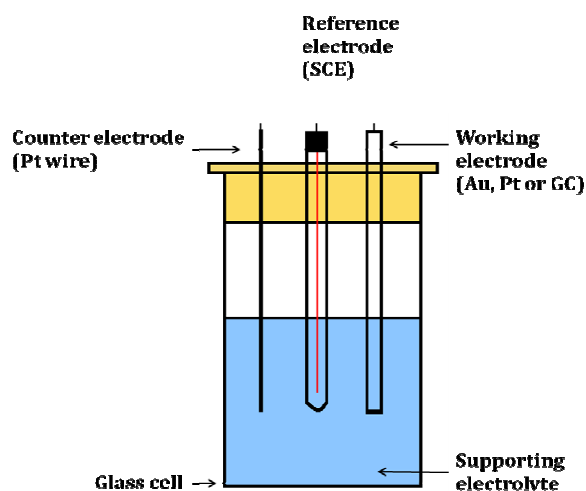


Figure 2.6: Diagram of electrode and electrochemical cell.

2.3.3 Electrode materials and preparation

Gold electrodes for EQCM experiments were purchased from IJ Cambria Scientific, used as received and disposed afterwards. All other electrode materials, of a purity grade of 99.9 %, were purchased from Goodfellow Metals. A scheme of the electrode assembly is shown in Figure 2.7. A glassy carbon (GC), gold or platinum wire was encased in a larger insulating Teflon sheath and set in place using epoxy resin. The electrical contact was achieved using a copper wire. The electrodes were polished using 1.0 μm diamond polish (Buehler

MetaDi Monocrystalline Diamond suspension) on a Buehler micro-cloth and washed with distilled water, to ensure a clean and smooth surface.

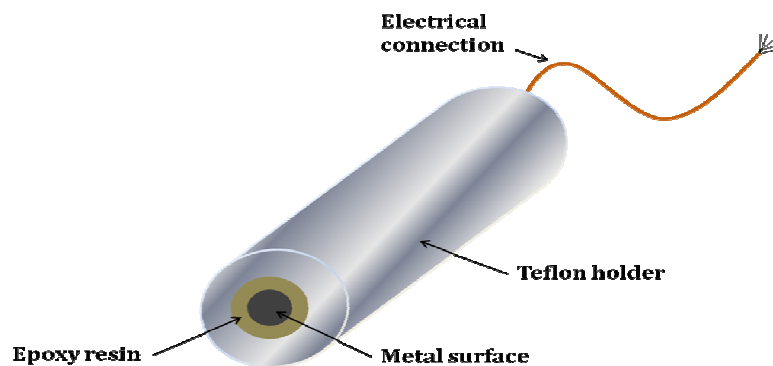


Figure 2.7: Schematic diagram of electrode assembly.

The electrodes described in Figure 2.7 were used for all the experiments apart from spectroelectrochemistry experiments, where an Indium Tin Oxide (ITO) electrode was employed. To ensure electrical contact a copper wire was connected to the ITO electrode with a conducting epoxy resin, as shown in Figure 2.8.

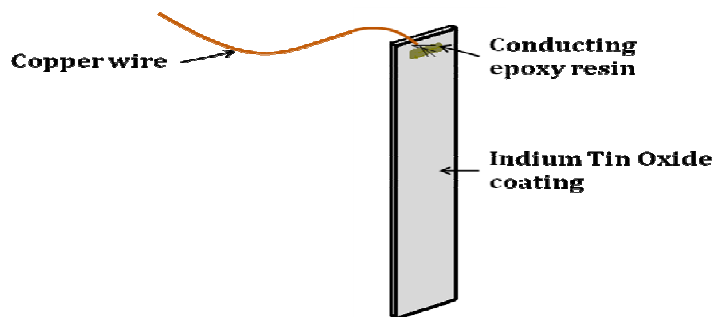


Figure 2.8: Schematic diagram of an ITO electrode.

2.4 Polymer electrosynthesis

All polymers were synthesized potentiostatically, by applying a constant potential to the electrode and then recording the current as a function of time. This method was employed to electrochemically deposit polypyrrole on the selected substrate.

Pyrrole, 0.20 M, was dissolved in the desired electrolytic solution. The supporting electrolyte has the fundamental functions to ensure the conductivity of the solution and to provide doping of the polymer. The dopants examined in the present study were the chloride anions (Cl^-), sulfated β -cyclodextrin ($\text{s}\beta\text{-CD}$) anions and carboxymethyl β -cyclodextrin ($\text{CM}\beta\text{-CD}$) anions. To dope the polymer with chloride, pyrrole was dissolved in a 0.10 M sodium chloride (NaCl) solution. When the sulfated β -cyclodextrin was the dopant, a 0.02 M solution of the sulfated β -cyclodextrin was combined with pyrrole and used as the electropolymerization solution. No supporting electrolyte was used. This negatively charged cyclodextrin is sufficiently conductive at 0.02 M to allow electropolymerization, due to the large number of ionized sulfate groups on the rim of the cavity. Likewise, no supporting electrolyte was necessary for electropolymerization in the presence of the carboxymethyl β -cyclodextrin. Again, a 0.02 M solution of $\text{CM}\beta\text{-CD}$ was used. However, the pH was adjusted to 4.0 with a small quantity of sulfuric acid (H_2SO_4), in order to promote electropolymerization. Otherwise the polymer growth was too slow.

To achieve the electropolymerization of pyrrole, the potential applied to the electrode of interest must exceed 0.5 V vs. SCE. The anodic voltages used in this work ranged from 0.6 to 0.8 V vs. SCE. Higher potentials were not employed as they are well known to give rise to over-oxidation of the polymer. The thickness of the polymer films was controlled by monitoring the charge and the experiment was stopped when the required amount of charge was obtained. Further details on the potentials and charges employed will be given in the experimental sections of the relevant chapters.

2.5 Experimental techniques

2.5.1 EQCM measurements

Additional information on the synthesis and electrochemical behaviour of the conducting polymers was obtained by means of the Electrochemical Quartz Crystal Microbalance (EQCM) technique. The experiments were performed on a CHI400 EQCM, a schematic of which is shown in Figure 2.9. The equipment consisted of a quartz crystal oscillator, a frequency counter, a fast digital function generator, a high-resolution and high-speed data acquisition circuitry, a potentiostat, a galvanostat and a computer. EQCM measurements calculate the mass change occurring at the electrode surface by monitoring the changes in the resonant frequency (f_0) of an oscillating quartz crystal. The frequency is related to the mass through the Sauerbrey equation, Equation 2.2:

$$\Delta f = - \frac{2 f_0^2 \Delta m}{A (\rho_q \mu_q)^{1/2}} \quad 2.2$$

where f_0 is the resonant frequency, Δm is the mass change, A is the surface area of the electrode or film, 0.203 cm^2 , ρ_q is the density of quartz, 2.648 g cm^{-3} , and μ_q is the shear modulus of quartz, $2.947 \times 10^{11} \text{ g cm}^{-1} \text{ s}^{-2}$. In this equation the change in frequency (Δf) is equal to minus the change in mass (Δm) per unit area (A) times a constant. The frequency, therefore, decreases as the mass increases.^{2,3}

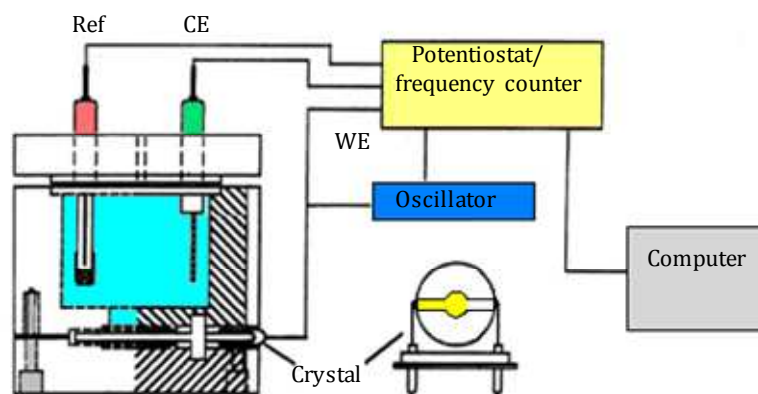


Figure 2.9: EQCM set-up.

2.5.2 *UV-Vis spectroscopy*

UV-Vis spectroscopy measures the amount of ultraviolet and visible light transmitted or absorbed by a sample placed in the spectrometer. The wavelength at which a chemical absorbs light is a function of its electronic structure and the intensity of the light absorption is related to the amount of the chemical between the light source and the detector. Therefore a UV-Vis spectrum can be used to identify some chemical species. Also, it is well suited for the quantitative study of association constants since the measured absorbance values are proportional to the respective concentration by the Beer-Lambert law.⁴

A Varian Cary series spectrophotometer was used for all of the analysis on monitoring the drug release and complexation studies. It comprises a Xenon lamp and has a maximum scan rate of 24,000 nm/min. This technique was employed to investigate the interaction between the β -CD with the viologen compounds, as dications. In all cases, a quartz cuvette with a length of 1 cm was used. The interval of wavelengths scanned was from 200 to 800 nm and the resolution of the instrument was 0.3 nm.

2.5.3 Spectroelectrochemical technique

In this technique, a UV-Vis spectrometer and a potentiostat are twinned together, as illustrated in Figure 2.10.

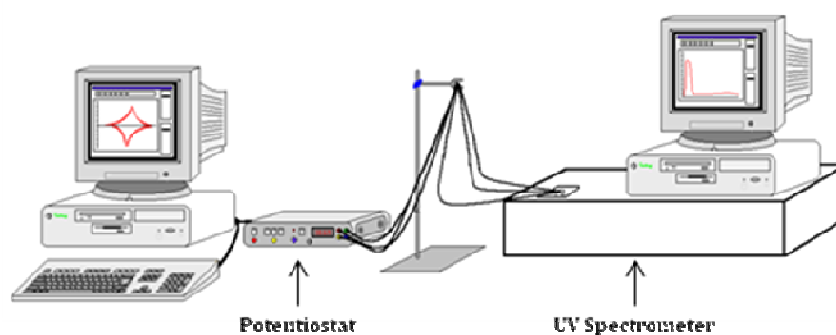


Figure 2.10: Schematic of the spectroelectrochemical apparatus.

The three electrodes were incorporated into the quartz cuvette described above. A transparent Indium Tin Oxide (ITO) coated glass served as the working electrode while the counter electrode consisted of a platinum wire of 1.0 mm diameter. Due to the size restrictions of the quartz cell, the standard SCE could not be used as reference electrode, therefore a silver wire of 1.0 mm diameter served as a quasi-reference electrode for this purpose. The lid of the quartz cell was designed to hold the electrodes in place and prevent the UV light path from being obstructed, as shown in Figure 2.11.

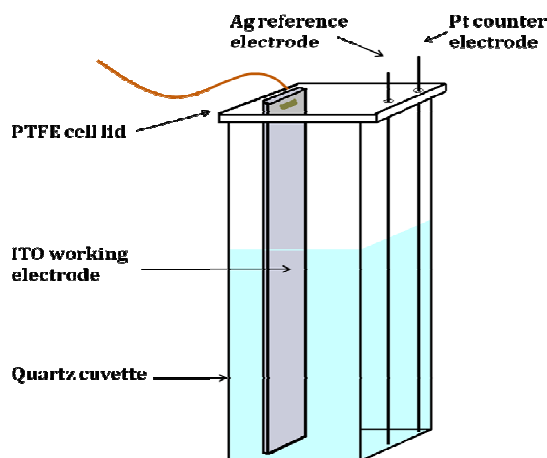


Figure 2.11: Schematic of electrodes set up in a UV cuvette.

This technique was used to study the interaction between the cyclodextrins and the viologens, in their radical state. A constant cathodic potential which is able to generate the radical cationic species from the viologen dication was applied while the UV spectrum was recorded. Further details are given in Chapter 6.

2.5.4 Cyclic voltammetry

Cyclic voltammetry (CV), involves sweeping the potential applied to the working electrode between two potential limits at a required scan rate, where the change in current is monitored.⁵ The resulting cyclic voltammogram is a plot of applied potential as a function of current. The working electrode serves as the surface where the electron transfer of the redox reaction takes place and the electrical current created is known as the faradic current. The CE balances this faradic process with an electron transfer in the opposite direction. (e.g., if oxidation takes place at the WE, reduction takes place at the CE). The redox reaction occurs within the potential range defined by the two chosen potential limits, and the potential at which the reduction or oxidation takes place provides qualitative information about the electroactive species under investigation. The working electrode can act as an electrochemical reductant or oxidant depending on the applied potential to the surface. As the applied potential becomes more negative, the electrode becomes a better reducing agent. Equally, as the applied potential becomes more positive, the electrode becomes a better oxidizing agent.

Cyclic voltammetry was used as an investigative tool to study the properties of the polymers.⁶ Secondly, it was used to determine the diffusion coefficient for the polymers doped with different anions.⁷ The scan rates employed in the specific experiments are illustrated in the figure captions or corresponding text in the results section. Thirdly, interactions between the sulfated β -cyclodextrin sodium salt ($s\beta$ -CD), β -cyclodextrin hydrate (β -CD), and the viologen compounds were studied by means of cyclic voltammetry. Finally, this technique was utilized for preliminary studies concerning the sensing properties of the cyclodextrin modified polymers to detect viologens in solution.

As detailed above, the CV experiment involves scanning the potential between two limits at a particular scan rate. It is particularly useful in studying the reversibility of a redox couple. For a simple redox couple, the voltammogram exhibits an oxidation wave, with a peak current, and a corresponding reduction wave, centred at a peak potential.

For a reversible couple, the ratio of the reverse-to-forward peak currents, i_{pr}/i_{pf} , is unity, while the separation between the peak potentials is given by Equation 2.3. Also, this peak separation is independent of the scan rate. Thus, the peak separation can be used to determine the number of electrons transferred, n , and as a criterion for the Nernstian behaviour:^{5,7}

$$\Delta E_p = E_{pa} - E_{pc} = \frac{57}{n} \text{ mV} \quad 2.3$$

In addition, the peak current for a reversible couple is given by the Randles-Sevcik equation, Equation 2.4:

$$i_p = K n^{3/2} A D^{1/2} c v^{1/2} \quad 2.4$$

where the constant, K , has a value of 2.69×10^5 , i_p is the peak current, n is the number of electrons transferred per mole of electroactive species, A is the area of the electrode in cm^2 ; D is the diffusion coefficient in $\text{cm}^2 \text{ s}^{-1}$; c is the concentration in mol cm^{-3} , v is the scan rate of the potential in V s^{-1} .⁷ The i_p is linearly proportional to the concentration, c , of the electroactive species and the square root of the scan rate, $v^{1/2}$. Thus, if linear plots of i_p vs $v^{1/2}$ are obtained, then the electrode reaction is under diffusion control, which is the mass transport of the electroactive species to the surface of the electrode across a concentration gradient. Using Equation 2.4, the diffusion coefficients were evaluated from the slopes of the corresponding, i_p vs $v^{1/2}$ plots. Diffusion of the reversible couple, $[\text{Fe}(\text{CN})_6]^{3-}/[\text{Fe}(\text{CN})_6]^{4-}$ (potassium ferricyanide, $\text{K}_3[\text{Fe}(\text{CN})_6]$), was studied at the bare GC electrode and at the three polymer films characterized in this thesis, ppyCl, ppys β -CD and ppyCM β -CD. The

ferricyanide was chosen for this study because its electrochemistry is highly reproducible and well known.^{8,9}

However, the situation is very different when the redox reaction is slow or when it is coupled with a chemical reaction. For an irreversible process (slow electron exchange), the redox peaks are reduced in size and are separated by a large potential. Totally irreversible systems are characterized by a shift of the peak potential with the scan rate, as detailed in Equation 2.5:

$$E_p = E_0 - \frac{RT}{\alpha nF} \left(0.78 - \ln \frac{k^0}{D^{1/2}} + \frac{1}{2} \ln \frac{\alpha nFv}{RT} \right) \quad 2.5$$

where α is the transfer coefficient and n is the number of electrons involved in the charge-transfer step. Thus, E_p occurs at potentials higher than E^0 , with the overpotential related to the rate of the reaction, k^0 , and α . For quasi-reversible systems (with $10^{-1} > k^0 > 10^{-5}$ cm s⁻¹) the peaks exhibit a larger separation in peak potentials compared to the reversible redox system, Equation 2.3.

2.5.5 Rotating disc voltammetry

Rotating Disc Voltammetry, (RDV), was employed in the determination of the diffusion coefficients of the viologens, in the absence and presence of an excess of β -CD dissolved in the solution. Data obtained were compared to the corresponding experiments recorded in the presence of β -CD, in order to probe the influence of the negative charges on the sulfated CD, in the interaction with the analytes. RDV was employed also to determine rate constants, as detailed below.

A schematic of the equipment involved is shown in Figure 2.12. A rotating disc electrode, similar to the electrode shown in Figure 2.7, was used for these studies. The RDV set-up consists of an electrode attached to a rotor spindle *via* a suitable electrical contact. When the circular disc is rotated at a particular rotation speed in solution, fresh reactant is brought to the surface. A well-defined flow pattern, shown in Figure 2.12 (b), is obtained where the rotating

electrode acts as a 'pump', dragging the solution perpendicular to the electrode surface which is subsequently thrown out in a radial direction on contact with the electrode surface.⁷

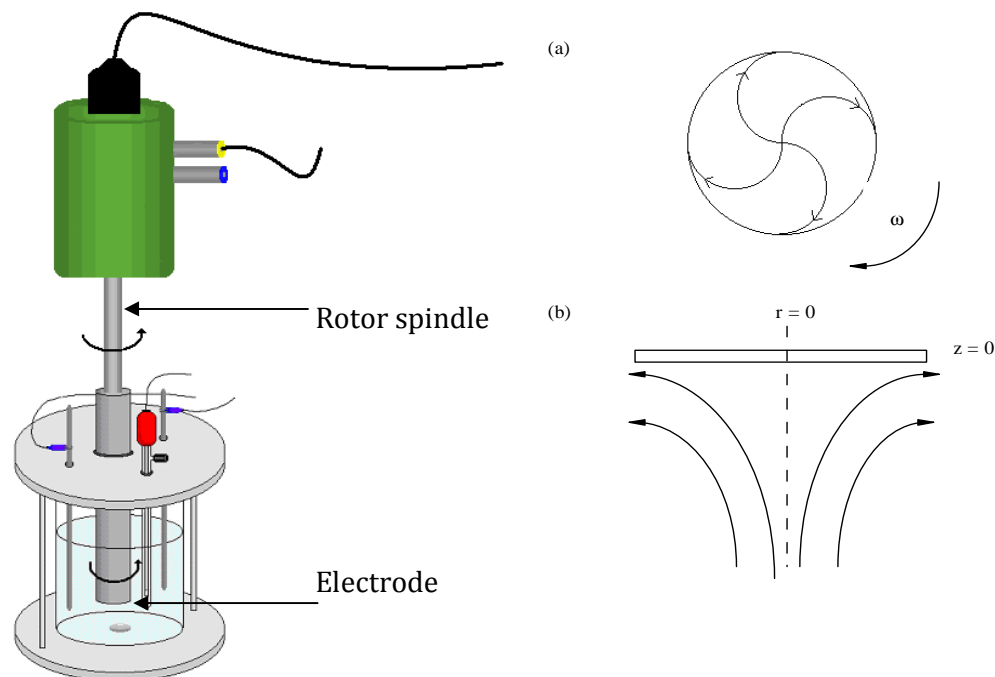


Figure 2.12: Schematic diagram of electrode in the RDV set-up. The patterns of flow to a rotating disc electrode (a) viewed from below the electrode face and (b) across its surface as viewed from the side.

This technique has an advantage over cyclic voltammetry, where the diffusion layer is time dependent. The thickness of the diffusion layer using RDV can be controlled by changing the rotation speed of the electrode. This approach leads to higher currents, greater sensitivity and improved reproducibility due to the increased transport of electroactive species to the electrode surface. The electrode is rotated at a known frequency, f , where the angular velocity, $\omega = 2\pi f/60$. The rotation of the electrode must not be so fast as to cause turbulence in the solution, therefore ensuring laminar flow of the substrate to the electrode surface.¹⁰ Since the current is proportional to the concentration, the observed

current should increase with an increase in ω . With this statement, the Levich equation is defined. This equation applies to the total mass-transport-limited condition at the electrode surface. Using the Levich equation⁷ for an electrochemical process, where the observed current is limited by diffusion, the limiting current can be related to the rotation speed of the electrode by Equation 2.6:

$$i_L = 0.621nFAD^{2/3}\nu^{-1/6}c\omega^{1/2} \quad 2.6$$

where,

$$\text{slope} = 0.621nFAD^{2/3}\nu^{-1/6}c$$

In this analysis, i_L is the limiting current, n is the number of electrons transferred, F is Faraday's constant (96485.3415 C mol⁻¹), A is the surface area, D is the diffusion coefficient, cm² s⁻¹, ν is the kinematic viscosity (0.0092 cm² s⁻¹)¹¹, c is the concentration and ω is the rotation speed in rad s⁻¹.

In the work for this thesis, the Levich equation was used to determine D_f and D_c , which are the diffusion coefficients of the viologens obtained in the absence and presence of an excess of β -CD or β -CD. In this case, the limiting current was recorded as a function of the rotation rate for a solution of viologen in the absence and presence of cyclodextrin. As the limiting current is directly proportional to the square root of the rotation speed, Levich plots, i_L vs. $\omega^{1/2}$, were generated giving a linear relationship. The diffusion coefficient, D , was then obtained from the slope using the known parameters n and c .

The Koutecky-Levich equation was also applied to the RDE data to evaluate the apparent rate constant, k , for the reduction of potassium ferricyanide, K₃[Fe(CN)₆], on a bare GC electrode and on the three polymers characterized in this thesis, ppyCl, ppys β -CD and ppyCM β -CD. The ferricyanide was chosen for this study because its electrochemistry is reproducible and well known.^{8,9} Moreover, the ferricyanide/ferrocyanide couple exhibits a well-behaved and

reversible redox process. The Koutecky-Levich equation is a modification of the Levich equation and is generally used if the Levich plot, i_L vs. $\omega^{1/2}$, deviates from linearity due to a kinetic limitation in the electron-transfer reaction.¹⁰ The Koutecky-Levich equation is given by Equation 2.7:

$$\frac{1}{i_L} = \frac{1}{i_K} + \frac{1}{i_{lev}} = \frac{1}{nFAk\Gamma c} + \frac{1.61}{nFA\nu^{-1/6}D^{2/3}c\omega^{1/2}} \quad 2.7$$

Here, i_L represents the measured limiting current, i_K is the current of the electron transfer between the electrode or the polymer and the ferricyanide, $[\text{FeCN}_6]^{3-}$, and i_{lev} is the Levich current, which corresponds to the mass transfer of $[\text{FeCN}_6]^{3-}$ in the solution. The i_K is not influenced by the rotation rate, as expressed in Equation 2.8:

$$i_K = nFAk\Gamma c \quad 2.8$$

where n is the number of electrons transferred, F is Faraday's constant (96485.3415 C mol⁻¹), A is the surface area, k is the reaction rate constant in cm s⁻¹, Γ is the surface coverage and c is the concentration.

In this instance, the Koutecky-Levich plot, $1/i_L$ vs. $1/\omega^{1/2}$, was used to estimate the rate constants of the reduction of $[\text{FeCN}_6]^{3-}$ to $[\text{FeCN}_6]^{4-}$ at the different polymer surfaces. Linear plots were obtained and the rate constant, k , was determined from the intercept of the Koutecky-Levich plot. Equation 2.7 was employed as well to estimate the charge transfer rate constants for the viologens, alone and in the presence of different amount of sβ-CD.

2.5.6 Differential pulse voltammetry (DPV)

Pulse Voltammetry is a frequently used method of ion detection that was first developed in the 1950s to improve the sensitivity of the polarographic measurements made by pharmaceutical companies.¹² When low concentrations of analytes are monitored using electrochemical measurements, problems occur

due to a double layer capacitance effect. Therefore, the current monitored is not totally faradaic, hence reducing the accuracy of the experiment. In order to improve the accuracy, different types of pulse voltammetry may be used. There are several types of pulse voltammetry, including normal, differential and square wave voltammetry.⁷ For this thesis, Differential Pulse Voltammetry (DPV) was used. With DPV, the base potential is incremented and increased at a fixed rate as shown in Figure 2.13 (b). The pulses applied are of the same magnitude each time. Unlike normal pulse voltammetry, in DPV the current is sampled twice, just prior to each pulse and then again at the end of the pulse, as shown in Figure 2.13 (c). The difference between these two values is calculated and the resulting current values ΔI , are plotted against the applied potential, V . This ΔI value would be zero if no oxidation or reduction of the analyte occurs at the working electrode.

In this study, DPV was utilized to reduce the background current due to the polypyrrole electroactivity and enhance the signal generated by the reduction of the viologens at the polymer surface, in order to increase the sensitivity and the detection properties of the polymer modified with cyclodextrins. The following parameters were used: pulse amplitude of 50.00 mV, pulse width of 0.10 s, a sampling width of 0.05 s, pulse period of 0.30 s, an increment of 3.00 mV and a potential window from 0.00 to -1.40 V vs SCE.

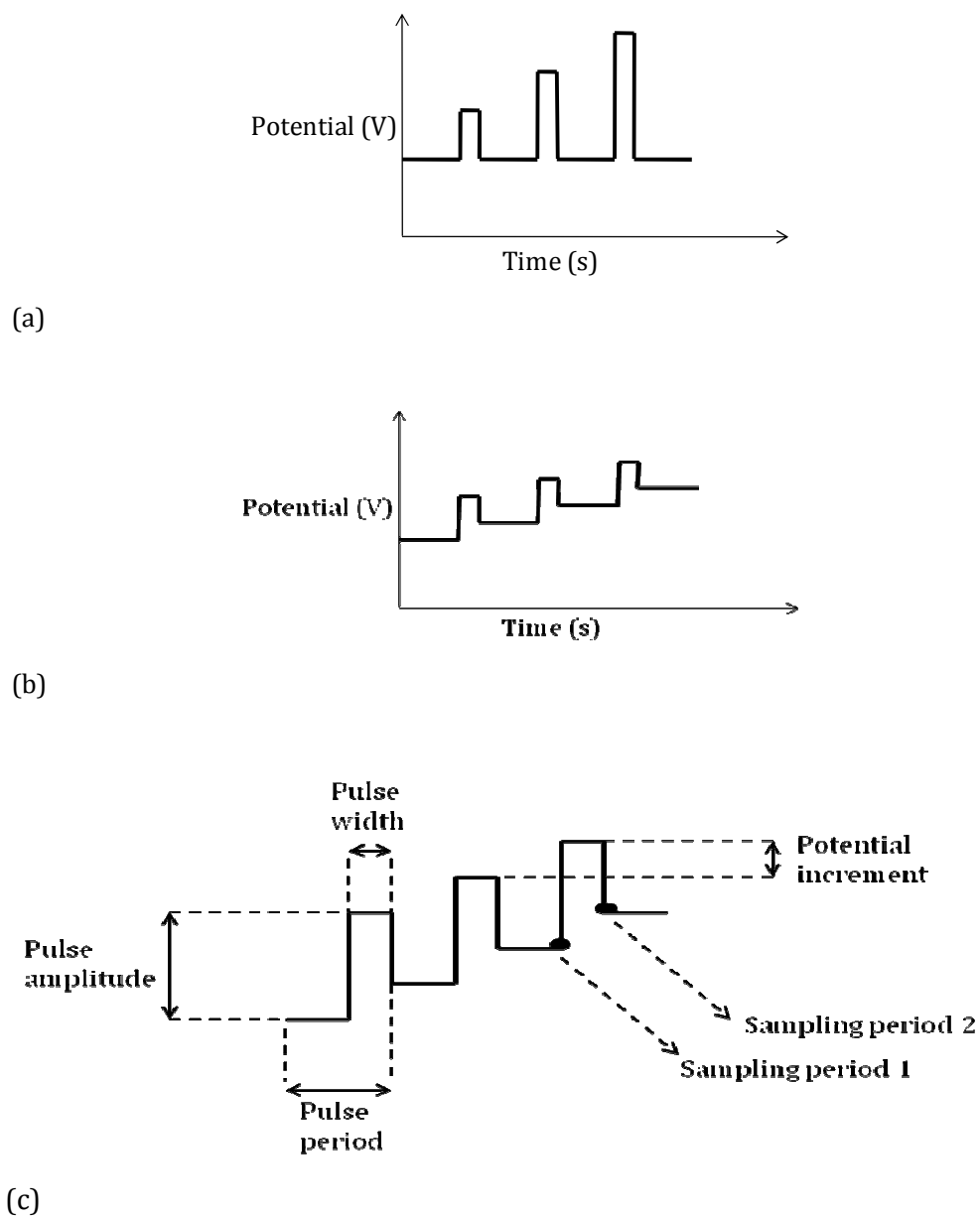


Figure 2.13: Schematic of normal pulse voltammetry (a), schematic of differential pulse voltammetry (b) and schematic of the parameters for DPV (c).

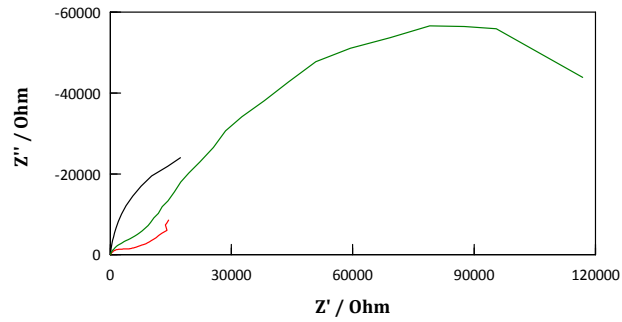
2.5.7 Electrochemical Impedance Spectroscopy

Electrochemical Impedance Spectroscopy (EIS) is a method used to examine several factors at the working electrode surface, including the stability, kinetics, and double layer capacitance.¹³ Impedance measurements involve the

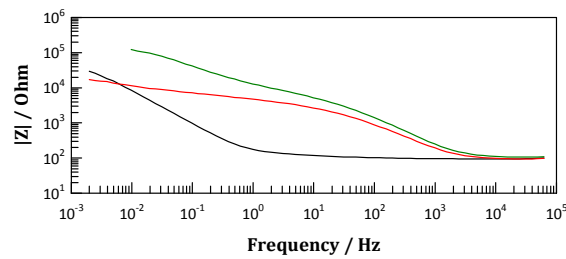
application of a small perturbing sinusoidal voltage of 5 mV, superimposed on the fixed baseline applied potential or versus the open-circuit potential. A shift in the phase and amplitude of this sinusoidal voltage may occur, resulting in an AC current. A frequency analyser measures this difference in amplitude and time lag, θ , over a variety of frequencies. Any shift in the phase or amplitude of the voltage is as a result of variations occurring in the electrochemical cell.

The total impedance of a system is determined by the impedance of the various components of the electrochemical cell, for example, electron-transfer kinetics, diffusion, passivating layers, solution resistance, etc.¹³ The relative contribution of the various components tends to exhibit a variation with frequency; for example, electron-transfer kinetics may dominate at high frequencies, whereas diffusion may dominate at lower frequencies. Measuring over a wide frequency range allows processes with different time scales to be detected within the same experiment. This is what makes EIS such a useful technique.

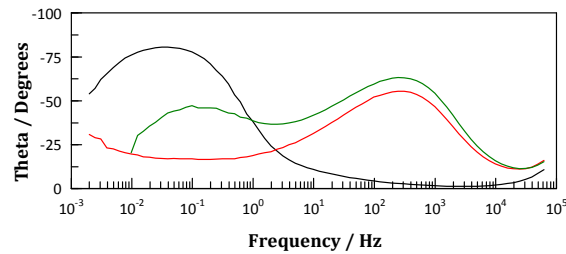
Experimental results are expressed as a real and imaginary part resulting from the shift in phase. The phase shift arises as a result of the AC potential applied to the cell, which can result in a phase shift between the applied AC potential and the AC current response. These components are plotted on a vector diagram known as a Complex Plane or “Nyquist” plot, with the real component (Z') on the x-axis and the imaginary component (Z'') on the y-axis, as illustrated in Figure 2.14 (a).



(a)



(b)



(c)

Figure 2.14: Example of a Complex Plane (or Nyquist) plot (a), Bode plot (b) and (c) for with Z in units of $\Omega \text{ cm}^2$ (a).

These data may also be presented as a Bode plot, Figure 2.14 (b) and (c), which displays the total impedance $|Z|$, typically in units of Ω , (Equation 2.9) on a logarithmic scale and phase angle, θ , as a function of the frequency on a logarithmic scale.

$$|Z| = \sqrt{(Z_{real})^2 + (Z_{imag})^2} \tag{2.9}$$

In this work impedance measurements were carried out in order to obtain information on the capacitance of the polymer films. The exact experimental conditions and details are described in detail in Section 3.7.2. However, in general, the polymer was conditioned for 60 min versus the open-circuit potential or at a fixed applied potential to ensure that a steady state was attained before the measurements were performed. This was further tested by recording the impedance data from high to low frequencies and then from low to high frequencies. If no hysteresis was observed, then it was concluded that steady-state conditions were achieved. The impedance response was then modelled using Z-view, a software package that models the data to appropriate equivalent electric circuit using a non linear least squares fitting routine that considers both the real and imaginary components of the data.

The aim in fitting experimental data to an equivalent circuit model is to mimic the actual impedance measurements with an artificial equivalent electric circuit, consisting of resistors, capacitors and constant phase elements. Z-view software is designed to accurately model impedance data. Each circuit element in the model is selected to correspond to a real physical component in the electrochemical cell. The fitting procedure involves a non-linear least squares method. Initial estimates for the parameters are required and the iterative process refines these values to select values that best fit the experimental data.

The main circuit elements used to model data in this thesis were resistors (R) and constant phase elements (CPE). A resistor has no imaginary component; hence its value is equal to the impedance for the real component. Therefore, the resistance value can account for the resistance elements in the electrolyte solution and the resistance for charge transfer. Constant phase elements can be used to determine the capacitance of the interface and also diffusion processes in the polymer layer. They are often used instead of capacitors, for systems that may not behave ideally. A constant phase element is defined by two parameters, an exponent (T) and an actual value (P). CPE-T gives information on the physical process occurring. If such a value is 1.0, it is correct to assume that the CPE

behaves as an ideal capacitor. However, values between 0.8 and 1.0 are acceptable capacitance exponents, being consistent with a porous surface. A value of 0.5 is indicative of a diffusion process and coincides with a phase angle of 45° . The CPE-T value gives the physical value of the constant phase element.

Using various components in series or in parallel an appropriate model based on the physical system is created. Figure 2.15 shows the two models used to evaluate impedance data in the present thesis. In this analysis, the simulated impedance is calculated based on the initial circuit parameters and values. This fit is then compared to the experimental data. The values of the circuit parameters are modified and the fit between the experimental and simulated data re-evaluated. This iterative process is continued until the difference between the simulated and the experimental data is minimized. The % errors shown in Figure 2.16 give the percentage by which the circuit element can be modified without any loss in fit between the simulated and the experimental data. This in turn, gives the actual errors in the values of each circuit component. In simple circuits, the error should be less than 2%. However, a percentage error up to 5 % is acceptable in complex models containing a greater number of circuit elements. When using this approach, it is important that each equivalent circuit element corresponds to a component of the electrochemical cell; otherwise the equivalent circuit has little meaning.

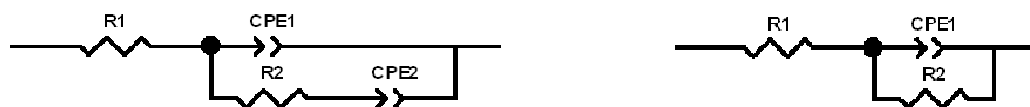
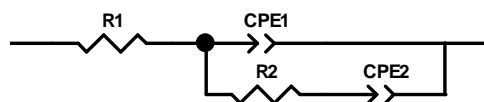


Figure 2.15: Equivalent circuits used to fit impedance data presented in Chapter 3.



<u>Element</u>	<u>Freedom</u>	<u>Value</u>	<u>Error</u>	<u>Error %</u>
R1	Free(+)	81.04	3.4149	4.2138
CPE1-T	Free(+)	0.00015157	4.0408E-6	2.666
CPE1-P	Free(+)	0.40898	0.0039444	0.96445
R2	Free(+)	1277	40.554	3.1757
CPE2-T	Free(+)	0.00053856	1.6121E-5	2.9934
CPE2-P	Free(+)	1.08	0.018453	1.7086

Figure 2.16: Data fitting routine, circuit parameters, values and errors.

2.5.8 Nuclear magnetic resonance spectroscopy

Proton (^1H) Nuclear Magnetic Resonance (NMR) is widely used for the determination of the structure of organic compounds. For the purpose of these studies it is the most effective structural tool for investigating the interaction between a cyclodextrin and a complexed species.⁴

^1H NMR spectroscopy is quantitative; the relative number of hydrogen nuclei can be measured by integrating the area under the peak. It also reveals the connectivity of the structure due to the coupling of the protons, and more importantly, for this research, the chemical shifts give a reliable indication of the local environment. Radio waves are used to study the energy level differences of ^1H nuclei. Hydrogen nuclei have a nuclear spin of a half and so have two energy levels: they can be aligned either with or against the applied magnetic field. The chemical shift provides much information and is a measure of the shielding of the nucleus by the electrons around it.¹⁴ In these studies, ^1H NMR spectroscopy was used to study the interaction of the α -CD and β -CD with the viologens and to determine the stoichiometry of the interaction between benzyl viologen and the α -CD. ^1H NMR experiments were performed on a Bruker 300 MHz NMR spectrometer at 293 K in D_2O .

2.5.9 Differential Scanning Calorimetry (DSC)

DSC is used to study the thermal transitions of polymers such as glass transitions, crystallization, melting interval, decomposition and even their purity.¹⁵ Figure 2.17 shows the different parts of the apparatus for a DSC analysis. An aluminium pan containing the polymer is placed in the heating chamber, close to an empty aluminium pan which acts as a reference.

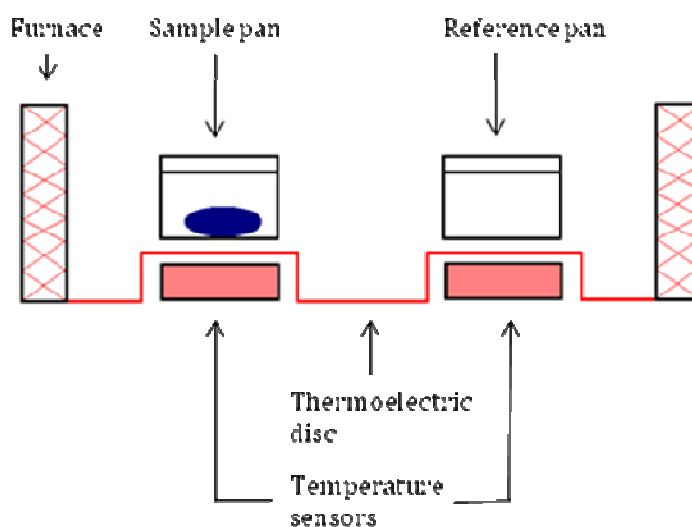


Figure 2.17: Schematic of Differential Scanning Calorimeter.

The furnace is set to increase or decrease the temperature at a fixed rate and the arrangement of the furnace and pans ensures that both pans are at identical temperature at any given time. The DSC measures the energy necessary to maintain both pans at an identical temperature. Therefore, the amount of heat absorbed or released by the polymer sample as it is heated or cooled at a particular rate is measured. Data are recorded as the heat change expressed as heat flow (mW) as a function of the temperature ($^{\circ}\text{C}$). For this work pans containing approximately 2 mg of samples were heated from 30 to 400 $^{\circ}\text{C}$, at a constant rate of 10 $^{\circ}\text{C}/\text{min}$, under a nitrogen atmosphere. The instrument used was a Perkin Elmer Pyris 6.0 apparatus and the results were recorded and analysed by means of Pyris Data Analysis software, which displays endothermic peaks as bell shaped curves and exothermic peaks as well curves. This

technique was utilized to investigate the thermal behaviour of the polymer doped with β -CD and with chloride anions in an attempt to provide evidence for the incorporation of the β -CD within the polymer matrix during electropolymerization.

2.5.10 Optical and scanning electron microscopy

Optical and Scanning Electron Microscopy (SEM) allows the observation and characterisation of samples on a micrometer (μm) to a nanometer (nm) scale, respectively. Optical images were performed on a Leica DMEP DFC-280 and an Olympus BX51M system using Leica application suite and Olympus DP Version 3.2, software, respectively. SEM images were obtained from an Avalon 8000, Princeton Gamma Technology. A flat GC electrode, 5 mm in diameter and encased within a PVC support, as detailed in Section 2.3.3, was used as the substrate. This electrode was specifically designed for both the optical and SEM microscopes, in order to fit on the flat stage where the samples were placed. The polymers were formed at the flat GC electrodes and then analyzed. For the SEM images, the polymer films were sputtered with a thin layer of gold using an Emitech K550x gold sputter coater.

2.5.11 Solution properties

Solution properties such as pH and ionic conductivity were determined using an Orion model 720A pH meter and a Jenway 4510 conductivity meter, respectively. The equipment was calibrated each time prior to experimental analysis using buffered solutions, pH 7.0 and 4.0 obtained from Fluka, and 0.1 mol dm⁻³ KCl from Sigma. Where necessary, the pH and conductivity of the solutions were adjusted by adding H₂SO₄.

2.6 Theory of experimental techniques and equations used

In order to understand the various processes occurring during the formation of a complex several theories and related equations were used. The following is an overview of the theories where the background is also provided.

2.6.1 Complexation studies

The term complex embraces a variety of different interactions between two molecules, *i.e.* host-guest interaction, ion pairing and charge-transfer interaction. In aqueous solutions, cyclodextrins are well known to form inclusion complexes with host molecules.⁴ However, host-guest complexation is not the only way of interaction between a cyclodextrin and an analyte. For example, the β -CD investigated in this research work is a negatively charged species. The viologens, in their dication and radical states are positively charged therefore electrostatic interaction can occur between these compounds and the β -CD. Complexation studies were carried out to elucidate if the interaction occurring between the anionic CD and the viologens was due to inclusion of the analytes in the hydrophobic cavity of the β -CD, to electrostatic interactions or alternatively to a combination of both effects.

In order to evaluate complexation between viologens and β -CD or β -CD the formation constant was determined using CV and RDV. Also, Job's method was employed to distinguish the stoichiometric value of the complex between the viologens and the β -CD. Data to construct the Job's plot were collected from UV-Vis and ¹H NMR measurements. Details on the exact experimental methodologies are provided in Chapter 5 and Chapter 6, while the related theory behind each of the equations used is described in the following sections.

2.6.1.1 Job's method

Before any structural or associative measures are performed on a complexation interaction, it is important to determine the stoichiometry of the complex. A common way to confirm this stoichiometric value is the well-known continuous variation or Job's method.^{16,17} This method is an experimental mixing technique widely used in the determination of stoichiometric ratios of each constituent involved. This method can be applied to various analytical techniques, such as Fluorescence,¹⁸ UV-Vis spectroscopy¹⁷ and ¹H NMR.¹⁹ In each method, the Job plot is based on the spectral change observed for the molecules forming the complex.

The Job's method was used to evaluate the stoichiometry of the complex between methyl, ethyl and benzyl viologen and the $s\beta$ -CD. This method involves the preparation of a series of solutions where the sum of the viologen [V] and $s\beta$ -CD [CD] concentrations is kept constant while changing the mole fraction. This is achieved by mixing different volumes of the two components, V and CD, such that the overall volume remains the same along the series. Experimentally, some property (such as chemical shifts in the NMR or absorbance values in UV-Vis) whose value changes when the two species form a complex, is measured in each solution.⁴

The data for the Job's plot are generated by taking the product of the mole fraction with the change of the property from that of an equal concentration of free viologen. This product is then plotted as a function of the mole fraction. The stoichiometry is determined from the x-coordinate at a maximum value of the Job's curve.

2.6.1.2 Formation constants

An equilibrium is established between these species and is expressed as the complex formation, stability, equilibrium or binding constant, K_f . The formation constant for complex has to be evaluated for the quantitative analysis.²⁰ In complexation studies, a simple way of determining the formation constant for a 1:1 complex is based on the following equilibrium:



with V representing the viologen, $s\beta\text{-CD}$ the sulfated β -cyclodextrin and $V-s\beta\text{-CD}$ the complex. From here, the formation constant can be defined as:

$$K_f = \frac{[V-s\beta\text{-CD}]}{[V][s\beta\text{-CD}]} \quad 2.11$$

where $[V]$ and $[s\beta\text{-CD}]$ are the equilibrium concentrations of the two species forming the complex. The encapsulation of the viologens inside a CD cavity or the electrostatic interactions between the two leads to alterations in the chemical and physical properties of the viologen. In this instance it is feasible to calculate the formation constant by monitoring these changes. Depending on the experiment being performed, a certain property is monitored. For example, in UV-Vis spectroscopy the absorbance change is monitored. In all of the following cases these methods are known as approximation methods, as each method includes one or more approximation. The two main approximations for these evaluations are: (i) the cyclodextrin is in excess of the analyte (viologen) and (ii) the stoichiometric value for complex is 1:1.

The formation of a complex between a redox-active molecule and cyclodextrin can be followed using electrochemical approaches, such as CV and RDV. The peak current and peak potential of the redox-active compound is measured in the absence and presence of a large excess of CD; the complexed molecule is the predominant species in the electrolyte, when a large excess of CD is used. As the CD is large and bulky the complexed viologen will diffuse more slowly than the free viologen giving rise to a reduction in the peak current. Likewise, a higher applied potential is required to oxidize the complexed species. These electrochemical changes attributed to the complexation of the analyte in the presence of cyclodextrins are well discussed in the literature.^{21,22} The formation constant for the complex can be calculated using changes in the peak current data by using Equation 2.12, expressed as follows:²³⁻²⁵

$$\frac{1}{[s\beta\text{-CD}]} = K_f \frac{1-A}{1-\frac{i}{i_0}} - K_f \quad 2.12$$

Here, $[s\beta\text{-CD}]$ is the concentration of sulfated $\beta\text{-CD}$, i_0 and i are the peak currents without and with the sulfated CD, respectively. A is a proportionality constant. This equation is valid when the concentration of the CD is in large excess of the analyte and a 1:1 relationship is obtained for the complex.

In order to follow the changes in the oxidation/reduction potential of the viologen as it is complexed by the CD the RDV technique is very useful. The equation originally proposed by Galus²⁶ and used by Coutouli-Argyropoulou *et al.*²⁷ and Ibrahim *et al.*²⁴ relates the shift in the oxidation/reduction potential of the analyte with the extent of complexation with the cyclodextrin and changes in the diffusion coefficient on complexation, Equation 2.12. As mentioned in Section 2.5.5, the limiting currents obtained using the RDV scale linearly with the square root of the rotation frequency. The diffusion coefficient can be determined by means of the Levich equation. The half-wave potentials can also be easily evaluated from the RDV data. With these values, the formation constant can be evaluated using Equation 2.13, which is adapted for the s β -CD as complexing system:

$$\left(\frac{F}{RT}\right)\{(E_{1/2})_c - (E_{1/2})_f\} = \ln(1 + K_f [CD]) + \ln\left(\frac{D_c}{D_f}\right)^{1/2} \quad 2.13$$

Here, F is Faraday's constant (96485.3415 C mol⁻¹), R is the gas constant and T is temperature in K, $(E_{1/2})_c$ and $(E_{1/2})_f$ are the half-wave potentials of the electroactive analyte obtained in the presence and absence of the s β -CD, respectively, while D_f and D_c are the diffusion coefficients of the analyte obtained in the absence and in the presence of a large excess of s β -CD, respectively. Again this equation is only valid when the concentration of the s β -CD is in excess of the analyte and a 1:1 relationship is obtained for the stoichiometry of the complex.

Equations 2.11 and 2.12 were used to analyse the CV and RDE data and to obtain the formation constant, K_f , for the complexes formed between the s β -CD and methyl, ethyl or benzyl viologen. Further details are provided in Chapter 5 and Chapter 6.

2.7 References

1. *Handbook of chemistry and physics*; CRC press, 1978.
2. Naoi K., Lien M. and Smyrl W. H.; *Journal of the Electrochemical Society*, 138, 1991, 440-445.
3. Baker C. K. and Reynolds J. R.; *Journal of Electroanalytical Chemistry*, 251, 1988, 307-322.
4. Dodzuik H.; *Cyclodextrins and Their Complexes*; Wiley-VCH, 2006.
5. Bull R. A., Fan F. R. F. and Bard A. J.; *Journal of the Electrochemical Society*, 129, 1982, 1009-1015.
6. Diaz A. F., Castillo J. I., Logan J. A. and Lee W. Y.; *Journal of Electroanalytical Chemistry*, 129, 1981, 115-132.
7. Greef R., Peat R., Peter L. M., Pletcher D. and Robinson J.; *Instrumental methods in electrochemistry*; Ellis Horwood Ltd, 1985
8. Collyer S. D., Davis F., Lucke A., Stirling C. J. M. and Higson S. P. J.; *Journal of Electroanalytical Chemistry*, 549, 2003, 119-127.
9. Ybarra G., Moina C., Florit M. I. and Posadas D.; *Electrochimica Acta*, 53, 2008, 4727-4731.
10. Fan F. R. F. and Bard A. J.; *Journal of the Electrochemical Society*, 133, 1986, 301-304.
11. Reece D. A., Ralph S. F. and Wallace G. G.; *Journal of Membrane Science*, 249, 2005, 9-20.
12. Monk P. M. S.; *Fundamentals of Electroanalytical Chemistry*; J. Wiley & Sons LTD: Manchester, 2001.
13. Barsoukov E. and Macdonald J. E.; *Impedance Spectroscopy. Theory, Experiment and Applications*, 2nd ed.; Wiley-Interscience, 2005.
14. Harris D. C. and Bertolucci M. D.; *Symmetry and spectroscopy*; Dover, 1978.
15. Höhne G. W. H., Hemminger W. F. and Flammersheim H. J.; *Differential scanning calorimetry*; Springer, 2003.
16. Job P.; *Annales de chimie*, 9, 1928, 113-203.
17. Landy D., Tetart F., Truant E., Blach P., Fourmentin S. and Surpateanu G.; *Journal of Inclusion Phenomena and Macrocyclic Chemistry*, 57, 2007, 409-413.
18. Xu B., Gao N. Y., Cheng H. F., Hu C. Y., Xia S. J., Sun X. F., Wang X. J. and Yang S. G.; *Journal of Hazardous Materials*, 169, 2009, 586-592.
19. Terekhova I. V., Kumeev R. S. and Alper G. A.; *Journal of Inclusion Phenomena and Macrocyclic Chemistry*, 59, 2007, 301-306.
20. Hirose K.; *Journal of Inclusion Phenomena and Macrocyclic Chemistry*, 39, 2001, 193-209.
21. Matsue T., Evans D. H., Osa T. and Kobayashi N.; *Journal of the American Chemical Society*, 107, 1985, 3411-3417.
22. Dang X. J., Nie M. Y., Tong J. and Li H. L.; *Journal of Electroanalytical Chemistry*, 448, 1998, 61-67.
23. Yanez C., Nunez-Vergara L. J. and Squella J. A.; *Electroanalysis*, 15, 2003, 1771-1777.
24. Ibrahim M. S., Shehatta I. S. and Al-Nayeli A. A.; *Journal of Pharmaceutical and Biomedical Analysis*, 28, 2002, 217-225.

25. Zhao G. C., Zhu J. J., Zhang J. J. and Chen H. Y.; *Analytica Chimica Acta*, 394, 1999, 337-344.
26. Galus Z.; *Fundamental of Electrochemical Analysis*; Ellis Harwood: Chichester 1976.
27. Coutouli-Argyropoulou E., Kelaidopoulou A., Sideris C. and Kokkinidis G.; *Journal of Electroanalytical Chemistry*, 477, 1999, 130-139.

Chapter 3

Synthesis and characterization of the polymer

3.1 Introduction

In the present chapter the procedure and the experimental conditions used for the electrochemical synthesis of the polymer are described. Then, the techniques employed to characterize the polymer are reported and the results obtained are analyzed. Furthermore, all the experiments carried out on the polymer of interest, which is polypyrrole doped with the large highly charged sulfated β -cyclodextrin (ppys β -CD), are repeated on a polymer doped with a small chloride anion (ppyCl), to enable a comparison. Polypyrrole doped with chloride anions is one of the most widely investigated conducting polymers.¹⁻⁴ On the other hand, very little literature is available on conducting polymers modified with sulfated cyclodextrins.⁵ Polypyrrole films doped with sulfated cyclodextrins have previously been reported.⁶ However, these films have been electrosynthesized at very high oxidation potentials, which lead to over-oxidation of the polymer backbone structure, giving rise to less conducting films.

Finally, preliminary experiments on the synthesis and characterization of a polymer doped with an anionic carboxy cyclodextrin with only an average of 3.5 negative charges, compared to an average of 9 in the case of the sulfated β -cyclodextrin (s β -CD), are reported. This cyclodextrin, with a small number of negative sites, was chosen to highlight the influence of the number of ionized and charged groups of the dopant species on the properties of polypyrrole. To the best of our knowledge, there have been no reports on the synthesis of polypyrrole doped with an anionic carboxy cyclodextrin.

3.2 Electrosynthesis of the polymer

The method adopted for the electrosynthesis of the polymers was chronoamperometry, which involves the application of a constant polarizing potential. The major advantage of this method is that the amount of charge consumed in the electropolymerization step can be controlled and the experiment terminated once the desired charge is obtained. With this

procedure, the thickness of the polymers can be controlled by the amount of charge passed, hence it is possible to produce uniform polymers in each experiment.^{5,7-9} Although cyclic voltammetry (CV) is normally used to generate compact conducting polymer films, potentiostatic deposition, is well known to yield polymers with consistent morphology.¹⁰

The experimental conditions applied to electrochemically synthesize the polymer films are provided in Section 2.4. Briefly, the electrodes were dipped into a glass cell containing 10 mL of polymerizing solution and then a suitable potential was applied to the working electrode. The solution was not stirred as this inhibits electropolymerization at the electrode interface, although oxidation of pyrrole proceeds.¹¹ Nucleation of the polymer at the electrode interface occurs only when the radical cation-radical cation recombination of the radical species of pyrrole leads to an oligomer chain that surpasses the solubility limit and deposits on the electrode surface. Thus solution stirring would disperse the radical species into the bulk solution, avoiding polymerization.

3.2.1 Polymer growth

The growth of a polypyrrole film in a β -CD solution is illustrated in Figure 3.1 (a) and (b) and compared to a corresponding polymer doped with chloride anions. The oxidation current, which represents the rate of polymer growth, is plotted as a function of the time in Figure 3.1 (a), while in Figure 3.1 (b), the charge consumed during the process is plotted as a function of time. The growth of ppyCl is typical for the electropolymerization of pyrrole in a simple dopant solution.¹ Although not evident in the current-time plot presented in Figure 3.1 (a), on application of the potential to the electrode there is an initial charging current, which arises from the charging of the double layer. This charging current decays rapidly, being governed by the RC time constant,^{12,13} which, in turn, is related to the size of the electrode and the conductivity of the solution, where C is the double layer capacitance and R is the solution resistance. Other factors that might contribute to the current during the initial milliseconds could be oxidation of pyrrole to form oligomeric species which are still soluble and/or

adsorption of pyrrole at the electrode interface.¹³ However, the concentration of pyrrole used in all these experiments, which is 0.2 M, is sufficiently high to promote a very fast initiation step for the polymerization reaction. The next portion, which extends to about 2.5 s, shows a rising transient current, resulting from the increasing area available for the electrochemical reaction, as conducting polypyrrole is deposited on the electrode surface. The current increases continuously from about 5 to 30 s, indicating that the electrical resistance of the film does not interfere with the polymer growth and the film remains conducting.

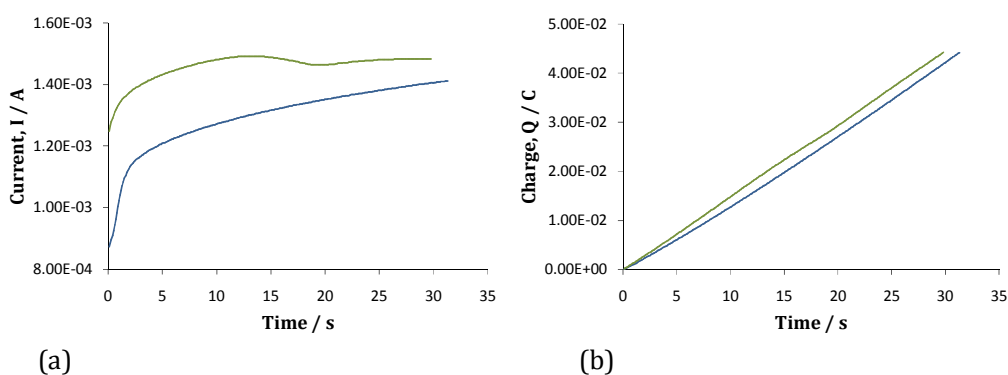


Figure 3.1: Current-time plot (a) and charge-time plot (b) for the electropolymerization of pyrrole on GC ($d = 4$ mm), at 0.8 V vs SCE until a charge of 4.42×10^{-2} C was consumed in — 0.20 M pyrrole and 0.02 M sβ-CD and — 0.20 M pyrrole and 0.10 M NaCl, both solutions at a pH of 5.0.

A different trend is observed for the growth of the sβ-CD doped polypyrrole films, ppysβ-CD. Firstly, the current is higher, particularly during the first 10 s, indicating a higher rate of electropolymerization. For example, the current at about 0.5 s is 1.25×10^{-3} A for ppysβ-CD and 9.00×10^{-4} A for ppyCl. The rising portion during the first few seconds of the transient is smaller for ppysβ-CD, probably because a shorter time is required for the nucleation process, being consistent with the higher rates of electropolymerization in the presence of the sβ-CD. However, after the first 12 s, there is a slight decrease in the current, which is not observed with the chloride system, and finally it reaches a steady-state value.

One possible explanation for this current-time behavior may be connected with the polyelectrolyte properties of the $s\beta$ -CD anions. As no supporting electrolyte was used, these polyanions will migrate to the positively charged platinum interface on application of the applied potential, giving a high local concentration of the $s\beta$ -CD anions. Once the monomer oxidation is initiated, the electropolymerization process proceeds at a fast rate in the presence of the high concentration of $s\beta$ -CD. As the electropolymerization proceeds, the concentration of the $s\beta$ -CD anions at the interface will drop and the rate of the electropolymerization reaction will now be dominated by the transport of the $s\beta$ -CD anions, through diffusion, giving rise to the slight dip in current at about 15 s. In particular, the diffusion of the $s\beta$ -CD anions is slow due to the large bulky nature of the anions. It appears that after 15 s the rate of electropolymerization is dominated by the diffusion of the bulky $s\beta$ -CD anions to the interface. This hypothesis was verified by applying the Cottrell equation, which is frequently used to confirm the potential range where an electrode reaction is diffusion controlled and/or to estimate the diffusion coefficient of the electroactive species.¹⁴ The Cottrell equation is given in Equation 3.1. The current, I , is proportional to the inverse of the square root of the time, t , and F is the Faraday constant (96,485.3415 C mol⁻¹), D is the diffusion coefficient in cm² s⁻¹, c is the concentration of the species and n is the number of electrons exchanged.

$$I = \frac{nFD^{1/2}c}{\pi^{1/2}t^{1/2}} \quad 3.1$$

For the ppys β -CD illustrated in Figure 3.1, current values between 15 and 20 s, corresponding to the slight decrease in the polymerization current, were fitted to the Cottrell equation (Equation 3.1). As evident in Figure 3.2, this gives a linear response with a correlation coefficient of 0.992, indicating clearly a diffusion-controlled process. However, the diffusion coefficient could not be calculated, as the $s\beta$ -CD is an electroinactive species. The $s\beta$ -CD moves to the electrode surface to balance the positive charge generated by the oxidation of the polypyrrole backbone, but the overall number of electrons involved in this

In Figure 3.3, the growth of polypyrrole films doped with chloride or β -CD anions are compared at a gold electrode. The plot shows three experiments for each dopant. In each experiment a fresh electropolymerization solution was employed and a constant potential of 0.8 V vs SCE was applied until a charge of 2.50×10^{-2} C was consumed. The plots overlap almost perfectly, as shown in Figure 3.3 (a) and (b). Both the current and charge recorded during electropolymerization are very reproducible. This high degree of reproducibility coupled with a constant electropolymerization charge suggests that polypyrrole films with a fixed thickness can be easily produced for both the ppys β -CD and ppyCl systems.

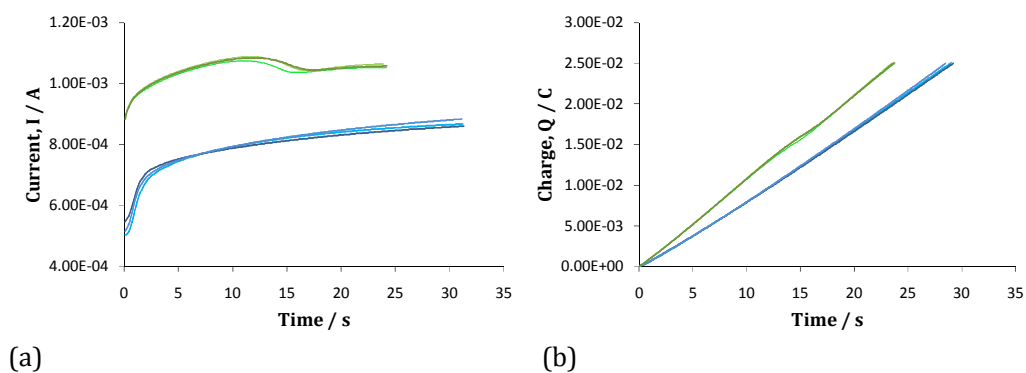


Figure 3.3: Current-time plot (a) and charge-time plot (b) for the electropolymerization of pyrrole on Au ($d = 3$ mm) at 0.8 V vs SCE until a charge of 2.50×10^{-2} C was consumed; electropolymerization in 0.20 M pyrrole and 0.02 M β -CD, pH = 5.0, 1 —, 2 —, 3 — and electropolymerization in 0.20 M pyrrole and 0.10 M NaCl, pH = 5.0, 1 —, 2 —, 3 —.

Similar results are presented in Figure 3.4 for the electrosynthesis of ppys β -CD and ppyCl films at a glassy carbon (GC) electrode by applying an oxidation potential of 0.7 V vs SCE. However, in this case a fresh electropolymerization solution was not used. One of the major concerns with the reuse of an aged solution is the formation of oligomeric species, which are intermediates in the pyrrole polymerization.¹⁵ An old solution contains a higher concentration of soluble oligomers which have different reactivity with respect to the pyrrole monomers. Therefore, the presence of oligomers might affect reproducibility. The currents for the three samples of ppys β -CD illustrated in Figure 3.4 (a) do

not overlap perfectly, indicating the presence of oligomeric species, although the reproducibility of the charge plots, shown in Figure 3.4 (b), is good. Better reproducibility is observed for the currents of the ppyCl samples when they are electropolymerized in the same solution.

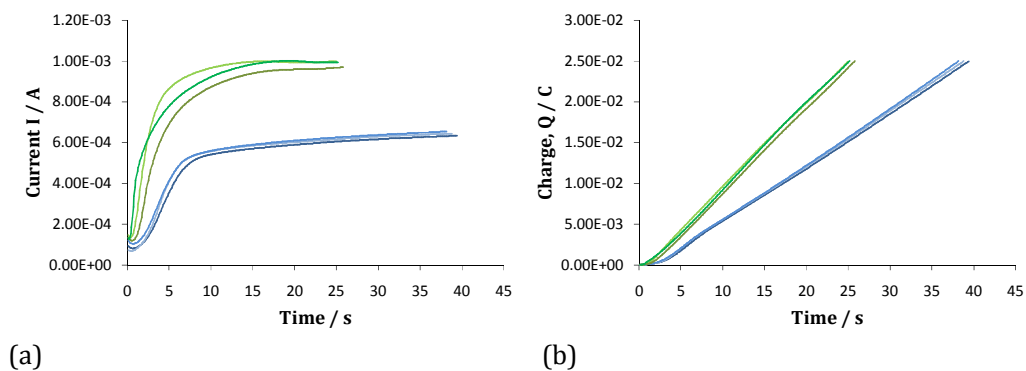


Figure 3.4: Current-time plot (a) and charge-time plot (b) for the electropolymerization of pyrrole on GC ($d = 4$ mm) at 0.7 V vs SCE until a charge of 2.50×10^{-2} C was consumed; electropolymerization in 0.20 M pyrrole and 0.02 M sβ-CD, pH = 5.0, 1 —, 2 —, 3 — and electropolymerization in 0.20 M pyrrole and 0.10 M NaCl, pH = 5.0, 1 —, 2 —, 3 —.

3.2.3 Influence of the substrate

Another important aspect that may influence the mechanism of electropolymerization is the nature of the electrode substrate. It has been shown that the substrate can alter the manner in which conducting polymers are formed.¹⁰ Differences are due, for example, to a different affinity of the analyte for the metal surface or to variations in the kinetics of electropolymerization. As there is no information available in the literature on the role of the metal substrate in the electropolymerization of pyrrole in the presence of highly sulfated CDs, the growth of ppyCl and ppysβ-CD at both GC and Au electrodes was compared.

Typical data are shown in Figure 3.5 where the current density, associated with the growth of ppysβ-CD and ppyCl, is plotted as a function of the time of electropolymerization at both Au and GC electrodes. Similar data, although

depicted as charge-time plots, are presented in Figure 3.6 (a) and (b). In general, higher current densities are observed with the Au substrate. This observation is in agreement with data reported in the literature.¹⁶ A possible explanation is that the growth of the polymer on Au involves the deposition of larger oligomeric species.¹⁶ In addition, the $s\beta$ -CD enhances to some extent the polymerization process on Au, since the different substrate has a lower influence on the deposition of ppyCl.

It is very clear from Figures 3.5 (a) and 3.6 (a) that the electropolymerization of pyrrole in the presence of the $s\beta$ -CD anions has a strong dependence on the nature of the substrate. The slopes of the charge-time plots for the formation of the ppy $s\beta$ -CD films at Au and GC are $1.49 \times 10^{-2} \text{ C cm}^{-2} \text{ s}^{-1}$ ($R^2 = 0.999$) and $1.18 \times 10^{-2} \text{ C cm}^{-2} \text{ s}^{-1}$ ($R^2 = 1.0$), respectively. This indicates a significant increase in the rate of the electropolymerization reaction at the Au interface. This enhancement in the rate of electropolymerization at the Au electrode is more moderate with the ppyCl system, as shown in Figures 3.5 (b) and 3.6 (b).

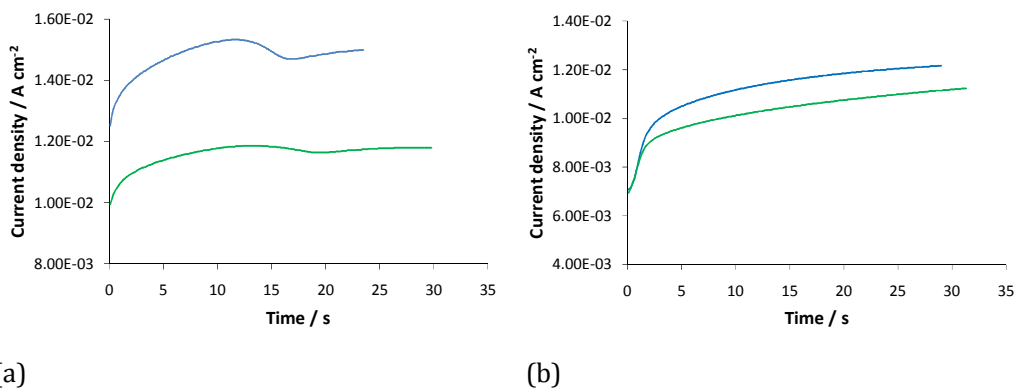


Figure 3.5: Current-time plots for the electropolymerization of pyrrole on Au — and GC —, electropolymerization in 0.20 M pyrrole and 0.02 M $s\beta$ -CD at 0.7 V vs SCE, pH = 5.0 (a) and electropolymerization in 0.20 M pyrrole and 0.10 M NaCl at 0.7 V vs SCE, pH = 5.0 (b).

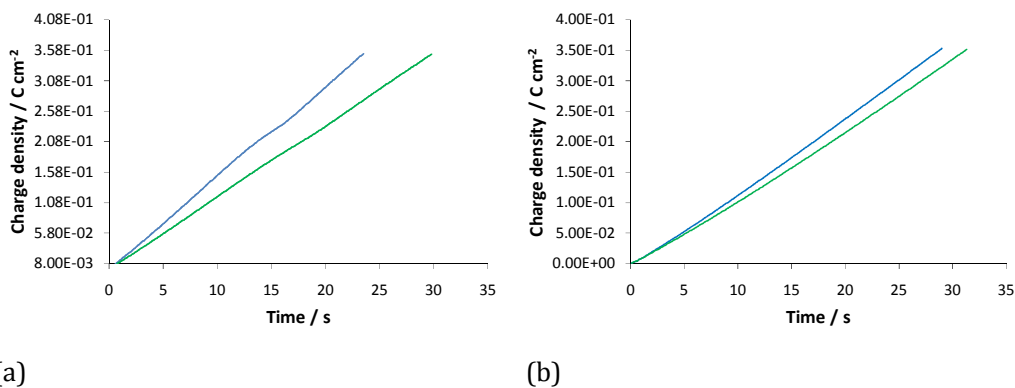


Figure 3.6: Charge-time plots for the electropolymerization of pyrrole on Au — and GC —, electropolymerization in 0.20 M pyrrole and 0.02 M s β -CD at 0.7 V vs SCE, pH = 5.0 (a) and electropolymerization in 0.20 M pyrrole and 0.10 M NaCl at 0.7 V vs SCE, pH = 5.0 (b).

3.2.4 Influence of the dopant

Finally, the last parameter considered in the electrosynthesis of the s β -CD modified polymer was the influence of the dopant. In addition to chloride, sodium dodecylsulfate (sds) was chosen. On dissociation, sds generates the dodecylsulfate anion, which is a large bulky dopant which may be compared to the sulfated β -cyclodextrin. However, it possesses only one negative charge and has very different properties to the cyclodextrin. The polymer doped with sds (ppysds) was synthesized under conditions similar to that used with the ppyCl and ppys β -CD films. The pyrrole concentration was 0.20 M, while the concentration of sds was 0.02 M. A potential of 0.8 V vs SCE was applied until a fixed charge of 2.50×10^{-2} C was consumed. Representative data are shown in Figure 3.7, where the growth of polypyrrole doped with s β -CD is compared to ppyCl and to ppysds. In each case, three separate experiments are presented to highlight the degree of reproducibility achieved between experiments.

In Figure 3.7 (a) only the first 30 s of the electropolymerization process are plotted. The current obtained during the formation of ppysds is significantly smaller than that measured with the other two systems. From Figure 3.7 (b) it is immediately evident that the rate of polymerization for ppysds is the slowest. Chloride anions have only one negative charge per molecule but they have a

high mobility due to their small size. For this reason their diffusion to the electrode surface is a fast process. In contrast, sds is a large species, it also has only one negative charge. The large size results in a low mobility and slow diffusion to the electrode surface. In addition, sds has surfactant-like properties.¹⁷ Therefore, the lower rate of electropolymerization may also be connected to the adsorption of the sds at the surface to give a lower surface area for deposition of the film. On the other hand, the s β -CD anions are large and bulky giving slow diffusion, but each CD has a large number of negative charges, giving rise to a very high ionic strength. The ionic strength can be calculated using Equation 3.2, where I represents the ionic strength of the solution, z the charge on the ion and c the concentration of the ion. The ionic strengths of the NaCl and sds solutions were calculated using Equation 3.2 and were found to be 0.10 M and 0.02 M, respectively. The ionic strength of the s β -CD solution was found to be in a range from 0.56 M to 0.90 M, when 7 or 9 sulfated groups per cyclodextrin molecule were considered, respectively.

$$I = \frac{1}{2} \sum z_i^2 c_i \quad 3.2$$

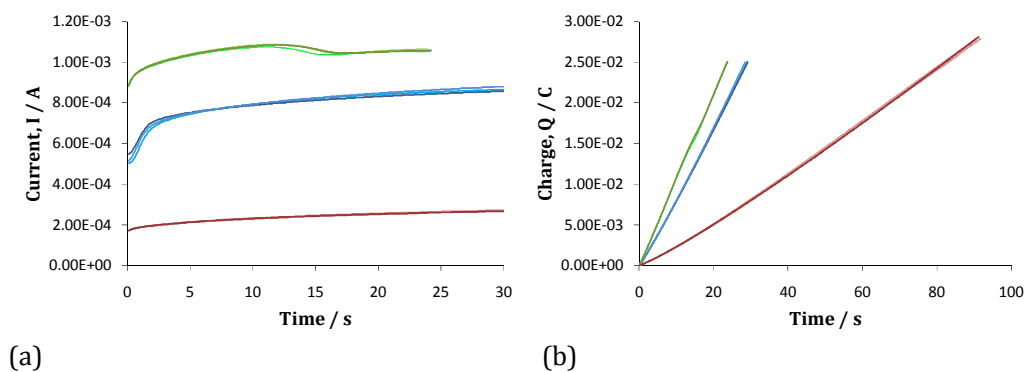


Figure 3.7: Current-time plot (a) and charge-time plot (b) for the electropolymerization of pyrrole on Au, ($d = 3$ mm), at 0.8 V vs SCE until a charge of 2.50×10^{-2} C was consumed; ppyCl (0.20 M pyrrole and 0.10 M NaCl, pH = 5.0) 1 —, 2 —, 3 —; pps β -CD (0.2 M pyrrole and 0.02 M S β -CD, pH = 5.0) 1 —, 2 —, 3 —; ppsds (0.20 M pyrrole and 0.02 M sds, pH = 5.0) 1 —, 2 —, 3 —.

Interestingly, the ratio of the steady-state currents obtained during the electropolymerization of pyrrole in the presence of the 0.02 M sds and 0.02 M β -CD, which is approximately 20, is close to the ratio of the respective ionic strengths, which is about 23. This highlights the significant role of the ionic strength of the solution in controlling the rate of electropolymerization. Indeed, when the NaCl concentration was increased to 0.56 M, similar charge-time plots with nearly identical slope values were obtained in both the chloride and β -CD solutions.¹⁸

3.3 Diffusion coefficient and rate constant of ferricyanide

An interesting aspect in the study of the conducting polymer matrix deposited on the metal substrate is the rate of diffusion of electroactive species to the electrode interface and the rate of the electron transfer at the polymer interface. To elucidate such behaviour at the polymer films described in Sections 3.1 and 3.2, a small electroactive molecule, potassium ferricyanide, $K_3Fe(CN)_6$, was chosen. This red crystalline material has been extensively exploited over the last few decades to characterize a variety of systems, because of its straightforward and reversible redox mechanism.^{19,20} Another application of this versatile compound is as an electron transfer mediator in amperometric biosensors.²¹

3.3.1 Diffusion coefficient and rate constant by means of cyclic voltammetry (CV)

By applying a suitable potential, the redox couple $Fe(III)(CN)_6^{3-}/Fe(II)(CN)_6^{4-}$ is generated. The ferri/ferrocyanide couple provides a quasi ideal electrochemical probe for the study of chemically modified surfaces since its reduction and oxidation both proceed via a simple one electron transfer process. In these studies, the diffusion coefficients and the rate constant for the $Fe(III)(CN)_6^{3-}/Fe(II)(CN)_6^{4-}$ system at the ppys β -CD interface were calculated and compared to values obtained for ppyCl and for the bare GC electrode. Other important information concerning the reversibility of the systems was extrapolated from the cyclic voltammetry data and will be discussed later in this section.

The formal redox potential of the ferri/ferrocyanide couple was first calculated at the bare GC electrode from the half-wave potential in a steady state rotating disc polarization curve, as shown in Figure 3.8. The half-wave potential was found to be 0.117 V vs SCE in a 0.10 M NaCl supporting electrolyte. At this potential polypyrrole is conductive but its electroactivity will not interfere with the ferricyanide signal, making this an ideal electroactive probe.

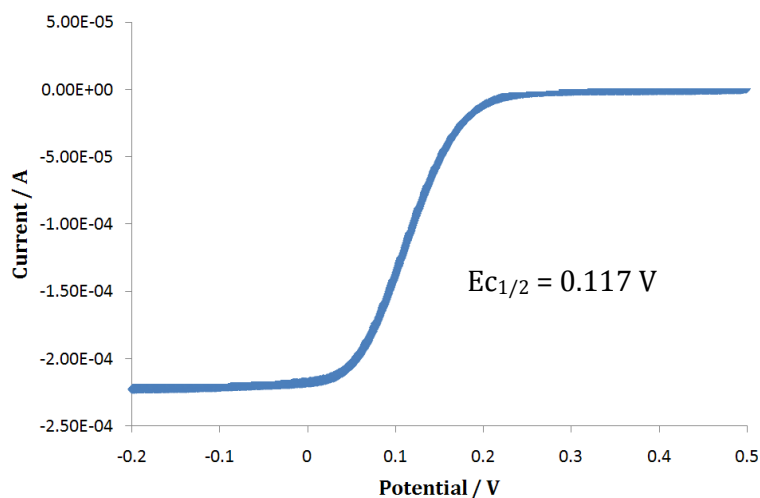


Figure 3.8: Current-potential curve at a GC rotating disk electrode ($d = 5$ mm), in 5.00×10^{-3} M $K_3Fe(CN)_6$ in 0.10 M NaCl at 250 rpm. Data recorded at 50 mV s^{-1} . Applied potential is relative to the SCE reference.

Cyclic voltammetry data for the ppys β -CD and ppyCl systems were recorded in a 5.00×10^{-3} M $K_3Fe(CN)_6$ solution in a 0.10 M NaCl supporting electrolyte. The potential window was varied from -0.2 to 0.5 V vs SCE, since the reduction and oxidation of the ferri/ferricyanide occurs within this range, as evident from Figure 3.8. Both ppys β -CD and ppyCl were first conditioned for 20 voltammetric cycles in the working solution at a scan rate of 75 mV s^{-1} . Then the scan rate was varied from low to high values and the voltammograms were recorded. Ten cycles were collected for each scan rate to determine the stability of the systems. In general, the data were taken from the 10th cycle, except in the case of the bare GC electrode where there was some evidence of poisoning of the surface with extended cycling.

Representative cyclic voltammograms for the bare GC, ppys β -CD and ppyCl systems are shown in Figures 3.9, 3.10 and 3.11, respectively. The characteristic oxidation and reduction peaks of the ferri/ferrocyanide couple are evident at the GC electrode, Figure 3.9. Furthermore, as shown in the inset in Figure 3.9, the peak currents vary in a linear manner as a function of the square root of the scan rate. A linear plot is observed for both the reduction and oxidation currents, indicating that the redox reactions of the ferri/ferrocyanide couple are under diffusion control.

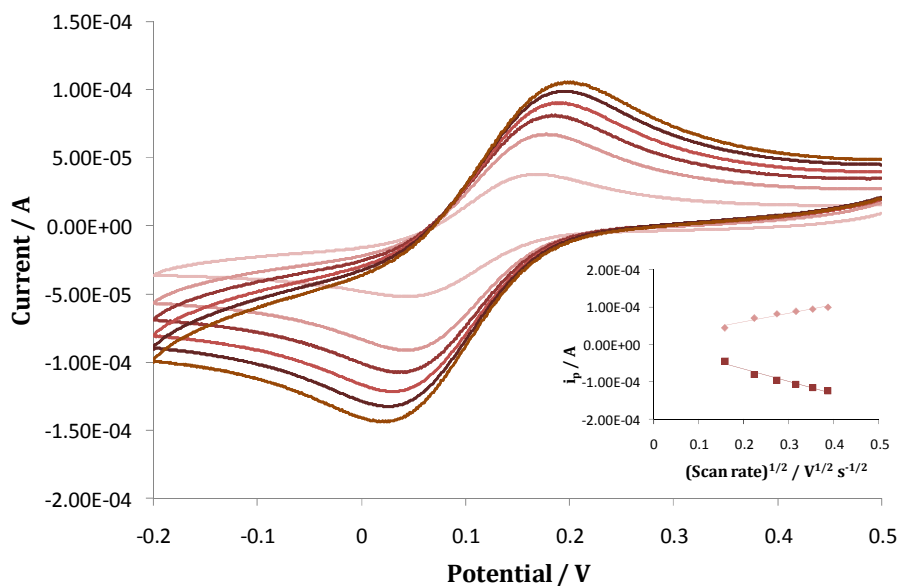


Figure 3.9: Cyclic voltammograms recorded in 5.00×10^{-3} M $K_3Fe(CN)_6$ and 0.10 M NaCl at 25, 50, 75, 100, 125, 150 $mV s^{-1}$ on GC electrode, ($d = 4$ mm). Scan direction is from 0.5 to -0.2 V. Inset shows the peak current, i_p , plotted as a function of the square root of scan rate. Applied potential is relative to the SCE reference.

Oxidation and reduction of the ferri/ferrocyanide couple is also clearly visible at the ppys β -CD and ppyCl films, Figures 3.10 and 3.11, respectively. However, in both cases, the capacitive current appears as a large background current. This limited the range of scan rates that could be employed. There was a considerable increase in the capacitive current of the polymer at scan rates higher than 150 $mV s^{-1}$. This made it particularly difficult to separate the

faradaic current due to the ferricyanide electroactivity from the capacitive current.

It is well known that for a potential step experiment the charging current dies after a certain time. On the other hand, for a potential sweep experiment a capacitive current, i_c , always flows, since the potential is continuously changing (Equation 3.3).

$$|i_c| = AC_d \nu \quad 3.3$$

While the faradaic current varies with the square root of the scan rate, as reported in Equation 3.4, the capacitive current varies with ν , Equation 3.3, so that i_c becomes more important at faster scan rates.²² For these reasons, the scan rates were only varied from 25 to 150 mV s⁻¹. In all cases, the capacitive background currents were subtracted from the peak currents to give the true i_p values. By plotting the peak current for the reduction of Fe(CN)₆³⁻ to give Fe(CN)₆⁴⁻ as a function of the square root of the scan rate, linear plots were obtained for ppys β -CD, ppyCl and for the bare GC electrode, as shown in the insets in Figures 3.9, 3.10 and 3.11. From the slope of each plot it was possible to calculate the diffusion coefficient, D , for the Fe(CN)₆³⁻ species using the Randles-Sevcik equation.¹⁴

$$i_p = K n^{3/2} AD^{1/2} c \nu^{1/2} \quad 3.4$$

In Equation 3.4, i_p is the peak current in A, K is a constant which has a value of 2.69×10^5 , A is the electrode area in cm², c is the concentration of the electroactive species in mol cm⁻³, D is the diffusion coefficient in cm² s⁻¹ and ν is the scan rate in V s⁻¹. This equation predicts that the peak current is proportional to the square root of the sweep rate and passes through the origin for a reversible reaction.

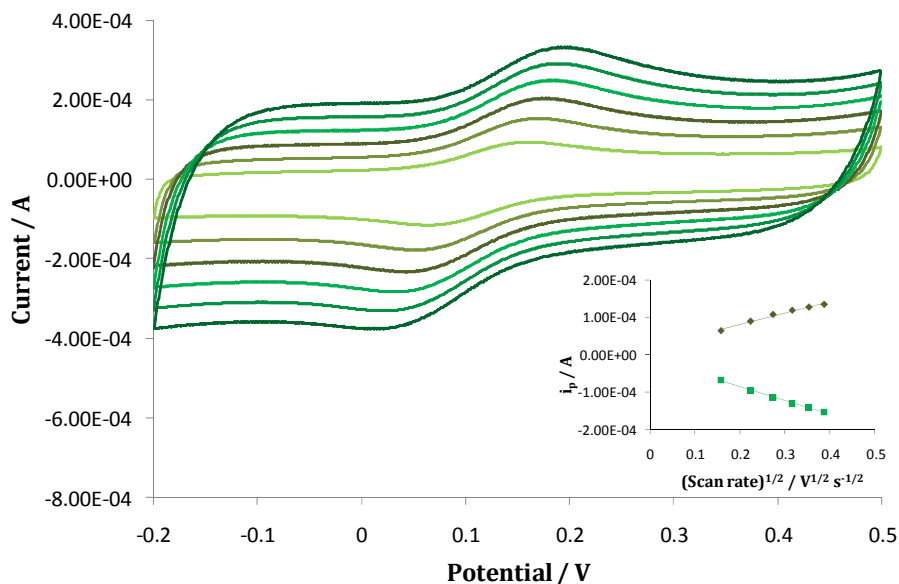


Figure 3.10: Cyclic voltammograms recorded in 5.00×10^{-3} M $K_3Fe(CN)_6$ and 0.10 M NaCl at 25, 50, 75, 100, 125, 150 $mV s^{-1}$ on ppys β -CD formed at 0.7 V to 2.50×10^{-2} C in 0.20 M pyrrole and 0.02 M $s\beta$ -CD on GC ($d = 4$ mm). Inset shows i_p plotted as a function of the square root of scan rate. Applied potential is relative to the SCE reference.

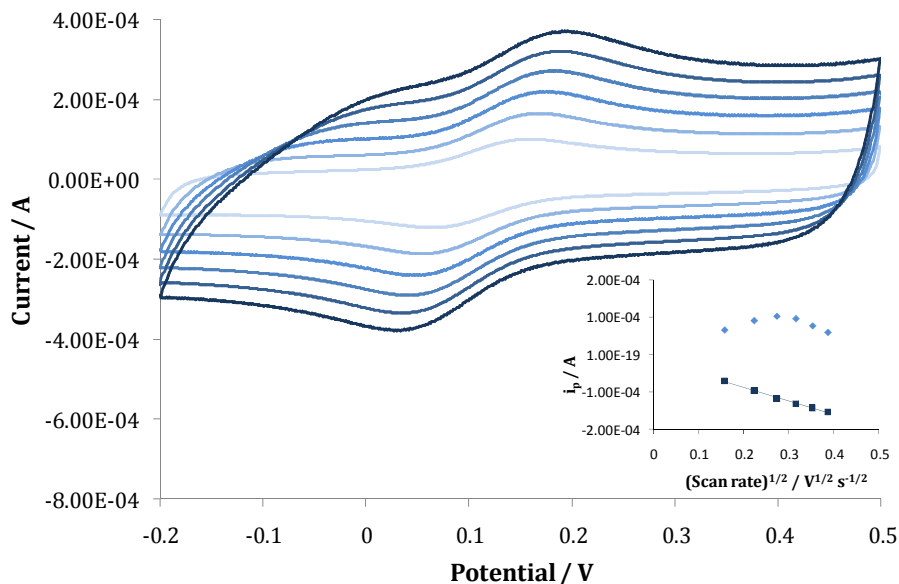


Figure 3.11: Cyclic voltammograms recorded in 5.00×10^{-3} M $K_3Fe(CN)_6$ and 0.10 M NaCl at 25, 50, 75, 100, 125, 150 $mV s^{-1}$ on ppyCl formed at 0.7 V to 2.50×10^{-2} C, in 0.20 M pyrrole and 0.10M NaCl on GC ($d = 4$ mm). Inset shows i_p plotted as a function of the square root of scan rate. Applied potential is relative to the SCE reference.

Data extracted from the insets in Figures 3.9, 3.10 and 3.11 are summarized in Table 3.1. It is important to note that for an ideal reversible reaction the linear plot should pass through the origin. This was not the case for the ppyCl and ppys β -CD coated electrodes, indicating a kinetic limitation. On the other hand, the linear plot crosses the origin for the bare GC electrode. In addition, the reoxidation of the ferro/ferricyanide couple on the ppyCl polymer is complicated by the electrochemistry of the polymer. This may explain the non linear relationship observed between the limiting current and the square root of the scan rate, as depicted in the inset of Figure 3.11.

Table 3.1: Diffusion coefficients, D , obtained from CV data recorded at 25, 50, 75, 100, 125 and 150 mV s^{-1} , for 5.00×10^{-3} M potassium ferricyanide in 0.10 M NaCl at the three different electrode surfaces. Geometrical surface area was used to compute D .

	Slope / $\text{A V}^{-1/2} \text{s}^{1/2}$	R²	D / $\text{cm}^2 \text{s}^{-1}$	Intercept / A
ppysβ-CD	3.68×10^{-4}	0.996	4.75×10^{-6}	1.22×10^{-5}
ppyCl	3.60×10^{-4}	0.995	4.54×10^{-6}	1.63×10^{-5}
GC	3.30×10^{-4}	0.961	3.86×10^{-6}	0.0

As clearly revealed in Table 3.1, the slope obtained for ppys β -CD is essentially the same as that obtained for ppyCl and hence the respective diffusion coefficients for the analyte at the ppys β -CD and ppyCl interface are very similar too. On the other hand, the diffusion coefficient is considerably smaller at the bare GC interface. As the diffusion coefficient of an analyte is constant at a fixed temperature, these variations in the apparent diffusion coefficients were explained in terms of variations in the surface area, A , Equation 3.4. When a polymer is deposited, its surface is not perfectly smooth but porous and rough. These factors contribute to an increase in the surface area that becomes larger than the geometrical area of the substrate electrode. Using the D value calculated at the bare GC electrode, $3.86 \times 10^{-6} \text{ cm}^2 \text{ s}^{-1}$, the true surface area of the polymers was estimated, as shown in Table 3.2. These data show that the surface areas of the polymer-modified electrodes are higher by a factor of 8.5%. Furthermore, it can be deduced that the surface areas of ppys β -CD and ppyCl

are very similar despite an enormous diversity in the size and charge of the two dopants.

Table 3.2: Geometrical surface area for GC electrode and calculated surface areas for ppys β -CD and ppyCl.

	Surface area / cm ²
GC	0.1257
ppysβ-CD	0.1394
ppyCl	0.1364

Next, CV data were fitted to the Kochi and Klinger equation and used to evaluate the electron transfer rate constant, k . Kochi and Klinger²³ in fact, developed a correlation between rate constant and separation of peak potentials, $E_p^a - E_p^c$, as shown in Equation 3.5.

$$k = 2.18 \left(\frac{\beta D n F \nu}{R T} \right)^{1/2} \exp \left[- \frac{\beta^2 n F}{R T} (E_p^a - E_p^c) \right] \quad 3.5$$

Here, k is the rate constant in cm s⁻¹, D is the diffusion coefficient in cm² s⁻¹, n is the number of electrons transferred, F is the Faraday's constant (96,485.3415 C mol⁻¹), ν is the scan rate in V s⁻¹, R is the gas constant (8.314 J K⁻¹ mol⁻¹) and T is the thermodynamic temperature in K. E_p^a and E_p^c are the anodic and cathodic peak potentials, respectively, expressed in V and β is the charge transfer coefficient.²³ By plotting $\ln \nu$ as a function of the potential separation, ΔE , ($\Delta E = E_p^a - E_p^c$), Figure 3.12, it was possible to compute β , from the slope of the plot and, finally k from the intercept, as shown by rearranging Equation 3.5 to give Equation 3.6. These computed rate constants are given in Table 3.3 and show that there is very little variation in the rate of electron transfer at the three electrodes. The β values are close to the typical value of 0.5 for the three electrodes²², indicating that the transition state is mid way between the Fe(CN)₆³⁻ and Fe(CN)₆⁴⁺ species.

$$\ln v = \frac{2\beta^2 nF}{RT} \Delta E + 2 \ln k - 2 \ln 2.18 - \ln \frac{\beta D n F}{RT} \quad 3.6$$

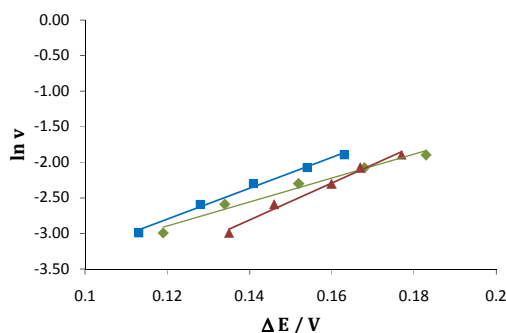


Figure 3.12: Plot of the logarithm of the scan rate, $\ln v$, as a function of the peak separation, ΔE , obtained from CV data recorded in 5.00×10^{-3} M $K_3Fe(CN)_6$ and 0.10 M NaCl at 50, 75, 100, 125, 150 $mV s^{-1}$ at ppys β -CD electrosynthesized at 0.7 V vs SCE to 2.50×10^{-2} C in 0.20 M pyrrole and 0.02 M s β -CD \blacklozenge ; at ppyCl electrosynthesized at 0.7 V vs SCE to 2.50×10^{-2} C in 0.20 M pyrrole and 0.10 M NaCl \blacksquare ; and at bare GC \blacktriangle ; ($d = 4$ mm).

Table 3.3: Electron transfer rate constant, k , and transfer coefficient, β , at the three different electrode surfaces, obtained from the plots in Figure 3.12. The diffusion coefficient was taken as $5.30 \times 10^{-6} cm^2 s^{-1}$, calculated from RDE measurement at 5 $mV s^{-1}$ (Table 3.5).

	Slope / V^{-1}	β	Intercept	R^2	$k / cm s^{-1}$
ppys β -CD	16.71	0.46	-4.90	0.98	1.82×10^{-3}
ppyCl	21.60	0.53	-5.39	0.99	1.53×10^{-3}
GC	25.81	0.58	-6.42	0.99	9.68×10^{-4}

3.3.2 Diffusion coefficient and rate constant by means of RDV

Although the electron transfer rate constant, k , was estimated from the peak separation with increasing scan rate, using the Kochi's method²³, sufficiently high scan rates could not be used due to the large capacitive current of the conducting polymers, limiting such an analysis. Instead, the ferri/ferrocyanide

couple was employed to evaluate the electron transfer rate constant by means of rotating disc voltammetry (RDV). In this case the data were fitted to the Koutecky-Levich equation, Equation 3.7.¹⁴

$$\frac{1}{i_L} = \frac{1}{n F A k c} + \frac{1.61}{n F A \nu^{-1/6} D^{2/3} c \omega^{1/2}} \quad 3.7$$

Here, i_L is the limiting current, n is the number of electrons transferred, F is Faraday's constant (96,485.3415 C mol⁻¹), k is the reaction rate constant, D is the diffusion coefficient in cm² s⁻¹, ν is the kinematic viscosity ($\nu = 0.0092$ cm² s⁻¹)²⁴, A is the surface area in cm², c is the concentration of the electroactive species expressed in mol cm⁻³ and ω is the rotational rate in rad s⁻¹. When i_L^{-1} is plotted as a function of $\omega^{-1/2}$, in the absence of kinetic complications, a linear plot is obtained. From the intercept it is possible to extrapolate and compute the rate constant, k .

As explained in detail in Chapter 2, the main advantages of this technique are the control of the diffusion layer and the increased mass transport of electroactive species to the electrode surface, leading to higher currents and consequently to greater sensitivity. Furthermore, from RDV data, diffusion coefficients for the bare GC, ppyCl and ppys β -CD were evaluated by applying the Levich equation (Equation 3.8) and compared to the values reported in Section 3.2.1, calculated using the Randles-Sevcik equation.

$$i_L = 0.621 n F A D^{2/3} \nu^{-1/6} c \omega^{1/2} \quad 3.8$$

In Equation 3.8, i_L is the limiting current, n is the number of electrons transferred, F is Faraday's constant (96,485.3415C mol⁻¹), D is the diffusion coefficient in cm² s⁻¹, ν is the kinematic viscosity (ν is 0.0092 cm² s⁻¹)²⁵, A is the surface area in cm², c is the concentration of the electroactive species in mol cm⁻³ and ω is the rotational rate in rad s⁻¹.

Typical RDV results collected using a scan rate of 5 mV s^{-1} are shown in Figure 3.13 for the bare GC, in Figure 3.14 for the ppys β -CD and in Figure 3.15 for the ppyCl system. Limiting currents were observed from about 0.0 to -0.2 V vs SCE and these increased with the rotation rate, according to the RDV theory, Equation 3.8. The voltammograms were also recorded at a higher scan rate of 50 mV s^{-1} . The results obtained were similar to those presented in Figures 3.13, 3.14 and 3.15, but with less well defined limiting currents. This indicates a kinetic limitation. At the higher scan rate, Nernstian equilibrium is not achieved due to a slow rate of electron transfer at the electrode interface.

Levich plots, where the limiting current was measured at -0.1 V vs SCE, are presented in Figure 3.16 for the three electrodes, GC, ppyCl and ppys β -CD, at both 5 and 50 mV s^{-1} . The diffusion coefficients calculated from the Levich plots are listed in Tables 3.4 and 3.5. They are in good agreement with those reported in Table 3.1, having similar magnitudes.

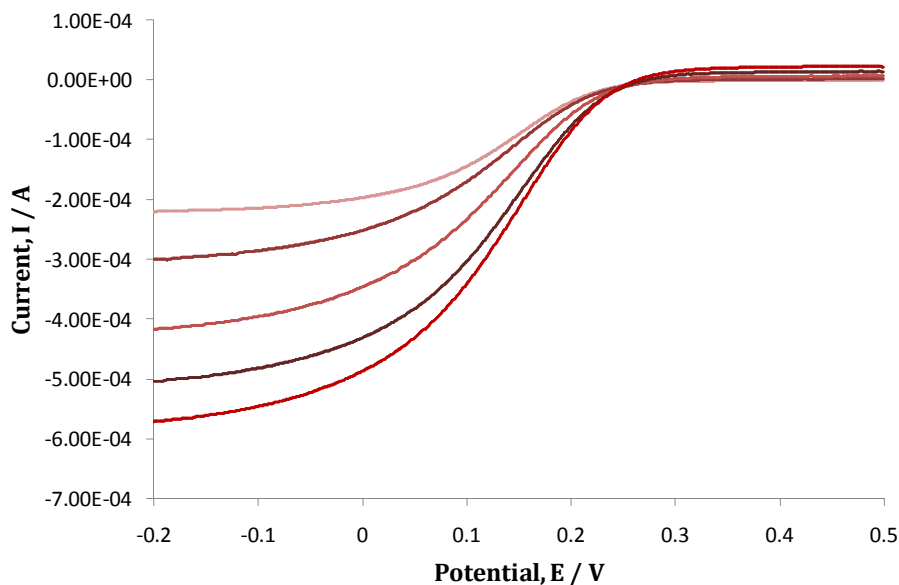


Figure 3.13: RDV data recorded in $5.00 \times 10^{-3} \text{ M K}_3\text{Fe}(\text{CN})_6$ and 0.10 M NaCl at 250, 500, 1000, 1500 and 2000 rpm, at a scan rate of 5 mV s^{-1} , on a GC electrode, ($d = 5 \text{ mm}$). Applied potential is relative to the SCE reference.

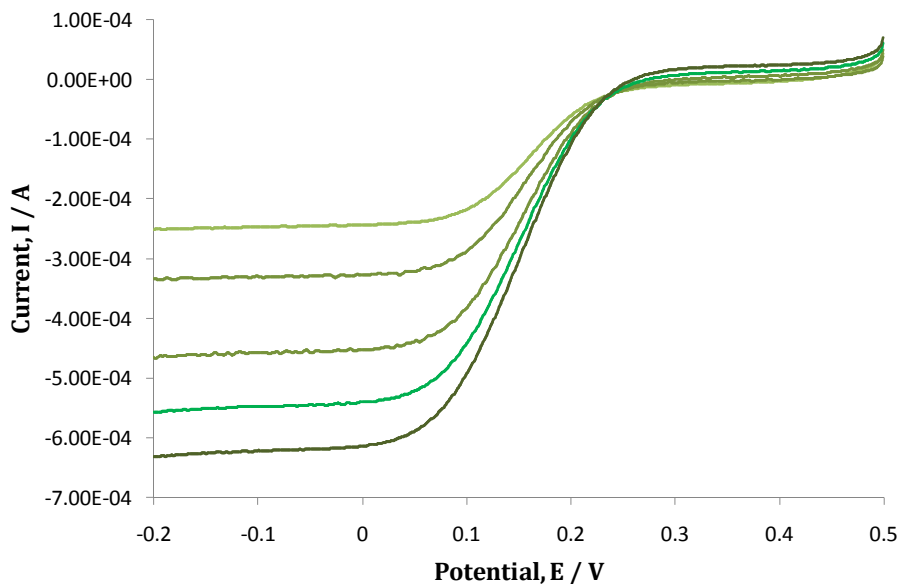


Figure 3.14: RDV data recorded in 5.00×10^{-3} M $K_3Fe(CN)_6$ and 0.10 M NaCl at 250, 500, 1000, 1500 and 2000 rpm, at a scan rate of 5 mV s^{-1} , on a ppys β -CD electrode electrosynthesized at 0.7 V to 3.90×10^{-2} C at GC ($d = 5 \text{ mm}$). Applied potential is relative to the SCE reference.

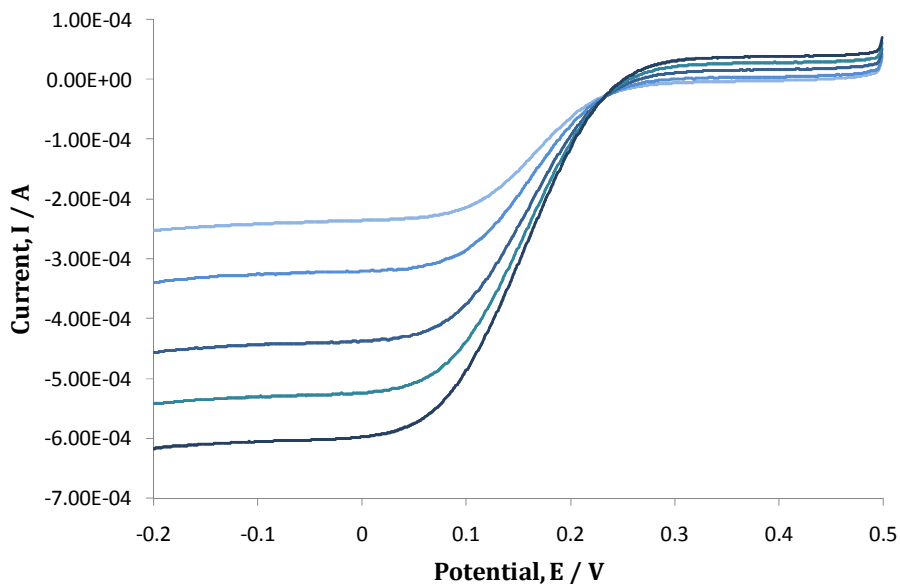


Figure 3.15: RDV data recorded in 5.00×10^{-3} M $K_3Fe(CN)_6$ and 0.10 M NaCl at 250, 500, 1000, 1500 and 2000 rpm, at a scan rate of 5 mV s^{-1} , on a ppyCl electrode electrosynthesized at 0.7 V to 3.90×10^{-2} C at GC ($d = 5 \text{ mm}$). Applied potential is relative to the SCE reference.

However, as clearly evident from either Table 3.4 or Figure 3.16 (a), the linear plots for ppys β -CD and ppyCl do not pass through the origin when the experiments are performed at a scan rate of 50 mV s⁻¹. The intercepts are consistent with kinetic limitations, and for this reason data recorded at the lower scan rate are more reliable. As shown in Table 3.5, data recorded at the slower scan rate give the theoretical zero intercept. Under these conditions, Nernstian equilibrium is maintained at the electrode interface throughout the cycle. The diffusion coefficients, D , calculated at 50 mV s⁻¹ are very similar for the three substrates, while at 5 mV s⁻¹, D is slightly larger at the ppys β -CD and ppyCl electrodes compared to the bare GC interface (Tables 3.4 and 3.5). As explained, earlier in Section 3.2.1, such a characteristic is probably connected with a larger surface area of the deposited polymers with respect to the geometrical area of the electrode. The actual surface areas for ppys β -CD and ppyCl are listed in Table 3.6. Here it is seen that they are higher by a factor of 14% and 11%, respectively. These percentage increases are larger than the 8.5% found by CV, Section 3.2.1. However, it is well known that the RDV method is more sensitive and accurate.¹⁴ Thus, the diffusion coefficients given in Table 3.5, derived from a rotating electrode are more accurate, especially at the lower scan rate.

Table 3.4: Diffusion coefficient for K₃Fe(CN)₆ at the three different electrode surfaces, calculated from the plots in Figure 3.16 where data were recorded at 50 mV s⁻¹.

	Slope / A s ^{1/2}	R ²	D / cm ² s ⁻¹	Intercept / A
ppysβ-CD	4.06 x 10 ⁻⁵	1.00	5.74 x 10 ⁻⁶	1.71 x 10 ⁻⁴
ppyCl	3.98 x 10 ⁻⁵	1.00	5.57 x 10 ⁻⁶	1.79 x 10 ⁻⁴
GC	3.92 x 10 ⁻⁵	0.97	5.44 x 10 ⁻⁶	0.0

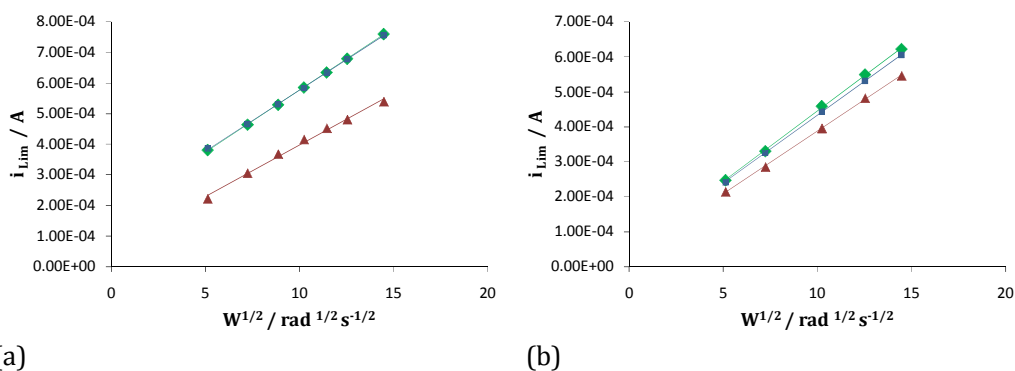


Figure 3.16: Levich plot for 5.00×10^{-3} M $K_3Fe(CN)_6$ in 0.10 M NaCl recorded at (a) 50 mV s^{-1} and (b) 5 mV s^{-1} . Bare GC electrode \blacktriangle ; ppys β -CD (synthesized from 0.20 M pyrrole and 0.02 M s β -CD at 0.7 V vs SCE to 3.90×10^{-2} C) \blacklozenge ; and ppyCl (synthesized from 0.20 M pyrrole and 0.10 M NaCl at 0.7 V vs SCE to 3.90×10^{-2} C) \blacksquare . The limiting current was read at -0.1 V vs SCE from the RDVs recorded at 250, 500, 750, 1000, 1250, 1500 and 2000 rpm.

Table 3.5: Diffusion coefficient for $K_3Fe(CN)_6$ at the three different electrode surfaces, calculated from the plots in Figure 3.16 where data were recorded at 5 mV s^{-1} .

	Slope / $A \text{ s}^{1/2}$	R ²	D / $\text{cm}^2 \text{ s}^{-1}$	Intercept / A
ppysβ-CD	4.40×10^{-5}	0.99	6.47×10^{-6}	0.0
ppyCl	4.28×10^{-5}	0.99	6.21×10^{-6}	0.0
GC	3.85×10^{-5}	0.99	5.30×10^{-6}	0.0

Table 3.6: Geometrical surface area for GC electrode and calculated area for ppys β -CD and ppyCl surfaces. RDV data obtained at 5 mV s^{-1} were fitted to the Levich equation and using a value of $5.30 \times 10^{-6} \text{ cm}^2 \text{ s}^{-1}$ for D , the area, A , was computed.

	Surface area / cm^2
GC	0.1963
ppysβ-CD	0.2243
ppyCl	0.2182

RDV measurements were also used to calculate the rate constant, k . This parameter is an expression of the rate at which the electrons are transferred

from the polymer to the electroactive species. By plotting the inverse of the limiting current as a function of the inverse of the square root of the rotation rate, a Koutecky-Levich plot was obtained for the three systems. The linear plot for ppys β -CD was found to overlap almost perfectly with that obtained for the ppyCl plot, both at a scan rate of 50 and 5 mV s⁻¹, as illustrated in Figure 3.17 (a) and (b). Similar intercepts, and hence similar rate constants, were calculated for the two polymers. These values together with the data for the bare GC electrode are summarized in Tables 3.7 and 3.8.

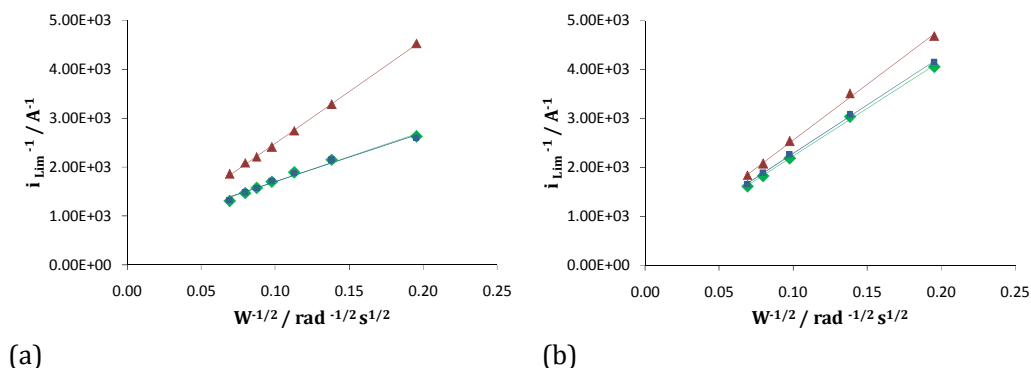


Figure 3.17: Koutecky-Levich plots for 5.00×10^{-3} M $K_3Fe(CN)_6$ in 0.10 M NaCl, recorded at (a) 50 mV s⁻¹ and (b) 5 mV s⁻¹. GC electrode \blacktriangle ; ppys β -CD (synthesized from 0.20 M pyrrole and 0.02 M s β -CD at 0.7 V vs SCE until a charge of 3.90×10^{-2} C was consumed) \blacklozenge ; and ppyCl (synthesized from 0.20 M py and 0.10 M NaCl at 0.7 V vs SCE until a charge of 3.90×10^{-2} C was consumed) \blacksquare . Limiting currents were read from the RDVs at -0.1 V vs SCE.

Again, the influence of scan rate can be seen. There is reasonably good agreement between the k values computed at 5 and 50 mV s⁻¹ for the bare GC electrode. However, for the two polymer modified GC interfaces, there is a two-fold increase in the k value when the scan rate is reduced from 50 to 5 mV s⁻¹. Again, this is consistent with a kinetic limitation at the polymer modified electrodes. As the scan rate is reduced the intercept becomes smaller indicating that the process is now more controlled by mass transfer to the interface. When the redox process occurs at the bare electrode interface, the electron is transferred efficiently from the electrode to the analyte. In the presence of a

polymer deposited on the electrode substrate, the electron flows from the metal to the conducting polymer and finally to the analyte. Results of this study support the conclusion that the overall electron transfer process is only slightly delayed by the presence of the polymer. When a sufficiently slow scan rate is used, to maintain Nernstian equilibrium at each applied potential, the rate constants for the three substrates are very close, as highlighted in Table 3.8.

Table 3.7: Rate constant, k , for 5.00×10^{-3} M $K_3Fe(CN)_6$ in 0.10 M NaCl at the three electrode surfaces at a scan rate of 50 mV s^{-1} .

	Intercept / A^{-1}	R^2	$k / \text{cm s}^{-1}$
ppysβ-CD	674.5	0.999	$1.56 \times 10^{-2} \text{ cm s}^{-1}$
ppyCl	702.6	0.984	$1.50 \times 10^{-2} \text{ cm s}^{-1}$
GC	375.2	1.00	$3.00 \times 10^{-2} \text{ cm s}^{-1}$

Table 3.8: Rate constant k , for 5.00×10^{-3} M $K_3Fe(CN)_6$ in 0.10 M NaCl at the three electrode surfaces at a scan rate of 5 mV s^{-1} .

	Intercept / A^{-1}	R^2	$k / \text{cm s}^{-1}$
ppysβ-CD	283.3	0.998	$3.73 \times 10^{-2} \text{ cm s}^{-1}$
ppyCl	317.8	0.999	$3.32 \times 10^{-2} \text{ cm s}^{-1}$
GC	291.3	0.998	$3.63 \times 10^{-2} \text{ cm s}^{-1}$

In summary, the diffusion coefficients calculated from the RDV data are consistent with those derived from CV. Moreover, they are in good agreement with those quoted in the literature.²⁶ The kinetic analysis clearly shows that the large dopant, $s\beta$ -CD, does not give rise to any significant reduction in the rate of electron transfer. Indeed, the rate constant, k , is slightly higher for the ppys β -CD electrode compared to the ppyCl electrode.

3.3.3 Reversibility

It is universally recognized in the literature that a redox reaction is classified as reversible if certain conditions are respected.^{14,22} Firstly, the peak potential, E_p , should be independent of the scan rate, secondly the peak potential separation

$(E_{pa} - E_{pc})$ should be equal to $57/n$ mV, where n is the number of electron equivalents transferred during the redox process. Another fundamental condition to be considered is the peak current ratio, I_{pa}/I_{pc} , which should be equal to one for all scan rates. Finally, the peak current should increase linearly as a function of the square root of the scan rate. An additional parameter useful for the evaluation of the reversibility is the peak width. Completely ideal reversible reactions are very hard to find in nature. Many redox processes can be defined as a quasi-reversible reaction. The electrochemistry of the ferri/ferrocyanide couple is a good example of a quasi-reversible reaction. The reversibility of this couple was studied at the GC and ppys β -CD and ppyCl modified electrodes and the parameters are summarized in Tables 3.9, 3.10 and 3.11.

As shown in Figure 3.9, a linear plot is obtained when the peak currents measured at the GC electrode are plotted as a function of the square root of the scan rate, indicating quasi-reversible behaviour. On the other hand, considering the peak current ratio, I_{pa}/I_{pc} , a value of unity is only achieved for the lowest scan rate investigated, as reported in Table 3.9. The parameter which deviates most from an ideal trend is the peak separation, ΔE_p , indicating some kinetic limitations. In the case of a reversible system, the electron transfer at the electrode interface is greater than the rate of diffusion at all scan rates. Therefore, Nernstian equilibrium is always maintained. If the rate of electron transfer is insufficient to maintain the Nernstian equilibrium, the shape of the cyclic voltammogram changes from the ideal shape. In particular, when the rate of diffusion becomes faster, the mass transport rate increases and becomes comparable to the rate of the electron transfer event. The most noticeable effect of this process is the increment in the peak potential separation, as evident in Table 3.9.

Table 3.9: Parameters extracted from CVs recorded at GC in the potential window 0.5 to -0.2 V vs SCE in 5.00×10^{-3} M $\text{K}_3\text{Fe}(\text{CN})_6$ in a 0.10 M NaCl supporting electrolyte.

Scan rate V s^{-1}	(Scan rate) ^{1/2} $(\text{V s}^{-1})^{1/2}$	Peak Current /A Fe³⁺/Fe²⁺	Peak Current /A Fe²⁺/Fe³⁺	$I_{\text{ox}}/I_{\text{red}}$	$E_{\text{pa}}-E_{\text{pc}}$ /V
		Fe³⁺/Fe²⁺	Fe²⁺/Fe³⁺		
0.025	0.1581	4.40×10^{-5}	4.44×10^{-5}	1.01	0.126
0.050	0.2236	8.05×10^{-5}	7.06×10^{-5}	0.88	0.135
0.075	0.2738	9.53×10^{-5}	8.17×10^{-5}	0.86	0.146
0.100	0.3162	1.06×10^{-4}	8.85×10^{-5}	0.83	0.160
0.125	0.3535	1.15×10^{-4}	9.45×10^{-5}	0.82	0.167
0.150	0.3872	1.24×10^{-4}	9.91×10^{-5}	0.80	0.177

Table 3.10: Parameters extracted from CVs recorded at ppys β -CD modified GC in the potential window 0.5 to -0.2 V vs SCE in 5.00×10^{-3} M $\text{K}_3\text{Fe}(\text{CN})_6$ in a 0.10 M NaCl supporting electrolyte.

Scan rate V s^{-1}	(Scan rate) ^{1/2} $(\text{V s}^{-1})^{1/2}$	Peak Current/A Fe³⁺/Fe²⁺	Peak Current /A Fe²⁺/Fe³⁺	$I_{\text{ox}}/I_{\text{red}}$	$E_{\text{pa}}-E_{\text{pc}}$ /V
		Fe³⁺/Fe²⁺	Fe²⁺/Fe³⁺		
0.025	0.1581	6.84×10^{-5}	6.44×10^{-5}	0.94	0.098
0.050	0.2236	9.51×10^{-5}	8.98×10^{-5}	0.94	0.119
0.075	0.2738	1.16×10^{-4}	1.08×10^{-4}	0.93	0.134
0.100	0.3162	1.30×10^{-4}	1.19×10^{-4}	0.91	0.152
0.125	0.3535	1.42×10^{-4}	1.28×10^{-4}	0.90	0.168
0.150	0.3872	1.53×10^{-4}	1.35×10^{-4}	0.88	0.183

Similar effects were observed with the ppys β -CD and ppyCl modified electrodes, Tables 3.10 and 3.11, respectively. For the polymer doped with s β -CD a linear relationship between the peak currents and $\omega^{1/2}$ is found for the reduction and oxidation of the ferri/ferrocyanide couple, as illustrated in Figure 3.10. Table 3.10 shows that an $I_{\text{pa}}/I_{\text{pc}}$ ratio of about 0.9 is obtained for all the scan rates, however, the peak potential separation increases with the increment of the scan rate, again suggesting kinetic limitations.

Table 3.11: Parameters extracted from CVs recorded at ppyCl modified GC in the potential window 0.5 to -0.2 V vs SCE in 5.00×10^{-3} M $K_3Fe(CN)_6$ in a 0.10 M NaCl supporting electrolyte.

Scan rate $V s^{-1}$	(Scan rate) ^{1/2} $(V s^{-1})^{1/2}$	Peak Current / A Fe³⁺/Fe²⁺	Peak Current / A Fe²⁺/Fe³⁺	I_{ox}/I_{red}	$E_{pa}-E_{pc}$ /V
0.025	0.1581	7.08×10^{-5}	6.56×10^{-5}	0.93	0.095
0.050	0.2236	9.78×10^{-5}	9.12×10^{-5}	0.93	0.113
0.075	0.2738	1.18×10^{-4}	1.03×10^{-4}	0.87	0.128
0.100	0.3162	1.31×10^{-4}	9.64×10^{-4}	0.73	0.141
0.125	0.3535	1.43×10^{-4}	7.71×10^{-5}	0.54	0.154
0.150	0.3872	1.54×10^{-4}	5.92×10^{-5}	0.38	0.163

In the case of the ppyCl modified electrode, Table 3.11, there is a significant reduction in the I_{pa}/I_{pc} ratios, which reaches values of about 0.38, with scan rates of 150 mV s^{-1} . This is mainly due to the electrochemistry of the polymer which makes the calculation of the peak current difficult. The peak separations are similar for all the three electrodes, suggesting similar rates of electron transfer.

The reversibility of the ferri/ferrocyanide couple at the three electrodes was further probed by applying the Heyrovsky-Ilkovic equation²⁷, Equation 3.9 to RDV data. The Heyrovsky-Ilkovic analysis provides a relationship between current and potential for a process under diffusion control.

$$E = E_{1/2} + \frac{2.303 RT}{nF} \log \frac{i_D - i}{i} \quad 3.9$$

Here, the intercept, $E_{1/2}$, is the half-wave potential in V, i is the Faradaic current in A, at the potential E and i_D is the limiting (diffusion) current. When the potential E is plotted as a function of the logarithm of $(i_D - i)/i$, as illustrated in Figure 3.18, the slope of the plot is equal to $2.303 RT/nF$, where n is the number of electrons exchanged, F is the Faraday's constant ($96,485.3415 \text{ C mol}^{-1}$), R is the gas constant ($8.31 \text{ J K}^{-1} \text{ mol}^{-1}$) and T is the thermodynamic temperature in K.

As evident from Figure 3.18, linear plots were obtained for all three electrodes. The experimentally observed slopes are compared with the theoretical slope value, which is calculated as 5.91×10^{-2} V at 298 K in Table 3.12. Also, provided are the intercept values and the measured $E_{1/2}$ values. In all cases, there is excellent agreement between the intercept and the $E_{1/2}$ values.

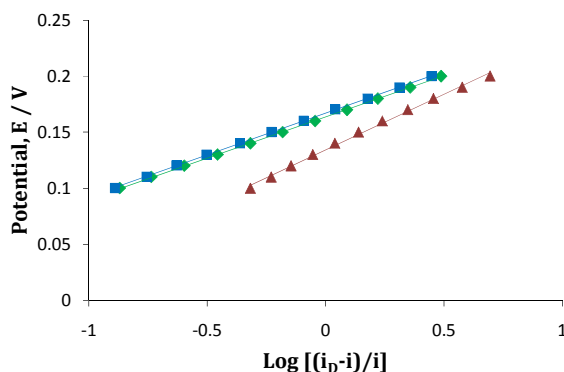


Figure 3.18: Heyrovsky-Illkovic plot derived from RDV data recorded in 5.00×10^{-3} M $K_3Fe(CN)_6$ in 0.10 M NaCl at 250 rpm and 5 mV s^{-1} , on ppys β -CD synthesized at 0.7 V, to 2.50×10^{-2} C, from 0.20 M pyrrole and 0.02 M s β -CD, pH = 5.0 \blacklozenge ; on ppyCl synthesized at 0.7 V, to 2.50×10^{-2} C, from 0.20 M pyrrole 0.10 M NaCl, pH = 5.0 \blacksquare ; and on GC \blacktriangle ; ($d = 5$ mm). Applied potential is relative to the SCE reference.

Table 3.12: Experimental slopes and intercepts derived from Figure 3.18 at the three different electrode surfaces.

	Slope / V	Intercept / V vs SCE	R ²	Experimental $E_{1/2}$ / V vs SCE
ppys β -CD	7.35×10^{-2}	0.164	0.999	0.164
ppyCl	7.48×10^{-2}	0.167	0.999	0.167
GC	9.88×10^{-2}	0.134	0.997	0.134

Interestingly, the half-wave potential, $E_{1/2}$, for the reduction of the ferricyanide is more positive at the ppys β -CD and ppyCl interfaces than at the GC electrode. The ferricyanide is reduced at more positive potentials on the ppy surface so both ppys β -CD and ppyCl have a catalytic effect on the ferricyanide reduction. This clearly highlights that the reaction is taking place at the polymer interface

and not at the GC substrate. There is some deviation between the experimental and theoretical slope values for all three electrodes, with the greatest deviation being observed with the bare GC electrode.

In summary, it is possible to state that the redox behavior of the ferri/ferricyanide couple at the three substrates investigated, GC electrode, ppys β -CD and ppyCl is a quasi-reversible process. The reversibility of the redox couple at the polymer of interest, ppys β -CD, is comparable to that of a bare GC substrate and better, in terms of that observed for ppyCl films. It is clear that the complex supramolecular chemistry of the large s β -CD dopant does not have a negative effect on the degree of reversibility of the ferricyanide electrochemistry. Furthermore, both polymeric substrates exhibit, to some extent, a catalytic effect on the reduction of the ferricyanide species.

3.4 Redox properties of the polymer: cyclic voltammetry

Cyclic voltammetry (CV) was used to provide general information about the redox activity and the ionic exchange of the conducting polymer, ppys β -CD. A corresponding polymer doped with chloride anions was studied for comparison. Typical cyclic voltammograms are presented in Figure 3.19 for ppys β -CD and ppyCl films grown to a charge of 3.80×10^{-1} C and cycled in 1.00 M NaCl. Similar data are presented in Figure 3.20 for thinner films grown to a charge of 2.50×10^{-2} C and cycled in 0.10 M NaCl. Clearly, the voltammograms are different for the ppys β -CD and ppyCl modified electrodes, indicating different redox behaviour.

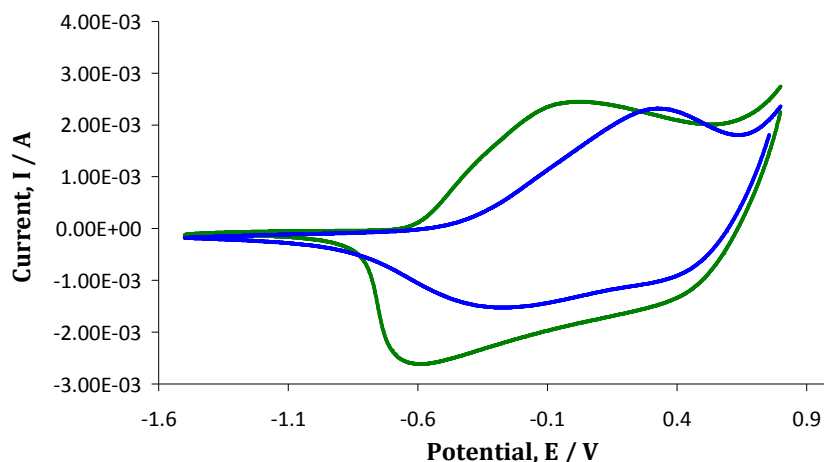


Figure 3.19: CV of ppyCl — and ppysβ-CD — cycled in 1.00 M NaCl, 10th cycle. Polymers were grown at 0.8 V to 3.80×10^{-1} C on a GC electrode ($d = 4$ mm); ppyCl was synthesized from 0.20 M pyrrole and 0.10 M NaCl, while ppysβ-CD was synthesized from 0.20 M pyrrole and 0.02 M sβ-CD, pH = 5.0. Applied potential is relative to the SCE reference.

In Figure 3.19, the reduction and subsequent oxidation for both ppysβ-CD and ppyCl are represented by broad waves. As a matter of fact it is more precise to describe a reduction/oxidation range rather than redox peaks. The reduction of ppysβ-CD begins at around 0.3 V vs SCE and continues until the potential reaches -1.0 V vs SCE, with a maximum current observed at -0.6 V vs SCE. The oxidation begins at -0.6 V vs SCE and extends up to 0.5 V vs SCE, with a maximum at -0.1 V vs SCE. These broad oxidation and reduction bands indicate a relatively slow exchange process. As the cyclodextrin is large and bulky it is not lost during the reduction of the polymer. Instead, reduction of the polymer is accompanied by the ingress of Na⁺ cations from the NaCl electrolyte. Concerning ppy doped with chloride anions, the polymer is reduced from about 0.1 to -1.0 V vs SCE, with a maximum current at approximately -0.2 V vs SCE. The interval of oxidation extends from approximately -0.5 to 0.6 V vs SCE, with a maximum rate of oxidation at approximately 0.3 V vs SCE. These data indicate that the ppyCl is slightly easier to reduce than the ppysβ-CD modified electrode. This is probably associated with the fact that reduction of the ppyCl is

accompanied by loss of the Cl^- anions, whereas the $\text{s}\beta\text{-CD}$ anion is too large to be expelled and the potential must be further lowered to facilitate the reduction of the polymer backbone and the ingress of Na^+ cations.

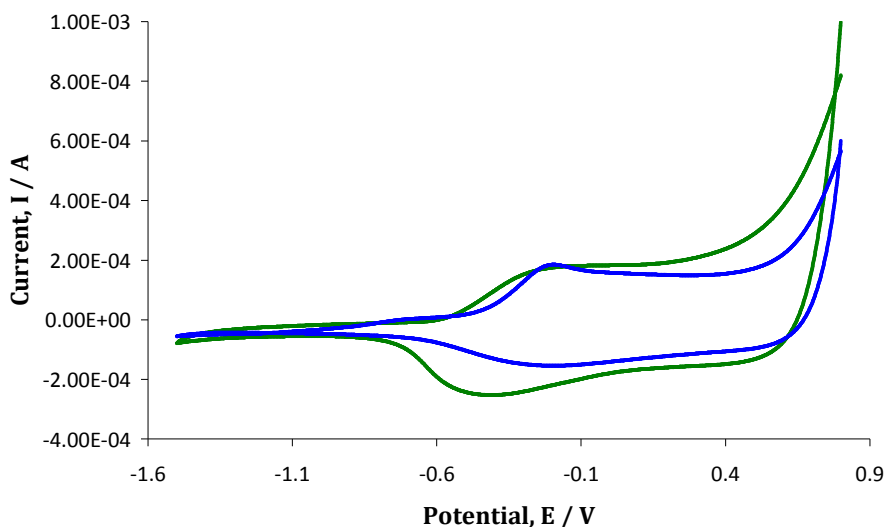


Figure 3.20: CV of ppyCl — and ppys β -CD — recorded in 0.1 M NaCl, 10th cycle. Polymers were grown at 0.7 V to 2.50×10^{-2} C on a GC electrode, ($d = 4$ mm); ppyCl was synthesized from 0.20 M pyrrole and 0.10 M NaCl; ppys β -CD was synthesized from 0.20 M pyrrole and 0.02 M β -CD, pH = 5.0. Applied potential is relative to the SCE reference.

An identical trend was observed for a thinner polymer, as shown in Figure 3.20. In this case, the reduction range recorded for ppys β -CD varies from 0.1 to -0.9 V vs SCE, while the oxidation wave starts at -0.6 V vs SCE and it is complete by 0.1 V vs SCE. On the other hand, ppyCl is reduced from -0.1 to -0.6 V vs SCE and oxidized from -0.5 to 0.0 V vs SCE. It is interesting to notice that the potential interval, or peak width, is narrower for the thinner polymer films. This can be explained by considering that a thick film is formed by a larger number of polymer layers so the electron transfer from the external layers to the GC substrate involves a longer path, which is reflected in a broader redox wave.

3.5 Doping levels and redox properties of the polymer: Electrochemical Quartz Crystal Microbalance (EQCM)

Using the EQCM technique it is possible to estimate the mass variation related to thin films deposited on the electrode surface. The Sauerbrey equation relates the mass change, Δm , expressed in g, to the resonant frequency shift of the crystal, Δf , expressed in Hz, Equation 3.10.²⁸

$$\Delta f = -\frac{2 f_0^2 \Delta m}{A(\rho_q \mu_q)^{1/2}} \quad 3.10$$

Here, f_0 is the resonant frequency of the unloaded crystal, A is the active area, ρ_q is the density of the quartz (2.648 g cm⁻³) and μ_q is the shear modulus of the quartz (2.947 x 10¹¹ dynes cm²).

This equation is valid if certain conditions are respected. The fundamental parameter to be considered is the polymer thickness. It has been previously demonstrated that when polymer films exceed about 500 nm, viscoelasticity effects play an important role and changes in the frequency are generated either by mass variation or by viscoelastic phenomena.¹² In order to apply the Sauerbrey equation to a polymer film, the film must behave as a rigid and perfectly elastic layer. The rigid film approximation is valid if the polymer thickness is small compared to the thickness of the crystal and if the overall mass loading results in a change of frequency that is small with respect to the resonant frequency of the unloaded crystal.¹² In order to satisfy the Sauerbrey relationship, polymer films were grown to a maximum charge of 5.00 x 10⁻³ C. The EQCM approach was applied to obtain an estimate of the doping levels in the ppys β -CD films and to probe further the redox properties of the film.

3.5.1 Doping level

Typical doping levels reported for ppy are in the ratio of 1:3 to 1:4 for dopant:pyrrole.²⁹ Previously, Wallace and co-workers³⁰ using microanalytical data, suggested that the doping level of the ppy films doped with either the α or the β sulfated CD, had a doping ratio of 1:4.5, slightly lower than the more

commonly reported doping levels. Several groups have used EQCM data to quantify polymer systems and to give an approximate calculation of the doping level.³¹ In the results presented here, EQCM measurements along with Equation 3.11, a derivation of Faraday's law, were used to estimate the doping levels. In this equation, M is the total mass of the deposited polymer, Q is the charge reached, M_m is the mass of the monomer, M_{dop} is the mass of the dopant, x is the doping level and F is Faraday's constant (96,485.3415 C mol⁻¹).

$$\frac{M}{Q} = \frac{M_m + (M_{dop})x}{(2 + x)F} \quad 3.11$$

Figure 3.21 demonstrates the experimental and theoretical results obtained for the growth of a ppy film doped with a small mobile chloride anion. These ppyCl films were deposited from a 0.10 M NaCl and 0.02 M pyrrole solution at 0.7 V vs Ag/AgCl. The theoretical curve was generated using Equation 3.11, assuming that the maximum doping level was achieved, i.e., $x = 0.33$. This gives a slope value of 3.50×10^{-4} g C⁻¹. A slope value of 3.20×10^{-4} g C⁻¹ was extrapolated from the experimental plot, which is somewhat lower than the theoretical slope value. However, in analyzing the initial growth, highlighted in Figure 3.21, there is very good correlation between the experimental and the theoretical data. However, as the film thickness (charge) increases a deviation from the theoretical slope is observed. This slight deviation from the theoretical slope is possibly due to the maximum doping level not being reached. Another reason for the lower experimental mass per unit charge is the formation on the electrode surface of soluble dimers or oligomers of pyrrole, which in turn consume the current and consequently the charge, but these are not involved in the deposition of the polymer to give the corresponding mass increase.

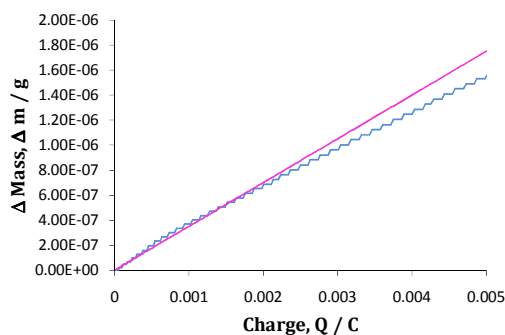


Figure 3.21: Mass -charge plot for the growth of ppyCl, deposited from 0.20 M pyrrole and 0.10 M NaCl at 0.7 V vs. Ag/AgCl until a charge of 5.00×10^{-3} C was reached. Theoretical — and experimental data —, ($n=3$).

As good agreement between the theoretical and experimental mass was obtained in Figure 3.21, this approach was used to estimate the doping level of the s β -CD doped polypyrrole films. As previously stated, the s β -CD is a cyclodextrin with 7-11 anions present on the outer rims. Unlike the chloride model, which has only one anion involved in the doping process, the cyclodextrin is a complex molecule with a minimum of 7 and a maximum of 11 anions possibly involved in the doping process. Although the majority of the molecules are more likely to possess 7 sulfated groups, the other fractions cannot be ignored.

In using Equation 3.11 to estimate the doping level for the ppys β -CD system, two hypotheses were necessary. In the first case, it was assumed that the maximum doping level of 0.33 was attained. Figure 3.22 shows the EQCM measurements, with mass as a function of charge, obtained for the growth of a ppys β -CD polymer at 0.7 V vs Ag/AgCl; these plots are marked as Exp on Figure 3.22 (a) and (b). The profiles labeled from 2 to 6 represent simulated data where the number of anions present on the CD and participating in the doping process was varied. In the case of the theoretical trace, Plot 1, Figure 3.22 (a), the estimated molar mass of the s β -CD, 2053.43 g, was used and each s β -CD provided only one anionic charge in the doping. It is obvious from these data displayed in Figure 3.22 (a) that there is a very large deviation from the theoretical and experimental slopes, 3.31×10^{-3} g C $^{-1}$ to 4.25×10^{-4} g C $^{-1}$

($R^2=0.997$), respectively. This clearly indicates that each s β -CD provides more than one sulfated anion to dope the polymer.

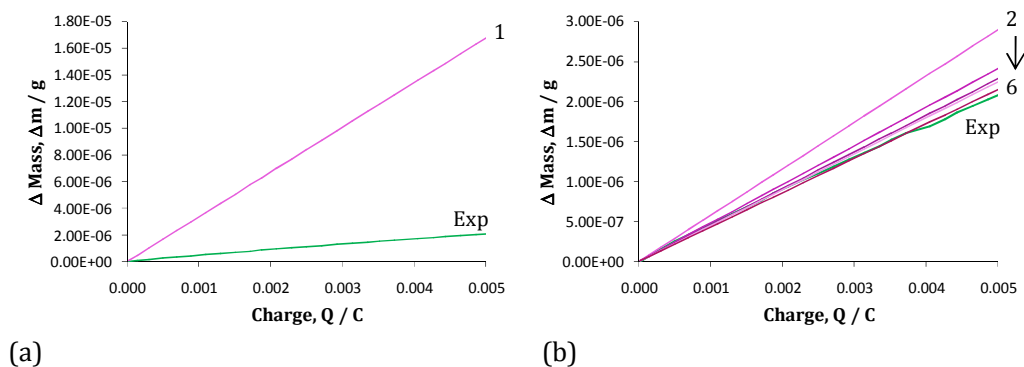


Figure 3.22: Mass -charge plot for the growth of ppys β -CD from 0.20 M pyrrole and 0.02 M s β -CD at 0.7 V vs. Ag/AgCl until a charge of 5.00×10^{-3} C was reached. Theoretical data — (Plots 1 to 6, details given in Table 3.13) and experimental data (Exp) —; ($n=3$).

Next, Equation 3.11 was used to estimate the mass charge relationship assuming that each S β -CD provided 11 anions in the doping process and the maximum doping level of 1:3 was maintained. This theoretical plot is provided as Trace 2 in Figure 3.22 (b). Although, the level of agreement between Trace 2 and the experimental plot is better than that observed between Trace 1 and the experimental plot, it is clear that there is still a significant gap between the theoretical and experimental profiles. Obviously, the doping level is considerably lower than 0.33. In order to test this hypothesis, doping levels of 0.10 and 0.08 were fitted into Equation 3.11, considering that the cyclodextrin provided 7 or 9 sulfated group to dope the polymers. The calculated theoretical m/Q slope values are summarized in Table 3.13 and further illustrated in Figure 3.22 (b), as Traces 3 to 6. The experimental data show the best agreement with Trace 6, which corresponds to a doping level of 0.08 with 7 sulfated groups participating in the doping process. In general, a reasonable hypothesis is that from 7 to 9 sulfated groups per cyclodextrin molecule participate in the doping process and the doping level ratio (dopant:monomer) varies from 1:10 to 1:12.

Table 3.13: Evaluated slopes for varying doping level and sulfated groups involved.

Plot	Negative groups of the s β -CD involved in doping	Doping level	Ratio dopant:monomer	Slope /g C ⁻¹
1	1	0.33	1:3	3.31 x 10 ⁻³
2	11	0.33	1:3	5.72 x 10 ⁻⁴
3	7	0.10	1:10	4.76 x 10 ⁻⁴
4	7	0.08	1:12	4.51 x 10 ⁻⁴
5	9	0.10	1:10	4.43 x 10 ⁻⁴
6	9	0.08	1:12	4.25 x 10 ⁻⁴
Exp	experimental	experimental	experimental	4.25 x 10 ⁻⁴

To sum up on this discussion, it was demonstrated that the maximum doping level, 0.33, with PPy films is not evident in the presence of the s β -CD. Due to the complexity of the s β -CD molecule, and the uncertainties in the number of substituted anionic sulfated groups, it is difficult to define the true level of doping. Although, Reece *et al.*³⁰ approximated a value of 1:4.5 (s β -CD:Py) and also stated the difficulties in evaluating the doping level due to the unknown degree of sulfation of the CD, our approximations point in the direction of a much lower doping level of 1:12. However, based on the assumption that all sulfated groups are involved in the compensation of the charge, it is highly unlikely that the doping level is higher than 0.10. At these levels it would mean that for about every 10 pyrrole units, 1 s β -CD would compensate for the charge. However, if all the sulfated groups on the s β -CD were involved in charge balance this would not only place strain on the cyclodextrin but also on the polymer. Therefore, it is highly probable that some free sulfonated groups are present within the polymer. Clearly, the doping level is very different with these large polyanionic dopants. Although the true doping level could not be obtained, the doping levels estimated between 0.08 and 0.10 seem reasonable in view of the large size of the s β -CD dopant.

3.5.2 Ionic exchange

In this work, films were grown to a maximum charge of 2.50 x 10⁻² C, in an attempt to avoid viscoelasticity complications so that the frequency shifts

measured were related to mass variations. A method to investigate if a polymer film can be considered as rigid is to plot the mass deposited on the electrode as a function of the charge consumed during polymerization. The mass is a linear function of the charge, according to Faraday's law, Equation 3.12:

$$q = \int_0^t i dt = m n F \quad 3.12$$

where q is the charge required to convert m moles of starting material to product in an electrode reaction involving the transfer of n electrons.¹⁴ As highlighted in Figure 3.23 (b), linear plots were obtained for the deposition of ppyCl and ppys β -CD films and hence polymers were assumed to be rigid. Another aspect clearly evident from the frequency-charge and mass-charge plots in Figure 3.23 is the higher mass deposited for ppys β -CD which is 1.00×10^{-5} g in comparison to the mass of ppyCl, 7.06×10^{-6} g. These data are consistent with the larger size of the s β -CD dopant. However, the mass of the ppys β -CD film is only larger by a factor of 1.3, yet the mass of the s β -CD is considerably higher than the chloride anion. This is in agreement with the low doping levels observed in Table 3.13.

Next, an examination into the ion and solvent flux observed during cycling of the ppys β -CD was carried out using the EQCM data. Both ppyCl and ppys β -CD were electrosynthesized at 0.7 V vs Ag/AgCl, on a gold working electrode connected to a piezoelectric quartz crystal and then cycled in a 1.00 M NaCl solution, from 0.6 to -1.2 V vs Ag/AgCl, using a scan rate of 50 mV s⁻¹. Ten cycles were recorded, in order to reach a steady state for the ionic exchange. A range of potentials where polypyrrole electroactivity is relevant are shown in Figures 3.24 and 3.25 for the first and 10th cycle. For the sake of clarity, only the reduction segments are presented. The frequency of the polymer doped with chloride anions, ppyCl, increased during reduction as depicted in Figure 3.24 (a), thus corresponding to a decrease in the mass of the polymer, as clearly illustrated in Figure 3.24 (b). When the polymer is reduced, ppy loses its positive charge and chloride anions are released from the polymer matrix into

the bulk solution in order to maintain electroneutrality, leading to a mass decrease ($\text{ppy}^+\text{Cl}^- + \text{e}^- \rightarrow \text{ppy} + \text{Cl}^-$).

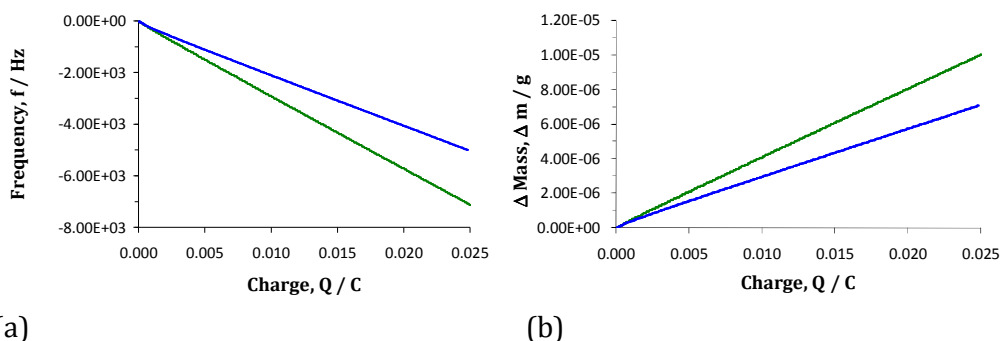
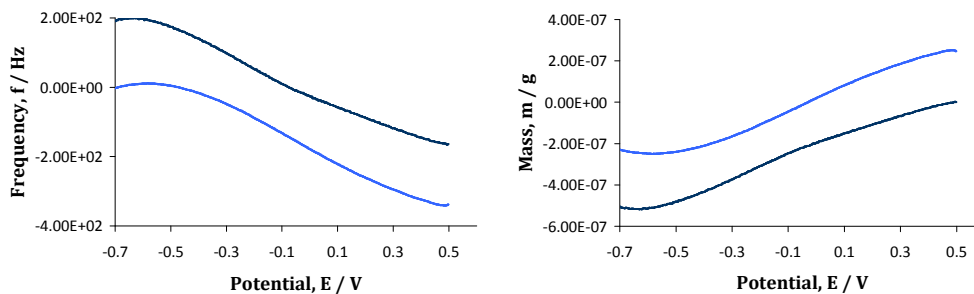


Figure 3.23: (a) Frequency-charge plot and (b) mass-charge plot for electropolymerization of pyrrole in 0.20 M pyrrole and 0.10 M NaCl, pH = 5.0 — and 0.20 M pyrrole and 0.02 M s β -CD, pH = 5.0 —. Both polymers were deposited onto a gold electrode, $A = 0.2033 \text{ cm}^2$, at 0.7 V vs Ag/AgCl until the final charge consumed was $2.50 \times 10^{-2} \text{ C}$.

The trend for ppyCl reduction is maintained from the 1st to the 10th cycle, as shown in Figure 3.24. A mass loss of $4.75 \times 10^{-7} \text{ g}$ is observed on reducing the polymer from 0.5 to -0.6 V vs Ag/AgCl during the first cycle, corresponding to about 7% of the mass of the polymer deposited during the synthetic process. A similar loss in mass of $4.74 \times 10^{-7} \text{ g}$ is recorded during the 10th cycle. However, it is also evident in Figure 3.24 that repetitive cycling leads to an overall increase in the mass at the electrode interface. This may indicate that not all the anions entering the polymer matrix during the oxidation process are expelled during the reduction step. Some of the chloride anions may be trapped within the polypyrrole matrix due to electrostatic or steric interactions with a consequent insertion of protons or sodium cations to balance the negative charge of chloride anions not expelled.



(a)

(b)

Figure 3.24: Frequency-potential plot (a) and mass-potential plot (b) for the redox activity of ppyCl in 1.00 M NaCl, at a scan rate of 50 mV s⁻¹ (ppyCl films were grown from 0.20 M pyrrole in 0.10 M NaCl, at Au electrode, A = 0.2033 cm², at 0.7 V vs Ag/AgCl, Q = 2.50 × 10⁻² C); 1st reduction segment —, 10th reduction segment —. Applied potential is relative to the Ag/AgCl reference.

Supposing that only chloride anions are expelled from the ppyCl during reduction, then the theoretical mass associated with the movement of chloride anions can be calculated from the charge, on the basis of Faraday's law. For a monoionic species, the charge is given as Equation 3.13.

$$Q_{M^-} = nF \quad 3.13$$

Here, F is the Faraday's constant (96,485.3415 C mol⁻¹) and n are the moles of the species carrying the charge. This equation can be rearranged to give Equation 3.14, where M_w is the molecular mass of the species carrying the charge and m its mass.

$$Q_{M^-} = \frac{m}{M_w} F \quad 3.14$$

From this formula m , which is the theoretical mass of chloride expected to be exchanged, was calculated. Using both the mass data presented in Figure 3.24 and the corresponding charge calculated from the simultaneous cyclic voltammogram, mass-charge plots were generated for the reduction of the polymer and compared to theoretical values calculated using Equation 3.15. The results are plotted in Figure 3.26 (a).

$$m = \frac{Mw}{F} Q_M. \quad 3.15$$

It is seen that the experimental plot, indicated by the blue trace, deviates from the theoretical slope, indicating that some of the charge is carried by a species with a mass lower than the chloride anions. This is particularly evident at the higher charge values, Figure 3.26 (a), which correspond to lower potentials in the cyclic voltammograms. These plots are consistent with the insertion of cations, protons or sodium in addition to the expulsion of chloride anions during the reduction of the polymer. If the ejection of the chloride anions is slow, then the negative charge of the chloride anions, trapped within the polymer matrix, will be balanced through the ingress of protons or sodium cations.

An opposite trend was observed when ppys β -CD was investigated. On reduction of the polymer a decrease in the frequency and consequently an increase in the mass were observed, as displayed in Figure 3.25 (a) and (b). The s β -CD is a large polyanion and cannot be expelled from the polymer backbone during reduction of polypyrrole because of its steric hindrance. As a consequence an increase of mass is registered on reduction of the polymer, as reduction is accompanied by the insertion of cationic species to maintain the electroneutrality of the system. (ppy⁺s β -CD⁻ + e⁻ → ppys β -CD⁻ Na⁺).

During the 1st reduction cycle, a mass increase of 1.74 x 10⁻⁶ g is observed, corresponding to a 14% increase in the mass of the electrode. Unlike the ppyCl system, the 1st and 10th cycles of the ppys β -CD system have different shapes, as clearly displayed in Figure 3.25. In particular, the gain in mass on reduction of the polymer is partially lost with proceeding cycles and the ionic movement observed during the 1st reduction cycle is completely different from the ionic exchange observed once the polymer has reached a steady state. Indeed, the 10th cycle indicates mixed cation and anion exchange properties. A small decrease in mass is observed on reducing the ppys β -CD from 0.5 to -0.1 V vs

Ag/AgCl, which is consistent with the loss of Cl⁻. On the other hand, an increase in mass is observed on reduction of the ppysβ-CD from -0.3 to -0.7 V vs Ag/AgCl, which can be attributed to the ingress of Na⁺ to balance the anionic sβ-CD.

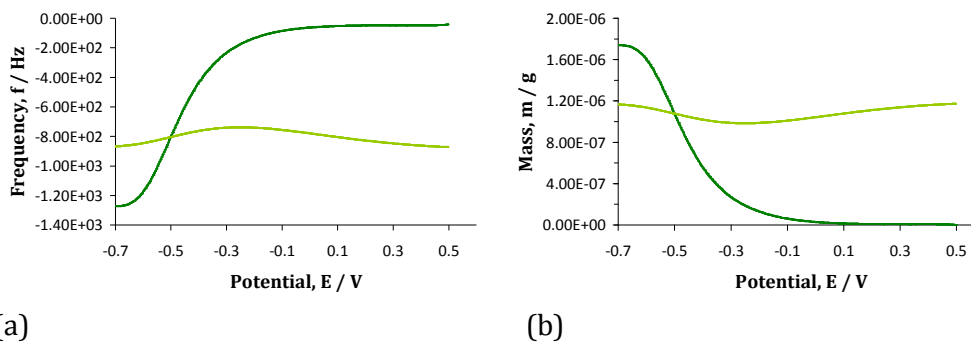


Figure 3.25: (a) Frequency-potential plot and (b) mass-potential plot for the redox activity of ppysβ-CD cycled in 1.00 M NaCl at a scan rate of 50 mV s⁻¹ (ppysβ-CD films were grown from 0.20 M pyrrole in 0.02 M sβ-CD, pH = 5.0, at 0.7 V vs Ag/AgCl, Q = 2.50 x 10⁻² C, at Au (A = 0.2033 cm²); 1st reduction segment —, 10th reduction segment —. Applied potential is relative to the Ag/AgCl reference.

As mentioned previously, the increase of mass recorded during the first reduction cycle is related to insertion of cations to balance the negative charge of the sβ-CD anions permanently trapped within the polymer matrix. Supposing that only Na⁺ takes part in the charge balance, then the mass change on reduction of the polymer can be calculated using Equation 3.15. This theoretical mass associated with Na⁺ exchange was calculated and plotted in Figure 3.26 (b) together with the experimental data. As shown in Figure 3.26 (b), the mass-charge plot for the experimental data is divided in two portions: the first one, at low charge values, where the charge is carried by species with a molecular mass lower than the Na⁺ and a second portion, at the higher charge values, where the mass carrying the charge is higher than the Na⁺. The first linear region corresponds to the potential interval from 0.5 to about -0.1 V vs Ag/AgCl and the lower experimental mass is probably related to the ingress of protons. Incorporation of protons into ppy films during electrochemical reduction in aqueous solutions has previously been demonstrated by Tsai *et al.*³² When the

potential becomes more negative, a dramatic increase in the mass carrying species is observed. This can be explained in terms of water incorporation, where the water accompanies the Na^+ forming a solvation shell around the Na^+ cation. The ingress of the solvated Na^+ is not observed at the more electropositive potentials suggesting that this phenomenon may be related to a change in the roughness and in the porosity of the reduced ppys β -CD. The more electronegative potentials may cause a rearrangement of the polymer structure that allows the entry of more water molecules of the solvation shell of the sodium cation.³³

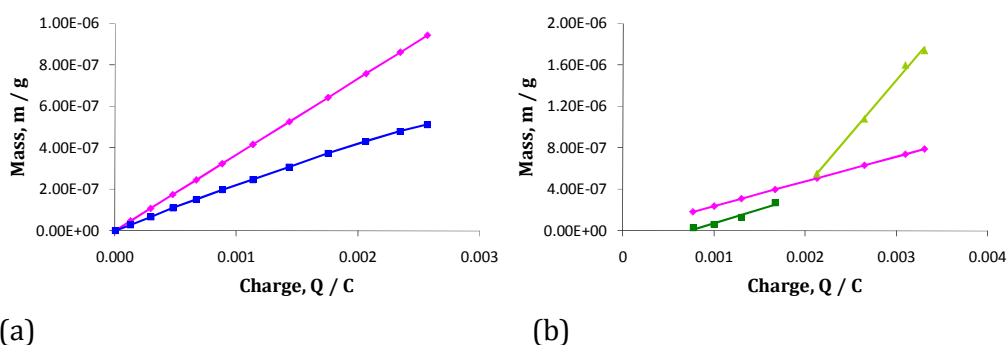


Figure 3.26: Mass-charge plot for the theoretical — and experimental, 1st cycle — redox activity of ppyCl (a) and the theoretical — and experimental, 1st cycle, —, — redox activity of ppys β -CD (b); ppyCl films were grown from 0.20 M pyrrole in 0.10 M NaCl and ppys β -CD films were grown from 0.20 M pyrrole in 0.02 M s β -CD, both at Au electrodes ($A = 0.2033 \text{ cm}^2$) at 0.7 V vs Ag/AgCl to a final charge, $Q = 2.5 \times 10^{-2} \text{ C}$.

Two different methods were used to evaluate the significance of the solvation shell involved in the sodium cation exchange. The first one is based on an analysis proposed by de Torresi *et al.*³⁴ In this analysis, the variation of mass, Δm , during reduction of the polymer is given by the mass of the sodium cation, $Mw_{\text{Na}^+} \xi_{\text{Na}^+}$, plus the mass of water from the solvation shell, $Mw_{\text{H}_2\text{O}} \xi_{\text{H}_2\text{O}}$, as described in Equation 3.16.

$$\Delta m = Mw_{\text{Na}^+} \xi_{\text{Na}^+} + Mw_{\text{H}_2\text{O}} \xi_{\text{H}_2\text{O}} \quad 3.16$$

Here, Mw_{Na^+} is the molecular mass of Na^+ and ξ_{Na^+} are the moles of Na^+ . Mw_{H_2O} and ξ_{H_2O} are the molecular mass and the moles of water, respectively. The electric charge, q , associated with the movement of the cation, Na^+ , is given by Equation 3.17, where F is Faraday's constant.

$$q = F \xi_{Na^+} \quad 3.17$$

If it is assumed that water molecules participating in the redox process belong to the hydration shell of the sodium cation, it is possible to write Equation 3.18,

$$\xi_{H_2O} = h \xi_{Na^+} \quad 3.18$$

where h is the hydration number of Na^+ . Combining Equations 3.16, 3.17 and 3.18, h can be expressed as follows in Equation 3.19.

$$h = \frac{F \Delta m}{q Mw_{H_2O}} - \frac{Mw_{Na^+}}{Mw_{H_2O}} \quad 3.19$$

By fitting the EQCM data for the ppys β -CD polymer to Equation 3.19, an h value of 4.08 for the solvation shell of Na^+ was computed. This value is in good agreement with the work of de Torresi *et al.*³⁴ who calculated an h value of 4.5 for Na^+ .

The second method used to give information on the solvation shell of Na^+ is based on a graphical construction, as depicted in Figure 3.27. In this analysis, the mass is plotted as a function of the charge for the reduction of the polymer between -0.3 and -0.7 V vs Ag/AgCl. The mass of sodium ion exchanged, m_{Na^+} , is given by line (a-b), while the mass of water associated with the process, m_{H_2O} , is given as line (c-b).

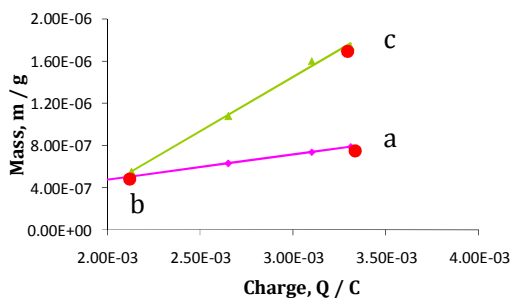


Figure 3.27: Magnification of Figure 3.26 (b), $a = 7.89 \times 10^{-7}$ g, $b = 4.90 \times 10^{-7}$ g, $c = 1.74 \times 10^{-6}$ g.

Dividing the calculated masses by the respective molecular mass, the moles of water and sodium ions were computed. The evaluated molar ratio between water and sodium was 4.01. This value is in excellent agreement with the solvation value previously obtained using the first method. In summary, it can be concluded that an average of 4 water molecules accompany the sodium cation when a fresh polymer pps β -CD is firstly reduced, i.e., first cycle in the CV.

On the other hand, after the significant cationic exchange observed during the 1st reduction cycle, the Δm is significantly reduced for the remaining cycles. As shown in Figure 3.26, the 10th cycle shows evidence of mixed anion and cation exchange. One possible explanation for this transition from cation exchange to mixed ion exchange may be that after the large ingress of Na⁺ observed on initial reduction, some of the Na⁺ cations become trapped within the polymer matrix, leading to a subsequent ingress of Cl⁻ anions to maintain electroneutrality as the polymer is oxidized.³⁵ Indeed, the Δm , at the end of the redox cycling is positive, signifying that some of the ionic species injected into the polymer are permanently incorporated.

3.6 Differential Scanning Calorimetry

To have an additional proof of the permanent immobilization of the sulfated β -CD into the polymer matrix, differential scanning calorimetry (DSC) experiments were performed. This technique was also employed to verify if a

reduced sample of ppys β -CD contained more water with respect to an oxidized polymer, as asserted in Section 3.5.2.

Prior to DSC measurements, the polymeric samples were dried in an oven at 50 °C, for 96 h to remove any excess water. In the DSC apparatus all samples were first held at a constant temperature of 50 °C for 5 min and then heated up to 400 °C, at a sweep rate of 10 °C min⁻¹. It is important to highlight that all the experiments were performed under N₂ atmosphere to prevent oxidation phenomena.

In Figure 3.28, a thermogram of the s β -CD is displayed. The first broad endothermic peak, from 50 to 120 °C, with a maximum around 82 °C was due to loss of water from the sample. A second endothermic peak is observed between 235 and 280 °C, with a maximum at 254 °C. This is seen more clearly in Figure 3.29. This endothermic peak is probably related to the decomposition of the CD. This deduction is in accord with the literature. For example, Veiga *et al.*,³⁶ in their thermal study of cyclodextrin derivatives, stated that cyclodextrins undergo decomposition above 240 °C. The sharp exothermic peak at 210 °C seems to be related to the presence of impurities in the s β -CD powder. As a matter of fact, if the thermogram of the sample is compared with a purified s β -CD powder, it is easy to notice that the exothermic peak is markedly reduced, as illustrated in Figure 3.30. The procedure used to purify the s β -CD and the relative impurities is presented in Section 2.2.1.

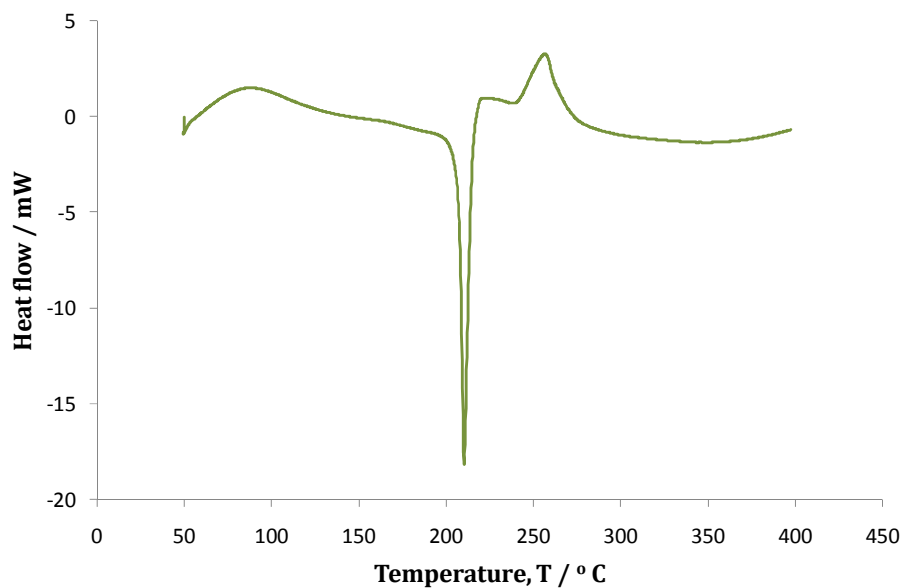


Figure 3.28: DSC of 3.50 mg sample of s β -CD, isothermal pretreatment at 50 °C for 5 min. Temperature was scanned from 50 up to 400 °C at a sweep rate 10 °C min⁻¹.

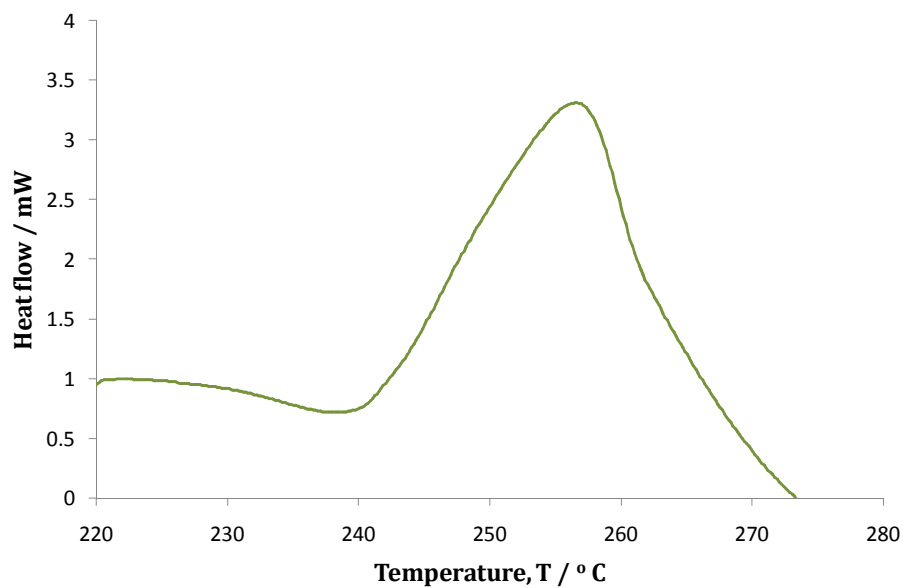


Figure 3.29: Magnification of Figure 3.28 in the temperature interval of 220 to 270 °C.

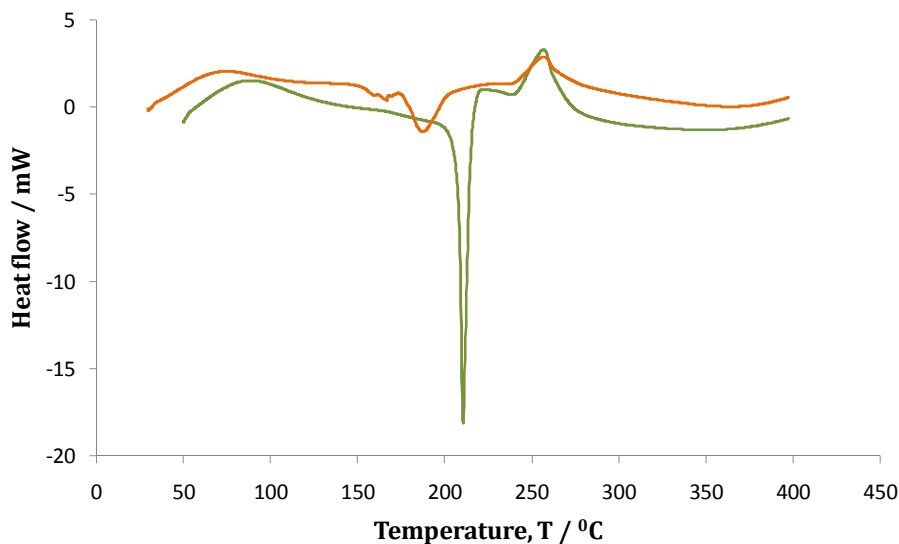


Figure 3.30: DSC of 3.50 mg of $s\beta$ -CD, isothermal pretreatment at 50 °C for 5 min. Temperature scanned from 50 up to 400 °C at a sweep rate 10 °C min⁻¹ — and DSC 2.0 mg of a purified sample of $s\beta$ -CD, with an isothermal pretreatment at 30 °C for 5 min. Temperature scanned from 50 up to 400 °C, sweep rate 10 °C min⁻¹ — .

Next, the thermal properties of ppys β -CD were investigated and compared to the thermal properties of ppyCl. Typical thermograms are depicted in Figure 3.31. The most important characteristic of the thermogram recorded for ppys β -CD is the presence of a broad endothermic peak between 170 and 370 °C, which is absent in the corresponding polymer doped with chloride anions. This peak is similar to the peak found for the $s\beta$ CD decomposition, shown in Figure 3.29. However, this peak is broader in the polymer sample, but it must be stressed that a DSC analysis considers a sample in its environment and the $s\beta$ -CD molecules within the film are surrounded by the ppy backbone. It is reasonable to expect that the decomposition of $s\beta$ -CD will be somewhat different when immobilized within the polymer matrix and when in a pure sample.

Another remarkable aspect evident from Figure 3.31 is the different water contents of the two polymers. Matveeva *et al.*³⁷ have suggested for polyaniline that the polymer contains water molecules bound in several ways. The residual water on the polymer surface can be easily removed by conventional drying, for example in an oven or in a flow of dried nitrogen. Then, water more strongly

bound can only be drawn off by means of high temperatures. Finally, irreversible absorbed water does not leave the polymer until it is thermally decomposed. As the ppys β -CD films were heated for 96 h at 50 °C, before thermal analyses, any residual water will be lost. Accordingly, the endothermic peak centred at about 90 °C can be attributed to strongly bound water. The water content for the pppys β -CD film is significantly higher than that of the ppyCl film, suggesting less strongly bound water in the later polymer film.

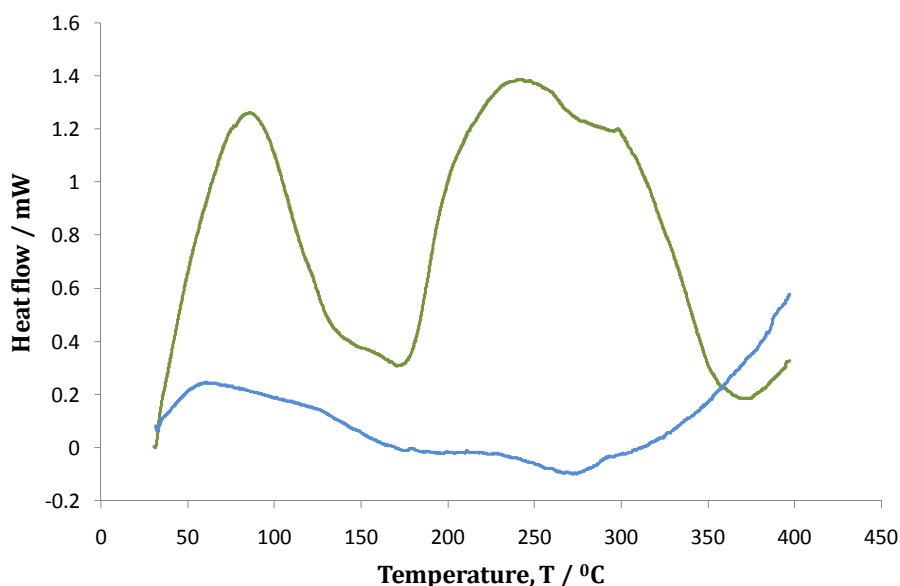


Figure 3.31: DSC of 1.50 mg sample of ppys β -CD —, and 1.60 mg sample of ppyCl —, isothermal pretreatment at 30 °C for 5 min. Temperature was scanned from 30 to 400 °C, at a sweep rate of 10 °C min⁻¹; ppys β -CD was synthesized from 0.20 M pyrrole and 0.02 M s β -CD and ppyCl was synthesized from 0.20 M pyrrole and 0.10 M NaCl, at 0.7 V vs SCE on a Pt electrode, (d = 4 mm), t = 60 min.

Concerning the ppyCl system, the data presented in Figure 3.31 are in good agreement with the literature.^{10,38} Chandrasekhar¹⁰ reported that exothermic transitions of ppy appeared to be related to a relaxation in the conducting polymer structure. In Figure 3.31 a broad exothermic transition of small magnitude is observed between 250 and 300 °C, consistent with the exothermic relaxation. In Figure 3.32, thermograms for both the reduced and oxidized ppys β -CD films are presented. Both samples were dried in an oven, at 50 °C for 96 h. As evident from Figure 3.32, the amount of water lost from the reduced

polymer is significantly higher and hence the DSC data are consistent with the incorporation of water within the polymer matrix as the films are reduced. When the polymer is reduced, the conformational rearrangement in its structure may allow the injection of more water molecules belonging to the solvation shell of the Na^+ . This supports the discussion in Section 3.4.2.

These DSC investigations clearly confirm the presence of the $\text{s}\beta\text{-CD}$ anions within the polypyrrole matrix and provide additional support for the incorporation of water into the polymer matrix as the films are reduced.

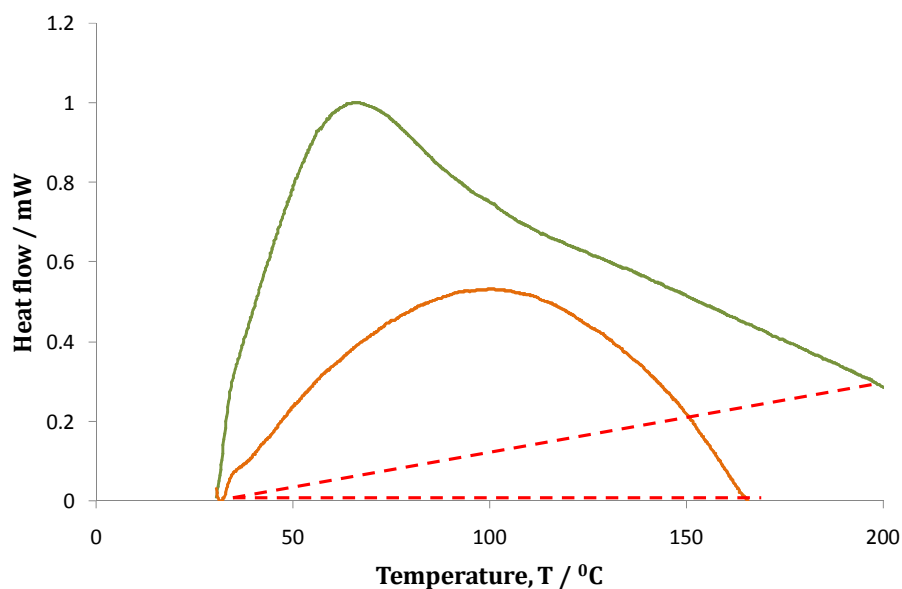


Figure 3.32: DSC of 2.10 mg sample of ppys β -CD reduced in 0.10 M NaCl at -0.6 V vs SCE for 30 min — and DSC of 2.10 mg sample of ppys β -CD in the oxidized state at 0.7 V vs SCE —. The ppys β -CD films were synthesized from 0.20 M pyrrole and 0.02 M $\text{s}\beta\text{-CD}$ at 0.7 V vs SCE on a Pt electrode, ($d = 4$ mm), $t = 60$ min.

3.7 Capacitance study

3.7.1 Cyclic Voltammetry

As evident in Figures 3.19 and 3.20, the background current in the cyclic voltammograms is large, indicating a high charging capacitance for the ppys β -CD films. The capacitance of ppys β -CD was determined and compared with

ppyCl using the relationship in Equation 3.20. In this equation, C represents the capacitance in F cm^{-2} , I is the current density in A cm^{-2} and dV/dt is the scan rate in mV s^{-1} .³⁹

$$I = C \frac{dV}{dt} \quad 3.20$$

Both polymers were grown to a charge of $1.98 \times 10^{-2} \text{ C cm}^{-2}$ and conditioned in 0.10 M NaCl, for 10 cycles, in a potential window from 0.7 to -1.0 V vs SCE. Then, they were cycled in 0.10 M NaCl at different scan rates of 5, 25, 50, 75, 100, 125, 150 and 200 mV s^{-1} . The electrochemical window was reduced to 0.15 to 0.25 V vs SCE, to avoid any faradaic currents and the current was read at 0.20 V vs SCE. The current recorded at 0.20 V was plotted as a function of the scan rate.

Representative current-scan rate plots are shown in Figure 3.33 (a) and (b) for polymers grown on gold and GC substrates, respectively. Good linear relationships are observed for all plots. Clearly, the capacitance values of ppys β -CD and ppyCl electrosynthesized on GC are very similar. Using Equation 3.20, a capacitance value of $1.09 \times 10^{-5} \text{ F cm}^{-2}$ is computed for ppys β -CD and a value of $1.01 \times 10^{-5} \text{ F cm}^{-2}$ for ppyCl, with correlation coefficients of 0.992 and 0.982, respectively. By contrast, the polymers behave moderately different when a gold electrode is used as the substrate. Ppys β -CD exhibits a capacitance of $1.94 \times 10^{-6} \text{ F cm}^{-2}$, with a correlation coefficient of 0.992 and ppyCl a capacitance of $1.29 \times 10^{-6} \text{ F cm}^{-2}$, with a correlation coefficient of 0.999. Furthermore, the capacitance of the polymers on GC is an order of magnitude higher with respect to the gold substrate. This suggests that the charge storage properties of the polymers grown to a charge/thickness of $1.98 \times 10^{-2} \text{ C cm}^{-2}$, depends on the nature of the substrate. Indeed, when the experiment was repeated using polymers ten times thicker, i.e., grown to charges of $1.98 \times 10^{-1} \text{ C cm}^{-2}$, the capacitance of the ppys β -CD was found to be $1.20 \times 10^{-3} \text{ F cm}^{-2}$, while for ppyCl a value of $6.10 \times 10^{-4} \text{ F cm}^{-2}$ was determined.⁴⁰

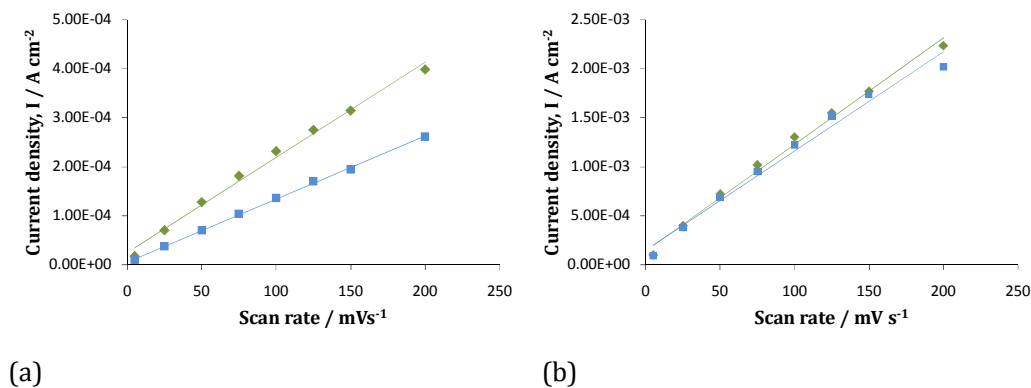


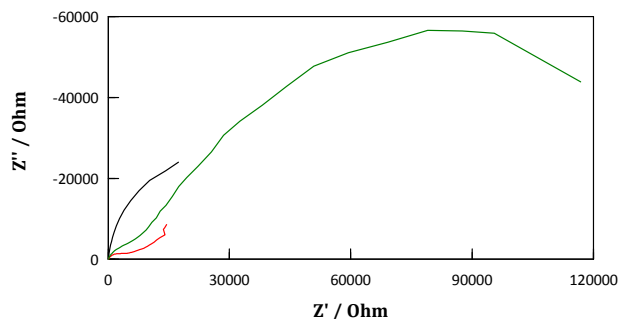
Figure 3.33: Current density measured at 0.20 V for ppyCl — and ppys β -CD — obtained from CVs recorded in 0.10 M NaCl as a function of the scan rate. Gold (a) and GC (b) substrates. Polymers were first conditioned in 0.10 M NaCl by cycling from 0.7 V to -1.0 V vs SCE for 10 cycles and then cycled between 0.15 and 0.25 V vs SCE to give the data in (a) and (b). The ppys β -CD films were grown at 0.7 V to a charge of 2.50×10^{-2} C on a GC electrode ($d = 4$ mm) or gold electrode ($d = 3$ mm), ppyCl was synthesized from 0.20 M pyrrole and 0.10 M NaCl, ppys β -CD was synthesized from 0.20 M pyrrole and 0.02 M β -CD. Applied potential is relative to the SCE reference.

The fact that the capacitance for the polymer doped with the anionic CD is higher indicates that more negative charge is stored within the ppys β -CD films. As a consequence more cations are attracted to the polymer surface. This is in good agreement with recent reports by Suematsu *et al.*⁴¹ who investigated the properties of ppy films doped with naphthalene rings substituted with sulfated groups. They found that a polymer doped with the tri-sulfated dopant had a higher capacitance than the di- or mono- sulfated naphthalene doped films. They attributed the larger capacitance to the presence of free sulfated groups in the film, which in turn enhance the concentration of cationic species bound within the polymer matrix. Ingram *et al.*⁴² worked with similar dopants and synthesized thick ppy films, of 10 μm , to employ in electrochemical supercapacitors. They showed that the polymers had a structure that enabled the rapid insertion and ejection of ionic species from the aqueous solution.

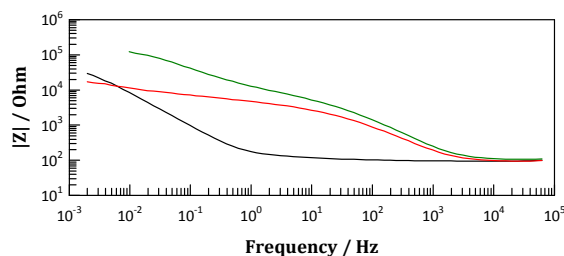
3.7.2 *Electrochemical Impedance Spectroscopy*

A complementary study on the ability of the ppys β -CD film to store charge was performed by means of electrochemical impedance spectroscopy. Again, the results were compared with those obtained for a corresponding polymer doped with chloride anions. Representative impedance plots, shown in the complex plane (Nyquist) and Bode formats, with the modulus of the impedance, Z , and phase angle presented as a function of frequency, are shown in Figure 3.34 (a), (b) and (c), respectively, for ppys β -CD films under open-circuit conditions, and polarized at -0.8 and 0.7 V vs SCE. In all cases, the data were recorded following a 60 min polarization period at the desired potential. Clearly, the applied potential, and in turn the oxidation state of the ppys β -CD, has a significant influence on the impedance response. The impedance profile changes from a simple one-time constant model when the polymer is reduced to a two-time constant model when the polymer is oxidized at 0.7 V vs SCE.

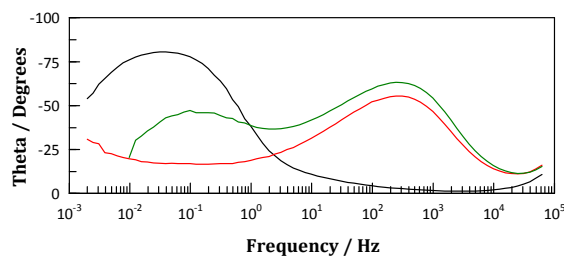
These data were fitted to the equivalent circuits depicted in Figure 3.35. The circuit shown in (a) was used to fit the experimental data when the ppys β -CD films were maintained in the oxidation state, while the simple Randles cell, presented in (b), was used to model the data when the polymer was reduced, or partially reduced. In these circuits, R_1 represents the solution resistance, R_2 represents the charge-transfer resistance, while CPE1 and CPE2 are constant phase elements.



(a)



(b)



(c)

Figure 3.34: Complex Plane (or Nyquist) plot (a), Bode plot (b) and (c) for ppys β -CD recorded in 0.10 M NaCl using a perturbation amplitude of 5.00 mV, measured at open circuit potential —, at a potential of -0.8 V — and 0.7 V —. The ppys β -CD films were synthesized at 0.7 V on a GC electrode ($d = 4$ mm) to charge 2.50×10^{-2} C. Applied potential is relative to the SCE reference.

CPEs are used frequently in fitting impedance data and are generally attributed to distributed surface reactivity, surface inhomogeneity, roughness or fractal geometry and electrode porosity.^{39,43} Mathematically, the impedance of the CPE is given by Equation 3.21, where Z is the impedance, Y is the admittance, ω is the angular frequency ($\omega = 2\pi f$, f being the frequency), n represents an exponent and Q gives the magnitude of the CPE element. When n is equal to 1.0, then Q^0 is

equal to the capacitance of the system and the CPE resembles a capacitor. Alternatively, when n approaches 0.5, then the CPE represents a diffusion controlled process.^{44,45}

An example of the fitting for the impedance of the ppys β -CD films, and the associated errors, is shown in Figure 3.36. In general, the errors were confined to < 8%. If errors, higher than 8% were achieved, then an alternative circuit was considered. In addition, all data were recorded under conditions, where steady-state, or near steady-state conditions, were maintained throughout the duration of the measurement.

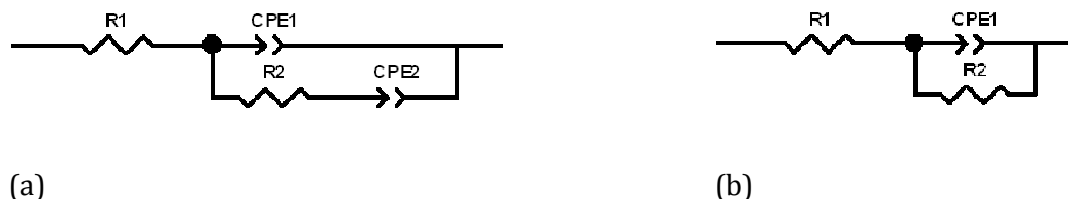
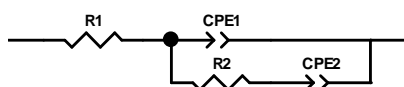


Figure 3.35: Equivalent circuits used to fit the data presented in Figure 3.34.



Element	Freedom	Value	Error	Error %
R1	Free(+)	101	0.99878	0.98889
CPE1-T	Free(+)	0.00040908	1.6133E-5	3.9437
CPE1-P	Free(+)	0.73392	0.0070159	0.95595
R2	Free(+)	610.2	40.762	6.6801
CPE2-T	Free(+)	0.00062241	2.285E-5	3.6712
CPE2-P	Free(+)	1.051	0.022826	2.1718

Figure 3.36: Data fitting routine, circuit parameters, values and errors.

The steady-state conditions were probed by collecting the impedance spectra as a function of time and comparing the circuit parameters. An example is presented in Table 3.14, which shows the magnitude of R1, CPE (Q and n) and

R2 for ppys β -CD films polarized at -0.5 V vs SCE in 0.10 M NaCl for three consecutive experiments, Exp 1, Exp 2 and Exp 3. The ppys β -CD film was polarized at -0.5 V vs SCE for 60 min before the first impedance measurement was made. As clearly evident from this analysis, the circuit parameters remain nearly constant, suggesting good stability and the establishment of steady-state conditions following a 60 min polarization period in the chloride supporting electrolyte.

Table 3.14: Circuit parameters (derived from Figure 3.35 (b)) for ppys β -CD, synthesized at 0.7 V vs SCE, 2.50×10^{-2} C, on a GC electrode ($d = 4$ mm) and then polarized at -0.5 V vs SCE for 60 min in 0.10 M NaCl; impedance data, Exp 1, 2 and 3, were recorded in 0.10 M NaCl at -0.5 V vs SCE using a perturbation amplitude of 5.0 mV.

ppys β CD	R1 / Ω	Q / F cm $^{-2}$	n	R2 / Ω
Exp 1	107	1.79×10^{-3}	0.93	24127
Exp 2	107	1.75×10^{-3}	0.83	20708
Exp 3	103	1.72×10^{-3}	0.83	18911

The impedance response of ppys β -CD films deposited onto GC electrodes was recorded as a function of the applied potential to probe the properties of the polymer at different levels of oxidation and reduction. The impedance data were fitted to the equivalent circuits shown in Figure 3.35. The data presented in Figure 3.37 show the capacitance of the ppys β -CD film (Q with $n \cong 1.0$) as a function of the applied potential, between 0.1 and 0.7 V vs SCE. The traces represented by the closed symbols show the variation of both CPE1 and CPE2, (derived from the circuit on the right of Figure 3.37), as a function of the applied potential. Both CPE1 and CPE2 remain essentially constant between 0.1 and 0.5 V vs SCE, reaching a capacitance value of about 5.00×10^{-3} F cm $^{-2}$, indicating a high charging capacitance. However, there is a considerable drop in the capacitance, as the potential is increased above 0.5 V vs SCE, reaching values as low as 1.00×10^{-5} F cm $^{-2}$ at 0.7 V vs SCE. This drop in the capacitance is consistent with the over-oxidation of the polypyrrole matrix⁴⁶, resulting in the

formation of a less conducting polymer substrate. Interestingly, identical impedance and capacitance values were determined by switching the ppys β -CD film between 0.1 and 0.5 V vs SCE. However, this was not the case when the potential was switched from 0.5 to 0.7 and back to 0.5 V vs SCE, as indicated by the additional points presented in Figure 3.37. In this case, there is a considerable reduction in the CPE1 element, after polarization at 0.7 V vs SCE, which clearly shows that the over-oxidation of the ppys β -CD is irreversible. A similar effect was observed on switching the polymer between 0.1 and 0.7 V vs SCE and back to 0.1 V vs SCE.

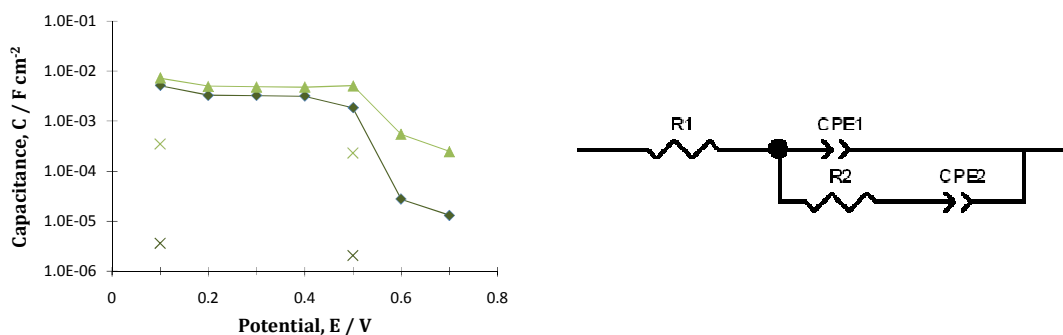


Figure 3.37: Capacitance, CPE1 — CPE2 —, and the equivalent circuit used in fitting, for ppys β -CD polarized at different potentials following a 60 min pre-polarization period. Data recorded by switching the applied potential from 0.5/0.1 to 0.7 V and then back to 0.5 and 0.1 V vs SCE (x, x). The ppys β -CD film was synthesized at 0.7 V, to a charge of 2.50×10^{-2} C from 0.20 M pyrrole and 0.02 M s β -CD. Applied potential is relative to the SCE reference.

A similar analysis recorded at more negative potentials is presented in Figure 3.38. In this case, the impedance data were fitted to the circuit depicted in Figure 3.35 and shown on the right in Figure 3.38. Again, the capacitance is essentially constant between -0.2 and -0.5 V vs SCE, reaching values of about 1.80×10^{-3} F cm⁻². Again, these high values are consistent with the charging capacitance of conducting polypyrrole.⁴⁷ As the potential is reduced further to -0.8 V vs SCE, there is a reduction in the charging capacitance. This is consistent with the formation of the reduced ppy⁰s β -CD·Na⁺ film, which is less conducting than the oxidized film. The transition observed after -0.5 V vs SCE is in good agreement with the CV data presented in Figure 3.19, which show the reduction

of the ppys β -CD film at potentials in the vicinity of -0.7 V vs SCE. In contrast to the data presented in Figure 3.37, the ppys β -CD film can be readily reversed from the reduced to the oxidized or partially oxidized state by switching the applied potential from -0.7 to -0.5 V vs SCE, as shown in Figure 3.38. Nearly identical capacitance values were recorded at -0.5 V vs SCE prior to and after reduction of the ppys β -CD film.

This high degree of reversibility is clearly evident in Figure 3.39. In this case, impedance data were recorded by switching the applied potential between the limits of 0.4 and -0.8 V vs SCE, as shown by the numbers added to Figure 3.39. Here, 1 represents the 1st experiment recorded at -0.2 V vs SCE, followed by data recorded at -0.5 V vs SCE, designated as 2, with the labels 3 to 6 showing the order of the subsequent experiments, which are all recorded with the same polymer. In each case, the impedance data were recorded following a pre-polarization period of 60 min at the required potential in order to achieve steady-state conditions. It is clearly evident that complete reversibility is achieved in the potential window spanning from -0.8 to 0.4 V vs SCE.

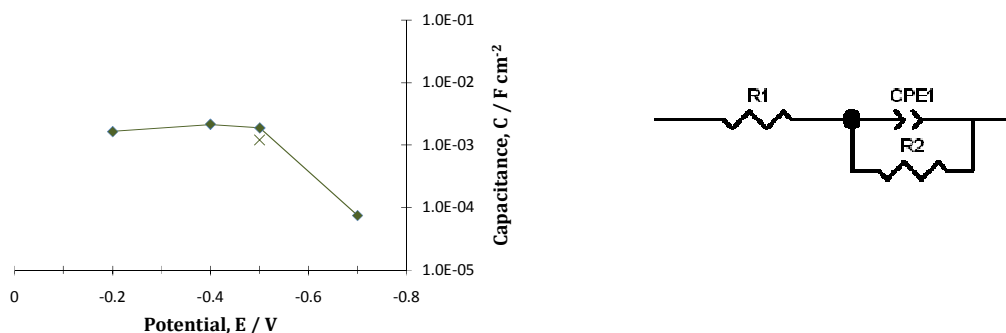


Figure 3.38: Capacitance values, CPE1 —, and equivalent circuit used in fitting, recorded as a function of the applied potential following a 60 min pre-polarization period, for ppys β -CD. Data recorded by switching the applied potential from -0.5 to -0.7 V and then back to -0.5 V (x). The ppys β -CD film was synthesized at 0.7 V vs SCE, to a charge of 2.5×10^{-2} C from 0.20 M pyrrole and 0.02 M s β -CD. Applied potential is relative to the SCE reference.

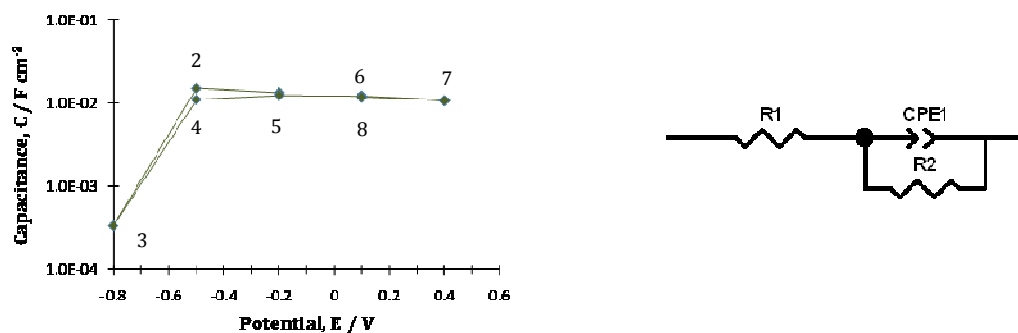


Figure 3.39: Capacitance, CPE1 —, and equivalent circuit used in fitting, for ppys β -CD recorded as a function of the applied potential following a 60 min pre-polarization period at each potential. The labels, 1 to 6, show the order of the experiments, with the polymer first polarized at -0.2 V and then switched to -0.5 , -0.8 , -0.5 , -0.2 , 0.2 , 0.4 and 0.2 V. The ppys β -CD film was synthesized at 0.7 V, to a charge of 2.50×10^{-2} C from 0.20 M pyrrole and 0.02 M s β -CD. Applied potential is relative to the SCE reference.

A similar analysis was performed on the ppyCl system and these data are presented in Figures 3.40 and 3.41. Figure 3.40, which is related to Figure 3.37 for the ppys β -CD, shows the variation of CPE1 and CPE2 as a function of the applied potential. Again, the capacitance is high and nearly constant between 0.1 and 0.6 V vs SCE, but is reduced considerably when the polymer is polarized at 0.7 V vs SCE, signifying the over-oxidation of the ppyCl. The magnitude of the CPE2 values is similar to that obtained with the ppys β -CD. However, the CPE1 values, which represent the charging capacitance of the polymer are somewhat lower for the ppyCl compared to the ppys β -CD films. It is also evident from a comparison of Figure 3.37 and 3.40 that the ppys β -CD film is over-oxidized at a lower potential of about 0.6 V vs SCE compared to 0.7 V vs SCE for the ppyCl system. Again, the over-oxidation of the ppyCl electrode is irreversible as shown by the additional points added to Figure 3.40 which were recorded after the polymer was subjected to 0.7 V vs SCE for 60 min and over-oxidized. As evident in Figure 3.41, there is a reduction in the CPE1 value as the applied potential is lowered from -0.2 to -0.5 V vs SCE. This corresponds to reduction of the ppyCl to form a more insulating polymer layer. This is in good agreement with the CVs shown in Figure 3.19, where the reduction wave is centred at approximately

-0.35 V vs SCE. On comparing Figure 3.41 with Figure 3.38, it is clear that the ppys β -CD film remains highly conducting at -0.5 V vs SCE, while the ppyCl film is partially reduced to give a more insulating polymer.

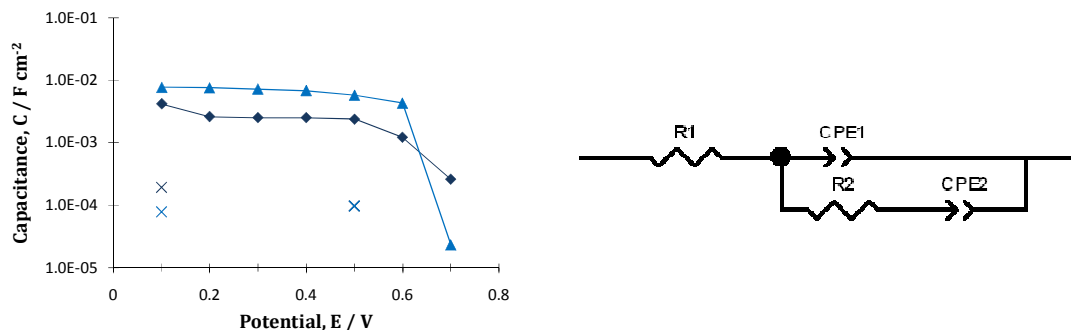


Figure 3.40: Capacitance values, CPE1 — CPE2 — and equivalent circuit used in fitting, for ppyCl recorded as a function of the applied potential following a 60 min pre-polarization period. Data recorded by switching the applied potential from 0.5/0.1 to 0.7 V and then back to 0.5 and 0.1 V (x, x). The ppyCl was synthesized at 0.7 V, to a charge of 2.50×10^{-2} C from 0.20 M pyrrole and 0.10 M NaCl. Applied potential is relative to the SCE reference.

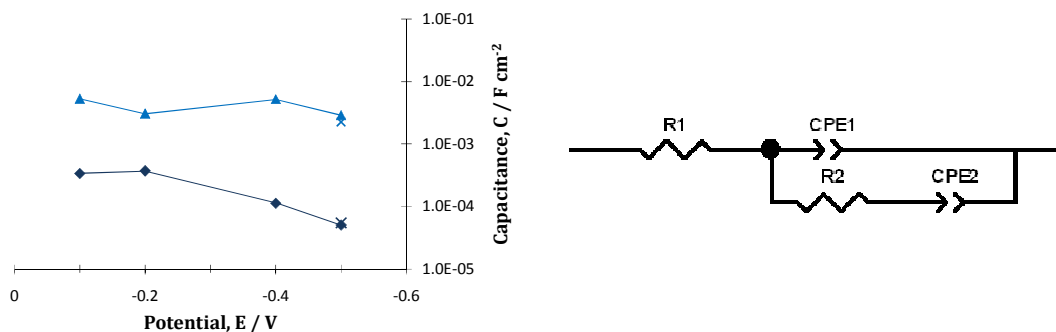
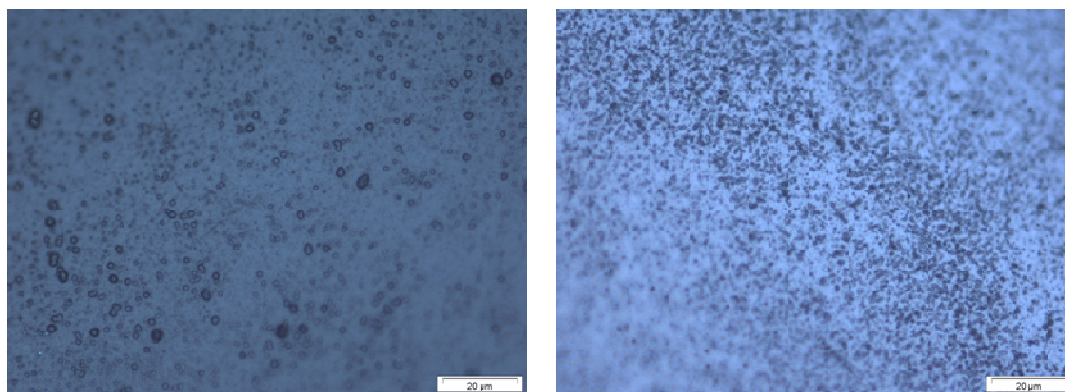


Figure 3.41: Capacitance values, CPE1 — CPE2 —, and equivalent circuit used in fitting, for ppyCl recorded as a function of the applied potential following a 60 min pre-polarization period. Data were recorded by switching the applied potential from -0.1 to -0.6 V and then the measurement was repeated at -0.5 V (x, x). The ppyCl was synthesized at 0.7 V, to a charge of 2.5×10^{-2} C from 0.20 M pyrrole and 0.10 M NaCl. Applied potential is relative to the SCE reference.

3.8 Morphology

Optical imaging techniques were performed on various polymers to obtain information on the morphology of the polymer. Films of polypyrrole doped with either β -CD or chloride anions were electrosynthesized and subsequently washed thoroughly with distilled water in order to remove any NaCl crystals or cyclodextrin molecules adsorbed on the modified electrode surface. Prior to the analysis, the polymers were dried by exposure to a gentle air flow, for 30 s. Optical images recorded for films of 0.20 C cm⁻² and 2.00 C cm⁻² thickness are shown in Figures 3.42 and 3.43, respectively. On thin polymers, Figure 3.42, no significant differences in the film morphology of ppyCl and ppys β -CD are observed. Small globular particles are evident with both polymers. On the other hand, when the thickness is increased by a factor of ten, the typical cauliflower structure is evident for both polymers, as illustrated in Figure 3.43 (a) and (b). In general, ppy films present a *cauliflower*-like morphology constituted by micro-spherical grains. It has been documented that such a particular structure is related to the dopant intercalation difficulty in the disordered polymeric chain.^{48,49} Interestingly, in the case of ppys β -CD the cauliflower structure behaves in a more organized manner as apparent from Figure 3.43 (a). The ppyCl micro grains are more randomly organized, with a larger variation in size and thickness as evidenced by the non focused areas in Figure 3.43 (b).

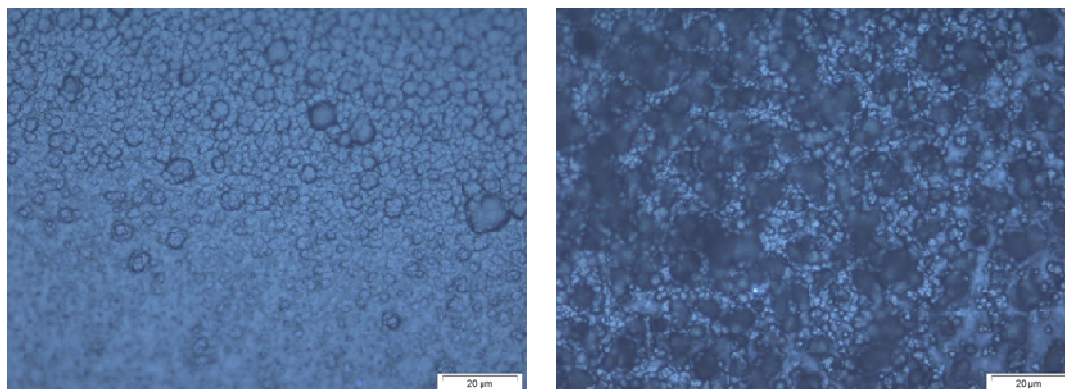
The globular particles seem to grow on a primary ppy layer, previously deposited. This is in agreement with the work of Suarez and Compton.³³ They made an *in-situ* atomic force microscopy study of polypyrrole synthesis suggesting two stages for ppy growth. The initial deposition of the polymer is essentially a two-dimensional process and the growth of the globular areas occurs after the formation of a thin polymer layer. A number of efforts have been directed towards the development of orientated and ordered structures in conducting polymers, in order to improve the conductivity, although this is very difficult. Some crystalline micro-islands have been observed on thin films at the initial state of electropolymerization^{50,51} and some molecular order for certain ppy thick films has been reported on the basis of X-ray analysis and neutron scattering experiments.^{52,53}



(a)

(b)

Figure 3.42: Optical images of ppysβ-CD (a) and ppyCl (b) on GC. Polymers were electrochemically deposited from aqueous solutions of 0.02 M sβ-CD and 0.10 M NaCl, in the presence of 0.20 M pyrrole at 0.7 V vs SCE to a charge of $2.00 \times 10^{-1} \text{ C cm}^{-2}$.



(a)

(b)

Figure 3.43: Optical images of ppysβ-CD (a) and ppyCl (b) on GC. Polymers were electrochemically deposited from aqueous solutions of 0.02 M sβ-CD and 0.10 M NaCl in the presence of 0.20 M pyrrole at 0.7 V vs SCE to a charge of 2.00 C cm^{-2} .

To overcome the lack of magnification and the difficulty in focusing the optical images, scanning electron microscopy (SEM) was also used to study the morphology. Typical SEM micrographs are shown in Figure 3.44 (a) and (b) for the ppysβ-CD and ppyCl films. In this case, the films were grown to a charge of $2.30 \times 10^{-1} \text{ C cm}^{-2}$ and then the surface was sputtered with a thin layer of gold.

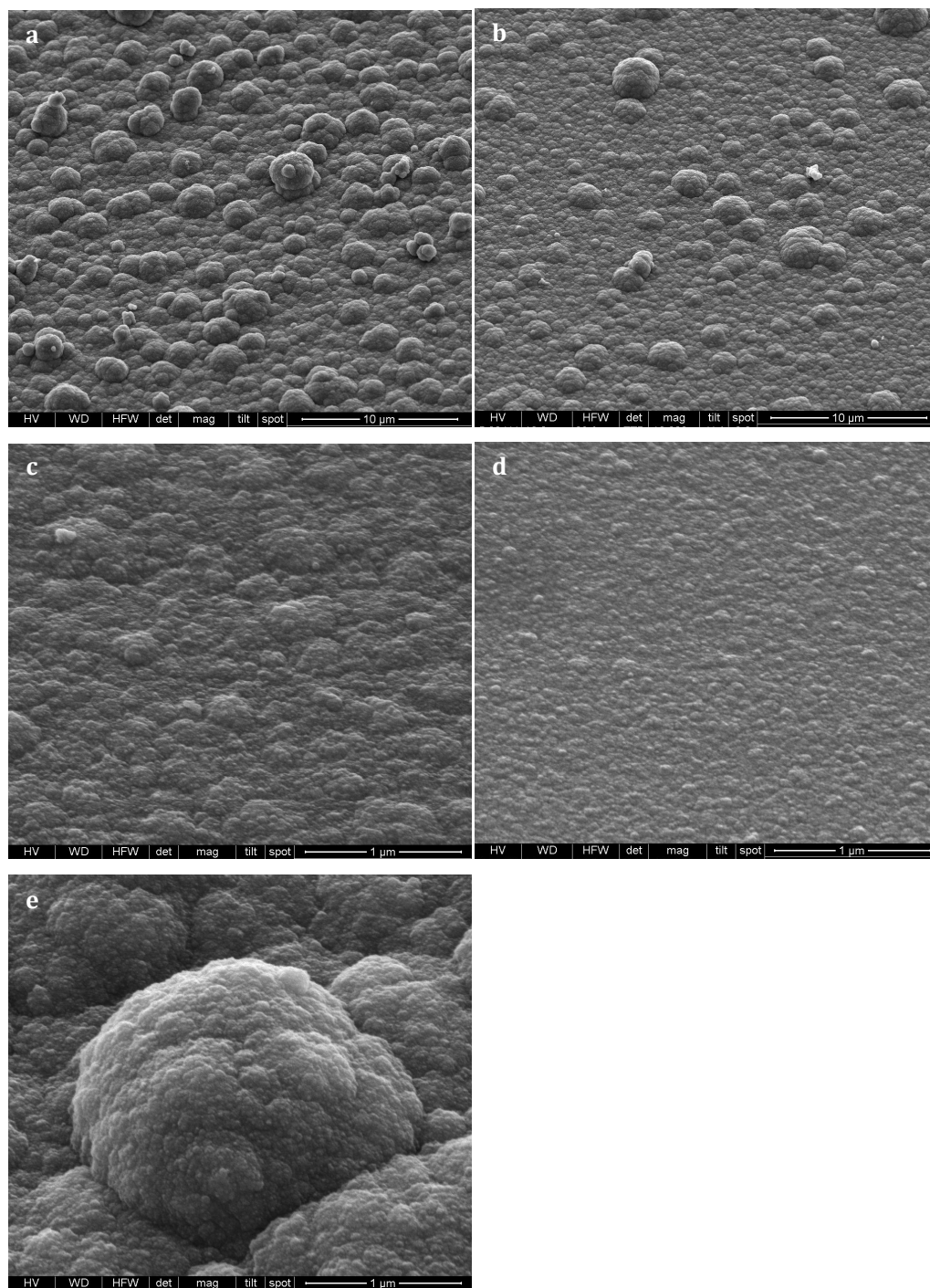


Figure 3.44: SEM micrographs of ppys β -CD films electrochemically deposited on GC from aqueous solutions of 0.02 M β -CD in the presence of 0.20 M py at 0.7 V vs SCE to a charge of 1.13 C cm⁻² (a) and (e), to a charge of 3.50×10^{-1} C cm⁻² (c) and to a charge of 9.80×10^{-2} C cm⁻² (d); ppyCl deposited under identical conditions from 0.20 M py/0.10 M NaCl to a charge of 1.13 C cm⁻² (b).

The cauliflower-like structure is clearly evident in these SEM micrographs. On comparing the micrographs of the ppys β -CD and ppyCl films, it is clear that the distribution of the globular particles is more homogeneous in the polymer doped with the large macrocycle. This aspect highlights again the importance of the dopant. Other authors who have investigated the morphology of ppy films doped with cyclodextrins have also observed a different organizational mode in comparison to ppy films doped with small anions.^{6,54} In Figure 3.44 (c), (d) and (e) it is interesting to observe how the morphology is influenced by the thickness of the polymer. The three pictures show identical magnification for three polymers grown to different charge. The characterization studies discussed in the previous sections of this chapter were done employing a polymer exhibiting the thickness and the morphology illustrated in Figure 3.44 (d). As the thickness increases this leads to growth of the globular particles, Figure 3.44 (d) and (e), in agreement with what Suarez and Compton postulated.³³

3.9 Preliminary study on polypyrrole doped with carboxymethyl β -cyclodextrin (ppyCM β -CD)

3.9.1 Introduction

As introduced in Section 3.1, a carboxymethyl β -cyclodextrin sodium salt was also used as a dopant anion. This CD was chosen as it contains an average of 3.5 carboxylated groups per CD molecule, and accordingly has a much lower charge density compared to the sulfated β -cyclodextrin sodium salt. This salt was dissolved in water, in the presence of pyrrole and used to form a new conducting polypyrrole film (ppyCM β -CD). Kaniewska *et al.*⁵⁵ have immobilized the carboxymethyl β -CD (CM β -CD) in a polyvinylchloride membrane in order to create a new chiral potentiometric sensor. They dissolved all the required components in THF and obtained the membrane by evaporation of the solvent. To the best of our knowledge, no publications have been reported on the immobilization *via* electrodeposition of a carboxymethyl β -cyclodextrin (CM β -

CD) in a conducting polymer matrix. Here, results are presented and discussed for the electrosynthesis and characterization of this new conducting, ppyCM β -CD film.

3.9.2 Electrosynthesis

The same method employed to electrochemically synthesize ppys β -CD was applied to generate the new polymer, but the experimental parameters were slightly altered to give efficient electropolymerization. Polypyrrole was deposited at an applied potential of 0.80 V vs SCE from a 0.30 M solution of pyrrole monomer and 0.02 M CM β -CD sodium salt. The pH of the solution was adjusted to 4.0 with a small volume of H₂SO₄. The concentration of pyrrole was increased from 0.20 M to 0.30 M and the pH reduced to facilitate electropolymerization, otherwise the growth of the polymer was too slow. In Figure 3.45, a plot representing the synthesis of ppyCM β -CD is shown. The current is plotted on the y-axis as a function of the time of electropolymerization.

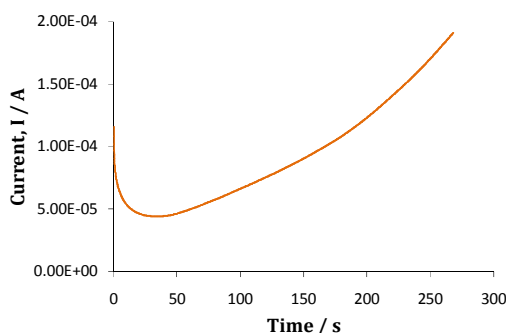


Figure 3.45: Current-time plot for the electropolymerization of pyrrole from a solution of 0.30 M pyrrole and 0.02 M CM β -CD at pH 4.0 at an applied potential of 0.80 V vs SCE on GC (d = 4 mm) until a charge of 2.50×10^{-2} C was consumed.

By comparing Figure 3.45 with Figure 3.3, it is clearly evident that the electropolymerization proceeds significantly slower in the presence of the CM β -CD anions compared to the s β -CD anions. One of the possible reasons could be the different ionic strength of the electropolymerization solutions, which was 0.56 M for a solution of 0.02 M s β -CD and 0.16 M for a 0.02 M CM β -CD solution. As a matter of fact, the conductivity of the 0.02 M s β -CD solution was found to be

7.62 mS at 23.5 °C compared to 3.10 mS measured for a 0.02 M solution of CM β -CD. Clearly, the conductivity has a role to play in the lower rate of electropolymerization observed for the ppyCM β -CD system.

Another important difference between the growth of ppys β -CD and ppyCM β -CD is the shape and profile of the current-time plot. Figure 3.45 shows that the current only begins to increase after 40 s and then the rate of the current increase is slow extending from 40 to 250 s. This indicates a slow nucleation process for the ppyCM β -CD film followed by a slow growth of the polymer on the deposited ppyCM β -CD at the electrode interface. On the other hand, the nucleation process is rapid in the case of ppys β -CD, while the current of electropolymerization reaches a quasi-plateau level after the first 15 s, as depicted in Figure 3.3. Finally, the overall current generated in the deposition of ppyCM β -CD is considerably lower, reaching a final value of 1.91×10^{-4} A, despite a current of 1.00×10^{-3} A recorded for ppys β -CD, Figure 3.3. As the ppys β -CD film was formed at a pH of 5.0 and from 0.20 M pyrrole, the ppys β -CD film was electrosynthesised under the conditions used for the ppyCM β -CD, to verify if the modified parameters of pH and pyrrole concentration had any influence on the electropolymerization of ppys β -CD. Current-time profiles similar to those illustrated in Figure 3.3 were obtained. However, the lower pH and higher pyrrole concentrations gave rise to an increase in the rate of polymer deposition.

In conclusion, although the rate of electropolymerization of the ppyCM β -CD is slower than the ppys β -CD system, it is clear from the data presented in Figure 3.45 that pyrrole can be successfully electropolymerized in the presence of the CM β -CD anions without a supporting electrolyte.

3.9.3 Diffusion and Rate Constant

To study the properties of ppyCM β -CD towards the diffusion of an analyte and the ability to transfer electric charge, the diffusion coefficient, D , and the rate constant, k , were evaluated. Again, the ferri/ferrocyanide was employed,

following the procedure described in Section 3.3.1. By plotting the peak current for the reduction of $\text{Fe}(\text{CN})_6^{3-}$ to give $\text{Fe}(\text{CN})_6^{4-}$ as a function of the square root of the scan rate, a linear plot was obtained, as shown in Figures 3.46. From the slope of the plot it was possible to calculate the diffusion coefficient, D , for the $\text{Fe}(\text{CN})_6^{3-}$ species using the Randles-Sevcik relation (Equation 3.4).

The calculated diffusion coefficient, D , for ppyCM β -CD was $3.00 \times 10^{-6} \text{ cm}^2 \text{ s}^{-1}$. This value is somewhat lower than the values found for ppyCl and ppys β -CD, Table 3.1. Indeed, as highlighted in Table 3.15, the diffusion coefficient at the ppyCM β -CD film is similar to that measured at the bare GC electrode. This may indicate a difference in the roughness and porosity of the ppyCM β -CD in comparison to the ppyCl and ppys β -CD electrodes. Another important aspect of this analysis is the existence of an intercept for the Randles-Sevcik plot, Figure 3.46 and Table 3.15. The fact that the linear plot does not pass through the origin is evidence of kinetic limitations.¹⁴ This is in agreement with the results presented for the ppys β -CD system, Table 3.1.

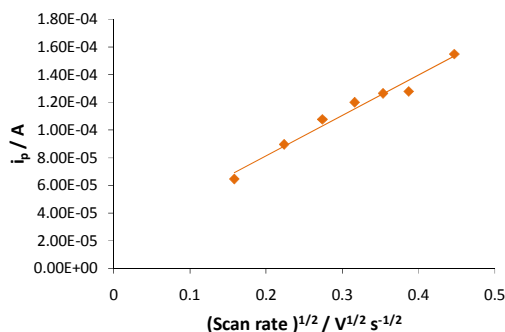


Figure 3.46: Randles-Sevcik plot for the diffusion of $\text{K}_3\text{Fe}(\text{CN})_6$ ($5.00 \times 10^{-3} \text{ M}$ in 0.10 M NaCl) to the ppyCM β -CD surface. Peak currents obtained from CV data recorded at 25, 50, 75, 100, 125 and 150 mV s^{-1} . The ppyCM β -CD film was synthesized from 0.30 M pyrrole and 0.02 M CM β -CD, pH 4.0, at 0.8 V vs SCE, to a charge of $2.50 \times 10^{-2} \text{ C}$.

Table 3.15: Diffusion coefficient, D , and other parameters obtained from a CV analysis at 25, 50, 75, 100, 125 and 150 mV s^{-1} , for $5.00 \times 10^{-3} \text{ M K}_3\text{Fe(CN)}_6$ in 0.10 M NaCl. Geometrical surface area was used to compute D .

	Slope / $\text{A V}^{-1/2} \text{ s}^{1/2}$	R²	D / $\text{cm}^2 \text{ s}^{-1}$	Intercept / A
ppyCMβ-CD	2.93×10^{-4}	0.973	3.00×10^{-6}	2.28×10^{-5}
GC	3.30×10^{-4}	0.961	3.86×10^{-6}	0.0

The ferri/ferrocyanide couple was also employed to evaluate the electron transfer rate constant, k , by means of rotating disc voltammetry (RDV), using the procedure described in Section 3.3.2. Experimental data were fitted to the Koutecky-Levich equation, Equation 3.7 and this plot is shown in Figure 3.47. A rate constant of $1.61 \times 10^{-2} \text{ cm s}^{-1}$ was computed using a scan rate of 50 mV s^{-1} . This value is very similar to the rate constant calculated for ppys β -CD at an identical scan rate, which was $1.56 \times 10^{-2} \text{ cm s}^{-1}$. No significant differences were found between the two polymers regarding the charge transfer rate. Another similarity concerns the influence of kinetic limitations. When RDV results for ppys β -CD were presented as the limiting current as a function of the square root of the rotation rate, an intercept of $1.22 \times 10^{-5} \text{ A}$ was noted, thus indicating non ideal behavior and the presence of kinetic limitations. Analogous results were obtained on analyzing the Levich plot for the ppyCM β -CD, Figure 3.48. An intercept of $2.28 \times 10^{-5} \text{ A}$ was extrapolated. As discussed previously, it is possible that at the scan rate of 50 mV s^{-1} the system did not maintain an Nernstian equilibrium during the measurements.

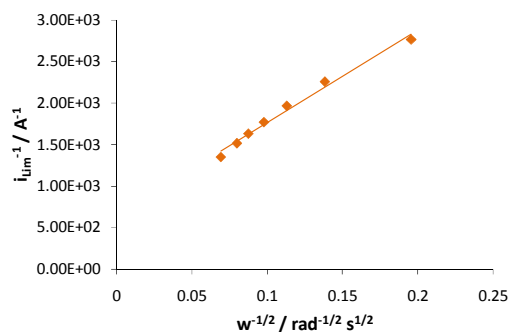


Figure 3.47: Koutecky-Levich plot for the reduction of 5.0×10^{-3} M $\text{K}_3\text{Fe}(\text{CN})_6$ in 0.1 M NaCl, at ppyCM β -CD deposited on GC ($d = 5.0$ mm) recorded at a scan rate of 50 mV s^{-1} . Rotation rates were 250, 500, 750, 1000, 1250, 1500 and 2000 rpm. Potential window was from -0.2 to 0.5 V vs SCE; ppyCM β -CD was synthesized from 0.30 M pyrrole and 0.02 M CM β -CD, pH 4.0, at 0.7 V vs SCE, 3.9×10^{-2} . Current was read at -0.1 V vs SCE.

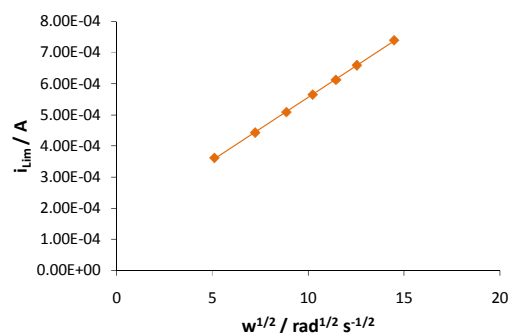


Figure 3.48: Levich plot for the reduction of 5.0×10^{-3} M $\text{K}_3\text{Fe}(\text{CN})_6$ in 0.10 M NaCl at ppyCM β -CD deposited at GC ($d = 5$ mm). Potential window was from -0.2 to 0.5 V vs SCE and the potential was scanned at 50 mV s^{-1} . The ppyCM β -CD was synthesized from 0.30 M pyrrole and 0.02 M CM β -CD, pH 4.0, at 0.7 V vs SCE, 3.90×10^{-2} C. Limiting current was read at -0.1 V vs SCE.

3.9.4 Capacitance measurement (by CV)

Next, cyclic voltammetry experiments were performed on the new system as detailed in Section 3.7.1 and, used together with Equation 3.20, to evaluate the capacitance for ppyCM β -CD. By plotting the current density as a function of the scan rate, a straight line was drawn, with a correlation coefficient of 0.999, as illustrated in Figure 3.49. From the slope of this plot, a capacitance of 6.11×10^{-6} F cm^{-2} was evaluated. The capacitance of a ppys β -CD film synthesized on a GC

substrate and grown to the same charge was $1.09 \times 10^{-5} \text{ F cm}^{-2}$. The lower value computed for the ppyCM β -CD indicates less capability of this polymer to store the charge. This is consistent with the lower number of negative sites of the carboxy methyl β -CD in comparison with the 7-9 negative groups of the s β -CD.

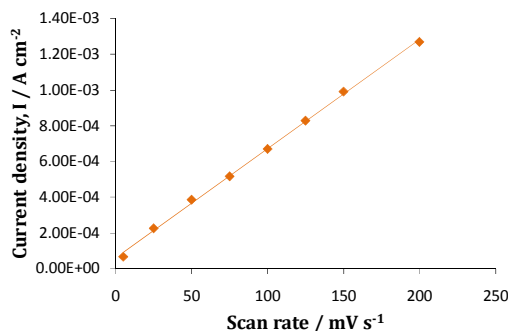


Figure 3.49: Current density at 0.20 V vs SCE for ppyCM β -CD in 0.10 M NaCl. The polymer was first conditioned in 0.10 M NaCl, for 10 cycles from 0.15 to 0.25 V vs SCE. The film was grown at 0.7 V vs SCE to a charge of $2.50 \times 10^{-2} \text{ C}$ on a GC electrode, ($d = 4 \text{ mm}$) from 0.30 M pyrrole and 0.02 M s β -CD, pH 4.0.

3.9.5 Cyclic Voltammetry and Quartz Crystal Microbalance

To acquire general information on the conductivity and redox properties of the ppyCM β -CD film, CV experiments in a 0.1 M NaCl solution were recorded. Figure 3.50 shows a typical voltammogram for a thin ppyCM β -CD film of 1.99 C cm^{-2} thickness. As outlined in Section 3.4, conducting polymers tend to produce broad redox peaks. For this reason, it is more correct to define an oxidation/reduction range, as opposed to a peak potential. As evident from Figure 3.50, oxidation of ppyCM β -CD begins at about 0.4 V vs SCE and continues until a potential of 0.7 V vs SCE is reached. The onset of the reduction wave is more difficult to determine. It seems to start around 0.0 V vs SCE, reaching a maximum rate at approximately -0.3 V vs SCE and the polymer is fully reduced at about -1.0 V vs SCE . Considering the corresponding plot for ppys β -CD, as illustrated in Figure 3.20, it is evident that there is little variation in the reduction of both polymers. In contrast, the polymer doped with CM β -CD is harder to oxidize, with an oxidation interval from -0.3 to 0.7 V vs SCE compared to -0.6 to 0.10 V vs SCE for ppys β -CD.

Another difference in both polymers, which is clearly evident by comparing Figures 3.50 and 3.20, is the considerable variation in the oxidation and reduction currents. The redox currents are nearly ten times smaller for the ppyCM β -CD system compared to those generated at the ppys β -CD film, even though both polymers were grown to similar charges. This suggests variations in the conductivity of the polymers, with the ppyCM β -CD film exhibiting the lower conductivity.

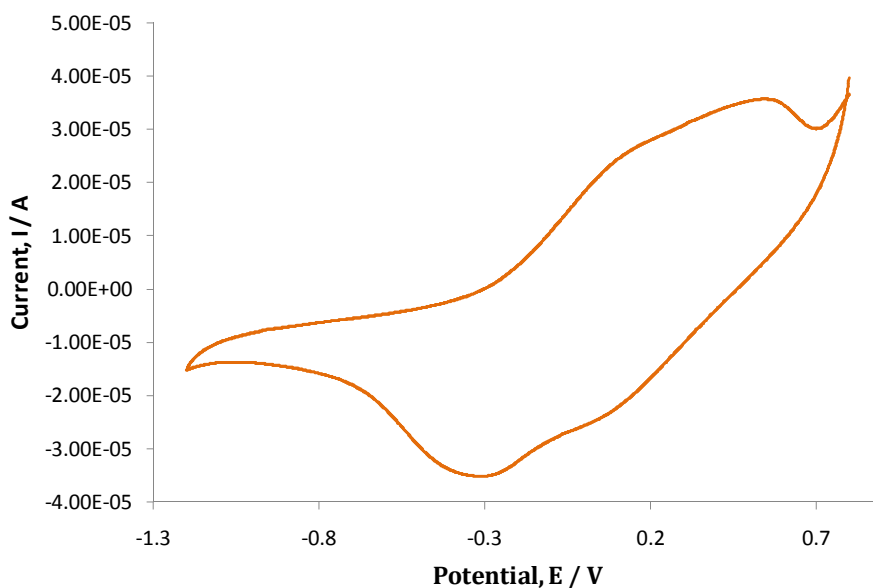


Figure 3.50: Cyclic voltammetry of ppyCM β -CD in 0.10 M NaCl, 10th cycle. Polymer was grown on GC (d = 4mm) at 0.80 V to a charge of 2.5×10^{-2} C from a solution of 0.30 M pyrrole and 0.02 M CM β -CD, pH 4.0. Applied potential is relative to the SCE reference.

Finally, attention was devoted to the ion flux observed during cycling of the ppyCM β -CD in NaCl. EQCM measurements were performed on a ppyCM β -CD polymer synthesized at 0.7 V vs Ag/AgCl, on a gold working electrode connected to a piezoelectric quartz crystal. Then, the polymer was cycled in 1.0 M NaCl from 0.5 to -1.2 V vs Ag/AgCl, using a scan rate of 50 mV s⁻¹. Plots, showing the frequency and mass determined from the Saurebrey equation, are presented in Figure 3.51. The traces are somewhat noisy as the change in mass is small and close to the detection limit of the instrument. However, it is clear that the frequency decreases during the reduction of the polymer, and consequently an

increase in the mass deposited on the electrode is registered. This is similar to the trend presented in Figure 3.25 for the ppys β -CD system.

The CM β -CD is a large polyanion and, similarly to the s β -CD anion, cannot be expelled from the polymer backbone, because of its steric hindrance, during reduction of polypyrrole. Accordingly, the increase in mass is due to the insertion of cationic species to maintain the electroneutrality of the system as the polymer is converted from the oxidized to the reduced state. The increase in mass observed on reduction of the ppyCM β -CD electrode was computed as 3.85×10^{-7} g. This is considerably smaller than the corresponding mass of 1.74×10^{-6} g obtained for the ppys β -CD system. Assuming that most of this mass is associated with the ingress of Na⁺, then, this corresponds to a considerable reduction in the moles of Na⁺ incorporated within the ppyCM β -CD film. This is not surprising given the lower charge on the CM β -CD cavity, with an average of 3.5 anionic groups compared to an average of 7 to 11 anionic sulfated groups on the s β -CD. However, the difference in the number of charged species, at a ratio of about 2.5, is not sufficient to account for the mass ratio, which is close to a factor of 4.0. This suggests that the ppyCM β -CD films incorporate less water compared to the ppys β -CD films.

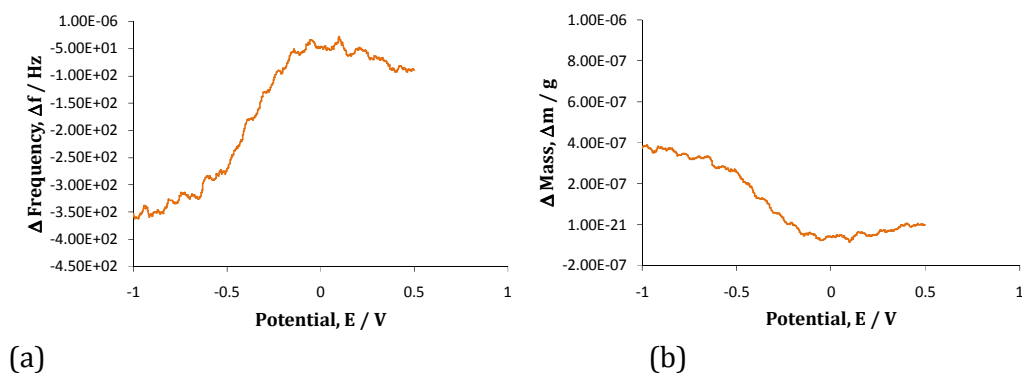


Figure 3.51: Frequency-potential plot (a) and mass-potential plot (b) for the redox activity of ppyCM β -CD in 1.00 M NaCl, at a scan rate of 50 mV s⁻¹ (ppyCM β -CD was grown from 0.30 M pyrrole in 0.02 M CM β -CD at Au electrode ($A = 0.2033$ cm²) at 0.7 V vs Ag/AgCl, $Q = 0.025$ C). Potential is relative to the Ag/AgCl reference.

3.9.6 Morphology

As already observed for ppys β -CD in Figure 3.44 (a), the ppy doped with CM β -CD also shows a typical globular organization. The modified polymer depicted in Figure 3.52 exhibits a higher grade of morphological organization in comparison to ppyCl (Figure 3.44 (b)). However the size of the microspherical grains is smaller with respect to ppys β -CD. This aspect might be connected to the different doping level or to different polymerization rate. The s β -CD solution has in fact higher conductivity in comparison to the CM β -CD solution, since it possesses a larger number of negative charges.

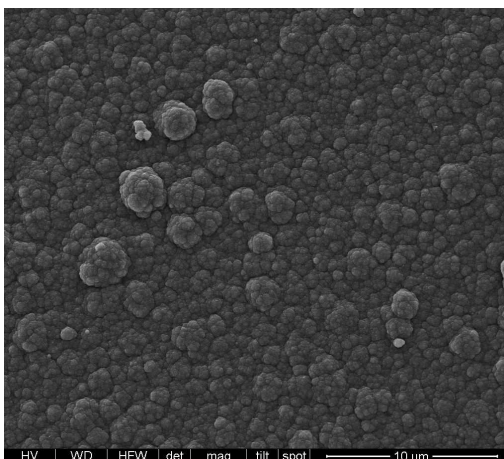


Figure 3.52: SEM micrographs of ppyCM β -CD films electrochemically deposited on GC from aqueous solutions of 0.02 M s β -CD in the presence of 0.30 M pyrrole (pH 4.0) at 0.8 V vs SCE to a charge of 1.13 C cm⁻².

3.10 Summary of results

In this chapter results are presented and discussed on the electrochemical synthesis of three ppy films, ppyCl, ppys β -CD and ppyCM β -CD. The ppyCl was used for comparison purposes. The dopants of major interest, the anionic s β -CD, and the anionic CM β -CD were found to be suitable electrolytes for the electrochemical polymerization of pyrrole. There was no need for the addition of any supporting electrolyte. A 0.02 M solution of s β -CD or CM β -CD was sufficient to enable the growth of polypyrrole films in a highly reproducible

manner, with nearly identical current-time transients being recorded during the electropolymerization period.

The potentiostatic electropolymerization of pyrrole was found to proceed at very high rates in the presence of 0.02 M β -CD, dissolved in an aqueous solution of 0.2 M pyrrole. The rate of polymer growth was compared to the rate of electropolymerization of pyrrole in chloride and dodecylsulfate-containing solutions. Much higher rates were observed in the β -CD solution; the steady-state electropolymerization currents were about 1.0×10^{-3} A in the presence of 0.02 M β -CD compared to 1.0×10^{-4} A in the presence of 0.1 M NaCl. This was explained in terms of the high ionic strength of the β -CD solution. The thickness of the films was controlled by fixing the electropolymerization charge. Optical images of ppys β -CD and ppyCl showed a more organized *cauliflower*-like morphology for the CD-modified polymer.

A redox active probe species, the ferri/ferrocyanide couple, was employed to investigate the behavior of ppys β -CD and ppyCl towards diffusion and charge transfer, i.e., the electron transfer rate constant, k . Both polymers exhibited similar results, indicating that the large dopant, β -CD, does not have a negative effect on the diffusion of electroactive species or on the rate of the electron transfer at the polymer interface. Similar rate constants, k , of 3.73×10^{-2} cm s⁻¹ and 3.32×10^{-2} cm s⁻¹ were determined for the reduction of 5.00×10^{-3} M ferricyanide at the ppys β -CD and ppyCl films, respectively.

The redox properties of the polymers were further examined by means of CV and EQCM in 1.00 M and 0.10 M NaCl. CV data demonstrated that the ppys β -CD was more difficult to reduce compared to the ppyCl film. This was explained in terms of the cation exchange properties of the ppys β -CD film, where reduction of the film is accompanied by the ingress of Na⁺ cations from the supporting electrolyte. On the other hand, the ppyCl film is a typical anion exchanger, where reduction of the film leads to the expulsion of the chloride anions. This was confirmed by EQCM investigations, which proved that ppys β -CD behaved like a cationic exchanger, due to the permanent immobilization of the large dopant

within the polymer matrix. In contrast, ppyCl exhibited anion exchange properties. In addition, the EQCM results provided evidence for solvent (H₂O) influx during the first reduction of the ppysβ-CD film. This was explained in terms of a rearrangement of the polymer film as the film was reduced, making it more susceptible to the influx of solvent molecules. These findings were further supported by a thermal analysis using DSC. The thermograms confirmed the permanent immobilization of the sβ-CD anion within the polymer matrix. Moreover, the thermograms showed evidence for the influx of large amounts of water during the reduction of the ppysβ-CD films. The EQCM data were also used to estimate the doping level of the ppysβ-CD films. It was shown clearly that the maximum doping level of 0.33 (1:3 dopant:pyrrole), which is seen with simple dopants, such as chlorides, was not achievable with the sβ-CD anions. Instead, a much lower doping level, varying from 1:10 or 1:12 (sβ-CD: pyrrole) was estimated.

The capacitance of the ppyCl and ppysβ-CD films was determined using CV. It was shown that the capacitance of relatively thin films depended on the nature of the substrate material, with higher values obtained at a GC electrode compared to an Au substrate. In general, higher capacitance values were computed for the ppysβ-CD films and this was attributed to the higher number of anionic charges within the polymer matrix.

Electrochemical impedance spectroscopy was used to study the properties of oxidized and reduced ppysβ-CD films. Near steady-state conditions were achieved on polarization of the films at the required potential for 60 min and provided applied potentials higher than 0.5 V vs SCE were not used, the polymer could be reversibly switched from one state to another giving identical impedance profiles. A two-time constant equivalent circuit was used to fit the data for the oxidized or partially oxidized ppysβ-CD films, while the simple Randles cell was used to model the data for the reduced ppysβ-CD films. A constant phase element, CPE, was used to represent the capacitance of the films. High capacitance values, approximately $5.00 \times 10^{-3} \text{ F cm}^{-2}$, were obtained on fitting the impedance data of ppysβ-CD films polarized at applied potentials

between 0.1 and 0.5 V vs SCE. On the application of higher applied potentials over-oxidation of the film occurred giving rise to a considerable reduction in the charging capacitance, reaching values of about $1.00 \times 10^{-5} \text{ F cm}^{-2}$ at 0.7 V vs SCE. A similar reduction in the capacitance of the film was observed on reduction of the film. The capacitance measured at -0.7 V vs SCE was approximately $1.00 \times 10^{-4} \text{ F cm}^{-2}$, being consistent with the formation of a more insulating film. However, the conducting and high charging capacitance of the film was restored on oxidation of the film. Similar behavior was observed for the ppyCl film. Over-oxidation of the ppyCl film was clearly observed on applying potentials higher than 0.6 V vs SCE, indicating that the ppyCl film is more resistant to the onset of over-oxidation compared to the ppys β -CD film. The charging capacitance was somewhat lower for the ppyCl film, consistent with the CV data.

Finally another macro-cyclic dopant, the anionic CM β -CD, was introduced and used to synthesize a new conducting polymer, ppyCM β -CD. This polymer was deposited from a solution of pyrrole and CM β -CD, without any further electrolyte, but the pyrrole concentration was increased and the pH was lowered to 4.0 to enable efficient polymerization. Polymerization proceeded slowly in comparison to ppys β -CD. This was attributed to a lower conductivity of the reaction solution. This new polymer, ppyCM β -CD, showed cation exchange properties and again this was explained in terms of the size of the CM β -CD dopant, with the dopant being too large and bulky to be expelled on reduction of the polymer film.

It is clearly evident from the results presented in this chapter that the ppys β -CD films have a high affinity for Na⁺. Indeed, Tamsamani and co-workers⁶ suggested that ppys β -CD films could be potentially useful for the extraction of metal cations due to the enhanced electrostatic effects with the sulfate moieties of the CDs. Using this unique property of the ppys β -CD films, these films were investigated in the sensing and uptake of three different cationic species, methyl, ethyl and benzyl viologens. Methyl viologen is the well-known pollutant paraquat. These findings are presented and discussed in Chapter 4.

3.11 References

1. Tamm J., Alumaa A., Hallik A., Silk T. and Sammelseg V.; *Journal of Electroanalytical Chemistry*, 414, 1996, 149-158.
2. Weidlich C., Mangold K. M. and Juttner K.; *Electrochimica Acta*, 47, 2001, 741-745.
3. Kupila E. L. and Kankare J.; *Synthetic Metals*, 55, 1993, 1402-1405.
4. Weidlich C., Mangold K. M. and Juttner K.; *Electrochimica Acta*, 50, 2005, 1547-1552.
5. Tamm J., Hallik A., Alumaa A. and Sammelseg V.; *Electrochimica Acta*, 42, 1997, 2929-2934.
6. Tamsamani K. R., Mark H. B., Kutner W. and Stalcup A. M.; *Journal of Solid State Electrochemistry*, 6, 2002, 391-395.
7. Diaz A. F., Castillo J. I., Logan J. A. and Lee W. Y.; *Journal of Electroanalytical Chemistry*, 129, 1981, 115-132.
8. Bull R. A., Fan F. R. F. and Bard A. J.; *Journal of the Electrochemical Society*, 129, 1982, 1009-1015.
9. Qi Z. G., Rees N. G. and Pickup P. G.; *Chemistry of Materials*, 8, 1996, 701-707.
10. Chandrasekhar P.; *Conducting Polymers, Fundamental and Applications*; Kluwer Academic Publishers, 1999.
11. Miller L. L., Zinger B. and Zhou Q. X.; *Journal of the American Chemical Society*, 109, 1987, 2267-2272.
12. Baker C. K. and Reynolds J. R.; *Journal of Electroanalytical Chemistry*, 251, 1988, 307-322.
13. Scharifker B. R., Garciapastoriza E. and Marino W.; *Journal of Electroanalytical Chemistry*, 300, 1991, 85-98.
14. Greef R., Peat R., Peter L. M., Pletcher D. and Robinson J.; *Instrumental methods in electrochemistry*; Ellis Horwood Ltd, 1985
15. Appel G., Schmeisser D., Bauer J., Bauer M., Egelhaaf H. J. and Oelkrug D.; *Synthetic Metals*, 99, 1999, 69-77.
16. Garfias-Garcia E., Romero-Romo M., Ramirez-Silva M. T., Morales J. and Palomar-Pardave M.; *ECS Transactions*, 15, 2008, 121-131.
17. Steed J. W. and Atwood J. L. *Supramolecular Chemistry*; Wiley & Sons, 2000.
18. Hendy G. M.; Polypyrrole modified with sulfonated β -cyclodextrin: Controlled release of dopamine and host-guest complexation properties, Ph.D thesis, NUIM, Department of Chemistry, 2009.
19. Collyer S. D., Davis F., Lucke A., Stirling C. J. M. and Higson S. P. J.; *Journal of Electroanalytical Chemistry*, 549, 2003, 119-127.
20. Ybarra G., Moina C., Florit M. I. and Posadas D.; *Electrochimica Acta*, 53, 2008, 4727-4731.
21. Dzyadevych S. V., Arkhypova V. N., Soldatkin A. P., El'skaya A. V., Martelet C. and Jaffrezic-Renault N.; *Ingenierie et Recherche Biomedicale*, 29, 2008, 171-180.
22. Fini P., Longobardi F., Catucci L., Cosma P. and Agostiano A.; *Bioelectrochemistry*, 63, 2004, 107-110.
23. Klingler R. J. and Kochi J. K.; *Journal of Physical Chemistry*, 85, 1981, 1731-1741.

24. Lyman W. J., Reidy P. J. and Levy B. S.; *Mobility and degradation of organic contaminants in subsurface environments*; C.K. Smoley Inc, 1992.
25. http://www.engineeringtoolbox.com/water-dynamic-kinematic-viscosity-d_596.html.
26. Vasantha V. S. and Chen S. M.; *Electrochimica Acta*, 51, 2005, 347-355.
27. Rieger P. H.; *Electrochemistry*, Second ed.; Chapman & Hall, 1994.
28. Naoi K., Lien M. and Smyrl W. H.; *Journal of the Electrochemical Society*, 138, 1991, 440-445.
29. Wallace G. G., Spinks G. M., L. A. P. Kane-Maguire L. A. P. and Teasdale P. R.; *Conductive Electroactive Polymers: Intelligent Materials Systems*; CRC Press, 2003.
30. Reece D. A., Ralph S. F. and Wallace G. G.; *Journal of Membrane Science*, 249, 2005, 9-20.
31. Syritski V., Opik A. and Forsen O.; *Electrochimica Acta*, 48, 2003, 1409-1417.
32. Tsai E. W., Jang G. W. and Rajeshwar K.; *Journal of the Chemical Society-Chemical Communications*, 1987, 1776-1778.
33. Suarez M. F. and Compton R. G.; *Journal of Electroanalytical Chemistry*, 462, 1999, 211-221.
34. Vidotti M. and de Torresi S. I. C.; *Journal of the Brazilian Chemical Society*, 19, 2008, 1248-1257.
35. Arca M., Mirkin M. V. and Bard A. J.; *Journal of Physical Chemistry*, 99, 1995, 5040-5050.
36. Veiga M. D., Merino M., Fernandez D. and Lozano R.; *Journal of Thermal Analysis and Calorimetry*, 68, 2002, 511-516.
37. Matveeva E. S., Calleja R. D. and Parkhutik V. P.; *Synthetic Metals*, 72, 1995, 105-110.
38. Thieblemont J. C., Brun A., Marty J., Planche M. F. and Calo P.; *Polymer*, 36, 1995, 1605-1610.
39. Brett C. M. A. and Oliveira A. M.; *Electrochemistry. Principles, Methods and Applications*; Oxford Science Publications, 1993.
40. Harley C. C.; The Formation of an Electrochemical Sensor for the Selective Detection of Dopamine, Ph.D thesis, NUIM, Department of Chemistry, 2009.
41. Suematsu S., Oura Y., Tsujimoto H., Kanno H. and Naoi K.; *Electrochimica Acta*, 45, 2000, 3813-3821.
42. Ingram M. D., Staesche H. and Ryder K. S.; *Solid State Ionics*, 169, 2004, 51-57.
43. Barsoukov E. and Macdonald J. E.; *Impedance Spectroscopy. Theory, Experiment and Applications*, 2nd ed.; Wiley-Interscience, 2005.
44. Hallik A., Alumaa A., Tamm J., Sammelselg V., Vaartnou M., Janes A. and Lust E.; *Synthetic Metals*, 156, 2006, 488-494.
45. Zoltowski P.; *Journal of Electroanalytical Chemistry*, 443, 1998, 149-154.
46. Mostany J. and Scharifker B. R.; *Synthetic Metals*, 87, 1997, 179-185.
47. Iroh J. O. and Levine K.; *Journal of Power Sources*, 117, 2003, 267-272.
48. Liu A. S. and Oliveira M. A. S.; *Journal of the Brazilian Chemical Society*, 18, 2007, 143-152.
49. Bazzaoui M., Martins L., Bazzaoui E. A. and Martins J. I.; *Electrochimica Acta*, 47, 2002, 2953-2962.

50. Wang J. J., Zheng G. J., Yang L. and Sun W. R.; *Analyst*, 126, 2001, 438-440.
51. Caple G., Wheeler B. L., Swift R., Porter T. L. and Jeffers S.; *Journal of Physical Chemistry*, 94, 1990, 5639-5641.
52. Mitchell G. R., Davis F. J. and Legge C. H.; *Synthetic Metals*, 26, 1988, 247-257.
53. Dyreklev P., Granstrom M., Inganas O., Gunaratne L., Senadeera G. K. R., Skaarup S. and West K.; *Polymer*, 37, 1996, 2609-2613.
54. Bouchta D., Izaoumen N., Zejli H., El Kaoutit M. and Temsamani K. R.; *Biosensors & Bioelectronics*, 20, 2005, 2228-2235.
55. Kaniewska M., Sikora T., Katakly R. and Trojanowicz M.; *Journal of Biochemical and Biophysical Methods*, 70, 2008, 1261-1267.

Chapter 4

Conducting ppys β -CD as a sensor for viologens

4.1 Introduction

Conducting polymers (CPs) are being increasingly studied for applications in the field of sensors. They offer a remarkably active matrix that can be sensitive to gas vapours, ions and biomolecular systems. Furthermore, these polymers have a unique doping/dedoping process, which is associated with the movement of ions into/out of the polymer matrix. This property was exploited in the late 1980s, by Miller *et al.*,¹⁻³ for the electro-controlled delivery of charged biological substances. Both glutamate and salicylate were released, playing the role of doping anions. Li and Dong⁴ applied the doping/dedoping processes of CPs to investigate the controlled delivery of ATP. Miller and Zhou⁵ studied the electro-controlled delivery of protonated dopamine and procaine because these cationic species behave as *pseudo*-doping agents (or counterions). In recent years, Yang *et al.*⁶ developed a sensor based on poly(N-acetylaniline) modified with β -CD to detect cinchonine, an important antimalarial drug. Izaoumen *et al.*⁷ studied the detection properties of a polypyrrole film doped with β -CD towards oxidation of the neurotransmitters dopamine and norepinephrine. A reason why polymer film modified electrodes are so attractive lies in the fact that they are easy and simple to fabricate. Moreover, their surface offers more active sites than some other modified electrodes made through covalent bonding or adsorption.⁸

Among the wide range of CPs currently available, ppy is one of the most attractive and extensively used materials.⁹ This is due to its large surface area, good environmental stability, controllable surface biochemical properties, simple electrochemical preparation and also because it is a biocompatible polymer.¹⁰ This polymer, ppy, may be synthesized chemically or electrochemically, however the latter method has several advantages over the chemical polymerization approach because the film thickness, the morphology, the permeation and the charge transport can be controlled by adjusting the electrochemical parameters. Moreover, ppy films electrochemically synthesized have good adherence to the electrode substrate and also exhibit good conductivity.⁹

In this chapter the ability of ppys β -CD to detect three different viologen compounds was studied. As discussed above, cyclodextrin modified polymers have been used for the controlled delivery and detection of biomolecules.¹¹⁻¹³ However, in this case ppy was doped with an anionic sulfated β -CD to give the modified ppys β -CD electrode. Methyl (MV), ethyl (EV) and benzyl (BV) viologen were employed as molecular models to explore the β -CD-modified polypyrrole characteristics. The three substances belong to the same family of compounds. They differ in the side chain, as discussed in Section 1.4, and they were investigated also to determine how the substituents affect the interaction with the polymer. Furthermore, the methyl viologen is the highly toxic herbicide, paraquat. The development of a cheap and easy to manage sensor able to detect paraquat and, possibly, to remove it from aqueous solutions would be a step forward in pollution remediation.

Interaction between the polymer and the three viologens was explored by means of two electrochemical techniques: cyclic voltammetry (CV) and differential pulse voltammetry (DPV). In addition, a constant potential amperometry (CPA) study was performed to sense methyl viologen. Initially, CV voltammograms of ppys β -CD in relatively high concentrations of the viologens were recorded to figure out how the ppys β -CD interacts with the analytes. After this preliminary study, attention was focused on benzyl viologen with the aim to optimize the experimental conditions, in order to improve the sensitivity of the ppys β -CD towards the detection of the viologens. Various parameters were investigated, including a study on the potential applied during the electrodeposition of the polymer, the thickness of the film and the influence of the supporting electrolyte. With the best experimental parameters selected, DPV experiments were performed to increase the detection ability of the polymer. Finally, an additional study, using CPA was performed to sense methyl viologen because it is one of the most used herbicides worldwide.

4.2 Electrochemistry of the viologens

Prior to presenting and discussing the results concerning the interaction of ppys β -CD with the three viologens, a brief summary of their electrochemistry is provided. As described in more detail, in Section 1.4, viologen molecules exist in nature in the stable form of dication. When an appropriate potential is applied, they can undergo electron transfer reactions by two consecutive one-electron reductions. Figure 4.1 clearly shows the two steps of reduction, leading firstly to the generation of a radical species followed by the formation of a neutral compound. Moreover, Figure 4.1 indicates the counter ions and the three different substituents of the 4,4'-bipyridinium ring: a methyl group in the case of paraquat, an ethyl chain for the ethyl viologen and finally a benzyl substituent in the case of benzyl viologen.

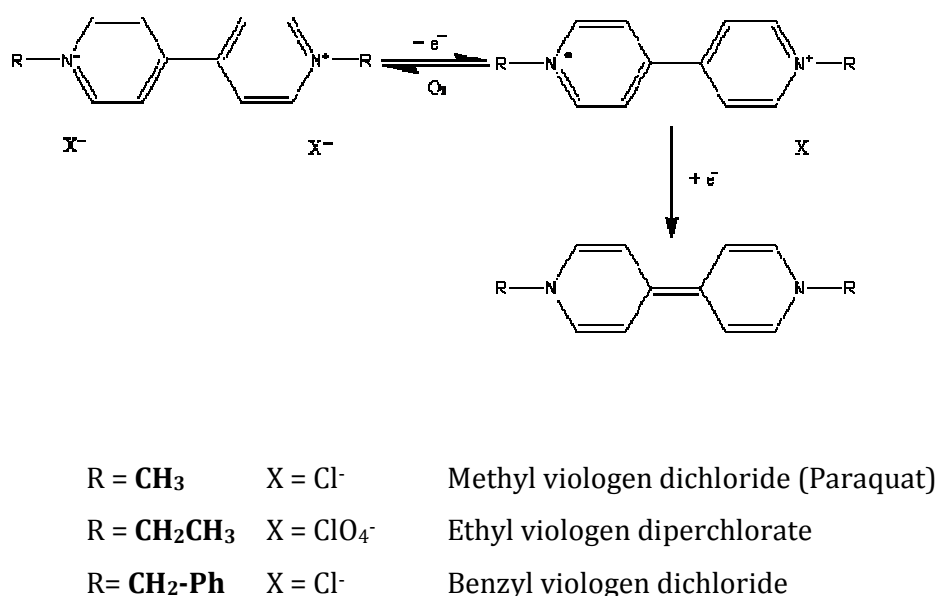


Figure 4.1: Scheme representing the first and second reduction for the viologen compounds.

Figure 4.2, Figure 4.3, and Figure 4.4 represent cyclic voltammograms for a 5.00×10^{-3} M solution of MV, EV and BV, respectively, on a bare gold electrode. A supporting electrolyte was necessary to ensure conductivity of the solution. For this purpose the solutions were prepared in 0.1 M NaCl. The first and second

reductions are clearly evident. The related reduction potentials are listed in Table 4.1. These experimental values are in good agreement with previous works reviewed by Bird and Kuhn.¹⁴ However, a larger discrepancy was noticed for the second reduction of methyl viologen. The extrapolated peak potential was -1.032 V vs SCE, i.e., 89 mV more positive than the value reported by Bird and Kuhn. The potential of -1.121 V vs SCE described by the authors corresponds to experiments performed in phosphate buffer and Bard has suggested that there is pH dependence for the second reduction of methyl viologen.¹⁵

As evident from the three voltammograms, the oxidation waves resulted in more complicated voltammograms and were difficult to analyze. While the first reduction of the viologens is known to be highly reversible, there is good agreement in the literature in considering the second reduction step to be less reversible. One of the reasons is that the neutral form is often insoluble in water. As a matter of fact, some authors, such as Hunig^{16,17}, stated that reversible potentials for viologens can only be obtained in organic solvents in which all the reactants and products are highly soluble. In addition, during the reduction process, the viologens can undergo several secondary reactions, summarized in Table 4.2 that might affect the subsequent oxidation process. These side reactions on the electrode surface involve generally the cation radical and the neutral molecule and contribute to the irreversibility of the second reduction.¹⁴ Conproportionation and dimerization reaction will be further discussed in Chapter 5. To minimize the reaction with oxygen, all solutions containing viologens were purged with nitrogen for 20 min.

As the oxidation waves are complex with complications arising from the secondary reactions, the results presented and discussed in this chapter will focus on the reduction waves.

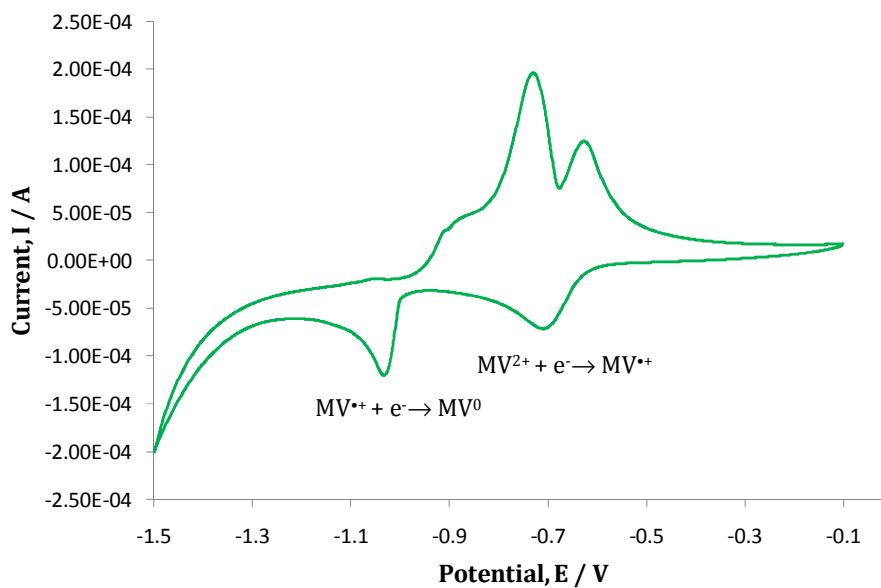


Figure 4.2: CV recorded at a bare Au electrode, $d = 3.0$ mm in a 5.00×10^{-3} M MV/0.10 M NaCl solution. Scan rate: 50 mV s^{-1} . Potential refers to the SCE reference scale.

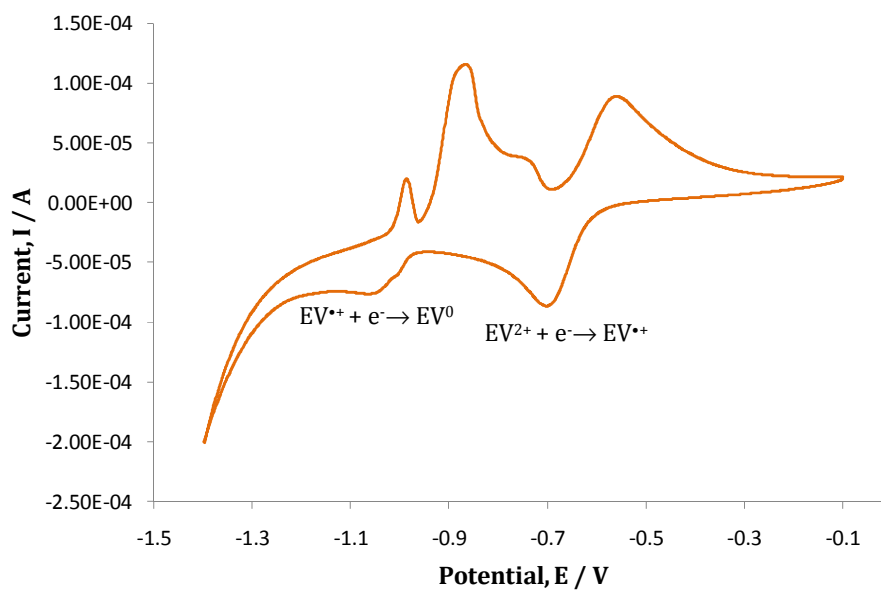


Figure 4.3: CV recorded at a bare Au electrode, $d = 3.0$ mm in a 5.00×10^{-3} M EV/0.10 M NaCl solution. Scan rate: 50 mV s^{-1} . Potential refers to the SCE reference scale.

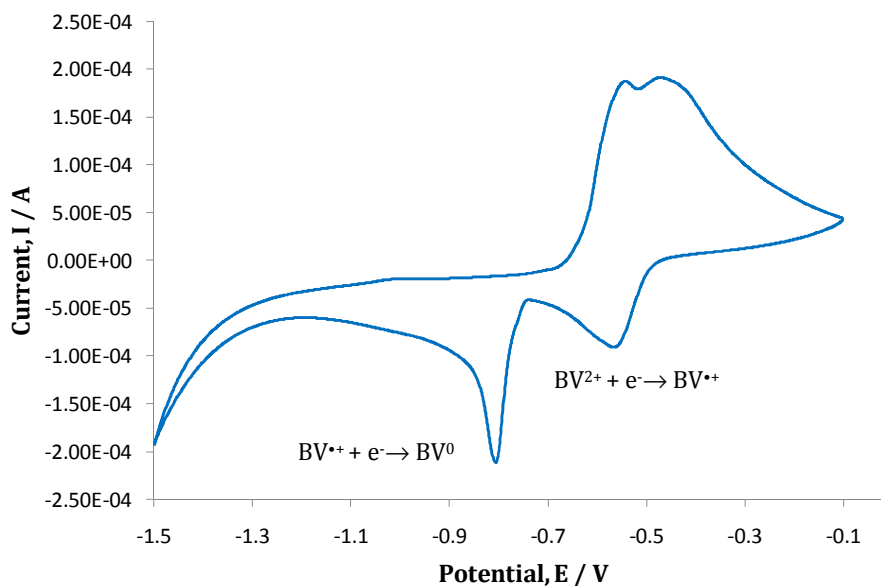


Figure 4.4: CV recorded at a bare Au electrode, $d = 3.0$ mm, in a 5.00×10^{-3} M BV/0.10 M NaCl solution. Scan rate: 50 mV s^{-1} . Potential refers to the SCE reference scale.

Table 4.1: A comparison of the experimental and literature values¹⁴ for the peak potentials of the first and second reduction waves of the three viologen compounds.

Compound	Experimental values		Literature values	
	Potential, E / V vs SCE		Potential, E / V vs SCE	
	$V^{2+} + e^- \rightarrow V^{\bullet+}$ 1 st reduction	$V^{\bullet+} + e^- \rightarrow V^0$ 2 nd reduction	$V^{2+} + e^- \rightarrow V^{\bullet+}$ 1 st reduction	$V^{\bullet+} + e^- \rightarrow V^0$ 2 nd reduction
MV	-0.709	-1.032	-0.687	-1.121
EV	-0.704	-1.050	-0.690	/
BV	-0.567	-0.806	-0.573	-0.790

Table 4.2: Summary of the side reactions that can occur during the redox process of a viologen, V^0 = neutral viologen, V^{2+} = dication, $V^{\bullet+}$ = radical cation.

Conproportionation	$V^0 + V^{2+} \rightarrow 2 V^{\bullet+}$
Disproportionation	$2 V^{\bullet+} \rightarrow V^0 + V^{2+}$
Dimerization	$2V^{\bullet+} \rightarrow (V^{\bullet+})_2$
Reaction with oxygen	$2 V^{\bullet+} + \frac{1}{2} O_2 \rightarrow 2 V^{2+} + 2 OH^-$

4.3 The detection of methyl, ethyl and benzyl viologens by means of cyclic voltammetry (CV)

In this section, the ability of the ppys β -CD film to detect the three viologens is explored. This is followed by a discussion on the mode of interaction between the viologens and the polymer during the sensing events. In the QCM section discussed in Chapter 3, ppys β -CD was described to behave as a cation exchanger and the controlled uptake or release of cations was reached by switching the oxidation state of the film. The applied voltage is responsible for the electronic state of the polymer backbone. When ppy is oxidized, positive charges are generated and neutralized by the negative charge of the s β -CD dopant. Once ppy is reduced, an insulating neutral polymer is formed. This promotes a flux of cations from the bulk solution to the electrode to balance the negative charges of the large anionic dopant immobilized within the ppy matrix. Hence, the electroneutrality of the system is maintained. The driving forces controlling this process are mainly electrostatic interactions. Viologen compounds, also, in their fully oxidized and radical states have a cationic nature. Therefore, they could interact electrostatically with the polymer. Another possible hypothesis on the viologen-polymer interaction regards the supramolecular structure of the s β -CD. As widely documented in Section 1.3, cyclodextrins can form inclusion complexes with a variety of guest molecules. Their hydrophobic cavity can host species of proper size and shape, by means of hydrogen bonding, electrostatic interactions, Van der Waals forces and hydrophobic effects.

4.3.1 Influence of the substrate

The working electrodes examined in this study were platinum (Pt), glassy carbon (GC) and gold (Au). Figure 4.5 shows the cyclic voltammetric behaviour of EV at a bare Pt, GC and Au electrode. Pt was found to be the electrode with the most limitations. To completely reduce a viologen compound, the applied potential has to reach negative values of -0.80/-1.10 V vs SCE. At these potentials, Pt is well known to catalyze hydrogen reduction.¹⁸ As a matter of fact, it is clear from the current density plot of Pt, represented by a blue trace in Figure 4.5 that hydrogen evolution sharply increases at potentials more negative than -0.90 V vs SCE. As a consequence of the huge signal due to hydrogen reduction, it is not possible to monitor the second reduction of the viologens or indeed to distinguish the re-oxidation peaks for EV in the reverse cycle.

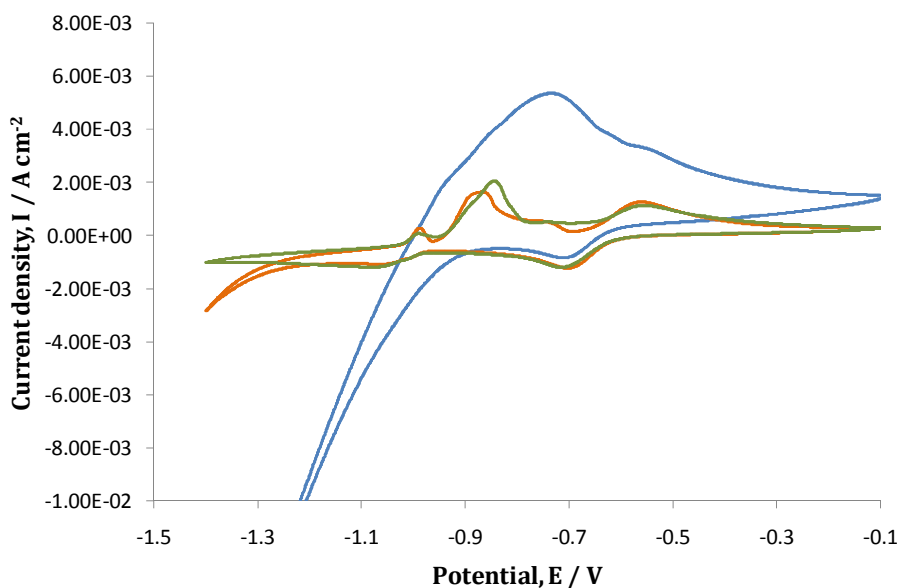


Figure 4.5: CV of a 5.00×10^{-3} M EV / 0.10 M NaCl solution, at a scan rate 50 mV s^{-1} , on Pt —, Au — and GC —. Potential refers to the SCE reference scale.

GC and Au gave similar voltammograms for the reduction and subsequent oxidation of EV. Peaks were slightly better defined on Au. After these preliminary experiments the gold electrode was chosen as the working electrode. Despite the fact that its response is very similar to that of GC, the

latter is harder to manage because of its fragility. Moreover, the electrode cleaning procedure is easier when a black ppy film has to be removed from a gold yellow surface than from a black GC substrate.

4.3.2 Redox behavior of viologens at ppys β -CD investigated by CV and QCM

Cyclic voltammograms of a ppys β -CD film grown to a charge of $3.50 \times 10^{-1} \text{ C cm}^{-2}$ in a $5.00 \times 10^{-3} \text{ M}$ solution of methyl, ethyl and benzyl viologen are shown in Figure 4.6, Figure 4.7 and Figure 4.8, respectively. The main difference between the signals recorded on the polymer and on the bare electrode (Figure 4.2, Figure 4.3 and Figure 4.4) was the presence at the polymer of an intense reduction peak around -1.0 V vs SCE . This peak was common to all three solutions of viologens.

Peak potential values for the first and second reduction processes of the three compounds are listed in Table 4.3 and compared to data collected at the bare electrode. In addition, the peak potential of the third reduction wave, which occurs only on the polymer-modified electrode, is also reported. The first reduction potential was slightly affected by the presence of the polymer on the electrode. Shifts of 9 mV for MV, of 17 mV for EV and of 12 mV for BV, towards more negative potentials were recorded. These slight shifts to more electronegative potentials can be attributed to the resistance of the polymer films. Although the polymer is conducting, it is a less efficient conductor than the bare electrode. Alternatively, the viologen dications can interact electrostatically with the negative sulfate groups which are present on the $s\beta$ -CD dopants. Indeed, Ren and Pickup¹⁹ published a paper where they discuss the formation of ion pairs between a viologen and the sulfate groups of a conducting polymer doped with poly(styrenesulfonate) anions. Ion pairing at the ppys β -CD surface between the sulfate groups of the $s\beta$ -CD and the quaternary nitrogens of the viologens would increase the electron density of the viologen dications. As a consequence, the reduction would be more difficult and a more electronegative potential would be required to reduce the viologen. This explanation is consistent with the findings of the studies outlined in Chapter 5.

In contrast, the second reduction of BV and EV was more facile on the polymer surface, as seen by the values presented in Table 4.3. As a matter of fact, EV^{•+} is reduced at -0.978 V vs SCE showing an electropositive shift of 72 mV, while BV^{•+} is reduced at -0.767 V vs SCE, to give a positive potential shift of 39 mV with respect to the bare electrode. This characteristic can be explained in terms of the accumulation of the radical species in the polymer matrix. In Chapter 5 it will be shown that the electrostatic interactions between the sulfate groups and the dicationic species are stronger than those between the sulfate groups and the radical species. However, as the ppys β -CD has a porous structure in comparison to the bare gold electrode, the generated radicals can be trapped and hence accumulate within the polymer matrix. This accumulation and local increase in the concentration of the radical species would account for the easier reduction.

Table 4.3: Peak potentials for reduction of the three viologens on a bare gold electrode and on ppys β -CD. The ppys β -CD films were synthesized on Au, d = 3.0 mm, from a 0.20 M py/ 0.02 M s β -CD solution, at 0.80 V vs SCE and to a charge of 2.5×10^{-2} C.

Compound	Bare Au		ppys β -CD		
	Potential, E /V vs SCE		Potential, E /V vs SCE		
	V ²⁺ + e ⁻ → V ^{•+} 1 st reduction	V ^{•+} + e ⁻ → V ⁰ 2 nd reduction	V ²⁺ + e ⁻ → V ^{•+} 1 st reduction	V ^{•+} + e ⁻ → V ⁰ 2 nd reduction	Adsorption peak
MV	-0.709	-1.032	-0.718	-1.045	-1.245
EV	-0.704	-1.050	-0.721	-0.978	-1.137
BV	-0.567	-0.806	-0.579	-0.767	-0.923

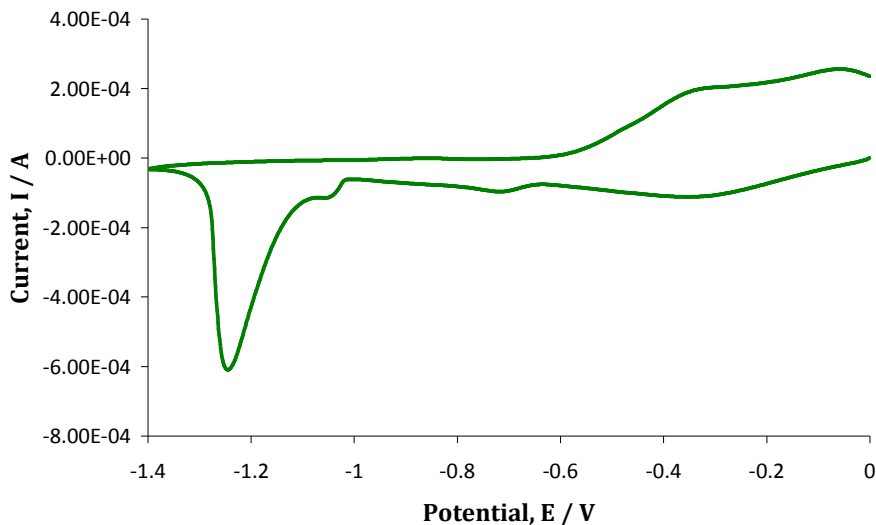


Figure 4.6: CV of 5.00×10^{-3} M MV in 0.10 M NaCl solution, scan rate 50 mV s^{-1} , on ppys β -CD after conditioning of the polymer in the MV solution, for 10 cycles from -0.1 V to -0.6 V vs SCE. The ppys β -CD was synthesized on Au, $d = 3.0$ mm, from a 0.20 M pyrrole/0.02 M β -CD solution, at 0.80 V vs SCE and until a charge of 2.50×10^{-2} C was consumed. Applied potential refers to SCE reference.

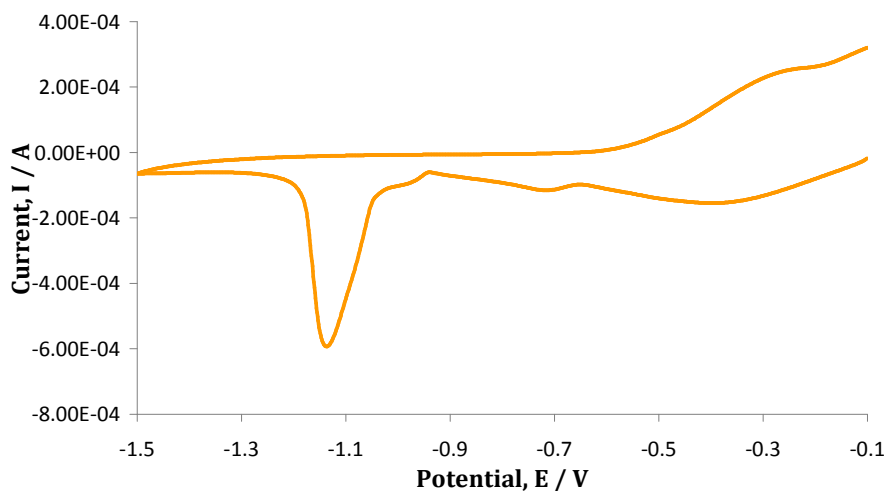


Figure 4.7: CV of 5.00×10^{-3} M EV in 0.10 M NaCl supporting electrolyte, scan rate 50 mV s^{-1} , on ppys β -CD after conditioning of the polymer in the EV solution, for 10 cycles from -0.1 V to -0.6 V vs SCE. The ppys β -CD was synthesized on Au, $d = 3.0$ mm, from a 0.20 M pyrrole/ 0.02 M β -CD solution, at 0.80 V vs SCE until a charge of 2.50×10^{-2} C was consumed. Applied potential refers to SCE reference.

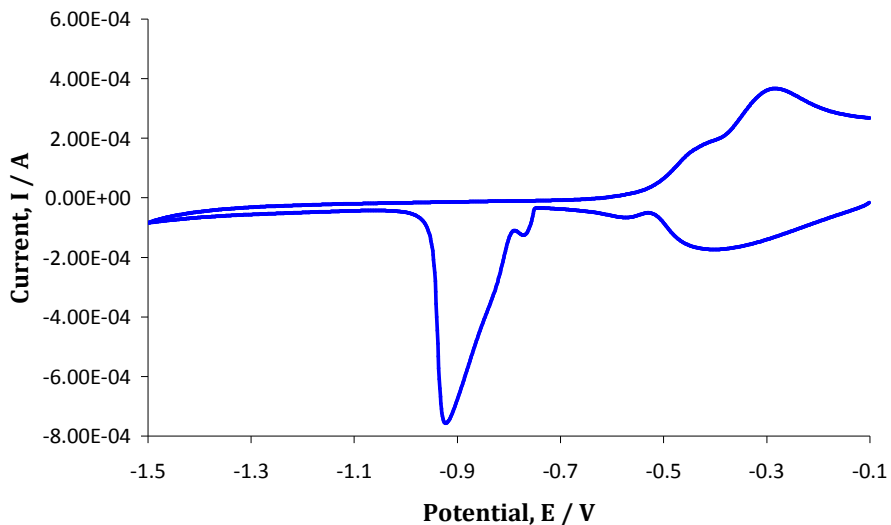


Figure 4.8: CV of 5.00×10^{-3} M BV in 0.10 M NaCl supporting electrolyte, scan rate 50 mV s^{-1} , on ppys β -CD after conditioning of the polymer in the BV solution, for 10 cycles from -0.1 V to -0.5 V vs SCE. The ppys β -CD was synthesized on Au, $d = 3.0 \text{ mm}$, from a 0.20 M pyrrole/ 0.02 M s β -CD solution, at 0.80 V vs SCE until a charge of $2.50 \times 10^{-2} \text{ C}$ was consumed. Applied potential refers to SCE reference.

The large peaks recorded at -1.245 V for MV, at -1.137 V for EV and at -0.923 V vs SCE for BV had the typical shape and asymmetry of a redox process involving adsorbed species.²⁰ Another indication that suggests these peaks can be treated as adsorption peaks was the substantial dependency of the peak potential on the scan rate, as illustrated in Figure 4.9 for the benzyl viologen. While the first and second reduction of the BV are minimally affected by the increase of the scan rate, the third peak potential was found at -0.923 V vs SCE when a scan rate of 50 mV s^{-1} was used and at -1.347 V vs SCE for the highest scan rate investigated which was 400 mV s^{-1} . This large shift of the peak potential indicated that the third reduction was a slow and irreversible process. This was confirmed by the absence of the corresponding peak in the oxidation wave.²⁰ It is well known from the literature that the peak current involved in an adsorption process is proportional to the scan rate, ν , while proportionality between the peak current and $\nu^{1/2}$ is consistent with a reaction controlled by the diffusion of the electroactive molecule to the electrode surface.²⁰⁻²²

However, when the peak current for this third reduction peak of BV was plotted as a function of the scan rate, a linear relationship was not found, Figure 4.10 (a). On the other hand, when the peak current was plotted as a function of the square root of the scan rate, a straight line with a correlation coefficient of 0.995 was obtained, Figure 4.10 (b).

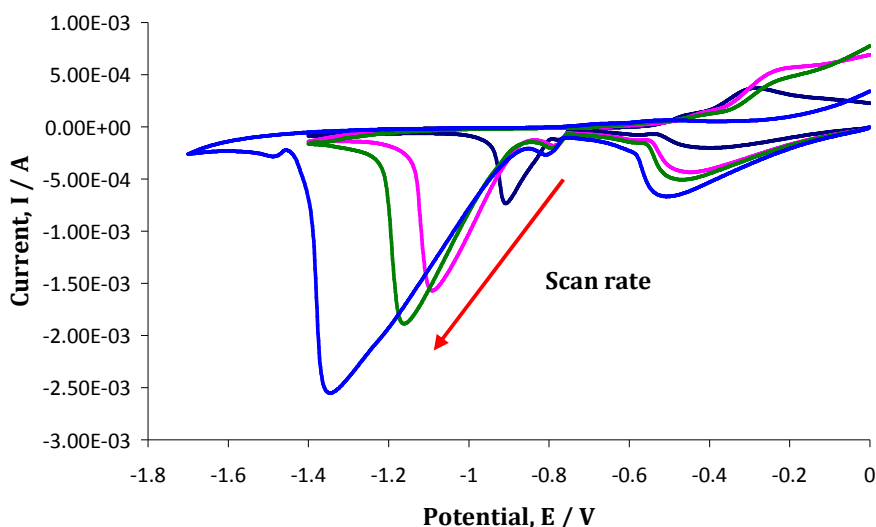
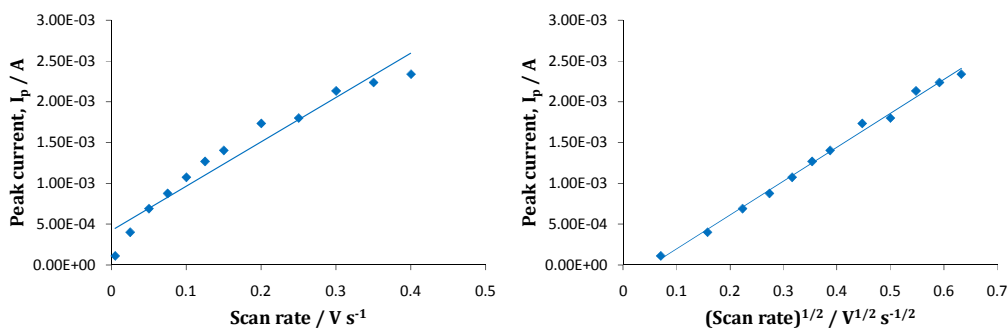


Figure 4.9: CVs (potential vs SCE) of a 5.00×10^{-3} M BV/0.10 M NaCl solution, scan rate 50, 150, 200 and 400 mV s^{-1} , on ppys β -CD. The ppys β -CD was synthesized on Au, $d = 3.0 \text{ mm}$, from a 0.20 M pyrrole/ 0.02 M s β -CD solution, at 0.80 V vs SCE and to a charge of 2.50×10^{-2} C.



(a) (b)
Figure 4.10: Peak current for the peak at more negative potential plotted vs the scan rate (a) or vs the square root of the scan rate (b). A new polymer was synthesized for every scan rate measurement. The ppys β -CD was deposited on Au, $d = 3.0 \text{ mm}$, from a 0.20 M pyrrole/ 0.02 M s β -CD solution, at 0.80 V vs SCE and to a charge of 2.50×10^{-2} C.

The data presented in Figure 4.10 suggest a diffusion controlled process with the peak current depending on the square root of the scan rate. In contrast, the shape of the peak and the irreversibility of the wave suggest the existence of adsorption phenomena. To clarify this issue, additional tests were performed.

Quartz crystal microbalance experiments for ppys β -CD cycled in different concentrations of BV were carried out and the results are shown in Figure 4.11 (a). Furthermore, the QCM scan performed in 5.00×10^{-3} M BV was compared with the signal recorded when ppys β -CD was cycled in 1.00 M NaCl and these data are shown in Figure 4.11 (b). In all cases, the potential was cycled from 0.0 to -1.2 V vs Ag/AgCl. The Δ mass was computed from the frequency data, as detailed in Section 2.5.1.

The change in mass on cycling ppys β -CD in 1.0 M NaCl from 0.0 to -0.7 V vs Ag/AgCl was 1.74×10^{-6} g and this was attributed to the injection of sodium cations and water molecules from the ions solvation shell during reduction of the polymer, as outlined in Section 3.5.2. When the polymer was cycled in 5.00×10^{-3} M BV, three linear regions exhibiting different slopes could be identified in the mass-potential plot, as shown in Figure 4.11 (b). The first fragment is connected with the ppy electroactivity. Around -0.5 V vs Ag/AgCl the slope of the mass plot changes, as highlighted by the red dotted line. This second section of mass increase occurred from -0.5 V to -0.8 V vs Ag/AgCl which is the potential region corresponding to the first and second reduction of the BV at the polymer-modified electrode (see Table 4.3). Finally, the potential window for the last portion of the mass plot, from -0.80 V to -1.20 V vs Ag/AgCl is related to the third intense peak of reduction. By decreasing the BV concentration from 5.00 to 2.50×10^{-3} M, the Δ mass involved in the overall process was nearly halved, from 7.23×10^{-6} g to 3.05×10^{-6} g. When the BV concentration was reduced to 1.00×10^{-3} M, a Δm of 2.03×10^{-6} g was obtained for the reduction wave, Figure 4.11 (a).

Clearly, there is a considerable increase in mass as the polymer is cycled in the BV-containing solutions. In particular, the dotted slope of Figure 4.11 (b)

indicates that both the radical and the neutral species generated from the reduction of the viologen within the solution are deposited to some extent on the polymer. The dashed trace, corresponding to the potential interval from -0.8 V to -1.2 V provides evidence of a further increase of mass on the polymer.

A reasonable explanation for the mass increase between -0.8 V and -1.2 V is that the neutral species, BV^0 , forms and accumulates on the large ppys β -CD surface area. It then undergoes a comproportionation reaction with the dication BV^{2+} , which is the predominant species within the bulk solution. The comproportionation reaction (Table 4.2) of the adsorbed BV^0 generates more radicals which, in turn, are reduced again, in a cyclic reaction, as illustrated in Scheme 4.1. As the result of the combination of these chemical and electrochemical reactions, the intense peak around -0.9 V vs Ag/AgCl is observed. Therefore, this large peak is the result of a chemical reaction between an adsorbed species, BV^0 , with a species in solution, BV^{2+} . This could explain why the peak has the shape and behaviour of an adsorption process but it is also under diffusion control.

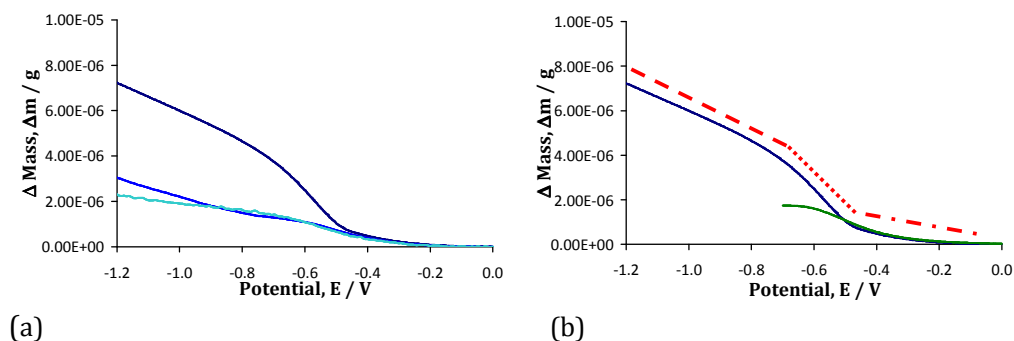
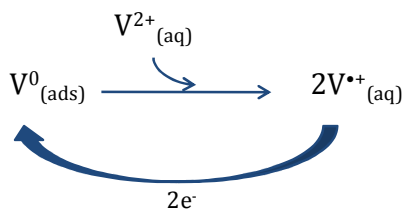


Figure 4.11: QCM data recorded for ppys β -CD in 5.00×10^{-3} M BV / 0.10 M NaCl —, in 2.50×10^{-3} M BV / 0.10 M NaCl — and in 1.00×10^{-3} M BV / 0.10 M NaCl — using a scan rate of 50 mV s^{-1} (a). QCM for ppys β -CD cycled in 5.00×10^{-3} M BV/0.10 M NaCl — compared to ppys β -CD cycled in 1.00 M NaCl — (b). The ppys β -CD was synthesized on Au, surface area 0.2033 cm^{-2} , from a 0.20 M pyrrole/ 0.02 M β -CD solution, at 0.80 V vs Ag/AgCl and to a charge of 2.50×10^{-2} C.



Scheme 4.1: Scheme for the viologen conproportionation reaction coupled with an electrochemical reduction of the radical at the ppys β -CD surface, which results in an increase in the amount of V⁰ and V^{•+} adsorbed.

In addition, in Figure 4.12, typical results from QCM experiments carried out at a constant potential for ppys β -CD in NaCl solution and in a BV solution are illustrated. At the applied potential of -1.0 V vs Ag/AgCl the polymer is fully reduced. The BV also at this potential is totally reduced. The Δ mass recorded in NaCl increases significantly in the first two seconds, indicating a flux of Na⁺ cations into the polymer to balance the negative sulfate groups of the s β -CD dopants.

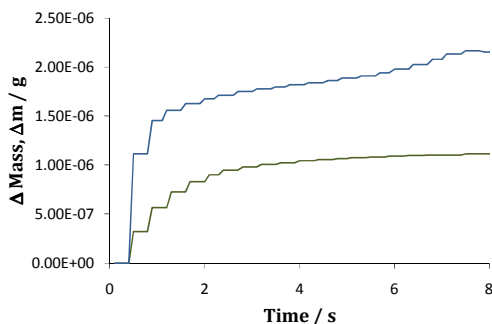


Figure 4.12: Potentiostatic mass-time curves recorded for ppys β -CD in 1.00 M NaCl, at -1.0 V vs Ag/AgCl, — and in 5.00 x 10⁻³ M BV in 0.10 M NaCl, at -1.0 V vs Ag/AgCl —. The ppys β -CD was synthesized on Au, surface area 0.2033 cm², from a 0.20 M pyrrole/0.02 M s β -CD solution, at 0.80 V vs Ag/AgCl and to a charge of 2.50 x 10⁻² C.

Then the mass reaches a plateau. When the polymer is cycled in the BV solution the Δ mass increase in the first two seconds is dramatically enhanced. This indicates a flux of species with larger mass. Then the plateau region, which occurs between 2 and 6 s is followed by a further increment of mass. The benzyl viologen competes with the Na⁺ cation to balance the negative charges of the reduced polymer. At the same time the benzyl viologen is reduced. The last

increase of the Δ mass could be due to several factors, such as the deposition of the neutral BV^0 within the ppys β -CD film, and the influx of BV dications and sodium cations to replace the reduced viologen in neutralizing the negative charges of the $s\beta$ -CD dopant molecules .

4.3.3 Comparison of the $s\beta$ -CD to a small anionic dopant

In Section 4.3.1, a gold substrate was chosen as the working electrode. Here the detection properties of ppys β -CD deposited at gold are compared to those of a corresponding polymer doped with a smaller species, the chloride anion. Both ppys β -CD and ppyCl were electrosynthesized potentiostatically on gold, at 0.80 V vs SCE to a charge of 2.50×10^{-2} C and then cycled in the analyte solutions from -0.1 V to -1.5 V vs SCE. Only the data for the EV system are shown, as similar electrochemical responses were obtained in the MV and BV solutions.

In Figure 4.13 the redox properties of EV at Au and at the ppyCl surface are represented, while Figure 4.14 illustrates the response at Au and at the ppys β -CD modified electrode. As shown in Figure 4.13, the reduction and oxidation of the EV species are very similar at the polymer doped with chloride anions and at the bare electrode. Similar peak currents and peak potentials are seen as the EV is reduced to the radical cation and further reduced to the neutral species. The reduction of gold oxides/hydroxides is evident in the vicinity of -1.3 to -1.5 V vs SCE. However, the presence of the polymer inhibits these reactions and low currents are observed for the polymer modified electrode.

On the other hand, the redox reactions of EV at the ppys β -CD doped polymer are very different, Figure 4.14. A broad peak around -0.70 V vs SCE is observed for the first reduction of EV. This is followed by a peak around -1.00 V vs SCE corresponding to the second reduction step of EV. However, this wave is partially masked by the intense and overlapping peak centred at -1.137 V vs SCE. This intense peak exhibited some fluctuations in the peak current when a reproducibility test was performed, as shown in Table 4.4. In addition, its intensity was noticed to decrease significantly with repeated cycling, as shown

in Figure 4.15. Although the peak current is very high in the first cycle, it drops to values closer to the magnitude of the other reduction waves on continued cycling. One possible explanation for these observations is the deposition of the reduced viologen, EV^0 , on the active polymer surface. This would result in a decrease of the peak current in the following cycles. In addition, the oxidation response is completely suppressed at the ppys β -CD film, thus confirming the irreversibility of the redox processes at the ppys β -CD.

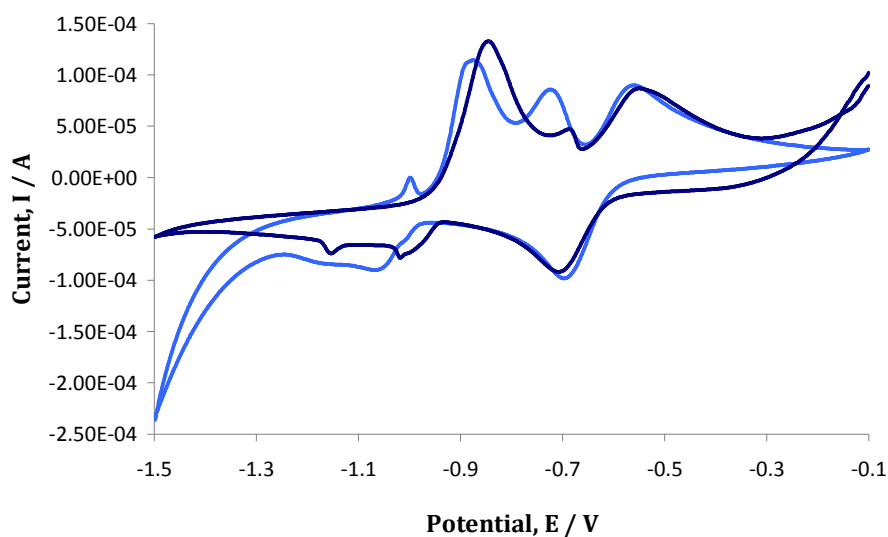


Figure 4.13: CV of 5.00×10^{-3} M EV / 0.10 M NaCl solution, scan rate 50 mV s^{-1} on ppyCl — and bare Au — . The ppyCl was synthesized on Au, $d = 3.0 \text{ mm}$, from a 0.20 M pyrrole/ 0.10 M NaCl solution, at 0.80 V Vs SCE to a charge of 2.50×10^{-2} C. Potential refers to the SCE reference scale.

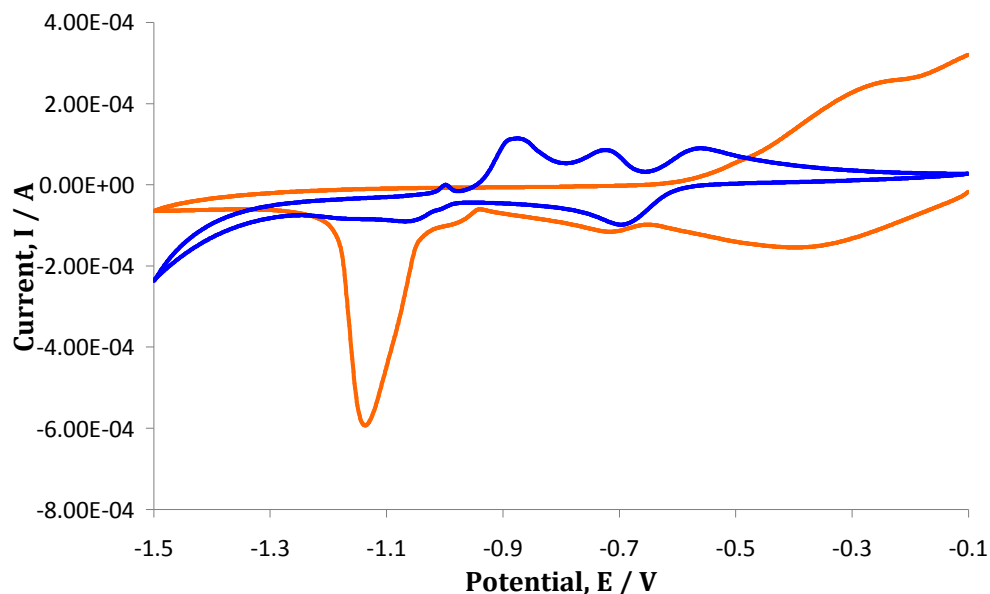


Figure 4.14 CV of 5.00×10^{-3} M EV in 0.10 M NaCl solution, scan rate 50 mV s^{-1} , on ppys β -CD — and bare Au —. The ppys β -CD was synthesized on Au, $d = 3.0$ mm, from a 0.20 M pyrrole/0.02 M s β -CD solution, at 0.80 V Vs SCE to a charge of 2.50×10^{-2} C. Potential refers to the SCE reference scale.

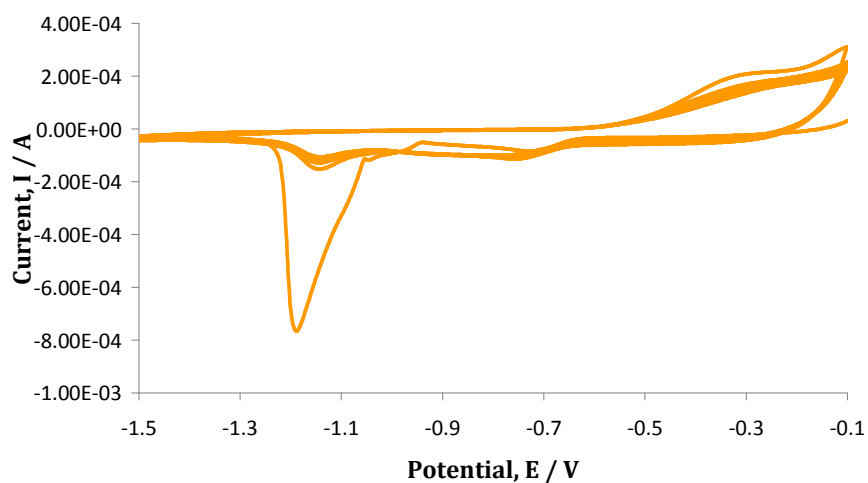


Figure 4.15: CV of 5.00×10^{-3} M EV in 0.10 M NaCl solution, scan rate 50 mV s^{-1} , on ppys β -CD —. The ppys β -CD film was synthesized on Au, $d = 3.0$ mm, from a 0.20 M pyrrole/ 0.02 M s β -CD solution, at 0.80 V Vs SCE to a charge of 2.50×10^{-2} C. Potential refers to the SCE reference scale.

Table 4.4: Reproducibility of the peak centred at - 1.100 V vs SCE obtained from CVs recorded in 5.00×10^{-3} M EV in 0.1 M NaCl, from - 0.10 to -1.50 V vs SCE, on ppys β -CD. The ppys β -CD was synthesized on Au, d = 3.0 mm, from a 0.20 M py/0.02 M s β -CD solution, at 0.80 V Vs SCE to a charge of 2.5×10^{-2} C.

Sample	Potential / V vs SCE	Current / A
1 Ppys β -CD	- 1.144	5.103×10^{-4}
2 Ppys β -CD	- 1.143	4.851×10^{-4}
3 Ppys β -CD	- 1.137	5.861×10^{-4}

4.3.4 Influence of the electrochemical window

The response described in Figure 4.15 was not observed if the potential was applied in the reverse direction. Figure 4.16 shows typical voltammograms recorded for a 5.00×10^{-3} M EV solution at a ppys β -CD film. The polymer, in this case, was cycled from - 1.5 V to - 0.1 V vs SCE. None of the peaks described in Figure 4.15 were observed, thus highlighting the importance of the direction of the potential scan. Only the redox activity of the ppys β -CD film is observed in the vicinity of -0.60 to -0.10 V vs SCE. As the initial cathodic potential of -1.50 V vs SCE is applied, the viologen is reduced to the neutral species, EV⁰, which is deposited within the polymer matrix. As a consequence the polymer matrix is deactivated. This is clearly evident from Figure 4.16.

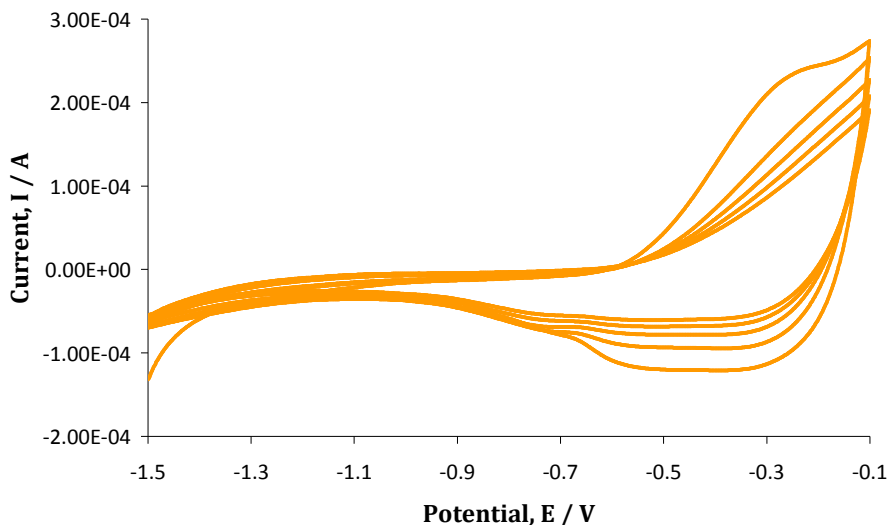


Figure 4.16: CV of a 5.00×10^{-3} M EV in 0.10 M NaCl solution, scan rate 50 mV s^{-1} , on ppys β -CD. Potential was switched from -1.5 V to -0.1 V vs SCE. The ppys β -CD was synthesized on Au, $d = 3.0 \text{ mm}$, from a 0.20 M pyrrole/ 0.02 M s β -CD solution, at 0.80 V vs SCE and to a charge of $2.50 \times 10^{-2} \text{ C}$.

4.3.5 Calibration curves

Preliminary experiments were performed by means of CV to elucidate if the modified sensor, ppys β -CD, had any ability in the sensing of different concentrations of the analytes. The reduction peak for the viologen adsorbed on ppys β -CD was used to construct calibration curves for the three compounds. This peak was detected around -0.9 V vs SCE for benzyl viologen, and around -1.1 V vs SCE for the ethyl and methyl viologens, as illustrated in the CVs shown in Figure 4.6, Figure 4.7 and Figure 4.8. Each CV experiment was repeated three times and a fresh polymer was used at all times. The modified polymer was first conditioned by cycling in the required viologen solution in the potential window from 0.0 to -0.5 V vs SCE in the case of BV and from 0.0 to -0.6 V vs SCE for MV and EV. Then the polymer was cycled in a potential window from 0.0 to -1.5 V and the peak currents of the first cycle were considered.

The resulting calibration plots are depicted in Figure 4.17(a), (b) and (c) for the methyl, ethyl and benzyl viologens, respectively. A linear relationship was obtained for methyl and ethyl viologens. In contrast, a polynomial curve was

constructed for the BV, thus suggesting a saturation of the active sites on the polymer at high concentration of the dication. Unfortunately, the lowest concentrations detected at the polymer surface were high. As a matter of fact, the polymer did not show any signal for MV or EV at concentrations lower than 1.00×10^{-3} M. The detection of the BV was slightly better, since a concentration of 5.00×10^{-4} M still gave a visible and reproducible signal.

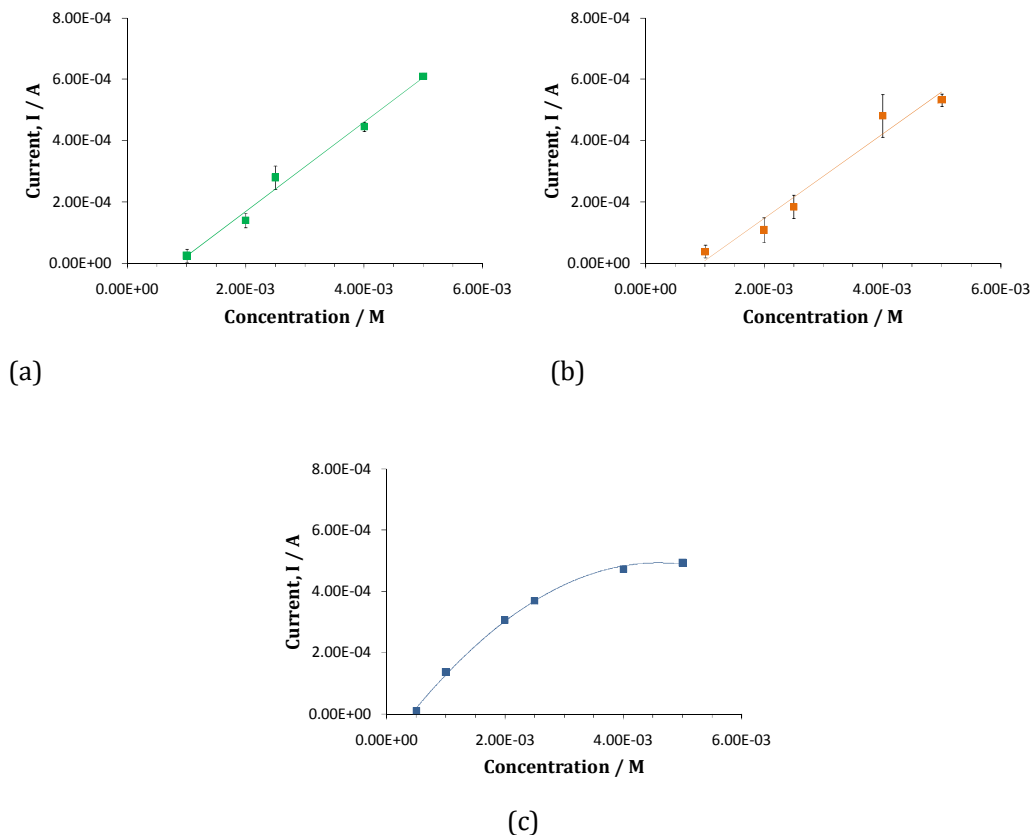


Figure 4.17: Calibration curve for the adsorption peak current as a function of the concentration of MV (a), EV (b) and BV (c) at the modified ppys β -CD. Fresh polymers were conditioned in the required viologen solution (made up in 0.10 M NaCl supporting electrolyte) by cycling 10 times in the potential interval from -0.1 to -0.6 (MV, EV) and from -0.1 to -0.5 (BV). Then the polymers were cycled in the viologen solutions from 0.0 to -1.5 V vs SCE at 50 mV s^{-1} . The ppys β -CD was synthesized on Au, $d = 3.0 \text{ mm}$, from a 0.20 M pyrrole/ 0.02 M β -CD solution, at a potential of 0.8 V vs SCE to a charge of $2.50 \times 10^{-2} \text{ C}$. (a) $y = 1.46 \times 10^{-1}x - 1.00 \times 10^{-4}$, $R^2=0.962$; (b) $y = 1.46 \times 10^{-1}x - 1.00 \times 10^{-4}$, $R^2=0.962$; (c) $y = -28.27x^2 + 2.60 \times 10^{-1}x - 1.00 \times 10^{-4}$, $R^2=0.998$.

These high concentration values highlight the limitations of the CV method in the sensing of the three compounds. One of the probable reasons was the high contribution of the capacitive current. When low concentrations of an analyte are used, low Faradaic currents are generated. On the other hand, the capacitive current due to the double layer charge separation at the polymer solution interface still gives a similar contribution. As a consequence, the small variations in the Faradaic currents are masked by capacitive effects. In an attempt to reduce the capacitive contribution of the polymer matrix, DPV and CPA experiments were performed and the results are presented in Sections 4.5 and 4.6. Furthermore, the experimental parameters were optimized in order to enhance the sensing ability of the ppys β -CD and the best experimental conditions are discussed in Section 4.4.

4.4 Optimization of the experimental parameters

Since the modified polymer, ppys β -CD, exhibited poor detection towards the sensing of the three viologens examined, an investigation into the experimental parameters was performed. The aim of this study was to optimize the experimental conditions in order to increase the detection of MV, EV and BV at the ppys β -CD surface. The study was focused on two different aspects: the characteristics of the polymer film and the supporting electrolyte used to dissolve the analytes. In the following section the potential at which the polymer was synthesized, the polymer thickness and the influence of the supporting electrolyte are discussed. Firstly, the growth potential of ppys β -CD was considered, in Section 4.4.1. Then, for polymers grown at the best potential selected in Section 4.4.1, the influence of the thickness was explored in Section 4.4.2. With the optimum charge and polymer thickness achieved, the affect of the supporting electrolyte was examined, in Section 4.4.3. Results are shown for the sensing of BV. For each experiment, the polymer synthesized under the established condition was abundantly rinsed with distilled water; then immersed in a 1.00×10^{-3} M BV solution, in 0.10 M NaCl, unless otherwise stated and cycled in a potential window ranging from 0.0 V to -1.4 V vs SCE. Ten cycles were recorded. Currents shown in the following plots (Figure 4.18, Figure 4.19

and Figure 4.20) represent the peak currents for the reduction wave around -0.9 V vs SCE of the BV adsorbed on the polymer matrix. The values presented refer to the first, second and last voltammetric cycle (cycle 10) at -0.9 V vs SCE, depicted in Figure 4.8. All experiments were performed at least twice.

4.4.1 Electrosynthesis potential

The first parameter studied was the potential applied to grow the polymer films. Polymers were grown on a gold substrate, from a 0.20 M solution of pyrrole, in 2.00×10^{-2} M s β -CD, to a charge of 2.50×10^{-2} C. The electrosynthesis potentials examined ranged from 0.6 V up to 0.9 V vs SCE, as shown in Figure 4.18. Once the polymer was deposited, it was rinsed and dipped into a solution 1.00×10^{-3} M of BV, in 0.10 M NaCl supporting electrolyte. It was then cycled in the BV solution. The currents represented by the blue trace in Figure 4.18 correspond to the peak currents at -0.9 V vs SCE recorded for the first cycle. It is evident from the plot that lower currents are measured for polymer films synthesized at potentials exceeding 0.7 V vs SCE. It is well known that during potentiostatic growth, polymerization proceeds faster at higher potentials although the resistance of the film may increase due to over-oxidation of the polymer backbone.^{23,24} Lewis and coworker²⁵ showed that polypyrrole over-oxidation begins at 0.65 V (at pH 6.0) but such phenomena became significant at potentials higher than 0.8 V vs SCE. In this work, polymers grown at lower potentials showed enhanced detection towards the sensing of benzyl viologen. In particular, an applied voltage of 0.6 V vs SCE gave rise to the synthesis of the polymer measuring the highest current. Differences in the peak current values among the samples prepared at different applied potentials were less meaningful when the second and last cycles were considered, as depicted by the green and orange traces, respectively, in Figure 4.18. From this study, it was concluded that the best potential to grow the ppys β -CD was 0.6 V vs SCE.

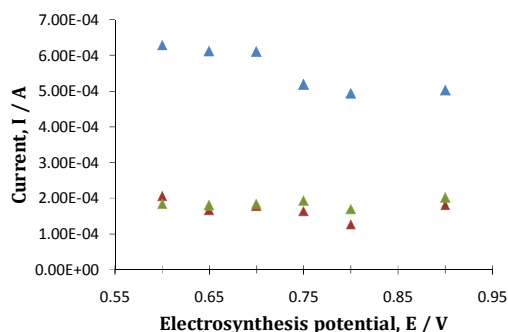


Figure 4.18: Peak currents for the reduction at -0.9 V vs SCE of 1.00×10^{-3} M BV in 0.1 M NaCl on ppys β -CD grown at different potentials. The ppys β -CD was synthesized on Au, $d = 3.0$ mm, from a 0.20 M pyrrole/ 0.02 M β -CD solution, to a charge of 2.50×10^{-2} C. The polymer was cycled in the BV solution from 0.0 V to -1.4 V vs SCE. 1st cycle \blacktriangle , 2nd cycle \blacktriangle and last cycle (10th) \blacktriangle .

4.4.2 Polymer thickness

To inspect the effect of the thickness of the ppys β -CD films, the polymers were electrosynthesized on an Au electrode at 0.6 V vs SCE until various charges, ranging from 2.10×10^{-1} C cm^{-2} to 2.83 C cm^{-2} , were consumed. Subsequently, the polymer was rinsed and cycled in the 1.00×10^{-3} M BV solution. The peak current and peak potential for the first, second and last cycle, corresponding to the reduction of the adsorbed BV were recorded and these are illustrated in Figure 4.19 (a) and (b). The peak reduction currents increase with charge, reaching a maximum for a polymer thickness corresponding to 2.12 C cm^{-2} , as shown in Figure 4.19 (a). This result was expected, considering the fact that as the thickness of a polymer film is increased, the porosity of the matrix increases too.²⁶ Hence, the surface of the polymer at which the BV can react at is larger, leading to higher currents. After the maximum at 2.12 C cm^{-2} , the peak currents start to decrease, as depicted in Figure 4.19. To reach these higher charges, the polymer is exposed to the oxidation potential for a longer time. This induces overoxidation to some extent, even at an applied voltage of 0.6 V vs SCE.

In Figure 4.19 (b) it is shown that as the thickness of ppys β -CD is increased, the corresponding peak potential for the reduction of the BV adsorbed on the polymer surface is shifted to more negative potentials. This indicates that the

system requires higher energy for reducing the analyte. For thick polymers, the higher active surface available for the electrochemical reaction is counterbalanced by a higher resistance of the film, since the electrons have to travel from the metal substrate through the polymer backbone.^{27,28} As a consequence, the choice of the optimum polymer thickness was a compromise between current intensity and potential shift. For this reason, a charge of 1.13 C cm^{-2} was selected, as depicted by the red arrows in Figure 4.19 (a) and (b).

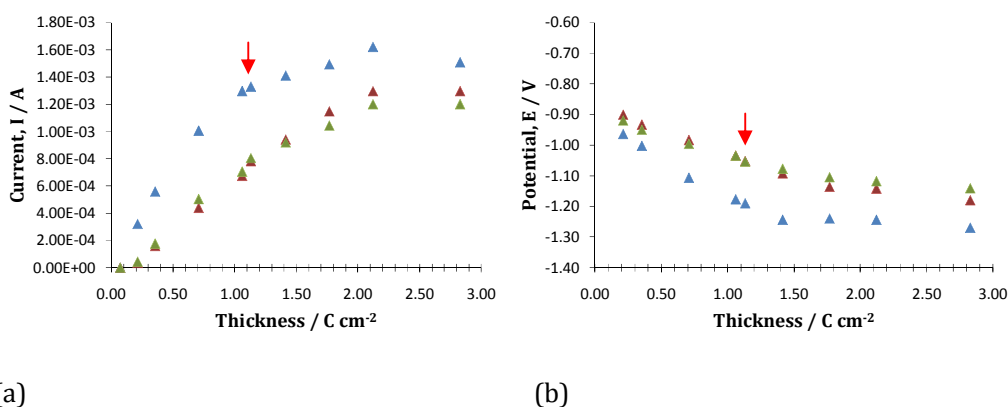


Figure 4.19: Peak current (a) and peak potential (b) for the reduction of $1.00 \times 10^{-3} \text{ M}$ BV in 0.10 M NaCl on ppys β -CD as a function of the polymer thickness, which is expressed as charge density. The ppys β -CD was synthesized on Au, $d = 3.0 \text{ mm}$, from a $0.20 \text{ M pyrrole} / 0.02 \text{ M s}\beta\text{-CD}$ solution, at a potential of 0.6 V vs SCE . The polymer was cycled in the BV solution from 0.0 V to -1.4 V vs SCE . 1st cycle \blacktriangle , 2nd cycle \blacktriangle and last cycle (10th) \blacktriangle .

4.4.3 Supporting electrolyte

The supporting electrolyte used for all the experiments was 0.10 M NaCl . In order to evaluate the influence of the NaCl in the sensing of the benzyl viologen, the ppys β -CD modified electrode was immersed in varying solutions of BV (5.00×10^{-4} , 1.00×10^{-3} and $2.50 \times 10^{-3} \text{ M}$) made up in different supporting electrolytes: 0.10 M NaCl , $0.1 \text{ M Na}_2\text{SO}_4$ and 0.1 M KCl . The polymer films were deposited at 0.6 V vs SCE and grown to a charge of 1.13 C cm^{-2} , as previously established in Section 4.4.1 and 4.4.2. Again, the peak current for the reduction

of the BV adsorbed on the electrode surface was evaluated. The first, second and last cycles were considered and the corresponding data are shown in Figure 4.20.

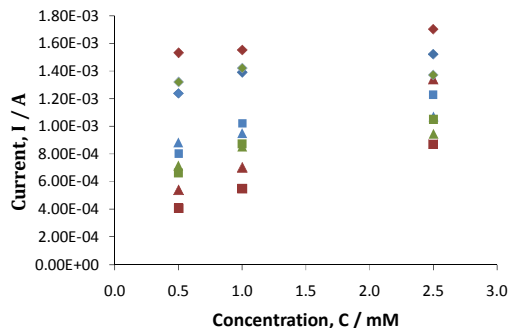


Figure 4.20: Peak current for the reduction of 1.00×10^{-3} M BV in 0.10 M NaCl \color{green} —, in 0.10 M Na₂SO₄ \color{red} — and 0.10 M KCl \color{blue} — on ppys β -CD as a function of the BV concentration. The ppys β -CD was synthesized on Au, $d = 3.0$ mm, from a 0.20 M pyrrole/ 0.02 M s β -CD solution, at a potential of 0.6 V vs SCE. The polymer was cycled in the BV solution from 0.0 V to -1.4 V vs SCE. 1st cycle $\color{black}\blacklozenge$, 2nd cycle $\color{black}\blacksquare$ and last cycle (10th) $\color{black}\blacktriangle$.

Using Na₂SO₄ higher currents were detected in the first cycle, with respect to signals recorded for BV in NaCl or KCl. However, a large drop in the current was recorded in the following cycles when Na₂SO₄ was employed as the supporting electrolyte. Similar peak currents were observed using NaCl and KCl, although at lower concentrations (5.00×10^{-4} M and 1.00×10^{-3} M BV solution), slightly higher currents were measured in the first cycle when NaCl was used as the supporting electrolyte. Since all the experiments before this study were performed in NaCl and other electrolytes did not show a significant improvement of the sensitivity, NaCl was selected as the supporting electrolyte.

Another important characteristic to consider for the choice of the supporting electrolyte was the cation exchange properties of the ppys β -CD. In Figure 4.21 voltammograms of ppys β -CD films in varying concentration of EV are presented.

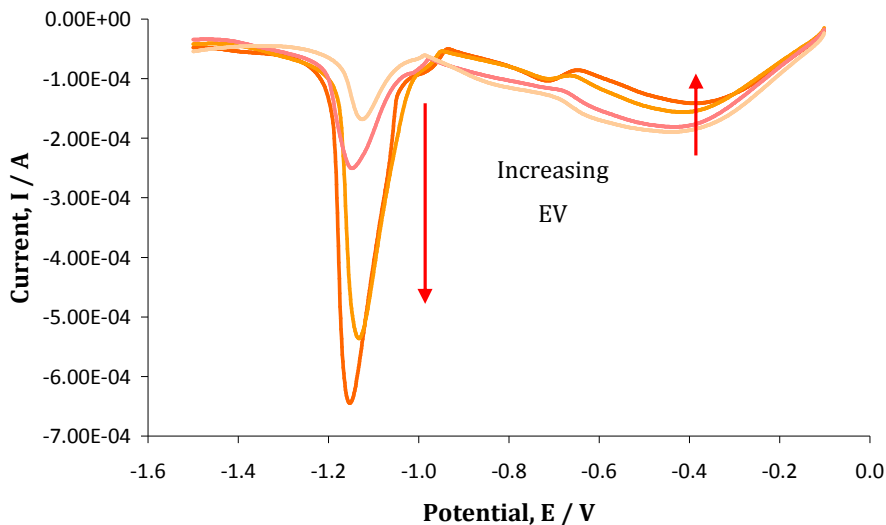


Figure 4.21: CV of ppys β -CD in EV solutions of varying concentrations: 5.00×10^{-3} M, 4.00×10^{-3} M, 2.50×10^{-3} M, 2.00×10^{-3} M in 0.1 M NaCl. The ppys β -CD was synthesized on Au, $d = 3.0$ mm, from a 0.20 M pyrrole/ 0.02 M s β -CD solution, at a potential of 0.6 V vs SCE.

It is visible from the plot that the current for the polymer electroactivity, between -0.2 and -0.5 V vs SCE, decreases as the EV concentration increases. In this potential interval the viologens are still inert and hence present in solution as dications. When the polymer starts to be reduced, a competition occurs between Na^+ and the EV^{2+} to influx into the polymer, in order to maintain the electroneutrality of the ppy backbone. High concentrations of the viologen promote the dication exchange over the Na^+ exchange. These phenomena are represented by a lower redox current of the polymer as a result of the lower mobility of the viologen (due to its larger size) compared to the Na^+ cation. At lower concentrations of EV, the contribution of the sodium becomes higher. For these reasons the optimum NaCl concentration was selected at 0.05 M. This latter concentration can still ensure the conductivity of the solution. At the same time the Na^+ exchange is decreased and that for the viologens is favoured.

4.5 Differential pulse voltammetry (DPV)

Differential pulse voltammetry (DPV) is a technique largely developed to provide enhanced sensitivity in analytical studies as compared to other methods such as CV.²¹ The main advantage over CV is the possibility with DPV to control and minimize the background noise and hence to enhance the detection properties of the system investigated.²¹ In this work DPV experiments were performed in an attempt to increase the sensing of the modified electrode, ppys β -CD, towards the detection of methyl, ethyl and benzyl viologens.

The experimental parameters for the DPV study were set up in accordance with the details reported in Section 2.5.6. A fresh polymer was electrosynthesized for each DPV experiment, at the applied potential of 0.6 V vs SCE, until a charge of 1.13 C cm⁻² was consumed. The viologen solutions were made up in 0.05 M NaCl, as this concentration was found to ensure conductivity of the solution and to reduce the background current. Prior to recording the DPV experiments, ppys β -CD was conditioned for 40 cycles in the desired viologen solution by means of CV, using a potential window from 0.0 to -0.5 V vs SCE for the benzyl viologen and from 0.0 to -0.6 V vs SCE for the methyl and ethyl viologens. The viologens are inert within these potential windows, while the polymer backbone is electroactive. The reason for conditioning was to accumulate the viologen on the polymer surface by using the cation exchange properties of the ppys β -CD film. In the study of the redox behaviour of the polymer matrix, a competition between the sodium cations and the viologen dication species was observed. As explained in Section 3.5.2, when the ppys β -CD is reduced, the polymer backbone becomes neutral. As the anionic β -CD is a large dopant, it cannot be released into the bulk solution, thus cations are required within the polymer matrix to balance the negative charge of the dopants and maintain electroneutrality of the system. The viologens are dicationic species; hence they compete with the Na⁺ cations to enter the polymer and neutralize the negative charge of the sulfate groups of the β -CD dopant.

In Figure 4.22, Figure 4.23 and Figure 4.24, DPV plots of 1.00 x 10⁻³ M MV, EV and BV in 0.05 M NaCl are shown. As observed with the CV experiments, 3

reduction peaks can be distinguished for the electrochemistry of the BV at the polymer modified surface. The first peak, around -0.6 V vs SCE corresponds to the reduction of the dication to generate the radical species ($BV^{2+} + e^- \rightarrow BV^{\bullet+}$), the signal around -0.8 V vs SCE was assigned to the second reduction of the benzyl viologen ($BV^{\bullet+} + e^- \rightarrow BV^0$). The wave at -1.0 V vs SCE is the typical reduction peak observed at the ppys β -CD surface and discussed in Section 4.3.2. Figure 4.22 and Figure 4.23 show that the second reduction process is less defined for the methyl and ethyl viologens, and it appears as a shoulder of the adsorption peak.

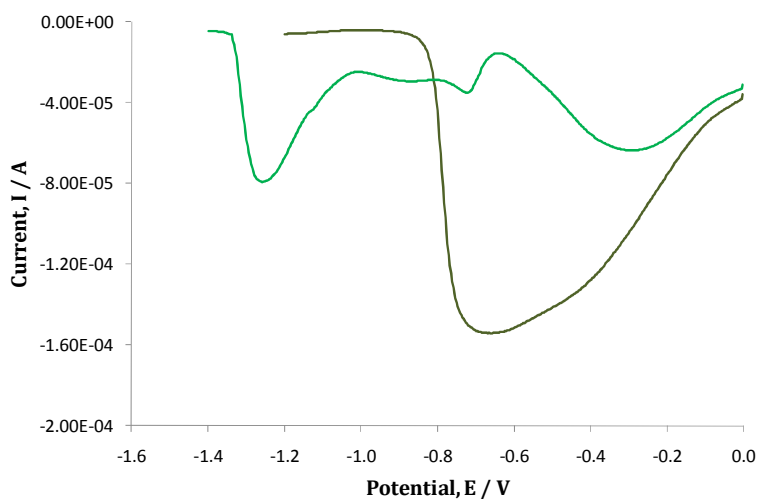


Figure 4.22: DPV of ppys β -CD in 1.00×10^{-3} M MV in 0.05 M NaCl — and in 0.05 M NaCl —. DPV set up: pulse amplitude 50.00 mV, pulse width 0.10 s, sampling width 0.05 s, pulse period 0.30 s, increment 3.00 mV. The ppys β -CD was electrodeposited on Au, $d = 3.0$ mm, from 0.20 M pyrrole/0.02 M s β -CD, at 0.6 V vs SCE until a charge of 1.13 C cm^{-2} was consumed. The polymer was conditioned in 1.00×10^{-3} M MV in 0.05 M NaCl using CV, 40 cycles, scan rate 50 mV s^{-1} , potential window 0.0 to -0.5 V vs SCE.

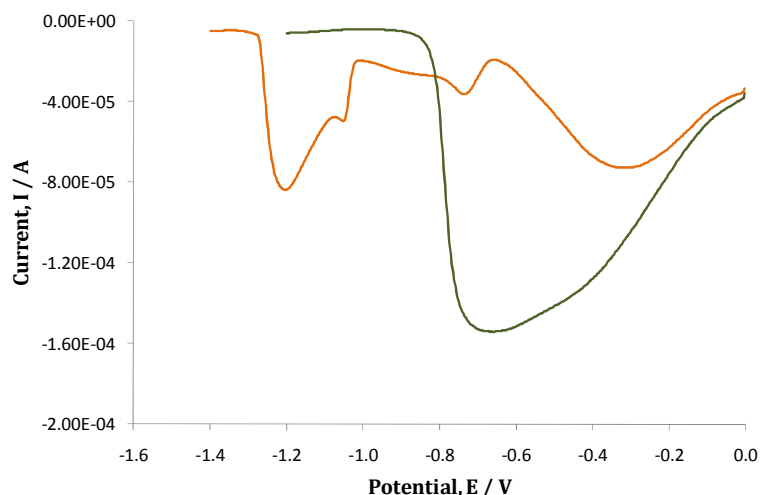


Figure 4.23: DPV of ppys β -CD in 1.00×10^{-3} M EV in 0.05 M NaCl — and in 0.05 M NaCl —. DPV set up: pulse amplitude 50.00 mV, pulse width 0.10 s, sampling width 0.05 s, pulse period 0.30 s, increment 3.00 mV. The ppys β -CD was electrodeposited from 0.20 M pyrrole/0.02 M s β -CD, at 0.6 V vs SCE until a charge of 1.13 C cm^{-2} was consumed. The polymer was conditioned in 1.00×10^{-3} M EV in 0.05 M NaCl using CV, 40 cycles, scan rate 50 mV s^{-1} , potential window from 0.0 to -0.5 V vs SCE.

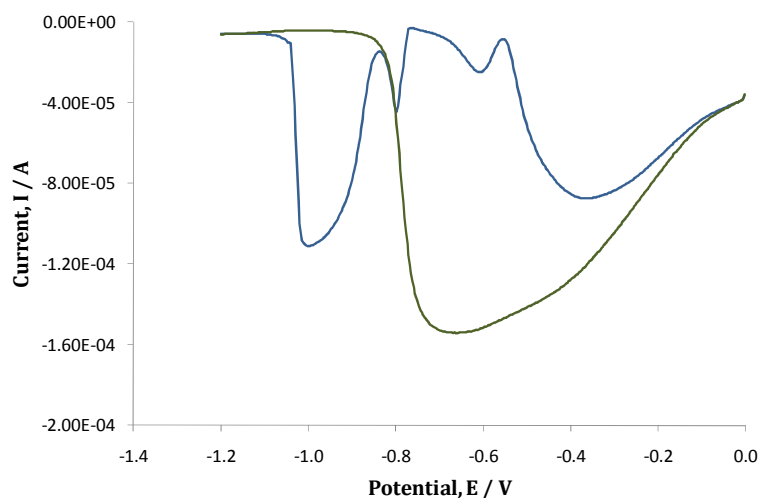


Figure 4.24: DPV of ppys β -CD in 1.00×10^{-3} M BV in 0.05 M NaCl — and in 0.05 M NaCl —. DPV set up: pulse amplitude 50.00 mV, pulse width 0.10 s, sampling width 0.05 s, pulse period 0.30 s, increment 3.00 mV. The ppys β -CD was electrodeposited on Au, $d = 3.0 \text{ mm}$, from 0.20 M pyrrole/0.02 M s β -CD, at 0.6 V vs SCE until a charge of 1.13 C cm^{-2} was consumed. The polymer was conditioned in 1.00×10^{-3} M BV in 0.05 M NaCl using CV, 40 cycles, scan rate 50 mV s^{-1} , potential window 0.0 to -0.5 V vs SCE.

The sensing ability of the ppys β -CD was compared to that of a polymer grown under identical conditions but doped with a large non-macrocyclic anion, sodium dodecyl sulphate (sds). As already stated in Section 3.2.4, sds anions are large bulky dopants, they possess only one negative charge and exhibit very different properties to the cyclodextrin. The sds-doped ppy (ppysds) showed no detection ability for the sensing of the methyl, ethyl and benzyl viologens, as revealed in Figure 4.25 (a), (b) and (c). The dramatic difference between ppysds and ppys β -CD might be due to the different amount of negative charges possessed by the two different dopants. The s β -CD has an average of 7 sulfate groups per molecule. On the other hand, sds anions have only one negative charge per molecule. It would appear that the interaction between ppys β -CD and the viologens is mainly driven by electrostatic forces. Results recorded at the ppysds surface suggest that the sensing ability of the ppys β -CD sensor is related to the number of negative charges exhibited by the dopant. Further investigations on the interaction between the s β -CD and the viologens will be provided in Chapters 5 and 6.

The adsorption peaks for the three compounds are straightforward to analyze when the viologen concentration is relatively high, *e.g.* 1.00×10^{-3} M, as shown in Figures 4.22, 4.23 and 4.24. Unfortunately, as the concentration of the viologen was decreased, the peak potential shifted. These features made the peak currents hard to analyze as a function of the viologen concentration. However, as previously mentioned, the viologens were found to compete with sodium cations for the ionic exchange during the redox processes of the polymer backbone. It was found that the background signal for the polymer electroactivity increased as the viologen concentration was decreased. This characteristic has been already discussed in Section 4.4.3. The dark green traces in Figure 4.22, Figure 4.23 and Figure 4.24 represent the electrochemical signal of ppys β -CD in a 0.05 M NaCl solution. As visible in the three figures, the current due to the polymer electroactivity is substantially diminished in the presence of the viologens. Due to the difficulties encountered in determining the current intensity changes of the adsorption peak, the background current (signal for the polymer reduction) was followed.

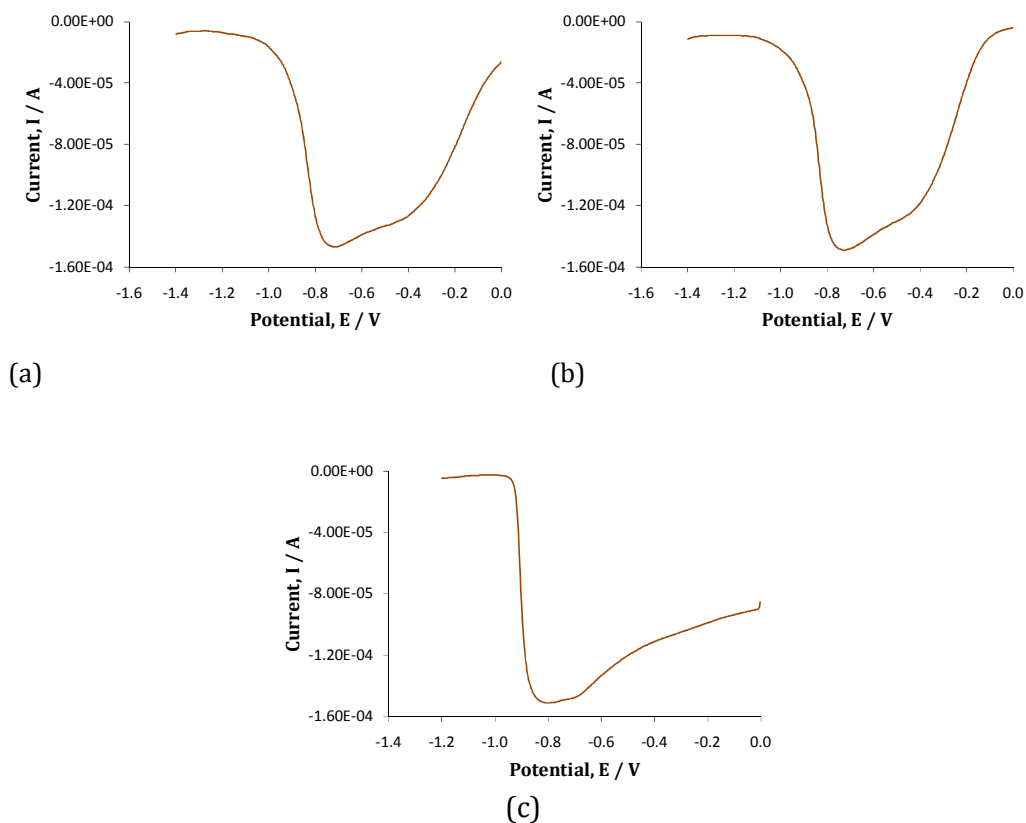
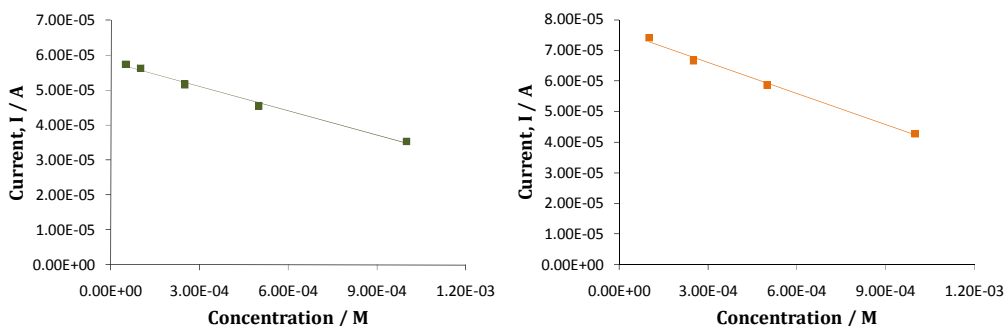
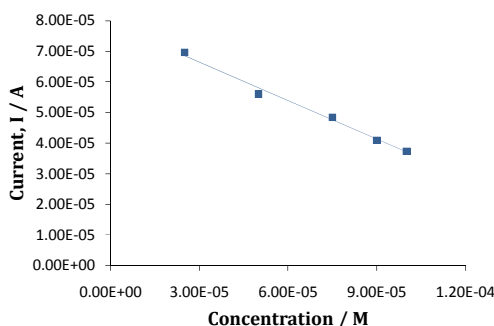


Figure 4.25: DPV of ppysds in 1.00×10^{-3} M MV/0.05 M NaCl (a), 1.00×10^{-3} M EV/0.05 M NaCl (b), 1.00×10^{-3} M BV/0.05 M NaCl (c). DPV set up: pulse amplitude 50.00 mV, pulse width 0.10 s, sampling width 0.05 s, pulse period 0.30 s, increment 3.00 mV. The ppysds was electrodeposited on Au, $d = 3.0$ mm, from 0.20 M pyrrole/0.02 M sds, at 0.6 V vs SCE until a charge of 1.13 C cm^{-2} was consumed. The polymer was conditioned in 1.00×10^{-3} M MV in 0.05 M NaCl using CV, 40 cycles, scan rate 50 mV s^{-1} , potential window 0.0 to -0.5 V vs SCE.

Figure 4.26 (a), (b) and (c) shows that good linearity was obtained for all three viologen compounds. For ethyl viologen, good linearity was observed only down to 1.00×10^{-4} M. However, more satisfactory results were obtained for methyl and benzyl viologens. They exhibited linear relationships down to 5.00×10^{-5} M and 2.50×10^{-5} M, respectively.



(a) $y = 2.33 \times 10^{-2}x + 6.00 \times 10^{-5}$, $R^2=0.994$ (b) $y = 3.39 \times 10^{-2}x + 8.10 \times 10^{-5}$, $R^2=0.994$



(c) $y = 4.20 \times 10^{-1}x + 7.98 \times 10^{-5}$, $R^2=0.990$

Figure 4.26: Background current of ppysβCD as a function of the methyl (a), ethyl (b) and benzyl (c) viologen concentrations. Data obtained from DPV measurements. DPV set up: pulse amplitude 50.00 mV, pulse width 0.10 s, sampling width 0.05 s, pulse period 0.30 s, increment 3.00 mV. The ppysβ-CD was electrodeposited on Au, $d = 3.0$ mm, from 0.20 M pyrrole/0.02 M sβ-CD, at 0.6 V vs SCE until a charge of 1.13 C cm⁻² was consumed. The polymer was conditioned in the viologen solutions in 0.05 M NaCl using CV, 40 cycles, scan rate 50 mV s⁻¹, potential window 0.0 to -0.5 V vs SCE.

4.6 Constant potential amperometry (CPA)

Constant potential amperometry (CPA) is an electrochemical technique originally designed to investigate the efficiency of electrode coating and membrane formation. An additional use of CPA is to study reaction kinetics.²⁹ In the present study, it was used to increase the detection properties of ppysβ-CD towards methyl viologen. The CPA experiments were carried out at a constant reduction potential of -0.9 V vs. SCE. The current of reduction was measured

before and after addition of measured aliquots of methyl viologen to a 0.10 M NaCl electrolyte solution. The working electrode was a rotating disc and the speed was set at 2000 rpm.

The sensitivity of CPA ensures a direct correlation of current with concentration and hence an accurate detection limit can be obtained. In this experiment the potential was fixed at -0.9 V vs. SCE in order to monitor the reduction of MV²⁺ to give MV^{•+}. In Section 4.5 the lowest concentration of methyl viologen that gave a signal detectable by means of DPV at the modified electrode was 5.00×10^{-5} M. It is important to highlight the main difference between the two electrochemical methods used. With DPV, variations in the current corresponding to the polymer backbone electroactivity were monitored as a function of the concentration of the viologens. The CPA experiment followed the current corresponding to the first reduction of MV as a function of the MV concentration. The CPA experiment was performed with the purpose to increase the detection limit for the highly toxic herbicide, methyl viologen, and possibly to reach the detection of concentrations reported in the legislative limits outlined by the EPA and the EU.³⁰

Hence, the reduction of the dication species was monitored and a characteristic CPA plot is depicted in Figure 4.27. The advantage of using a rotating working electrode is that all species at the polymer surface are reduced and a steady state is reached, as indicated in Figure 4.27 by the limiting current recorded following the addition step. On addition of the methyl viologen aliquots, a clear increase in the reduction current was observed. On the other hand if ppy is doped simply with sulfate anions, no detection is observed for the methyl viologen since the small dopants are released when the polymer is reduced (data not shown).

The response time of ppys β -CD, in which a steady-state current was reached following the additions of methyl viologen aliquots, was 36 s. This response time was larger than the values typically recorded in the literature.³¹ However the polymer was polarized at a reduction potential of -0.9 V vs SCE for a long

time frame, in order to minimize the capacitance current. At this reduction potential, ppy is less conducting and this can affect the response time

When the increase in current was plotted as a function of the methyl viologen concentration, the curve depicted in Figure 4.28 was obtained. It is evident from the plot that at lower concentrations of the analyte there is a linear relationship, while the curve deviates from linearity at higher concentrations. The currents recorded at lower concentrations of the herbicide are presented in Figure 4.29, and the linear plot exhibits a correlation coefficient of 0.990. The experimental detection limit taken from Figure 4.29 was 1.56×10^{-5} M. This can also be computed in accordance with Equation 4.1, in which C_m is the limit of detection (M), S_b is the standard deviation of the background current and m is the slope of the linear calibration curve ($A\text{ cm}^{-2}\text{ M}^{-1}$).

$$C_m = \frac{3S_b}{m} \quad 4.1$$

Using Equation 4.1, the calculated limit of detection was computed as 1.36×10^{-5} M, which is almost a 5-fold increase with respect to DPV, indicating the efficiency of this technique to reduce the contribution of the background current. This is in good agreement with the experimental value of 1.56×10^{-5} M. However, this detection limit is still not sufficient in terms of the legislative limits outlined by the Environmental Protection Agency (EPA) and the European Community (EC) of $3.0\ \mu\text{g L}^{-1}$ and $0.1\ \mu\text{g L}^{-1}$, respectively.³⁰

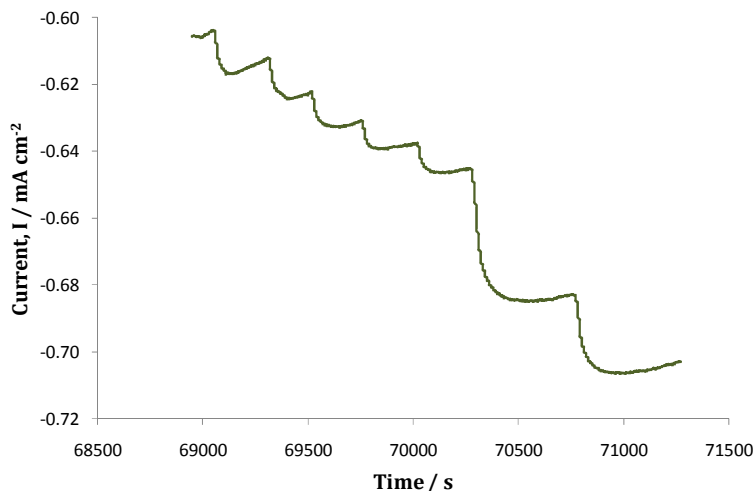


Figure 4.27: CPA plot of current as a function of time. Aliquot additions ranging from 50 μ l to 5 ml of 2.00×10^{-3} M methyl viologen to a 0.10 M NaCl electrolyte solution. The ppys β -CD was electrosynthesized from a 2.0×10^{-1} M pyrrole/ 2.0×10^{-2} M s β -CD, on Au, at a potential of 0.6 V vs SCE and to a charge of 1.13 C cm^{-2} . CPA was recorded at -0.9 V vs SCE at a rotation speed of 2000 rpm.

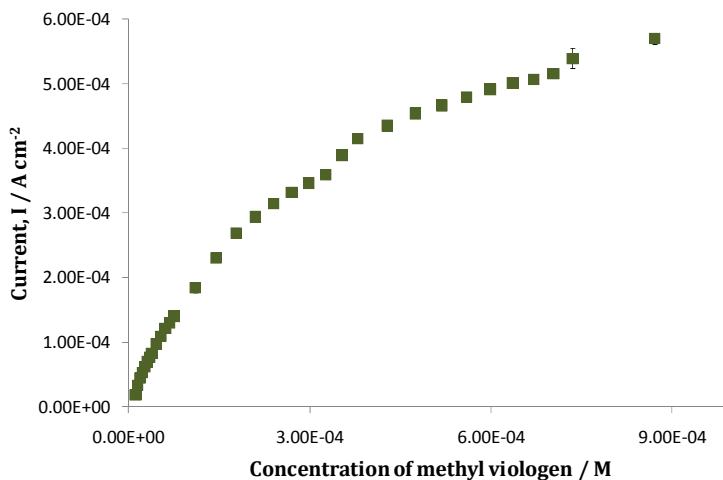


Figure 4.28: Limiting currents as a function of methyl viologen concentration for the reduction of MV^{2+} to give MV^{+} at the ppys β -CD surface. Data were recorded by means of CPA. The ppys β -CD polymer was electrosynthesized from a 2.0×10^{-1} M pyrrole/ 2.0×10^{-2} M s β -CD, on Au, at a potential of 0.6 V vs SCE and to a charge of 1.13 C cm^{-2} . CPA was recorded at -0.9 V vs SCE at a rotation speed of 2000 rpm.

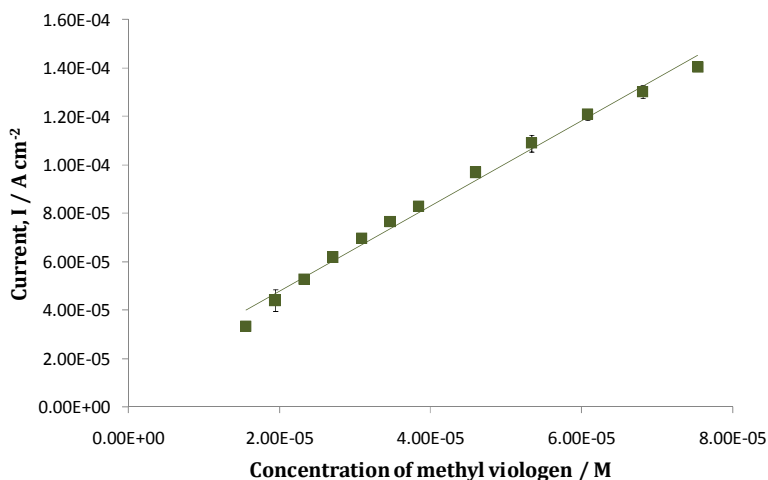


Figure 4.29: Linear region of the plot shown in Figure 4.28.

4.7 Summary of results and conclusions

In this chapter the use of ppys β -CD as a sensor for methyl, ethyl and benzyl viologen was explored. CV investigation showed three different electrochemical signals at the polymer surface. The first and the second corresponded to the first and second reduction processes of the viologens within the solution, as summarized in Figure 4.1. The third intense peak indicated the existence of adsorption phenomena. It has been attributed to the reduction of the radical species generated from the comproportionation reaction of the neutral viologen, V^0 , deposited on the polymer surface with the dicationic species V^{2+} in large excess within solution.

The adsorption peak exhibited great potential in the sensing of the three viologens, since it was very intense in comparison to the current signal recorded for the reduction processes of the species in the bulk solution. For this reason it was decided to follow the trend of such a peak as a function of the viologen concentration. Unfortunately results obtained by means of CV showed very poor detection. However, they were very useful in the understanding of the interactions between the viologens and the ppys β -CD and in the study of the best experimental conditions. From CV experiments it was deduced that the viologens in their dicationic state can take part in the cation exchange

properties of the polymer matrix when the polymer is reduced, to balance the negative charges of the β -CD dopants. It would appear that the main interaction between the polymer and the analytes is driven by electrostatic forces.

To increase the sensing ability of the ppys β -CD, DPV experiments were performed and compared to those obtained for polypyrrole doped with a large non-macrocyclic dopant, sds. The ppysds films did not show any signals for the reduction of the analytes. On the other hand, improvements were obtained for the ppys β -CD. The lowest concentrations that could be experimentally sensed were 1.00×10^{-4} M for the ethyl viologen, 5.00×10^{-5} M for the methyl viologen and 2.50×10^{-5} M for the benzyl viologen.

In addition a CPA study was performed for the methyl viologen, since this molecule is one of the most commonly used herbicides, also known as paraquat. In this case the reduction of the dication to give the radical was followed ($MV^{2+} + 1 e^{-} \rightarrow MV^{\bullet+}$). With CPA a further increase in the sensitivity was reached since the detection limit evaluated was 1.56×10^{-5} M.

However, this value is considerably higher than the limit established by the Environmental Protection Agency (EPA) which is $3 \mu\text{g L}^{-1}$ (1.17×10^{-8} M) and by the European Union, which value is $0.1 \mu\text{g L}^{-1}$ (3.89×10^{-10} M).

4.8 References

1. Miller L., Chang A. C. and Zhou Q. X.; *Studies in Organic Chemistry*, 30, 1987, 361-363.
2. Miller L. L., Zinger B. and Blankespoor R. L.; *Abstracts of Papers of the American Chemical Society*, 189, 1985, 60-COLL.
3. Blankespoor R. L. and Miller L. L.; *Journal of the Chemical Society-Chemical Communications*, 1985, 90-92.
4. Li Y. J. and Dong S. J.; *Journal of the Chemical Society-Chemical Communications*, 1992, 827-828.
5. Miller L. L. and Zhou Q. X.; *Macromolecules*, 20, 1987, 1594-1597.
6. Yang Y., Yang X., Yang H.-F., Liu Z.-M., Liu Y.-L., Shen G.-L. and Yu R.-Q.; *Analytica Chimica Acta*, 528, 2005, 135-142.

7. Izaoumen N., Bouchta D., Zejli H., El Kaoutit M. and Temsamani K. R.; *Analytical Letters*, 38, 2005, 1869-1885.
8. Zhao H., Zhang Y. Z. and Yuan Z. B.; *Analytica Chimica Acta*, 441, 2001, 117-122.
9. Ramanavicius A., Ramanaviciene A. and Malinauskas A.; *Electrochimica Acta*, 51, 2006, 6025-6037.
10. Nishizawa M., Nozaki H., Kaji H., Kitazume T., Kobayashi N., Ishibashi T. and Abe T.; *Biomaterials*, 28, 2007, 1480-1485.
11. Bidan G., Lopez C., Mendesviegas F., Vieil E. and Gadelle A.; *Biosensors & Bioelectronics*, 10, 1995, 219-229.
12. Hendy G. M.; Polypyrrole modified with sulfonated β -cyclodextrin: Controlled release of dopamine and host-guest complexation properties, Ph.D thesis, NUIM, Department of Chemistry, 2009.
13. Harley C. C.; The Formation of an Electrochemical Sensor for the Selective Detection of Dopamine, Ph.D, NUIM, Department of Chemistry, 2009.
14. Bird C. L. and Kuhn A. T.; *Chemical Society Reviews*, 10, 1981, 49-82.
15. Bard A. J., Ledwith A. and Shine H. J.; *Advances in Physical Organic Chemistry*, 13, 1976, 155-278.
16. Hünig S., Garner B. J., Ruider G. and Schenk W.; *Liebigs Annalen der Chemie*, 1973, 1036-1060.
17. Hunig S., Gross J. and Schenk W.; *Liebigs Annalen der Chemie*, 1973, 324-338.
18. Fry A. J.; *Synthetic Organic Electrochemistry*, 2nd ed.; Wiley-Interscience, 1989.
19. Ren X. M. and Pickup P. G.; *Journal of Physical Chemistry*, 97, 1993, 5356-5362.
20. Bard A. J. and Faulkner L. K.; *Electrochemical Methods Fundamental and Applications*, 2nd edition 2001 ed.
21. Greef R., Peat R., Peter L. M., Pletcher D. and Robinson J.; *Instrumental methods in electrochemistry*; Ellis Horwood Ltd, 1985.
22. Rieger P. H.; *Electrochemistry*, Second ed.; Chapman & Hall, 1994.
23. Bazzaoui M., Bazzaoui E. A., Martins L. and Martins J. I.; *Synthetic Metals*, 128, 2002, 103-114.
24. Kaplin D. A. and Qutubuddin S.; *Polymer*, 36, 1995, 1275-1286.
25. Lewis T. W., Wallace G. G., Kim C. Y. and Kim D. Y.; *Synthetic Metals*, 84, 1997, 403-404.
26. Carquigny S., Segut O., Lakard B., Lallemand F. and Fievet P.; *Synthetic Metals*, 158, 2008, 453-461.
27. Saidman S. B. and Bessone J. B.; *Journal of Electroanalytical Chemistry*, 521, 2002, 87-94.
28. Yang N. J. and Wang X. X.; *Electrochimica Acta*, 52, 2007, 6962-6968.
29. Ennis J. N. and Buxton P. C.; *Current Separations*, 17, 1998, 75-77.
30. de Oliveira U. M. F., Lichtig J. and Masini J. C.; *Journal of the Brazilian Chemical Society*, 15, 2004, 735-741.
31. Santhiago M., Lima P. R., Santos W. D. R., de Oliveira A. B. and Kubota L. T.; *Electrochimica Acta*, 54, 2009, 6609-6616.

Chapter 5

Interaction of β -CD with viologens: electrochemical study

5.1 Introduction

In Chapter 4 the sensitivity of polypyrrole doped with sulfated β -cyclodextrin (s β -CD) towards the detection of three different viologens was investigated and discussed. To comprehend in more depth the interactions between methyl, ethyl, and benzyl viologens and the s β -CD further studies were carried out by means of several different techniques, which include both electrochemical and spectroscopic methods. In this chapter results obtained using cyclic voltammetry (CV) and rotating disk voltammetry (RDV) are presented, while in Chapter 6 spectroscopic investigations are examined.

The exact interactions between the s β -CD doped polymer and the viologens are hard to probe since the polymer support is in large excess of the cyclodextrin dopant. However, a study of the interaction between the s β -CD and the viologens within solution can be useful in understanding the probable interaction within the polymer matrix. To explain such interactions two fundamental aspects have to be taken into account. Firstly, the presence of anionic groups on the primary and possibly on the secondary rim of the s β -CD, as depicted in Figure 5.1, and, secondly, the presence of the macrocycle cavity. In addition, the presence of positive charge on the three analytes must be considered, Figure 5.2. Given these factors, the anionic cyclodextrin might interact electrostatically with the positively charged viologens. Also, the presence of the s β -CD cavity introduces the possibility of the formation of an inclusion complex with the viologen molecules. Alternatively, a combination of both effects might occur.

The electrochemistry of viologens is not straightforward to document because of different phenomena which occur in the vicinity of the electrode surface during the redox process and in particular, during the oxidation of the reduced species. There is often controversy in the literature on the interpretation and assignment of the electrochemical peaks recorded using cyclic voltammetry.^{1,2} In addition, oxidation peaks depend on the experimental conditions, with the number and shape of the peaks varying with the electrode substrate, the

solvent, the scan rate and the potential window used.¹⁻⁴ Another peculiarity of the viologens is that they form insoluble layers and adsorb onto the electrode substrate when they are fully reduced. The peak potentials and shapes of the peaks corresponding to the redox activity of the adsorbed species are influenced by the surface morphology of the substrate electrode.

To the best of our knowledge, no previous papers have been published on the complexation of viologens with s β -CD. On the other hand, the inclusion of MV and other viologen compounds in the cavity of a neutral β -cyclodextrin (β -CD) has been investigated by several research groups.^{3,5,6}

In the following sections, the electrochemical properties of the three viologens in the absence and presence of the anionic s β -CD at gold or glassy carbon electrodes are presented and discussed. These data are then compared with the corresponding results obtained in the presence of the neutral β -CD. The interactions between the viologens, in different oxidation states, and the cyclodextrins, either charged or neutral, are finally discussed.

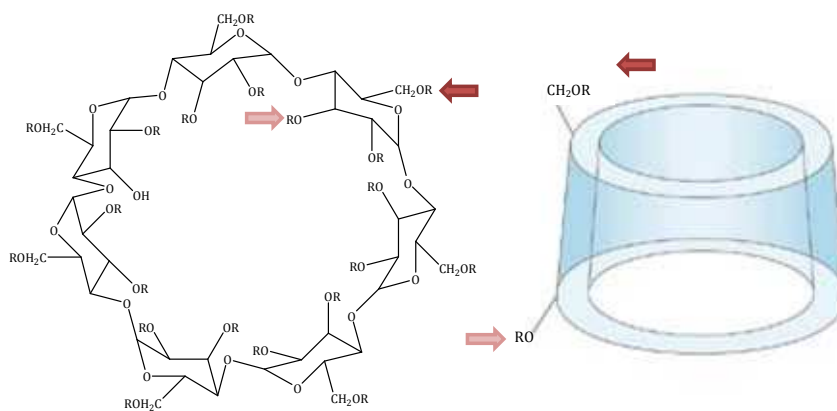


Figure 5.1: Structural and schematic representation of sulfated β -cyclodextrin (s β -CD). The arrows point to the primary and secondary rims and R represents $\text{SO}_3\text{-Na}^+$ or H with approximately 7-11 $\text{SO}_3\text{-Na}^+$ groups.

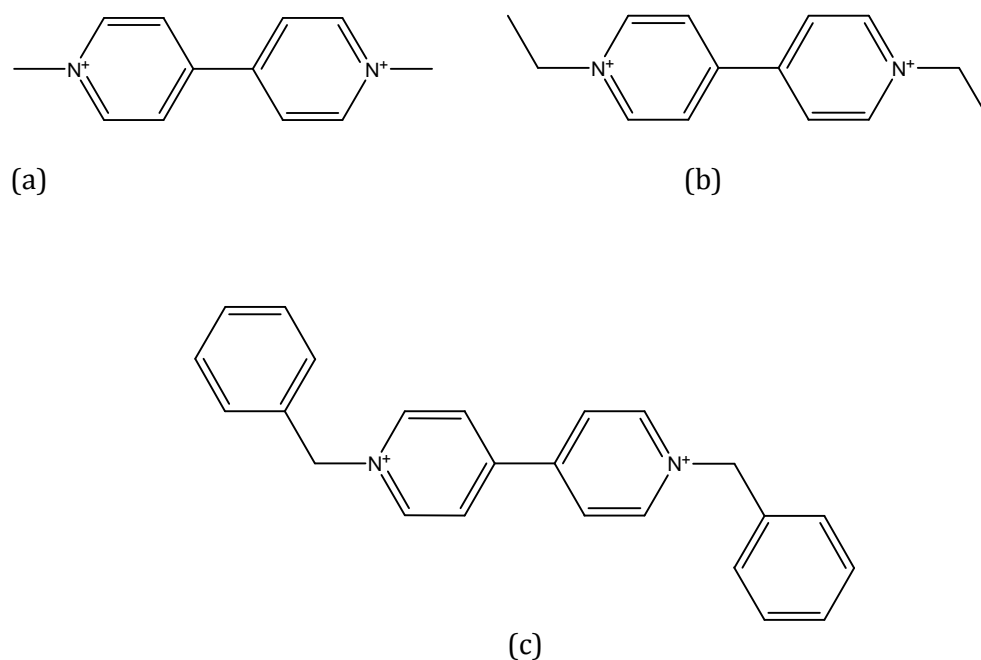


Figure 5.2: Molecular structure of methyl (a), ethyl (b) and benzyl (c) viologens.

5.2 Interaction of methyl viologen with β -CD and $s\beta$ -CD investigated by means of CV and RDV

5.2.1 Methyl viologen (MV) and β -cyclodextrin (β -CD)

The first viologen examined in this chapter is the methyl viologen (MV) or paraquat. The electroactivity of MV is shown in the cyclic voltammogram of Figure 5.3. The first reduction step, occurring at -0.727 V vs SCE, corresponds to the one electron reduction of the dication, as clarified in Equation 5.1. If the potential is stopped and reversed before the second electron transfer takes place, the first reduction wave shows high reversibility. This observation is supported by several publications^{2,3,5,7}. For example, Engelman and Evans² have demonstrated that the radical cation generated is soluble and it does not form a deposited layer on the electrode substrate. This gives rise to good reversibility. This assertion is valid for ethyl and benzyl viologens too. However, the radical cations become less soluble for viologens exhibiting long alkylic substituents. Engelman's conclusion was reinforced by studies with DPSC (double potential

step chronocoulometry) which have been found to be very sensitive to the deposition of the radical.²

A second cathodic wave is recorded around -1.051 V vs SCE. This corresponds to the reduction of the radical cation to form neutral MV. Such a process is described in Equation 5.2. The neutral species is poorly soluble and it tends to form a solid deposit adsorbed on the electrode surface.



When the potential is reversed, the anodic wave coupled to the second reduction does not show reversible behaviour. This is due to complications arising from the adsorption of the neutral form, $MV^0_{(s)}$. The broad oxidation wave around -0.900 V vs SCE, illustrated in Figure 5.3, represents the oxidation of the neutral form in solution, described in Equation 5.3. The sharp peak at -0.730 V vs SCE involves the oxidation of the neutral MV deposited on the gold surface, as described in Equation 5.4. Finally, Equation 5.5 illustrates the reaction related to the anodic peak coupled to the first reduction wave, observed at -0.660 V vs SCE, and partially overlapped by the adsorption peak. Xiao and co-workers⁸ have widely investigated the voltammetry of MV. They have assessed previously reported mechanisms for the redox process of this viologen and have suggested an interpretation involving adsorption, in good agreement with the experimental results presented here.



When a 4-fold excess of hydrated β -cyclodextrin (β -CD) is added to a 2.50×10^{-3} M solution of MV, the anodic wave for the second reduction becomes more symmetrical and both redox steps appear to be more reversible, as visible from the blue trace in Figure 5.3. This is further highlighted by the I_{pa}/I_{pc} and ΔE_p parameters, which are listed in Table 5.1. The peak current ratio is close to unity and the peak separation is close to 59 mV. Furthermore, the adsorption peak is completely suppressed in the presence of the excess β -CD. These observations are consistent with complexation of the reduced MV^0 by the β -CD. The first reduction wave is not affected by the β -CD suggesting little or no interaction between the MV^{2+} and the neutral β -CD. In contrast, reduction of the radical cation to give the neutral species undergoes a 0.027 V positive potential shift when 1.00×10^{-2} M β -CD is added. This is also accompanied by a decrease of the peak current, indicating some changes in the diffusion profile at the surface. This positive shift in the peak potential can be explained by the higher affinity of the β -CD for the neutral product which is generated. Works published by Sivagnanam and Palaniandavar³, Jeon *et al.*⁹ and Matsue *et al.*⁶ are in very good agreement with these observations.

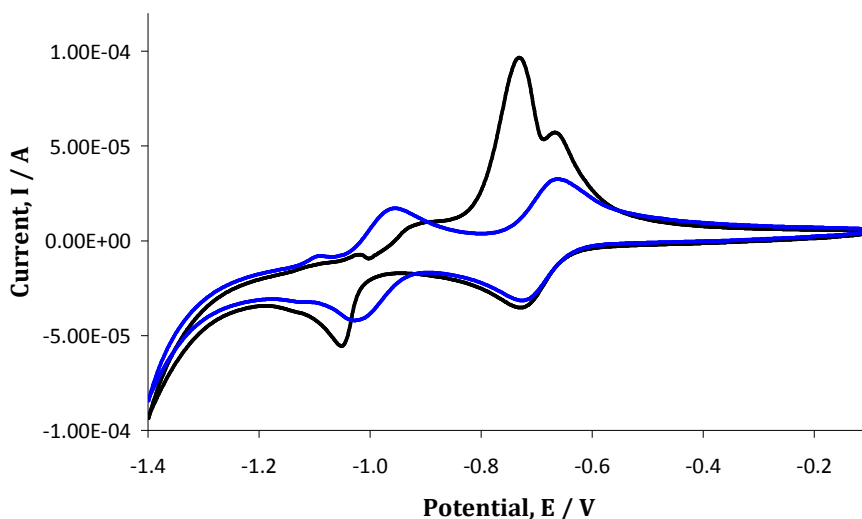


Figure 5.3: CV of a 2.50×10^{-3} M solution of MV in 0.10 M NaCl — and of a 2.50×10^{-3} M solution of MV in 0.10 M NaCl and 1.00×10^{-2} M β -CD — at a bare gold electrode ($d = 3.0$ mm), using a scan rate of 50 mV s^{-1} . Potential referred to SCE scale.

Table 5.1: Parameters for the MV redox processes on Au in a supporting 0.10 M NaCl electrolyte in the presence and absence of β -CD, potential window -0.2 / -1.4 V vs SCE, as shown in Figure 5.3.

Solution	1 st reduction couple		2 nd reduction couple	
	I_{pa}/I_{pc}	$E_{pa} - E_{pc} / V$	I_{pa}/I_{pc}	$E_{pa} - E_{pc} / V$
2.50 x 10⁻³ M MV	0.630	0.064	0.220	0.142
2.50 x 10⁻³ M MV + 1.00 x 10⁻² M β-CD	0.990	0.066	0.920	0.073

From Figure 5.4 it can be observed that a 4-fold excess of β -CD is necessary to completely suppress the deposition of MV^0 . As a matter of fact, a molar ratio of MV/β -CD of 1:1 or lower does not generate significant variations in the electrochemistry of MV. When the molar ratio reaches a 2:1 host/guest ratio, a positive potential shift and a reduction in the peak current is noticed for the second reduction, while the two oxidation peaks observed around -0.700 V vs SCE begin to merge into one signal, signifying the complexation of the neutral species. This CV study shows clearly that the β -CD makes an inclusion complex with the fully reduced MV^0 , while it has a very low affinity for the positively charged species, $MV^{\bullet+}$ and MV^{2+} .

In order to evaluate further the supramolecular chemistry of MV in solution with the neutral macrocyclic cage, RDV experiments were performed. RDV is considered to be more suited for these studies because it provides enhanced conditions for reversible charge transfer.¹⁰ Furthermore, it has been suggested that the shift in peak potential due to the presence of increasing concentrations of CD can be employed to determine the formation constant, K_f , of the complex.¹¹ To work out such constants, an excess of cyclodextrin is needed and the experiments should be performed at relatively slow scan rates. The sweep rate selected for these RDV experiments was 50 mV s⁻¹.

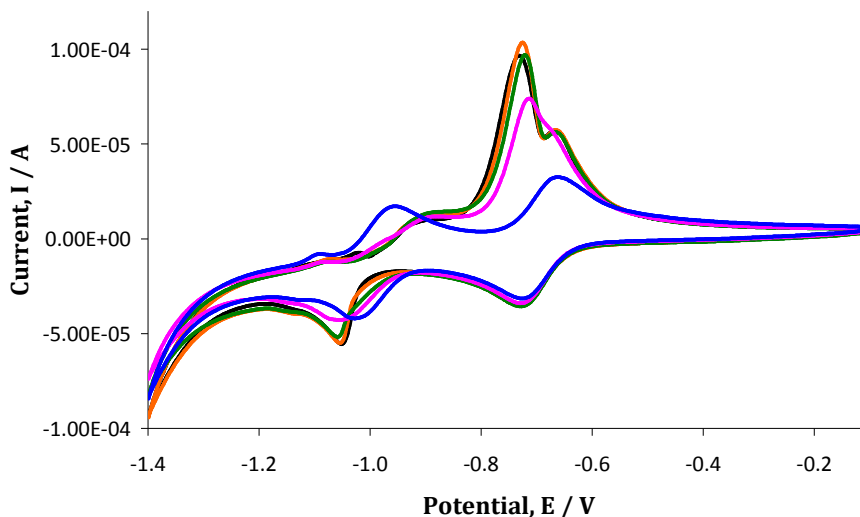


Figure 5.4: CV of a 2.50×10^{-3} M solution of MV in 0.10 M NaCl in the absence — and in presence of 1.00×10^{-3} M —, 2.50×10^{-3} M —, 5.00×10^{-3} M — and 1.00×10^{-2} M — β -CD on a bare gold electrode ($d = 3.0$ mm), using a scan rate of 50 mV s^{-1} . Potential referred to SCE reference scale.

Figure 5.5 shows the voltammograms for 1.00×10^{-3} M MV collected at a GC rotating disc electrode. The data presented in Figure 5.5(a) were recorded by sweeping the potential between 0.0 and -0.90 V vs SCE, while the data shown in Figure 5.5(b) were collected with a wider potential window, from 0.0 to -1.40 V vs SCE. It is evident from Figure 5.5(a) that the first reduction of MV, Equation 5.1, is a simple reversible process, the forward and reverse waves are nearly identical. However, adsorption phenomena take place when the molecule is fully reduced (Figure 5.5 (b)). Oxidation of the adsorbed species is clearly visible between -1.10 and -0.80 V vs SCE during the reverse sweep.

When a 10-fold excess of neutral β -CD is added to the solution, the adsorption peaks are suppressed. There is no evidence for the oxidation of any adsorbed species generated at the rotating disc electrode. These characteristics are clearly visible in Figure 5.6. It is also possible to appreciate a positive shift of 41 mV of the half-wave potential, $E_{1/2}$, corresponding to the second reduction of MV (Equation 5.2) in the presence of the β -CD. This positive shift and the absence of the adsorption peaks are consistent with the CV results and confirm

the affinity of the neutral cyclodextrin for the neutral species, MV^0 . On the other hand, the influence of the macrocycle on the first reduction process is negligible since no change in the limiting current or no potential shifts are noticed in the presence of β -CD.

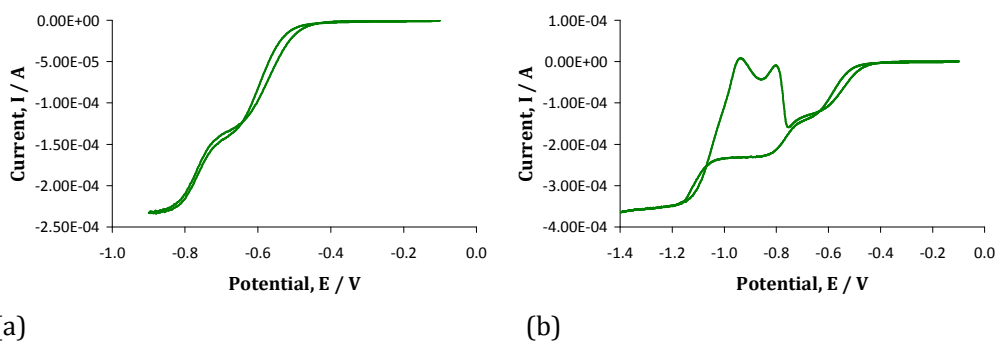


Figure 5.5: RDV voltammograms of 1.00×10^{-3} M MV in 0.10 M NaCl on a GC disc electrode ($d = 4.0$ mm), scan rate 50 mV s^{-1} , rotation frequency 2000 rpm, cycled from 0.0 to -0.9 V vs SCE (a) and from 0.0 to -1.4 V vs SCE (b). Potential axes are relative to SCE reference.

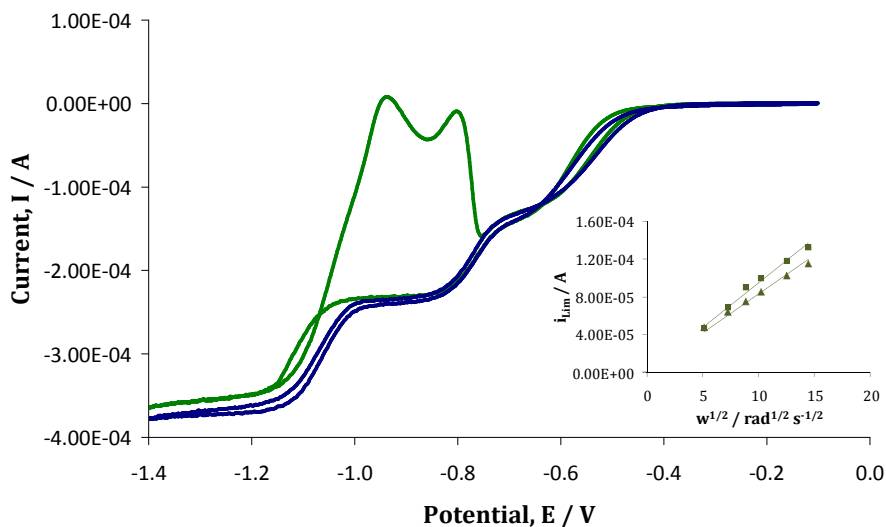


Figure 5.6: RDV voltammograms of 1.00×10^{-3} M MV in 0.10 M NaCl on a GC disc electrode ($d = 4.0$ mm) in absence (—) and presence (—) of 1.00×10^{-2} M β -CD, scan rate 50 mV s^{-1} , rotation frequency 2000 rpm. Inset shows limiting currents relating to the second reduction wave at -1.2 V vs SCE in the absence (\blacktriangle) and presence (\blacksquare) of 0.01 M β -CD as a function of the square root of the rotation rate. Potential axes are relative to SCE reference.

These RDV data were utilized to evaluate the formation constant for the complex between the β -CD and MV^0 by fitting the half-wave potential shifts, $\Delta E_{1/2}$, and the D_c/D_f ratio to Equation 5.6:

$$\left(\frac{F}{RT}\right)\{(E_{1/2})_c - (E_{1/2})_f\} = \ln(1 + K_f[CD]) + \ln\left(\frac{D_c}{D_f}\right)^{1/2} \quad 5.6$$

Here, F is Faraday's constant, 96,485.3415 C mol⁻¹, R is the gas constant, 8.3145 J K⁻¹ mol⁻¹, T is the temperature, $(E_{1/2})_f$ and $(E_{1/2})_c$ are the half-wave potentials for the free and for the complexed analyte, respectively, D_f is the diffusion coefficient of the free MV while D_c is the diffusion coefficient of MV^0 in the presence of β -CD. A problem encountered in the application of this equation was related to the low solubility of the electrogenerated free MV^0 , which in turn made impossible the calculation of the diffusion coefficient, D_f for the oxidation of the free MV^0 . However, in the literature there is good agreement about D_c/D_f ratios for complexed species and such a number is frequently reported to be 0.4.^{10,11} Furthermore, the $\Delta E_{1/2}$ was calculated using the reduction wave ($MV^{•+} + e^- \rightarrow MV^0$) because of non-Nernstian behaviour of the oxidation wave for the free MV^0 ($MV^0 \rightarrow MV^{•+} + e^-$). With the assumption of a D_c/D_f ratio of 0.4 and of a $\Delta E_{1/2}$ of 0.410 V, the formation constant of the complex, K_f , was computed by a rearrangement of Equation 5.6. A value of 681 ± 22 M⁻¹ was obtained for the complexation of MV^0 with β -CD. This value is somewhat lower than the value reported by Matsue *et al.*⁶ of 1400 M⁻¹, which was derived from cyclic voltammetry data. This discrepancy might be due to the different supporting electrolyte and pH that they have used. In addition they do not clearly explain the relationship employed to compute the K_f value.

The diffusion coefficients for the soluble radical $MV^{•+}$, alone and in the presence of the β -CD, were evaluated by plotting the limiting current as a function of the square root of the rotation rate. The Levich plot obtained showed good linearity (correlation coefficients were greater than 0.998), as illustrated in the inset of Figure 5.6. From the corresponding slopes, D_c and D_f were calculated, in accordance with Equation 5.7:¹²

$$i_L = 0.621 n F A D^{2/3} \nu^{-1/6} c \omega^{-1/2} \quad 5.7$$

In the Levich equation, i_L represents the limiting current, n is the number of electrons transferred through oxidation or reduction, F is the Faraday constant, 96485.3415 C mol⁻¹, A is the surface area in cm², D is the diffusion coefficient in cm² s⁻¹, ν is the kinematic viscosity in cm² s⁻¹, c is the concentration of the analyte in mol cm⁻³ and ω is the angular velocity in rad s⁻¹. A D_f of 1.15 x 10⁻⁵ cm² s⁻¹ and a D_c of 1.41 x 10⁻⁵ cm² s⁻¹ were evaluated for MV⁺⁺ free and in the presence of the guest, respectively; thus confirming the negligible interaction of the positively charged viologen with the neutral cyclodextrin.

5.2.2 Methyl viologen (MV) and sulfated β -cyclodextrin (s β -CD)

Prior to the analysis of the interactions within solution between the viologens and the sulfated β -CD (s β -CD), a test to verify the stability and the inertness of the anionic cyclodextrin was performed. Figure 5.7 illustrates that in the potential window of interest, from 0.0 to -1.4 V vs SCE, the s β -CD is not electroactive, as expected from the non-reducing nature of this macrocyclic oligosaccharide.¹³

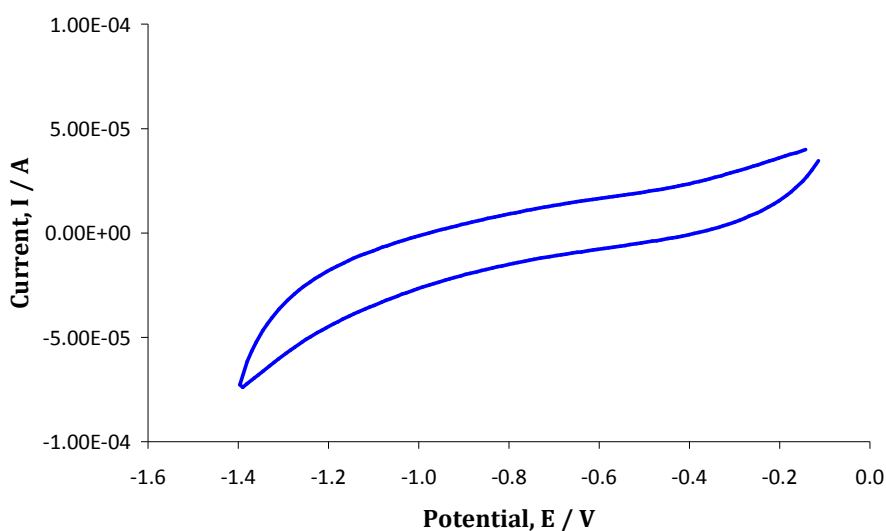


Figure 5.7: CV of solution of 2.00 x 10⁻² M s β -CD on a gold electrode ($d = 3.0$ mm). Potential referred to SCE reference scale.

To investigate the interaction between MV and the anionic cyclodextrin a titration was carried out using CV. Different quantities of s β -CD were added to a constant concentration of viologen in 0.10 M NaCl supporting electrolyte solution. Figure 5.8 illustrates the changes in the peak currents for both reduction processes described in Equations 5.1 and 5.2, upon addition of s β -CD. Furthermore, such a decrease of current is accompanied by a negative shift of the peak potential. The largest potential shift and drop of current are recorded for the highest concentration of s β -CD, which is at an 8-fold excess with respect to the MV concentration of 2.50×10^{-3} M.

The variations in the peak current and peak potential for both reduction reactions are plotted as a function of the s β -CD concentration in Figure 5.9 (a) and (b), respectively. A ΔE_p of 28 mV was calculated for the reduction of the dication to form the radical cation, while a ΔE_p of 37 mV was observed for the reduction of the radical to generate the neutral species in the presence of 2.0×10^{-2} M s β -CD. The peak potentials for both reductions are shifted towards more negative potential values. This is consistent with the formation of a complex.¹⁴⁻¹⁶ The complexation of MV with the s β -CD would make reduction of the viologen more difficult. Hence, the peak potential is shifted to more negative values. Nonetheless, the decrease in the peak currents is another important indication of complexation, since it is attributed to a lower diffusion coefficient of the complexed species.¹⁴⁻¹⁶ According to Ibrahim *et al.*¹⁴ and Zhao *et al.*¹⁷ the current decrease upon addition of the cyclodextrin can be employed to evaluate the formation constant, K_f , using the relationship depicted in Equation 5.8. Accordingly, by plotting the inverse of the cyclodextrin concentration as a function of $1/(1-i/i_0)$, it is possible to compute K_f from the intercept of the linear plot obtained. In this equation, [s β -CD] represents the cyclodextrin concentration in mol dm⁻³, A is a constant, i_0 and i are the peak currents without and in the presence of the cyclodextrin, respectively. This analysis is valid for the formation of a 1:1 complex and when an excess of CD is present.

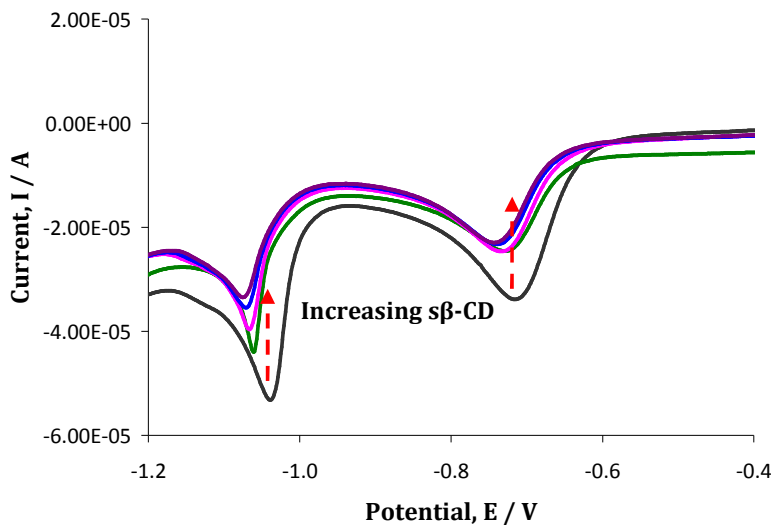


Figure 5.8: CV (reduction wave) of a 2.50×10^{-3} M solution of MV in 0.10 M NaCl in the absence — and in presence of β -CD at concentrations of 2.50×10^{-3} M —, 5.00×10^{-3} M —, 1.00×10^{-2} M — and 2.00×10^{-2} M — on a bare gold electrode ($d = 3.0$ mm), at a scan rate of 50 mV s^{-1} . Potential referred to SCE reference scale.

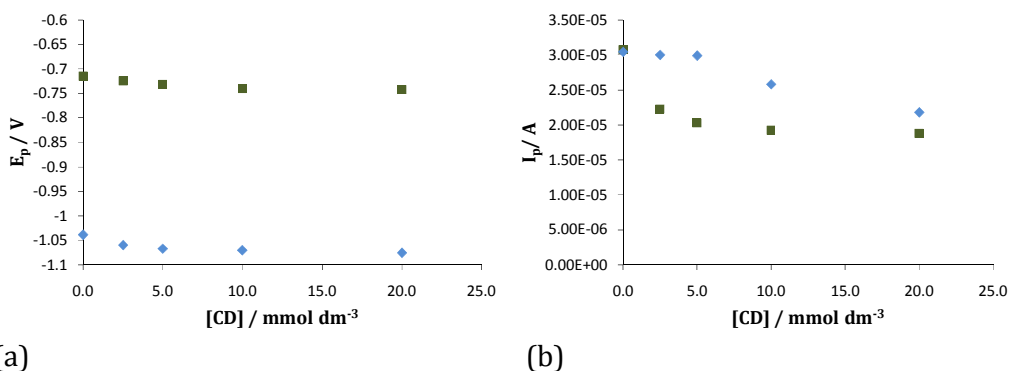


Figure 5.9: Reduction peak potentials (relative to SCE scale) (a) and reduction peak currents (b) for the first (■) and second (◆) reduction of 2.50×10^{-3} M MV in 0.10 M NaCl plotted as a function of increasing concentrations of β -CD.

As illustrated in Figure 5.10 (a), a linear graph was generated for the first reduction of MV, exhibiting a correlation coefficient of 0.999. From the intercept, a K_f of $743 \pm 26 \text{ M}^{-1}$ (3.5% error, $n=2$) was extrapolated for the dication, MV^{2+} . The K_f calculated from the plot presented in Figure 5.10 (b) relates to the radical cation, $\text{MV}^{\bullet+}$. This linear equation exhibited a correlation

coefficient of 0.996 and gave rise to a complexation constant of $248 \text{ M}^{-1} \pm 21$ (8.5% error, $n=2$) for the radical cation of MV.

$$\frac{1}{[s\beta\text{-CD}]} = K_f \frac{1-A}{1-\frac{i}{i_0}} - K_f \quad 5.8$$

Similar changes in the peak current and potentials are well documented within the literature and are indicative of inclusion complex formation.^{10,16,18} For instance, Dang *et al.*¹⁶ reported similar results for the complexation of anthraquinone and benzoquinone with β-CD. Oh and co-workers¹⁹ characterized the formation of an inclusion complex between ibuprofen and 2-hydroxypropyl-β-cyclodextrin and they computed an association constant of the same order of magnitude as the values calculated here. However, it is often reported that K_f values of several hundred are associated with a moderate affinity of the guest for the host, while a strong inclusion complex is confirmed by K_f values larger than about 1000 M^{-1} .²⁰ For example, Ugwu and co-workers²¹ studied the affinity of the anti-inflammatory drug, diflunisal, towards complexation with hydroxypropyl-β-cyclodextrin and found a complexation constant of 3892 M^{-1} , which is considerably larger than the values computed here. The relatively low value reported here may indicate another interaction, arising from electrostatic effects, such as ion-pairing or indeed the formation of a charge-transfer complex.^{22,23}

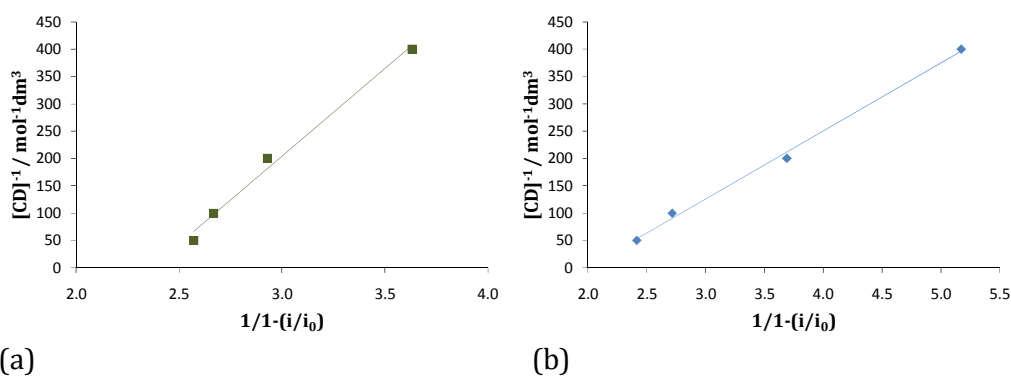


Figure 5.10: The inverse of the sβ-CD concentration plotted as a function of $1/(1-i/i_0)$ for the first reduction — (a) and second reduction — (b). Data taken from Figure 5.8 with a $2.50 \times 10^{-3} \text{ M}$ solution of MV in 0.10 M NaCl with added sβ-CD.

By comparing the results obtained with the neutral β -cyclodextrin and MV (Figure 5.4) with the data collected for the electrochemical response of MV in the presence of the anionic s β -CD (Figure 5.8), the anionic nature of the CD becomes evident. The data clearly show that the neutral CD has higher affinity for the neutral form of the viologen, MV⁰, while the anionic s β -CD interacts preferentially with the charged species, i.e, MV²⁺ and MV^{•+}. This highlights the significance of the negatively charged sulfate groups in determining the strength and nature of the interactions with the analyte.

As shown in Figure 5.3, the oxidation of the reduced viologens is made more difficult and complex by the presence of adsorbed species on the electrode substrate. Furthermore, other reactions can take place during the redox processes. These include a conproportionation reaction (Equation 5.9), a disproportionation reaction (Equation 5.10) and a dimerization (Equation 5.11). The extent of these secondary processes depends on the nature of the *R* substituents on the bipyridilium rings, on the solvent used and on the concentration of the viologen.⁷



As discussed in Section 5.2.1, the oxidation of MV shows three different oxidation waves: around -0.900 V vs SCE for the oxidation of the soluble neutral viologen to generate the radical cation, about -0.700 V vs SCE for the oxidation of the adsorbed neutral species and oxidation of the radical cation to generate the MV²⁺ species at about -0.660 V vs SCE. As shown in Figure 5.11, these oxidation waves are influenced by the presence of the s β -CD. There is a considerable reduction in the height of the adsorbed peak at -0.700 V vs SCE, indicating a lower concentration of the adsorbed MV⁰ in the presence of the s β -CD. This is consistent with the interaction between the s β -CD anion and the

cationic $MV^{•+}$ species during the forward reduction cycle. Less $MV^{•+}$ is converted to MV^0 and the resulting re-oxidation wave is lower in current. In addition, when the concentration of β -CD is present in large excess, 2.00×10^{-2} M, the oxidation peaks observed at -0.700 and -0.650 V vs SCE appear to merge into one single wave.

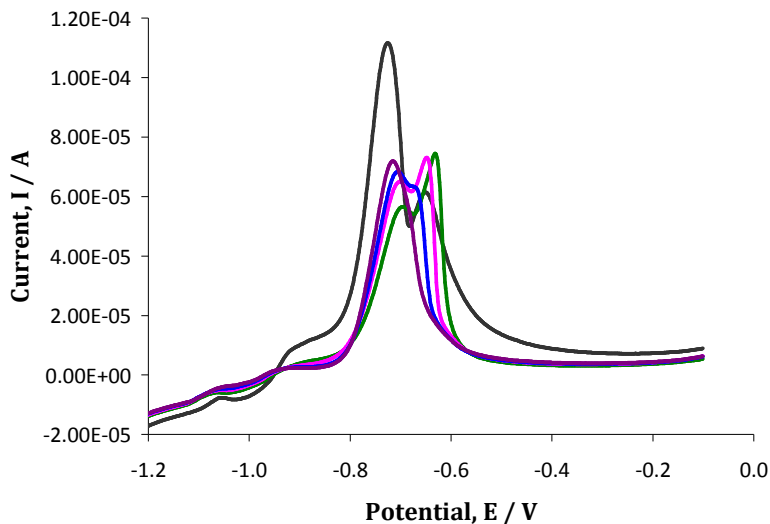


Figure 5.11: CV (oxidation cycle where the potential is cycled from -1.4 V to -0.1 V vs SCE) of 2.50×10^{-3} M MV in 0.1 M NaCl in the absence — and in presence of β -CD at concentrations of 2.50×10^{-3} M —, 5.00×10^{-3} M —, 1.00×10^{-2} M — and 2.00×10^{-3} M — on a bare gold electrode ($d = 3.0$ mm), using a scan rate of 50 mV s^{-1} . Potential referred to SCE reference scale.

In order to gain further information on the interactions between the viologen and the anionic macrocyclic cage, RDV experiments were carried out. The electrochemistry of MV in the presence of varying concentrations of β -CD was monitored at different rotation rates. From the voltammetric data at the rotating GC electrode, diffusion coefficients and heterogeneous charge transfer rate constants for the free viologen and for the compound in the presence of varying amounts of β -CD were calculated.

Figure 5.12 shows the RDV voltammograms for 1.00×10^{-3} M MV as a function of the rotation speed. The data collected at the GC disc electrode show that the

limiting current, i_L , of the analyte increases with increasing rotation frequency. This is observed for both the first and second reduction reactions of MV. A clear linear relationship between the limiting current and the square root of the rotation speed is shown in the inset of Figure 5.12, for both reduction processes, indicating that the system follows the Levich equation (Equation 5.7) and that the limiting current is mass transport controlled. As visible from Figure 5.12, the first reduction process seems to be split between two overlapping waves, extending between -0.400 and -1.000 V vs SCE. This leads to an overall limiting current for the first reduction step that is significantly higher than the second step of reduction. This is in contrast to that observed with the CV data, Figures, 5.3, 5.4 and 5.8. This phenomenon will be analyzed and discussed in more detail in Section 5.2.3.

Figure 5.13 illustrates the effect of a large excess of $s\beta$ -CD on the RDV voltammograms of MV. A dramatic drop in the redox currents is registered upon addition of the $s\beta$ -CD. In particular, the adsorption phenomena associated with the $MV^0(s)$ species are completely suppressed. This is similar to the effects observed in Figure 5.6 with the neutral β -CD. However, the significant decrease in the current observed could signify that the amount of MV^0 generated at the electrode surface does not reach the solubility limit and hence no deposit occurs. As a consequence, no adsorption peaks are observed. To verify this hypothesis, additional RDV experiments were carried out with free MV, using a concentration that originates an equal current to the one obtained with a 40-fold excess of $s\beta$ -CD. A profile similar to the trace recorded in the presence of the $s\beta$ -CD (pink trace) was observed. This provides conclusive evidence that the adsorption peak is simply absent due to the fact that an insufficient concentration of the reduced species was produced. Therefore, it is reasonable to conclude that the neutral MV^0 does not form an inclusion complex with the anionic $s\beta$ -CD. In contrast, the interaction of the positively charged MV^{2+} and $MV^{•+}$ species with the negatively charged $s\beta$ -CD leads to a sizeable decrease in the redox current and the production of considerably less MV^0 .

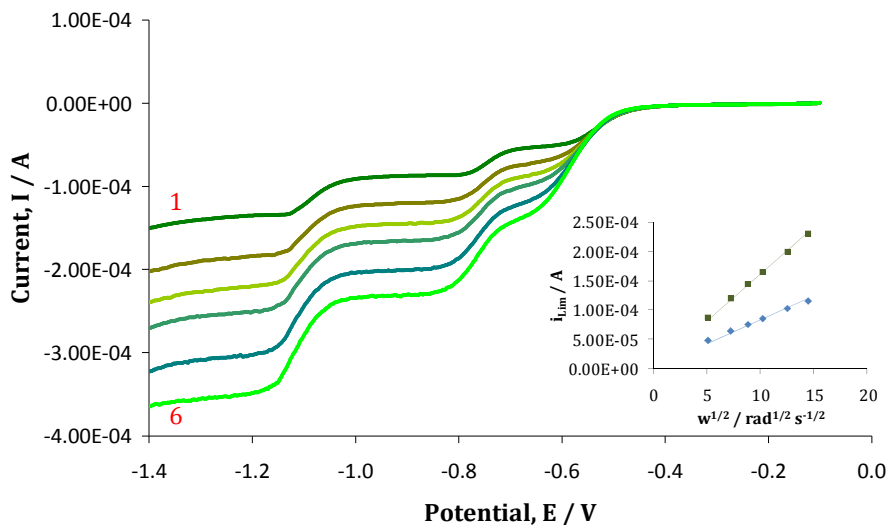


Figure 5.12: RDV voltammograms of 1.00×10^{-3} M MV in 0.10 M NaCl on a GC disc electrode ($d = 4.0$ mm), scan rate 50 mV s^{-1} , rotation frequency from 1 to 6: 250, 500, 750, 1000, 1500 and 2000 rpm. Inset shows Levich plots for the first (—) and second reduction (—) waves of MV. Limiting currents were read at -0.9 V vs SCE for the first and at -1.2 V vs SCE for the second reduction wave. Potential referred to SCE scale.

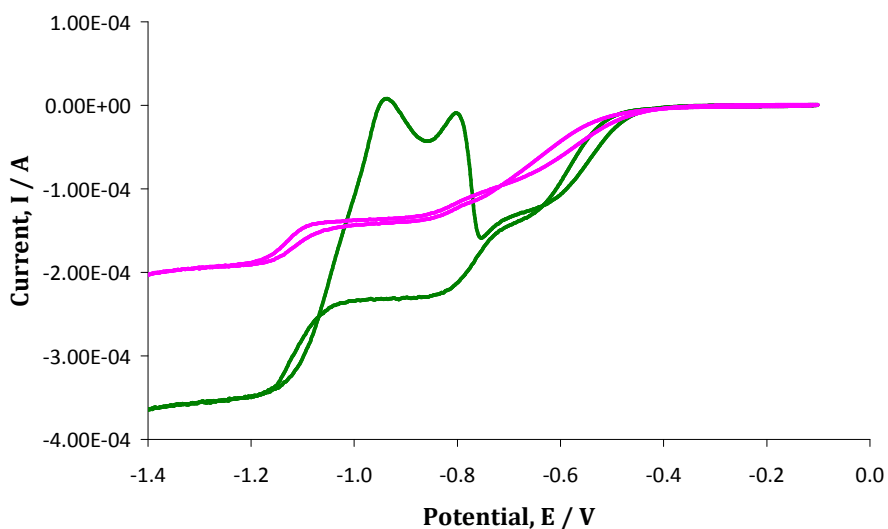


Figure 5.13: RDV voltammogram of 1.00×10^{-3} M MV in 0.10 M NaCl on a GC disc electrode ($d = 4.0$ mm), scan rate 50 mV s^{-1} , rotation frequency 2000 rpm, free (—) and in presence of 4.00×10^{-2} M β -CD (—). Potential referred to SCE reference scale.

In Figure 5.14 the influence of variations in the β -CD concentrations on the MV reduction processes are presented. It is seen that a 1:1 MV: β -CD ratio is sufficient to cause a large decrease in the limiting currents. A further decrease in the limiting current is noticed as the β -CD concentration is increased beyond the equimolar ratio. It is also evident that the presence of the β -CD minimizes the double wave phenomenon which occurs for the first reduction of the free MV.

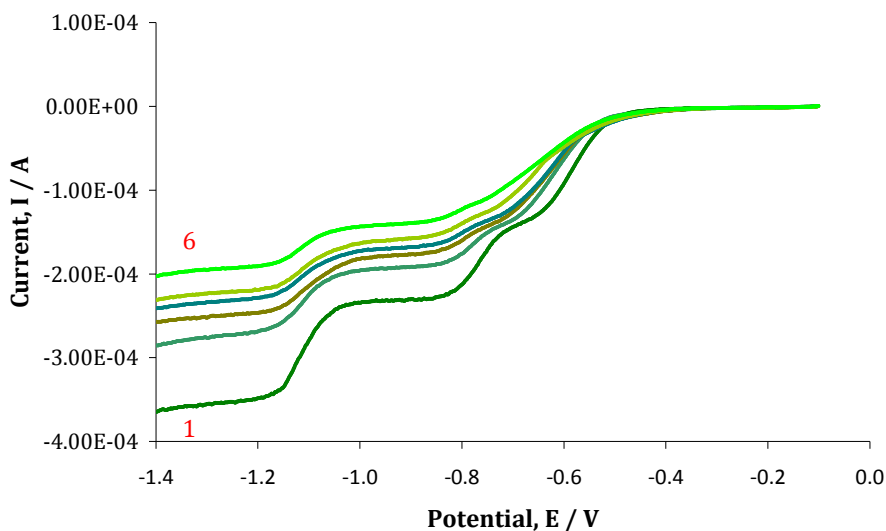


Figure 5.14: RDV voltammogram of 1.00×10^{-3} M MV in 0.10 M NaCl on a GC disc electrode ($d = 4.0$ mm), scan rate 50 mV s^{-1} , rotation frequency 2000 rpm, in the presence of different concentration of β -CD, from 1 to 6: 0.00, 1.00×10^{-3} , 5.00×10^{-3} , 1.00×10^{-2} , 2.00×10^{-2} , 4.00×10^{-2} M β -CD. Potential referred to SCE reference scale.

Levich plots, where the limiting current is plotted as a function of the square root of the rotation rate, are depicted in Figure 5.15 for MV in the presence of different concentration of β -CD. Good linear relationships are observed, confirming that the system is under diffusion control. Moreover, the diffusion from the bulk solution to the electrode surface of the electroactive MV^{2+} and of the partially reduced radical species, $\text{MV}^{•+}$, is diminished as the β -CD concentration increases. This is further revealed from the diffusion coefficients which were calculated by means of Equation 5.7. These are summarized and listed in Table 5.2. A decrease of the diffusion coefficient is a clear indication of

an interaction between the charged MV and the anionic sβ-CD. It is usually associated with the formation of an inclusion complex. However, confirmation of the host-guest interaction can only be achieved if there is an accompanying shift in the half-wave potentials, $E_{1/2}$, upon addition of the host molecules. From Figure 5.14 it can be seen that the shift of the $E_{1/2}$ value is small for both reduction processes.

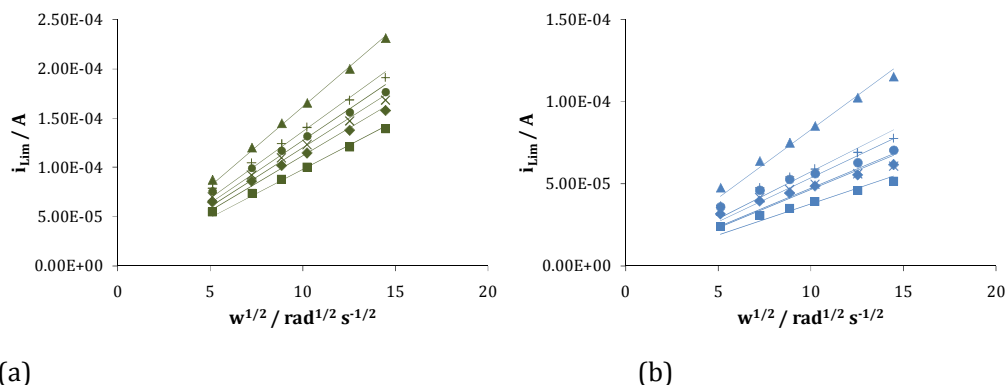


Figure 5.15: Levich plots for the limiting currents relative to the first (—) and second (—) reduction of 1.00×10^{-3} M MV in 0.10 M NaCl on a GC disc electrode ($d = 4.0$ mm), scan rate 50 mV s^{-1} , rotation frequency 250, 500, 750, 1000, 1500 and 2000 rpm, in the presence of different concentration of sβ-CD: 0.00 M (▲), 1.00×10^{-3} M (+), 5.00×10^{-3} M (●), 1.00×10^{-2} M (×), 2.00×10^{-2} M (◆), 4.00×10^{-2} M (■). Limiting currents were taken at -0.9 V vs SCE and at -1.2 V vs SCE.

Additionally, the heterogeneous charge transfer rate constant, k , was evaluated from RDV data for MV in the absence and presence of the varying concentrations of sβ-CD. Experimental values were fit to the Koutecky-Levich equation (Equation 5.12).

$$\frac{1}{i_L} = \frac{1}{i_K} + \frac{i}{i_{lev}} = \frac{1}{n F A k c} + \frac{1.61}{n F A \nu^{-1/6} D^{2/3} \omega^{1/2} c} \quad 5.12$$

In this analysis, i_L represents the measured limiting current, i_K is the current of the electron transfer between the viologen and the electrode and i_{lev} is the Levich current, which corresponds to the mass transfer of viologen in the

solution. The i_K is not influenced by the rotation rate, as expressed in Equation 5.13.

$$i_K = nF A k \Gamma c \quad 5.13$$

In these formulas n is the number of electrons transferred, F is the Faraday's constant (96485.3415 C mol⁻¹), A is the surface area in cm², k is the reaction rate constant, Γ is the surface coverage, c is the concentration, D is the diffusion coefficient of the viologen in cm² s⁻¹, ω is the rotational speed in rad s⁻¹ and ν is the kinematic viscosity (0.0092 cm² s⁻¹)²⁴.

Table 5.2: Diffusion coefficients of MV²⁺ and MV^{•+} as a function of the concentration of sβ-CD. Experiments were carried out on a GC disc electrode (d = 4.0 mm), at a scan rate 50 mV s⁻¹, using rotation frequencies of 250, 500, 750, 1000, 1500 and 2000 rpm. MV concentration was set at 1.00 x 10⁻³ M in 0.10 M NaCl.

[sβ-CD] / mol dm ⁻³	Diffusion coefficient (apparent) D / cm ² s ⁻¹ of MV ²⁺ 1st reduction: MV ²⁺ + e ⁻ → MV ^{•+}	Diffusion coefficient (apparent) D / cm ² s ⁻¹ of MV ^{•+} 2nd reduction: MV ^{•+} + e ⁻ → MV ⁰
0.00	3.16 x 10 ⁻⁵	1.10 x 10 ⁻⁵
1.00 x 10 ⁻³	2.43 x 10 ⁻⁵	6.67 x 10 ⁻⁶
5.00 x 10 ⁻³	2.19 x 10 ⁻⁵	6.02 x 10 ⁻⁶
1.00 x 10 ⁻²	2.02 x 10 ⁻⁵	4.97 x 10 ⁻⁶
2.00 x 10 ⁻²	1.82 x 10 ⁻⁵	4.85 x 10 ⁻⁶
4.00 x 10 ⁻²	9.79 x 10 ⁻⁶	3.56 x 10 ⁻⁶

In Figure 5.16 (a) and (b), the Koutecky-Levich plots for MV alone and in presence of different concentrations of the anionic macrocycle are illustrated both for the first and second reduction steps. By plotting the inverse of the limiting current, i_L^{-1} , as a function of the inverse of the square root of the scan rate, $\omega^{-1/2}$, linear relationships were obtained for all the CD concentrations, with correlation coefficients exceeding 0.994. From the intercept of each plot, k values were extrapolated and these are summarized in Table 5.3. It is evident that the rate constants for both reduction processes decrease upon addition of

the s β -CD. Such a decrease is attributed to the formation of a complex between the cationic MV (MV^{2+} and $MV^{\bullet+}$) and the anionic s β -CD. The nature of this complex will be discussed later in Section 5.5. It is reasonable to expect that the rate of the electron transfer reaction will be higher when the viologen is free in solution, compared to when it is complexed with the s β -CD. However, the slight increment in the rate constant noticed for very high concentrations of s β -CD can be explained in terms of enhanced conductivity of the solution. A conductivity value of 9.49 mS was measured for a 1.00×10^{-3} M solution of MV containing 0.10 M NaCl, while a value of 19.22 mS was measured for the same solution containing 4.00×10^{-2} M s β -CD (at 21.5 °C). It is well known that the rate constant depends on ionic strength and the 0.10 M NaCl supporting electrolyte is not sufficient to buffer the ionic strength at the higher concentrations of s β -CD. In the presence of the s β -CD, a larger decrease in the k value is noticed for the dicationic species when compared to the radical species. This result is consistent with the fact that MV^{2+} is more strongly bound to the anionic CD than the radical cation, $MV^{\bullet+}$.

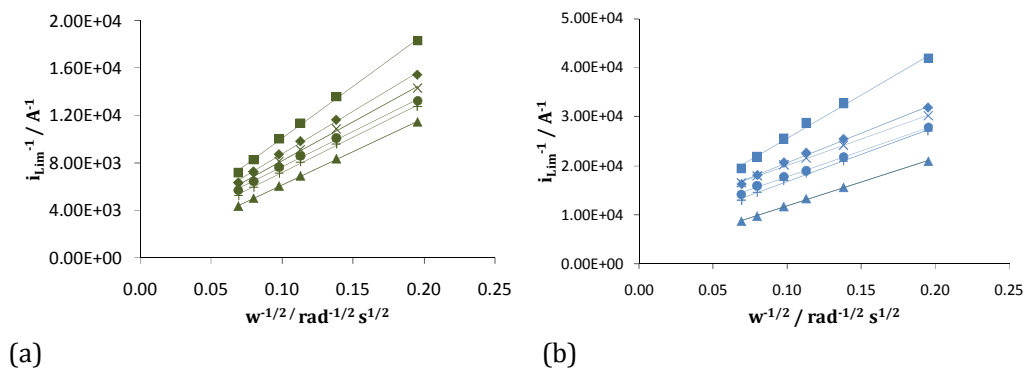


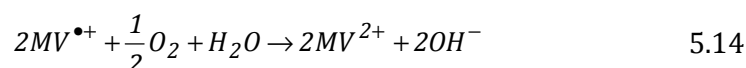
Figure 5.16: Koutechy-Levich plots for the limiting currents relative to the first (—) and second (—) reduction of 1.00×10^{-3} M MV in 0.10 M NaCl on a GC disc electrode ($d = 4.0$ mm), scan rate 50 mV s^{-1} , rotation frequency 250, 500, 750, 1000, 1500 and 2000 rpm, in the presence of different concentration of s β -CD: 0.00 M (\blacktriangle), 1.00×10^{-3} M (\blackplus), 5.00×10^{-3} M (\bullet), 1.00×10^{-2} M (\times), 2.00×10^{-2} M (\blacklozenge), 4.00×10^{-2} M (\blacksquare). Limiting currents were taken at -0.9 V vs SCE and at -1.2 V vs SCE.

Table 5.3: Rate constant values, k , for the reduction of MV^{2+} and $MV^{\bullet+}$ in the presence of varying amounts of sβ-CD. Experiments were carried out on a GC disc electrode ($d = 2$ mm), at a scan rate 50 mV s^{-1} , using rotation frequencies of 250, 500, 750, 1000, 1500 and 2000 rpm. MV concentration was set as $1.00 \times 10^{-3} \text{ M}$ in 0.10 M NaCl . Limiting currents taken at -0.9 V vs SCE and at -1.2 V vs SCE , for the reduction of MV^{2+} and $MV^{\bullet+}$, respectively.

[sβ-CD] / mol dm ⁻³	rate constant, k / cm s ⁻¹	rate constant, k / cm s ⁻¹
	1st reduction: $MV^{2+} + e^- \rightarrow MV^{\bullet+}$	2nd reduction: $MV^{\bullet+} + e^- \rightarrow MV^0$
0.00	1.61×10^{-1}	3.91×10^{-2}
1.00×10^{-3}	6.73×10^{-2}	1.44×10^{-2}
5.00×10^{-3}	4.89×10^{-2}	1.13×10^{-2}
1.00×10^{-2}	5.09×10^{-2}	8.83×10^{-3}
2.00×10^{-2}	5.22×10^{-2}	9.79×10^{-3}
4.00×10^{-2}	6.21×10^{-2}	1.04×10^{-2}

5.2.3 Influence of oxygen

To perform the RDV experiments discussed in Section 5.2.2, solutions of MV were previously purged with nitrogen for 15 min, in order to minimize oxygen evolution and to avoid the reaction described in Equation 5.14.



Bird and Kuhn have documented the fact that the viologen cation radical reacts rapidly with oxygen.⁷ As a matter of fact, such a reaction has been proposed as a means for determination of oxygen dissolved in water in low concentrations.^{25,26} Sun and co-workers²⁷ have published a paper where they assess the electrocatalytic activity of a sensor modified with MV towards oxygen reduction. They state that oxygen is efficiently reduced on the electrode surface while $MV^{\bullet+}$ is oxidized to MV^{2+} . On the other hand, molecular hydrogen interferes with the electrochemistry of viologens only when catalyzed.⁷

In the description of Figure 5.12, the existence of an atypical signal was noticed for the first reduction process of MV. The corresponding current seemed to be split in two overlaying waves. For each rotation rate, the amount of current passed during the first reduction wave was nearly double that of the second reduction step. This may indicate the existence of another electrochemical process between -0.400 and -0.600 V vs SCE. The presence of electrochemically active impurities in the batch of MV powder was immediately rejected after running an HPLC test of the compound. Next, the influence of the electrode substrate material was verified. RDV experiments were repeated on a gold electrode which was cleaned either chemically, using aqua regia (HNO_3/HCl 1:3) or *via* an electrochemical method (H_2SO_4 1.0 M, CV 0.0/1.5 V vs SCE, scan rate 0.5 V s^{-1} , 30 cycles).²⁸ None of these treatments was effective in the removal of the unknown electrochemical signal; hence the possibility of different active sites on the electrode material was excluded as well.

The last hypothesis postulated was again connected with the presence of oxygen within the viologen solutions. The blue trace in Figure 5.17 shows the absence of a double wave when the MV solution is purged with nitrogen for 60 min, prior to the RDV measurements. After the removal of oxygen, the voltammograms exhibit the typical feature expected for MV reduction, showing just one step for the generation of the radical and another limiting wave for the formation of the neutral species.

As shown in Figure 5.17, the amount of oxygen dissolved in the solution can affect the voltammograms in two ways. Firstly, oxygen evolution increases the overall reduction current, as clearly visible from Figure 5.17. Secondly, the presence of oxygen promotes the reaction described in Equation 5.14, so when the radical cation is generated it reacts with oxygen to form yet again the dicationic species, which in turn is reduced once more. The two phenomena lead to a larger current and to a double step for the first reduction process. Indeed, the ratio of the current evaluated for the first and the second reduction waves changed from 2.0, for the solution containing trace oxygen to 1.1, for the solution purged with nitrogen for 60 min. Given these facts, RDV experiments

for MV in the presence of β -CD were repeated in the absence of oxygen. Figure 5.18 illustrates that besides a decrease in the current, once oxygen has been removed, it is possible to appreciate a potential shift, both for the first and second reduction processes of MV, in the presence of the anionic cyclodextrin. These observations are in good agreement with the CV data and this now indicates changes in the ease of reduction of the charged MV species in the presence of the anionic cyclodextrin.

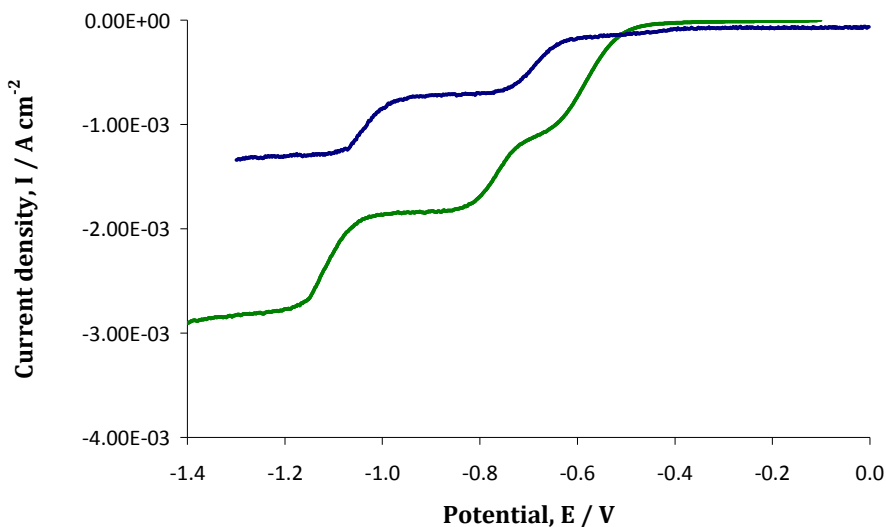


Figure 5.17: RDV voltammograms recorded for 1.00×10^{-3} M MV in 0.10 M NaCl on a GC disc electrode, at a scan rate 50 mV s^{-1} , rotation frequency of 2000 rpm, before — and after — complete saturation of the solution with N_2 .

The oxygen interference was not evident when CV experiments were performed, Figures 5.3, 5.4 and 5.8. As highlighted in Chapter 2, RDV is a technique which possesses greater sensitivity over CV, where the diffusion layer is time dependent. The better sensitivity is due to the increased transport of the electroactive species to the electrode surface. As a consequence, the transport of oxygen is more efficient at the rotating disc electrode, thus leading to an enhancement of its evolution current and to an enhancement of the reaction described by Equation 5.14.

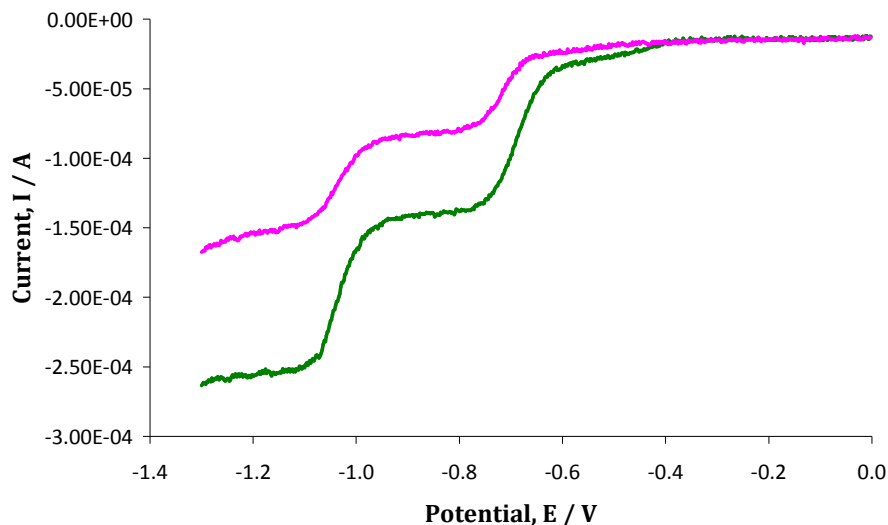


Figure 5.18: RDV voltammograms of 1.00×10^{-3} M MV in 0.10 M NaCl on a GC disc electrode ($d = 5.0$ mm), scan rate 50 mV s^{-1} , rotation frequency 2000 rpm, in the absence — and presence of 4.00×10^{-2} M β -CD —. Potential referred to SCE. Solutions were purged with nitrogen for 60 min.

For the reduction of the dication to form the radical molecule ($\text{MV}^{2+} + e^- \rightarrow \text{MV}^{\bullet+}$) a negative shift in the half-wave potential, $\Delta E_{1/2}$ of 0.042 V, was evaluated, while for the reduction of the radical to the neutral form ($\text{MV}^{\bullet+} + e^- \rightarrow \text{MV}^0$) a change of 0.038 V in the negative direction was computed upon addition of a 40-fold excess of β -CD (Figure 5.18). Combining both the decrease in the current and the potential shifts in the presence of the anionic CD, it was possible to evaluate the formation constants of the complex formed between the charged MV species and the anionic β -CD.

It has been suggested that as the peak potential shifts to more negative potentials, due to the presence of increasing concentration of CD, the shift can be employed to determine the K_f value of the complex.¹¹ Considering a 40-fold excess of the β -CD, a K_f of $171 \pm 5 \text{ M}^{-1}$ was computed for MV^{2+} and a K_f value of $135 \pm 4 \text{ M}^{-1}$ was calculated for $\text{MV}^{\bullet+}$, by fitting the RDV data to Equation 5.6. It is important to highlight that in Section 5.2.2 a D_c/D_f ratio given in the literature was used, due to the solubility limitations arising from the insoluble species examined, MV^0 . In the present case, the experimentally determined ratio for the

diffusion coefficient of the free and complexed viologen was employed since the positively charged MV $^{\bullet+}$ and MV $^{2+}$ are both soluble; hence their diffusion coefficients can be easily computed.

Using the CV technique, slightly higher formation constants were found, as summarized in Table 5.4. This variation may be related to the parameters used to compute the constants. RDV data were fit into Equation 5.6, which considers the potential shifts. These are connected with the ease of reduction of the complexed viologen compared to the free viologen. On the other hand, Equation 5.8 was applied to CV data and this analysis only considers changes in the peak current, which are related to changes in the rate of diffusion of the complexed viologen. However, from the data acquired from both techniques the conclusion can be drawn that the s β -CD interacts preferentially with the dicationic species, MV $^{2+}$.

As already mentioned, the formation constants evaluated do not suggest a strong host-guest inclusion complex, although they are considered a relevant indication of the interaction between the charged MV species and the s β -CD. However without any complementary analysis by means of other techniques, *i.e.* UV-Vis and ^1H NMR spectroscopy discussed in Chapter 6, the small K_f values are not sufficient to exclude the formation of an inclusion complex. In fact, other published works have reported formation constants of similar values, as a direct proof of host-guest inclusion complexation. For example, Yanez and Basquinnzay evaluated, by means of chronocoulometry, K_f values of 132, 247 and 276 M $^{-1}$ between estradiol and β -cyclodextrin, hydroxypropyl- β -cyclodextrin and sulfobutyl ether- β -cyclodextrin, respectively.²⁹

Furthermore, it was previously reported in Section 5.2.2 that the addition of a large excess of s β -CD caused the disappearance of the double signal for the first reduction, as visible from Figure 5.13 and Figure 5.14. This characteristic can be explained considering the complexation of MV $^{2+}$ with the s β -CD. The diffusion of the dication to the electrode surface is lowered by the complexation. As a consequence, less radical MV $^{\bullet+}$ is generated. In addition, part of the MV $^{\bullet+}$ formed

is complexed by the s β -CD. As a final result, a lower amount of MV^{•+} is available to react with oxygen. This is one explanation for the suppression of the double step in the rotating disc voltammograms, presented in Section 5.2.2.

Table 5.4: Summary of K_f values for MV species evaluated by means of CV and RDV.

Species	K_f / M^{-1} by RDV	K_f / M^{-1} by CV
MV ²⁺	171 \pm 5	743 \pm 21
MV ^{•+}	135 \pm 4	248 \pm 23

Additionally, diffusion coefficients and charge transfer rate constants were evaluated for the free MV and for the compound in solution with the s β -CD in the absence of oxygen. Figure 5.19 (a) and (b) show the Levich plots for MV free and for the analyte in solution with a 40-fold excess of s β -CD. Again, good linear relationships were found and the diffusion coefficients in the complete absence of oxygen were estimated by fitting the limiting currents into the Levich equation (Equation 5.7). For the free MV, diffusion coefficients, D_f , of 4.91×10^{-6} and $5.78 \times 10^{-6} \text{ cm}^2 \text{ s}^{-1}$ were calculated for the dication and radical species, respectively. The number computed for the dication is consistent with the value published by Ling and co-workers.³⁰ They evaluated a diffusion coefficient of $6.7 \times 10^{-6} \text{ cm}^2 \text{ s}^{-1}$ for MV²⁺. As expected, lower diffusion coefficients were calculated for the viologens with s β -CD. A diffusion coefficient equal to $2.10 \times 10^{-6} \text{ cm}^2 \text{ s}^{-1}$ was obtained for the MV²⁺, while a value of $2.74 \times 10^{-6} \text{ cm}^2 \text{ s}^{-1}$ was calculated for the MV^{•+} species in the presence of an excess of s β -CD. In Table 5.5 the ratios, D_c/D_f , are summarized and compared to the corresponding ratios obtained under conditions where oxygen was not totally removed from the electrolyte. As before, D_f indicates the diffusion coefficient for the free MV, whereas D_c refers to the complexed species. There is little change in the D_c/D_f values for the MV²⁺, while the ratio approaches a similar value of 0.47 for the MV^{•+} species in the absence of oxygen. D_c/D_f ratios of 0.47 have been reported in the literature in several publications and are usually taken to confirm an inclusion complex or

some other form of an association complex with a large bulky species, such as a cyclodextrin.^{10,11}

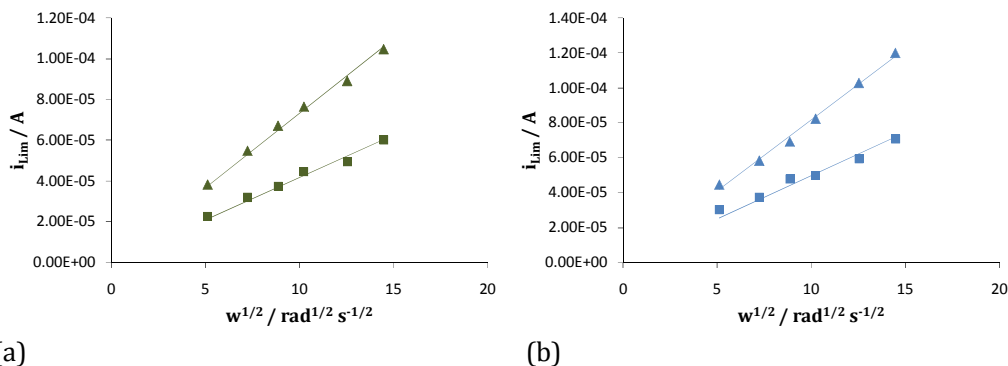


Figure 5.19: Levich plots for the limiting currents of the first (—) and second (—) reduction of wave of 1.00×10^{-3} M MV in 0.10 M NaCl on a GC disc electrode ($d = 2.50$ mm), scan rate 50 mV s^{-1} , rotation frequency 250, 500, 750, 1000, 1500 and 2000 rpm, in the absence (\blacktriangle) and presence of 4.00×10^{-2} M s β -CD (\blacksquare). Limiting currents were taken at -0.9 V vs SCE and -1.2 V vs SCE.

Table 5.5: Diffusion coefficient ratios, D_c/D_f , for MV^{2+} and $MV^{•+}$ in the presence and absence of dissolved of O_2 .

Solutions	D_c/D_f	D_c/D_f
	1 st reduction: $MV^{2++} e^- \rightarrow MV^{•+}$	2 nd reduction: $MV^{•++} e^- \rightarrow MV^0$
Solutions with O_2	0.42	0.33
Deoxygenated	0.43	0.47

Finally, the heterogeneous charge transfer rate constant, k , was evaluated in the deoxygenated samples, in the absence and presence of the varying concentrations of sulfated cyclodextrin. Experimental values were fit to the Koutecky-Levich equation (Equation 5.12). In Figure 5.20 the Koutecky-Levich plots for methyl viologen alone and in presence of the macrocycle are illustrated. By plotting the inverse of the limiting current, i_L^{-1} as a function of the inverse of the square root of the scan rate, $\omega^{-1/2}$, linear plots were obtained for

all the CD concentrations, with correlation coefficients exceeding 0.989. From the intercept of each plot, k values were extrapolated and compared to rate constants measured in the presence of trace amounts of oxygen (Table 5.6). Again, it is clearly evident that rate constants for both reduction processes decrease in the presence of the s β -CD. This decrease is attributed to the formation of a complex. It is clear that the presence of trace amounts of dissolved oxygen has little influence on the interactions between the charged viologen species and the s β -CD. Indeed, the rate constants are similar in magnitude regardless of the presence of dissolved oxygen. Some variation of the rate constant was recorded for the reduction of the dicationic species, MV²⁺, in solution with the s β -CD, in the absence and presence of dissolved oxygen. Moreover, the rate constant evaluated for the reduction of the free MV²⁺ ($1.13 \times 10^{-1} \text{ cm s}^{-1}$) is in perfect agreement with that published by Ling and co-workers ($1.00 \times 10^{-1} \text{ cm s}^{-1}$).³⁰

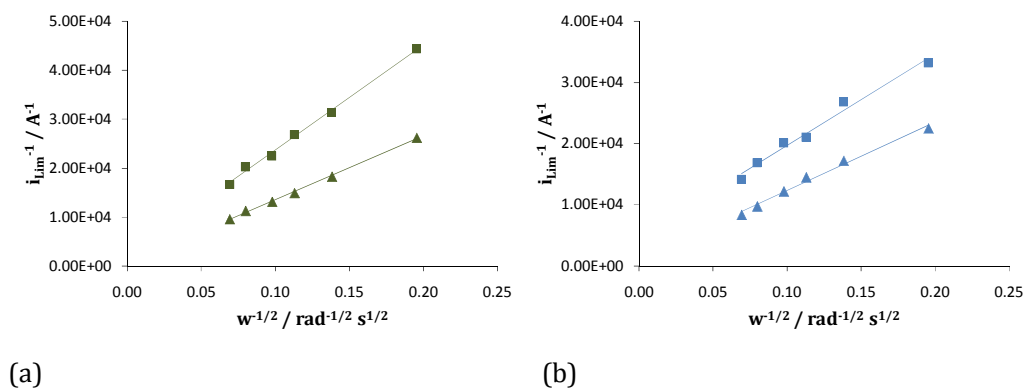


Figure 5.20: Koutechy-Levich plots for the limiting currents relative to the first (— \blacktriangle) and second (— \blacksquare) reduction of $1.00 \times 10^{-3} \text{ M}$ MV in 0.10 M NaCl on a GC disc electrode ($d = 2.50 \text{ mm}$), scan rate 50 mV s^{-1} , rotation frequency 250, 500, 750, 1000, 1500 and 2000 rpm, in the absence (\blacktriangle) and presence of $4.00 \times 10^{-2} \text{ M}$ s β -CD (\blacksquare). Limiting currents taken at -0.9 V vs SCE and -1.2 V vs SCE .

Table 5.6: Rate constants for 1.00×10^{-3} M MV in 0.1 M NaCl solution and for 1.00×10^{-3} M MV in 0.1 M NaCl with 4.00×10^{-2} M s β -CD, in the presence and absence of dissolved O₂.

Solutions	$k / \text{cm s}^{-1}$		$k / \text{cm s}^{-1}$	
	1 st reduction: $MV^{2+} + e^- \rightarrow MV^{\bullet+}$		2 nd reduction: $MV^{\bullet+} + e^- \rightarrow MV^0$	
	MV ²⁺	MV ²⁺ + s β -CD	MV ^{$\bullet+$}	MV ^{$\bullet+$} + s β -CD
Solutions with O ₂	1.61×10^{-1}	6.21×10^{-2}	3.91×10^{-2}	1.04×10^{-2}
Deoxygenated	1.13×10^{-1}	2.40×10^{-2}	4.55×10^{-2}	1.11×10^{-2}

5.3 Interaction of ethyl viologen with β -CD and s β -CD investigated by means of CV and RDV

5.3.1 Ethyl viologen and β -CD

With ethyl viologen (EV) the substituents bonded to the pyridinium rings are larger, as illustrated in Figure 5.2 (b). Therefore, by probing the interactions between EV and the neutral or anionic CDs the influence of small changes in the size of the viologen can be obtained. The electrochemistry of EV is similar to that of MV, as illustrated by the black trace in Figure 5.21. This voltammogram was recorded in 2.50×10^{-3} M EV in a 0.1 M NaCl supporting electrolyte. The first reduction peak occurs at -0.730 V vs SCE and this corresponds to the reduction of the dication to generate the radical cation, as clarified in Equation 5.1. The electrogeneration of the radical is then followed by a second reduction step, described in Equation 5.2, around -1.00 V vs SCE, which leads to the formation of the neutral viologen. On the reverse scan, the typical sharp adsorption wave around -0.850 V vs SCE reflects the poor solubility of the reduced species, EV⁰, in aqueous solutions.^{2,5} This peak features a small shoulder, and this can be associated with the oxidation of both the adsorbed species, EV⁰ (s), and soluble EV⁰ (aq) in solution. Finally, the oxidation peak at -0.600 V vs SCE is related to the oxidation of the radical cation back to the original dicationic state, EV²⁺, as described in Equation 5.5.

The voltammogram recorded in the presence of an excess concentration of neutral β -CD is very different, as illustrated in Figure 5.21. There is a considerable reduction in the adsorbed peak centred at -0.850 V vs SCE. Moreover, a larger oxidation peak, corresponding to the oxidation of the radical cation, is observed. These observations can be explained by considering the so-called conproportionation (Equation 5.9), disproportionation (Equation 5.10) and dimerization reactions (Equation 5.11) of the viologens.⁷ In particular, when the neutral viologen is electrogenerated it can undergo a conproportionation reaction with surrounding EV^{2+} to form the radical species. It appears that complexation of the neutral EV^0 , which is normally poorly soluble, by the β -CD increases the local concentration of soluble EV^0 at the electrode surface and thus the conproportionation reaction is promoted. The inclusion of the neutral EV^0 in the hydrophobic cavity of the β -CD should enhance its solubility and hence the anodic peak at around -0.850 V vs SCE, due to the oxidation of the adsorbed viologen, should disappear. On the other hand, the guest solubilized by the β -CD undergoes a conproportionation reaction whose product is the cation radical, $EV^{•+}$. This gives rise to an increase in the concentration of $EV^{•+}$ in the vicinity of the electrode surface. Accordingly, a larger peak for the oxidation of the radical cation is noticed. These data are in good agreement with a previous publication of Lee *et al*⁵, who gave a similar interpretation for the electrochemistry of N-methyl-N-heptyl-4,4'-bipyridium salt in the presence of β -cyclodextrin. Interestingly, the influence of the conproportionation processes was not observed in the cyclic voltammograms of MV (Figures 5.3 and 5.4). Clearly, other factors play a role such as the solubility of the precipitate, the hydrophobicity of the substituent bonded to the pyridilium ring and the geometry of the inclusion complex.⁵ Again, these findings are in good agreement with Xiao *et al.* and Lee *et al.* who observed no influence of conproportionation on the electrochemistry of MV.^{5,8}

Other relevant indications of the interaction between the neutral β -CD and the ethyl viologen can be found in the reduction wave, as shown in Figure 5.21. Currents for the first and second reduction waves are slightly decreased in the presence of the macrocycle, thus suggesting a somewhat slower diffusion to the

electrode surface for both the EV^{2+} and $EV^{•+}$ species. In both cases a small positive shift in the peak potentials was recorded. In particular, the second reduction wave occurs at a somewhat more positive applied potential value. Again, as discussed in Section 5.2.1 for MV, this is consistent with the higher affinity of the β -CD for the product of the reduction, i.e, EV^0 . In agreement with the data recorded for MV, an excess of β -CD is required to exert a significant effect on the electrochemical response of EV. Figure 5.22 shows the voltammograms recorded for 2.50×10^{-3} M EV in the presence of 1.00×10^{-3} , 2.50×10^{-3} , 5.00×10^{-3} and 1.00×10^{-2} M β -CD. Clearly, a molar ratio of about 2:1 is required for the β -CD/EV concentration before the β -CD influences the voltammetric signal of the viologen.

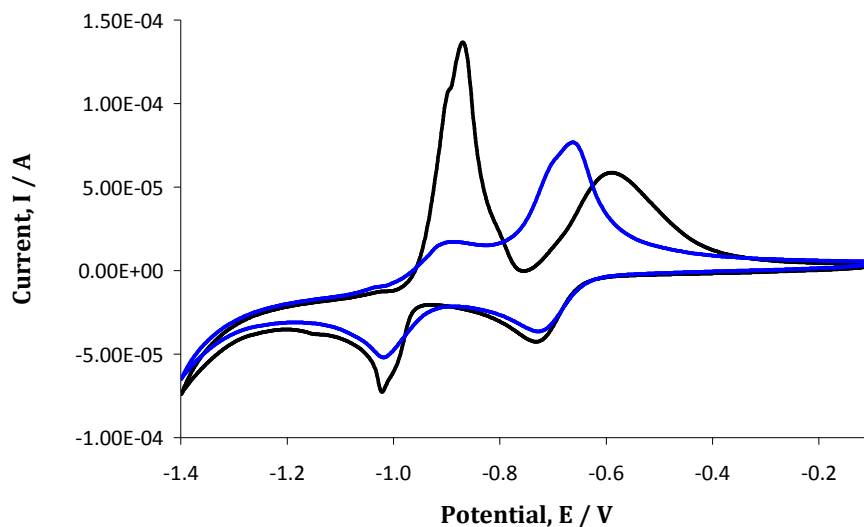


Figure 5.21: CV of a 2.50×10^{-3} M solution of EV in 0.10 M NaCl — and of a 2.50×10^{-3} M solution of EV in 0.10 M NaCl and 1.00×10^{-2} M β -CD — at a bare gold electrode ($d = 3.0$ mm) recorded at 50 mV s^{-1} . Potential referred to SCE reference.

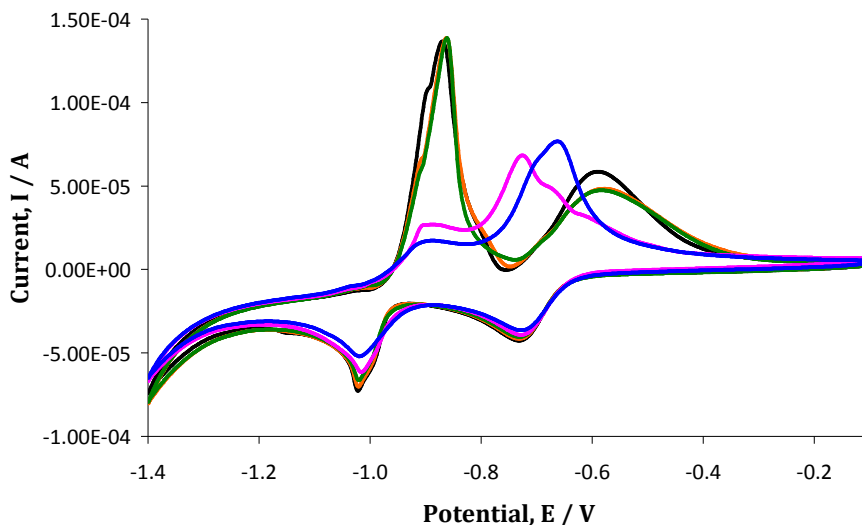


Figure 5.22: CV of a 2.50×10^{-3} M solution of EV in 0.10 M NaCl in the absence — and in the presence of β -CD at concentrations of 1.00×10^{-3} M —, 2.50×10^{-3} M —, 5.00×10^{-3} M — and 1.00×10^{-2} M — on a bare gold electrode ($d = 3.0$ mm). Potential referred to SCE reference.

To confirm and quantify the inclusion of EV within the hydrophobic cavity of the neutral β -CD, RDV measurements were carried out. Typical RDV data are presented in Figure 5.23. The data presented in Figure 5.23 (b) were recorded with a wider potential window, extending to -1.30 V vs SCE. In agreement with the data presented for MV, the reduction of the dication is a reversible process and the adsorption phenomena are only observed on the electrogeneration of the neutral species.

When a 10-fold excess of β -CD is added to the viologen solution, the voltammogram is dramatically changed, as depicted in Figure 5.24. The adsorption peaks are clearly suppressed. The redox behaviour of the molecule becomes reversible, thus suggesting that the neutral insoluble species, EV^0 , has been efficiently solubilized by inclusion in the hydrophobic cavity of the neutral β -CD. It is important to highlight that with RDV the enhancement of the comproportionation reaction upon addition of the cyclodextrin is not observed, since the electrogenerated species are quickly removed from the electrode surface by the rotation of the electrode.

For the first reduction process, the limiting currents in the absence and presence of β -CD are nearly identical. This is consistent with the CV results and confirms that the neutral macrocycle has little to no affinity for the dication, EV^{2+} . A small reduction in the current was monitored for the second reduction reaction upon addition of the β -CD, which leads to the formation of the neutral species, EV^0 . The diffusion coefficient for the free EV^{2+} species evaluated using the Levich equation (Equation 5.7), was equal to $1.74 \times 10^{-5} \text{ cm}^2 \text{ s}^{-1}$ while it was moderately decreased to $1.37 \times 10^{-5} \text{ cm}^2 \text{ s}^{-1}$ upon addition of the β -CD. The corresponding Levich plots are depicted in the inset of Figure 5.24 and the diffusion coefficients were computed from the slopes of the respective linear plots. A potential shift of about 0.027 V towards more positive potential values was observed for this second reduction step on addition of the neutral β -CD. This is in agreement with the findings of the CV experiments. As discussed for MV, a positive shift of the second reduction potential indicates a higher affinity of the neutral β -CD for the reduced ethyl viologen, EV^0 .

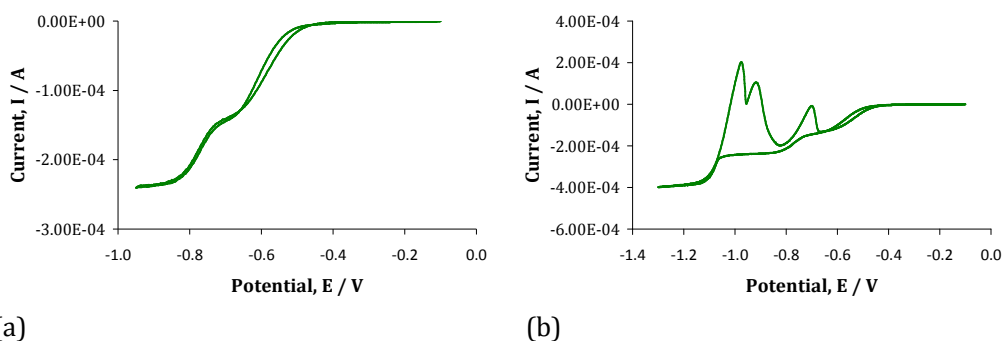


Figure 5.23: RDV voltammogram of $1.00 \times 10^{-3} \text{ M}$ EV in 0.10 M NaCl on a GC disc electrode ($d = 4.0 \text{ mm}$), scan rate 50 mV s^{-1} , rotation frequency 2000 rpm , from -0.1 to -0.9 V vs SCE (a) and from -0.1 to -1.3 V vs SCE (b). Potential referred to SCE reference scale.

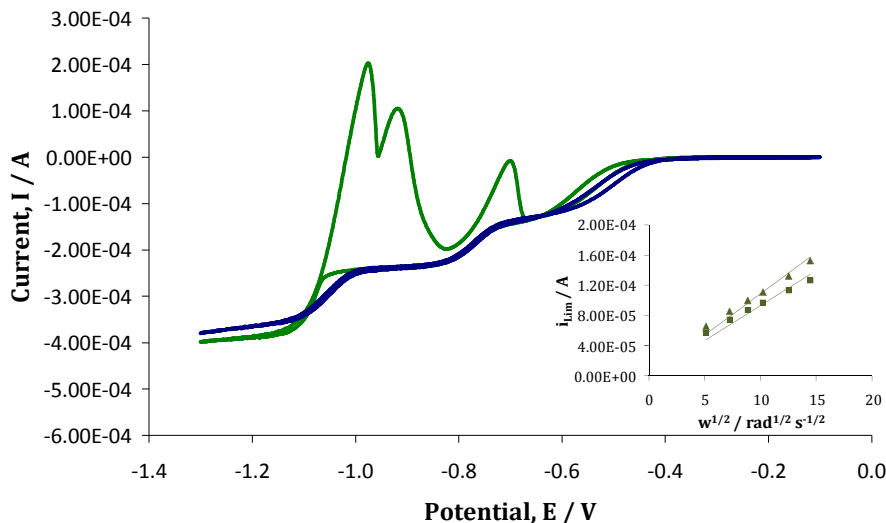


Figure 5.24: RDV voltammograms of 1.00×10^{-3} M EV in 0.10 M NaCl on a GC disc electrode ($d = 4.0$ mm) in the absence (—) and the presence (—) of 1.00×10^{-2} M β -CD, scan rate 50 mV s^{-1} , rotation frequency 2000 rpm. Inset shows limiting currents at -1.2 V relating to the second reduction of EV in the absence (\blacktriangle) and presence (\blacksquare) of β -CD, as a function of the square root of the rotation rate. Potential referred to SCE reference scale.

This interaction between the neutral β -CD and the reduced ethyl viologen, EV^0 , was quantified by evaluating the formation constant. The RDV data were fit to Equation 5.6. As already explained for methyl viologen, in Section 5.2.2; due to insolubility of the neutral species EV^0 , a diffusion coefficient for this species could not be evaluated. The D_c/D_f ratio was then approximated to 0.4, which is the value commonly obtained for complexed molecules with large cyclodextrins, while the experimental $\Delta E_{1/2}$ was estimated to be 27 mV. The formation constant, K_f , was computed as $336 \pm 15 \text{ M}^{-1}$. Although this does not indicate strong inclusion of the guest, it is sufficient to prevent the reduced viologen from depositing at the electrode surface.

5.3.2 Ethyl viologen and s β -CD

In Figure 5.25 voltammograms for the reduction of EV in the presence of different concentrations of sulfated β -cyclodextrin are presented. It is seen that the peak currents for both reduction steps decrease as more s β -CD is added.

These changes are plotted in Figure 5.26 (b), where the peak currents for the first and second reduction waves are plotted as a function of the s β -CD concentration. A marked drop in the current intensity is recorded after adding an equimolar amount of s β -CD. Then, a more moderate reduction is noticed for further increases in the concentrations of s β -CD. The peak potential for the first reduction wave varies on addition of the s β -CD, with a maximum shift of 0.026 V obtained for a 20×10^{-3} M concentration of the anionic macrocycle. The negative shift of the potential and the combined lower peak currents are a good indication of the complexation of the EV²⁺ dication with the s β -CD.^{10,16,18} When the second reduction wave (EV^{•+} + e⁻ → EV⁰) is examined, the considerable diminution in the peak current is not accompanied by an equally meaningful shift of the peak potentials, as revealed in Figure 5.26(a).

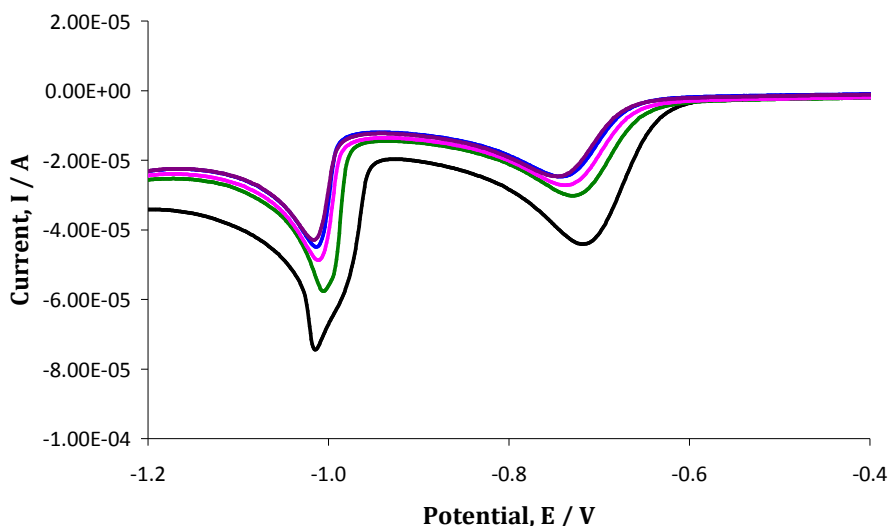


Figure 5.25: CV (reduction wave) of a 2.50×10^{-3} M solution of EV in 0.10 M NaCl in the absence — and in the presence of s β -CD at concentrations of 2.50×10^{-3} M —, 5.00×10^{-3} M —, 1.00×10^{-2} M — and 2.00×10^{-2} M — on a bare gold electrode ($d = 3.0$ mm) at 50 mV s^{-1} . Potential referred to SCE reference.

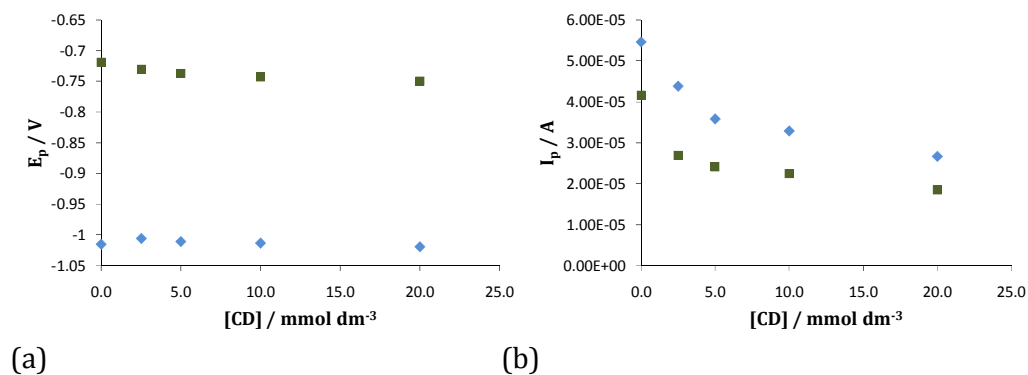


Figure 5.26: Reduction peak potentials (a) and reduction peak currents (b) for the first (■) and second (◆) reduction of 2.50×10^{-3} M EV in 0.10 M NaCl plotted as a function of increasing concentration of β -CD. Potential referred to SCE reference scale.

The inverse of the concentration of the β -CD was plotted as a function of $1/(1-i/i_0)$ in accordance with Equation 5.8. Typical plots are shown in Figure 5.27 for both reduction waves. Using these data, the formation constant between the radical cation, $EV^{•+}$, and the β -CD was computed as $170 \pm 7 \text{ M}^{-1}$ (4% error, $n=3$). This corresponds to a weak complexation process.²⁰ A larger association constant of $744 \pm 120 \text{ M}^{-1}$ (16% error, $n=3$) was obtained for the first reduction process, which indicates a higher affinity of the dicationic species, EV^{2+} , for the β -CD. Similar values were found for MV in Section 5.2.2. This suggests that the extension of the methyl to an ethyl substituent on the pyridilium ring does not affect significantly the extent of the interactions between the cationic viologens and the anionic β -CD.

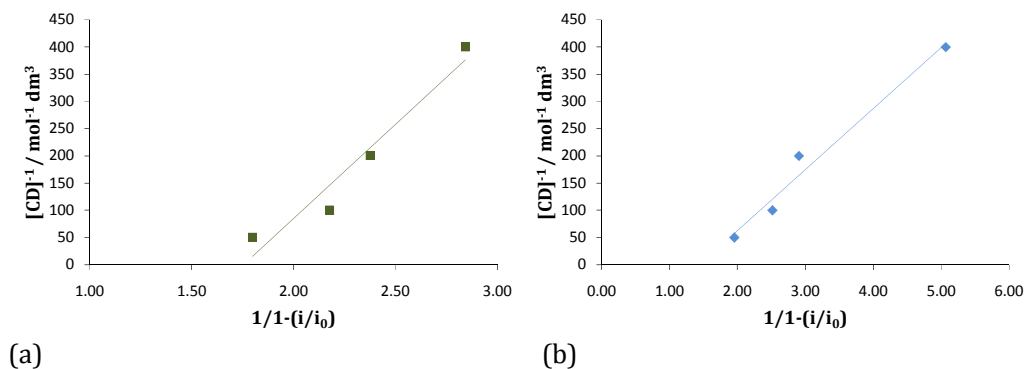


Figure 5.27: The inverse of the s β -CD concentration plotted as a function of $1/(1-i/i_0)$. A linear relationship was obtained for the first reduction — and for the second reduction — of 2.50×10^{-3} M EV in 0.10 M NaCl with added s β -CD at concentrations of 2.50×10^{-3} , 5.00×10^{-3} , 1.00×10^{-2} and 2.00×10^{-2} M. Data were extrapolated from CV measurements on a gold electrode ($d = 3.0$ mm), using a scan rate of 50 mV s^{-1} .

The oxidation profiles of the electrogenerated EV^0 and $\text{EV}^{\bullet+}$ species in the absence and presence of s β -CD are compared in Figure 5.28. The voltammograms recorded in the presence of s β -CD are considerably more complicated than the corresponding voltammograms recorded in free EV, or in the presence of the neutral β -CD, as illustrated in Figure 5.22. The peaks arising from the oxidation of the adsorbed EV species appear to be divided into three separate signals. The largest peak centred at -0.900 V vs SCE corresponds to the oxidation of the adsorbed EV^0 species, which is seen at -0.850 V vs SCE for the free ethyl viologen. However, two extra peaks around -1.0 V vs SCE, not present in the voltammogram of the free analyte, are recorded, reflecting a different environment in the proximity of the electrode surface. These new signals may be due to co-adsorbed EV^0 and s β -CD on the gold substrate. The fact that these signals increase with the s β -CD concentration supports such a hypothesis. Indeed, Kostela and co-workers³¹ have postulated too the possibility of co-adsorption of the viologen with micelles on the electrode substrate, to explain the existence of extra peaks with respect to the free viologen. In this work the authors investigated the electrochemistry of the asymmetrical viologen, TMV (N-tetradecyl-N'-methyl viologen) in the presence of different types of micelles. In particular, they observed the presence of extra peaks for TMV in solutions with micelles of polyoxyethylene-8-lauryl ether.

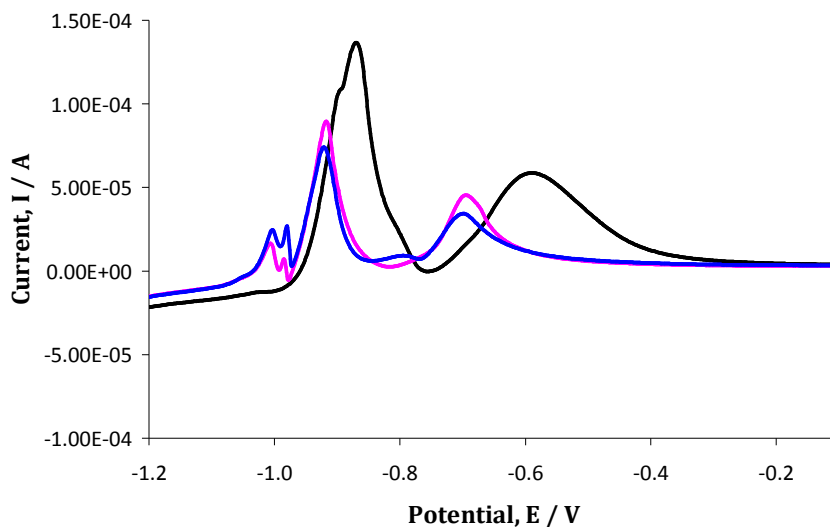


Figure 5.28: CV (oxidation wave) of a 2.50×10^{-3} M solution of EV in 0.1 M NaCl in the absence — and in the presence of s β -CD at concentrations of 5.00×10^{-3} M —, and 1.00×10^{-2} M — on a bare gold electrode ($d = 3.0$ mm) at 50 mV s^{-1} . Potential referred to SCE reference.

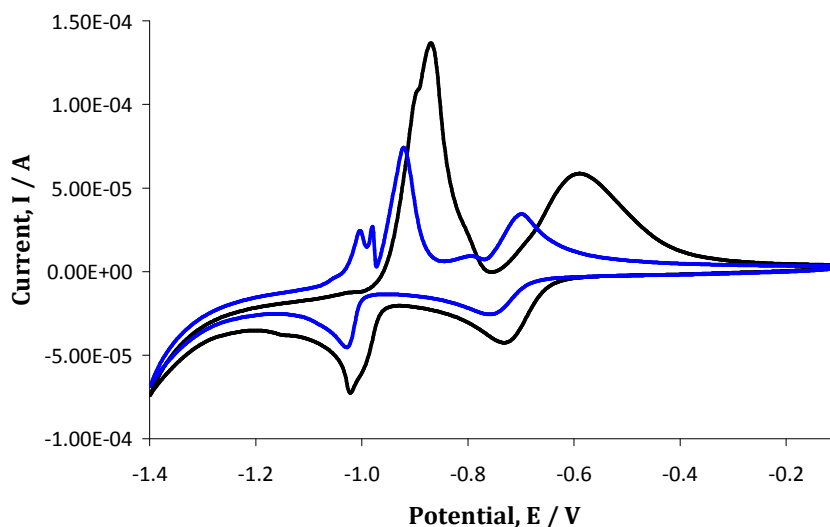


Figure 5.29: CV of a 2.50×10^{-3} M solution of EV in 0.10 M NaCl in the absence — and in the presence of 1.00×10^{-2} M s β -CD — on a bare gold electrode ($d = 3.0$ mm) at 50 mV s^{-1} . Potential referred to SCE reference.

It is clear that s β -CD does not suppress the adsorption peak arising from the oxidation of the fully reduced ethyl viologen, EV⁰, which is adsorbed onto the electrode surface. This is consistent with the data presented in Figure 5.25

which show that it is the oxidized form of the analyte, EV²⁺, which is more strongly bound to the anionic s β -CD than either the partially, EV^{•+}, or fully reduced, EV⁰, species. Only the fully reduced species interacts preferentially with the neutral β -CD while the s β -CD does not favour interaction with EV⁰. Furthermore the s β -CD appears to enhance adsorption phenomena of EV⁰ which is inconsistent with included species. These characteristics highlight again the relevance of the negative charges surrounding the anionic CD, in the interaction with the charged analytes.

The influence of the s β -CD on the oxidation of the electrogenerated EV^{•+} species to produce EV²⁺ is also evident in Figure 5.28. The peak current is lower in the presence of the s β -CD. Moreover, the peak undergoes a remarkable potential shift of 0.169 V to more negative potentials, giving an additional indication of the higher affinity of the s β -CD for the dicationic species, EV²⁺. As shown in Figure 5.29, an excess of s β -CD contributes to making the first reduction more reversible. In fact, a ΔE_p of 0.141 V and an I_{pa}/I_{pc} ratio of 0.680 were evaluated for the free EV, while a ΔE_p of 0.061 V, with an I_{pa}/I_{pc} ratio of 0.830 were calculated in the presence of 1.00×10^{-2} M s β -CD.

In order to obtain more detailed information on the interactions between EV and the sulfated β -cyclodextrin, RDV measurements were performed. In Figure 5.30 the current measured for the reduction of EV is plotted as a function of the applied potential. The limiting current, i_L , increases with increasing rotation frequency and this is clearly observed for both the first and second reduction waves of EV. As already observed for MV, the process corresponding to the reduction of the dicationic molecule EV²⁺ to its radical cation EV^{•+} is split into two separate steps, due to the presence of oxygen. A comparison of data collected before and after the removal of O₂ will be analyzed in Section 5.3.3.

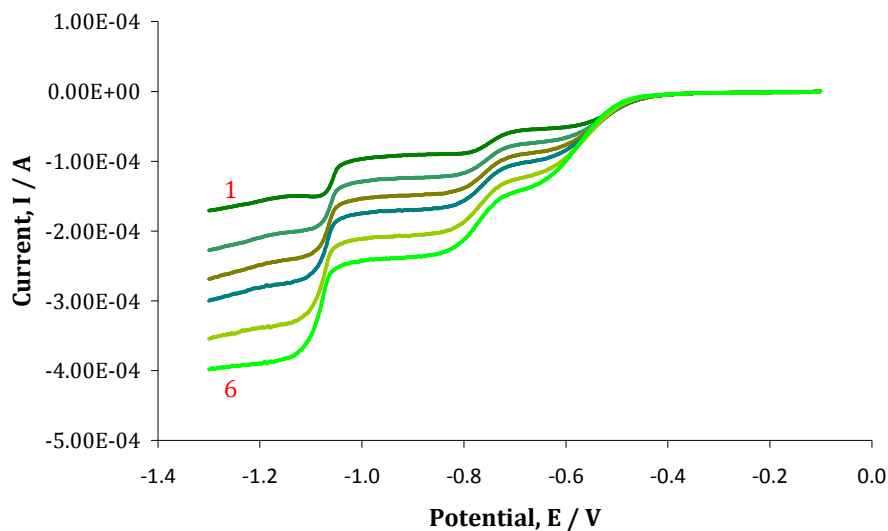


Figure 5.30: RDV voltammogram of 1.00×10^{-3} M EV in 0.10 M NaCl on a GC disc electrode ($d = 4.0$ mm), scan rate 50 mV s^{-1} , rotation frequency from 1 to 6: 250, 500, 750, 1000, 1500 and 2000 rpm. Potential referred to SCE reference.

Figure 5.31 shows that a significant reduction in the limiting currents occurs upon addition of $s\beta$ -CD. This provides proof for the interaction of the EV species with the anionic $s\beta$ -CD. When the limiting currents for both reduction waves are plotted against the square root of the rotation rate, linear plots are obtained. These plots are shown in Figure 5.32 (a) and (b) for the EV^{2+} and $\text{EV}^{•+}$ species, respectively. These data, together with the Levich equation (Equation 5.7), were used to compute the diffusion coefficients for the free EV species and for the molecule in solution with the $s\beta$ -CD. The computed values are shown in Table 5.7. A clear decrease in the diffusion coefficients is observed as the $s\beta$ -CD concentration is increased from 0.0 to 4.00×10^{-2} M.

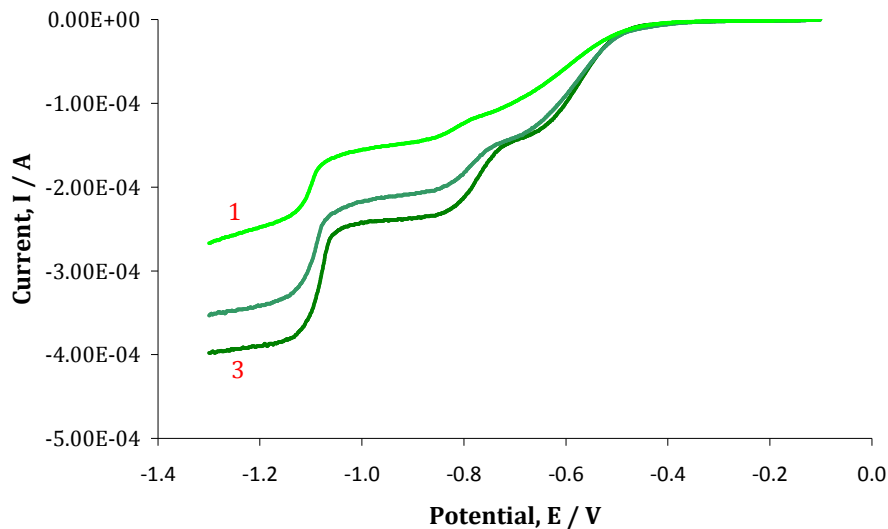


Figure 5.31: RDV voltammogram of 1.00×10^{-3} M EV in 0.10 M NaCl on a GC disc electrode ($d = 4.0$ mm), scan rate 50 mV s^{-1} , rotation frequency 2000 rpm, in the presence of different concentration of β -CD, from 1 to 3: 0.00, 1.00×10^{-3} , 4.00×10^{-2} M. Potential referred to SCE reference scale.

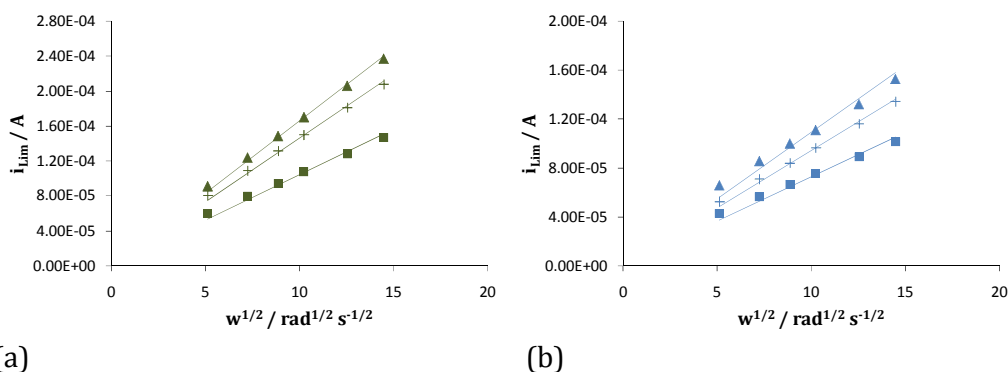


Figure 5.32: Levich plots for the limiting currents for the first (—) and second (—) reduction waves of 1.00×10^{-3} M EV in 0.10 M NaCl on a GC disc electrode ($d = 4.0$ mm), scan rate 50 mV s^{-1} , rotation frequency 250, 500, 750, 1000, 1500 and 2000 rpm, in the presence of different concentration of β -CD: 0.00 (\blacktriangle), 1.00×10^{-3} (\oplus), 4.00×10^{-2} (\blacksquare) M. Limiting currents taken at -0.9 V vs SCE and -1.2 V vs SCE .

Table 5.7: Diffusion coefficients for EV²⁺ and EV^{•+} in the presence of varying amount of s β -CD. Experiments were carried out on a GC disc electrode at a scan rate 50 mV s⁻¹, using rotation frequencies of 250, 500, 750, 1000, 1500 and 2000 rpm. EV concentration was set as 1.00 x 10⁻³ M EV.

[s β -CD] / mol dm ⁻³	Diffusion coefficient (apparent) D / cm ² s ⁻¹ for EV ²⁺ 1st reduction: EV²⁺ + e⁻ → EV^{•+}	Diffusion coefficient (apparent) D / cm ² s ⁻¹ for EV ^{•+} 2nd reduction: EV^{•+} + e⁻ → EV⁰
0.00	3.27 x 10 ⁻⁵	1.74 x 10 ⁻⁵
1.00 x 10 ⁻³	2.70 x 10 ⁻⁵	1.40 x 10 ⁻⁵
4.00 x 10 ⁻²	1.62 x 10 ⁻⁵	9.49 x 10 ⁻⁶

In addition, the charge transfer rate constants were evaluated using the procedures outlined earlier. The kinetics of the electron transfer is expected to be higher when the analyte is free in solution, compared to when it is complexed with the anionic cyclodextrin.

In order to evaluate the rate constants, Koutechy-Levich plots were constructed. Representative plots are depicted in Figure 5.33 (a) and (b) for the first and second reduction waves, respectively. The k values were estimated from the intercept using Equation 5.12. As anticipated, for both reduction processes, a lower rate constant was evaluated for the samples containing a 40-fold excess of cyclodextrin. For the first electron transfer (EV²⁺ + e⁻ → EV^{•+}), k values of 1.32 x 10⁻¹ and 2.90 x 10⁻² cm s⁻¹ were computed for the free and complexed EV²⁺, respectively. In the case of the second reduction (EV^{•+} + e⁻ → EV⁰), k values of 3.71 x 10⁻² cm s⁻¹ and 2.94 x 10⁻² cm s⁻¹ were calculated, for the free and bound EV^{•+}, respectively. The larger reduction in the rate constant for the first reduction process is consistent with the higher affinity of the anionic cyclodextrin for the dicationic form of the ethyl viologen, EV²⁺.

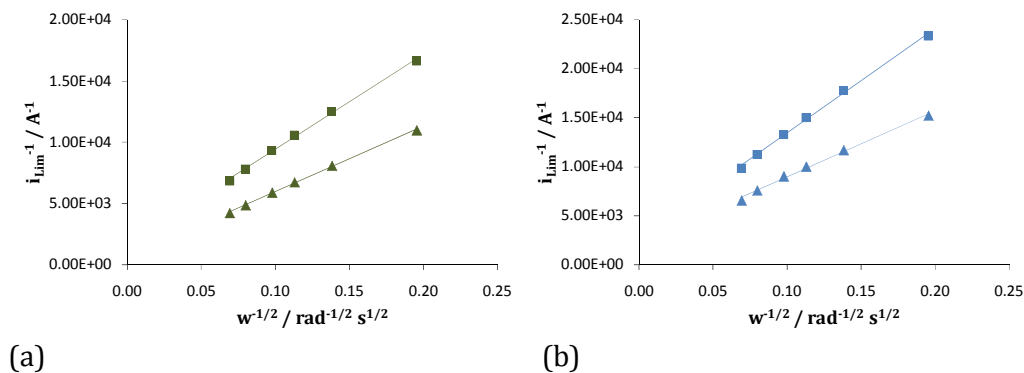


Figure 5.33: Koutechy-Levich plots for the limiting currents for the first (—) and second (—) reduction of 1.00×10^{-3} M EV in 0.10 M NaCl on a GC disc electrode ($d = 4.0$ mm), scan rate 50 mV s^{-1} , rotation frequency 250, 500, 750, 1000, 1500 and 2000 rpm, in the absence (\blacktriangle) and presence (\blacksquare) of 4.00×10^{-2} M s β -CD. Limiting currents were taken at -0.9 V vs SCE and at -1.2 V vs SCE.

5.3.3 Influence of oxygen

In the previous section, Section 5.2.3, the influence of oxygen on the electrochemistry of the MV at the rotating electrode was described. To understand the role of oxygen a similar set of experiments was carried out with the EV solution which was rigorously saturated with nitrogen. In Figure 5.34 the signals before and after removal of the oxygen are depicted. After purging of the solution with nitrogen for 60 min, the double wave observed during the first reduction step was suppressed, leading to a similar ratio of the limiting currents involved in the first and second steps of reduction. As discussed earlier for the MV system, these changes are due to the effects of dissolved oxygen.

When a 40-fold excess of s β -CD was added to the EV solution, a clear cathodic shift of 0.035 V in the half-wave potential, $E_{1/2}$, for the first reduction wave was observed, as shown in Figure 5.35. This corresponds to the reduction of the dication species, EV^{2+} . A smaller change of 0.012 V was registered for the half-wave potential of the second reduction. As shown in Figure 5.36 (a) and (b), good linear relationships were obtained between the limiting currents and the square root of the rotation wave, in agreement with the Levich equation (Equation 5.7). Using these linear plots, the experimental diffusion coefficients

ratio, D_c/D_f , for both reduction steps were computed as 0.35 and 0.38, for the first and second reduction step, respectively. These ratios are somewhat lower than the corresponding values computed in the presence of trace amounts of oxygen. Using these diffusion coefficients together with the observed potential shifts, the formation constants of the complex were obtained by fitting the data to Equation 5.6. A K_f of $122 \pm 8 \text{ M}^{-1}$ was computed for the complex formed between EV^{2+} and s β -CD, while a value of $40 \pm 3 \text{ M}^{-1}$ was obtained for the $\text{EV}^{\bullet+}$ /s β -CD complex.

In Table 5.8 the formation constants derived from the two methods, RDV and CV, are summarized. With both techniques a higher K_f was obtained for the EV^{2+} species. However, as already observed with MV, there is some variation in the magnitude of K_f when the RDV and CV approaches are compared.

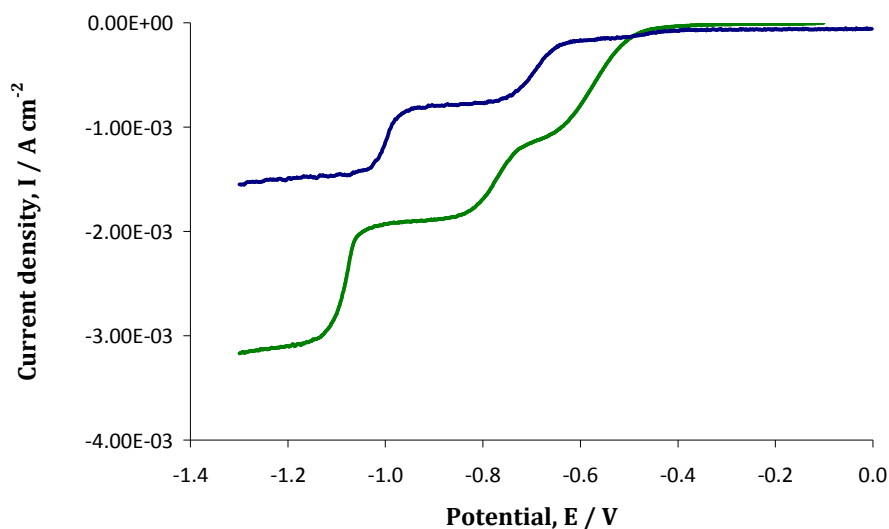


Figure 5.34: RDV voltammogram showing current densities for $1.00 \times 10^{-3} \text{ M}$ EV in 0.10 M NaCl on a GC disc electrode, at a scan rate 50 mV s^{-1} , rotation frequency 2000 rpm , before — and after — saturation of the solution with N_2 .

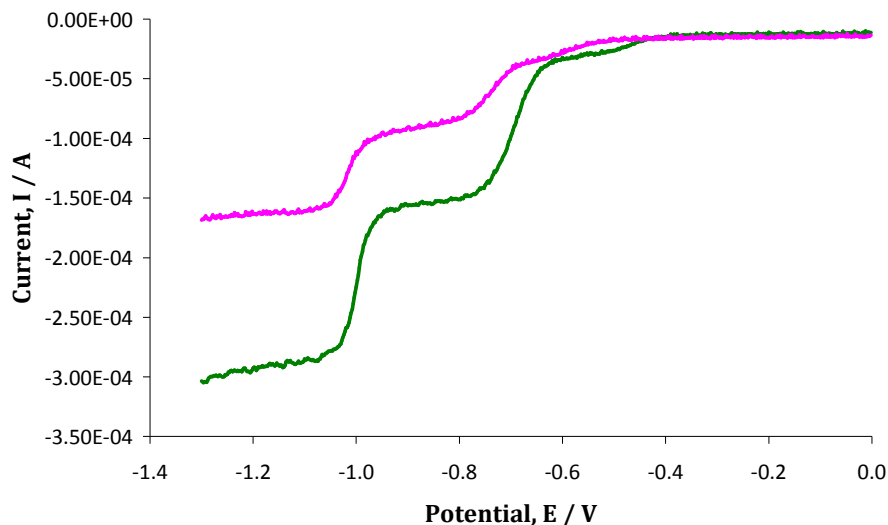


Figure 5.35: RDV voltammogram of 1.00×10^{-3} M EV in 0.10 M NaCl on a GC disc electrode ($d = 5.0$ mm), scan rate 50 mV s^{-1} , rotation frequency 2000 rpm, in the absence — and the presence of 4.00×10^{-2} M s β -CD —. Potential referred to SCE reference. Prior to RDV measurements, solutions were purged with nitrogen for 60 min.

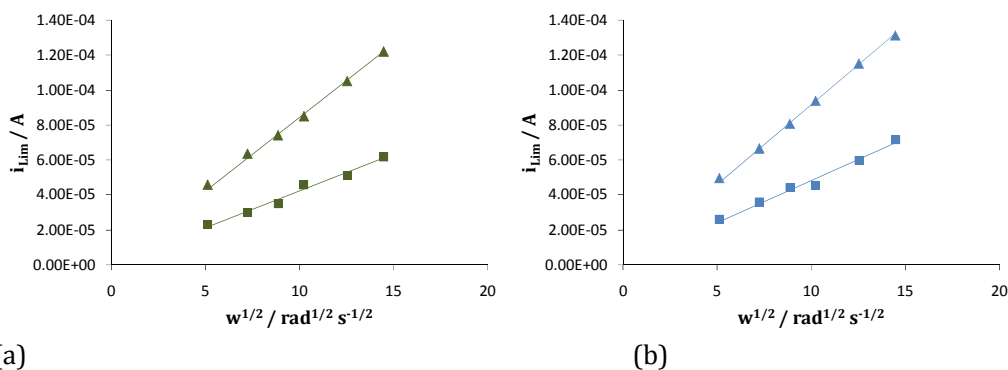
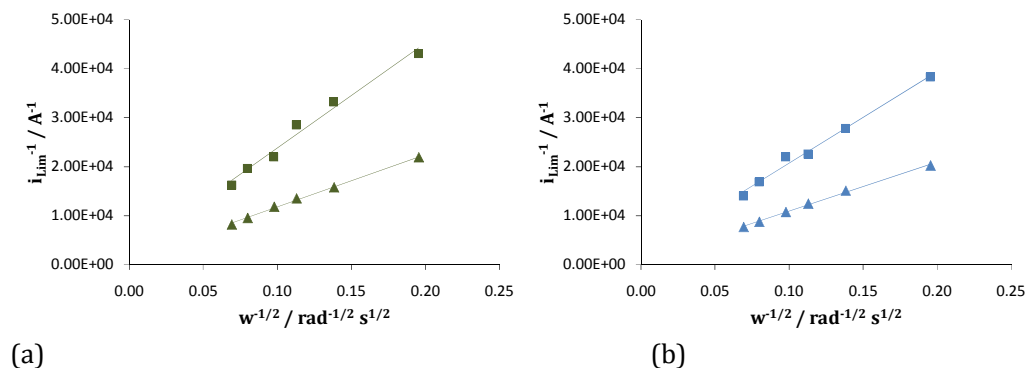


Figure 5.36: Levich plots for the limiting currents for the first (—) and second (—) reduction of 1.00×10^{-3} M EV in 0.10 M NaCl on a GC disc electrode ($d = 2.50$ mm), scan rate 50 mV s^{-1} , rotation frequency 250, 500, 750, 1000, 1500 and 2000 rpm, in the absence (▲) and the presence of 4.00×10^{-2} M s β -CD (■). Limiting currents taken at -0.9 V vs SCE and at -1.2 V vs SCE.

Table 5.8: Summary of K_f values for EV species evaluated by means of CV and RDV.

EV species	K_f / M^{-1} by RDV	K_f / M^{-1} by CV
EV^{2+}	122 ± 8	744 ± 120
$EV^{•+}$	41 ± 3	170 ± 7

**Figure 5.37:** Koutechy-Levich plots for the limiting currents of the first (—) and second (—) reduction of 1.00×10^{-3} M EV in 0.10 M NaCl on a GC disc electrode ($d = 2.50$ mm), scan rate 50 mV s^{-1} , rotation frequency 250, 500, 750, 1000, 1500 and 2000 rpm, in the absence (\blacktriangle) and the presence of 4.00×10^{-2} M sβ-CD (\blacksquare). Limiting currents taken at -0.9 V vs SCE and at -1.2 V vs SCE.**Table 5.9:** Rate constants for the reduction of EV^{2+} and $EV^{•+}$ in 1.00×10^{-3} M EV in 0.10 M NaCl and in 1.00×10^{-3} M EV, 0.10 M NaCl and 4.00×10^{-2} M sβ-CD, in the presence and absence of dissolved O_2 .

Solutions	$k / \text{cm s}^{-1}$		$k / \text{cm s}^{-1}$	
	1 st reduction: $EV^{2++} e^- \rightarrow EV^{•+}$		2 nd reduction: $EV^{•++} e^- \rightarrow EV^0$	
	EV	EV+sβ-CD	EV	EV+sβ-CD
With O_2	1.32×10^{-1}	2.90×10^{-2}	3.71×10^{-2}	2.94×10^{-2}
Deoxygenated	4.80×10^{-2}	2.23×10^{-2}	6.07×10^{-2}	2.64×10^{-2}

5.4 Interaction of benzyl viologen with β -CD and s β -CD investigated by means of CV and RDV

The last compound examined in the present chapter is the benzyl viologen, where the aliphatic chain of MV and EV has been replaced by a benzylic moiety. As the alkyl substituent is attached to an aromatic ring, this confers a higher hydrophobicity to the system. Therefore, it was interesting to verify how this molecule may interact with the sulfated β -cyclodextrin.

5.4.1 Benzyl viologen and β -CD

The electrochemistry of BV is similar to the other two viologens, as illustrated by the black trace in Figure 5.38. This voltammogram was recorded in 2.50×10^{-3} M BV in a 0.1 M NaCl supporting electrolyte. The first reduction peak occurs at -0.580 V vs SCE and it corresponds to the reduction of the dication to generate the radical cation, as clarified in Equation 5.1. The electrogeneration of the radical is then followed by a second reduction step, described in Equation 5.2, around -0.770 V vs SCE, which leads to the formation of the neutral viologen. On the reverse scan, the typical sharp adsorption wave around -0.600 V vs SCE reflects the poor solubility of the reduced species, BV⁰, in aqueous solutions. A ΔE_p of 0.170 V for the BV⁰/ BV^{•+} couple is in fact evidence of a reaction showing non-reversible behaviour. Finally, the anodic peak at -0.470 V vs SCE is related to the oxidation of the radical cation back to the original dicationic state, BV²⁺, also described in Equation 5.5. Figure 5.38 illustrates that as increasing concentrations of β -CD are added, the E_p for the reduction of the dication (BV²⁺ + e⁻ → BV^{•+}) undergoes a positive shift, while the cathodic peak for the reduction of the radical to form the neutral molecule (BV^{•+} + e⁻ → BV⁰) moves to more negative potential values and is accompanied by a significant decrease of the current. The peak current for the reduction of BV^{•+} is reduced from 5.46×10^{-5} A to 3.09×10^{-5} A on addition of the neutral β -CD (1.0×10^{-2} M), while the peak potential is shifted from -0.765 V to -0.821 V vs SCE in the absence and presence of 1.00×10^{-2} M β -CD.

These electrochemical characteristics of the benzyl viologen are significantly different to that observed with the methyl and ethyl viologens. The current and potential shifts recorded for methyl and ethyl viologens indicated the affinity of the neutral β -CD for the fully reduced state of the analytes. In contrast, the voltammograms depicted in Figure 5.38 indicate that the β -CD interacts preferentially with the partially reduced species of the benzyl viologen, $BV^{+\cdot}$.

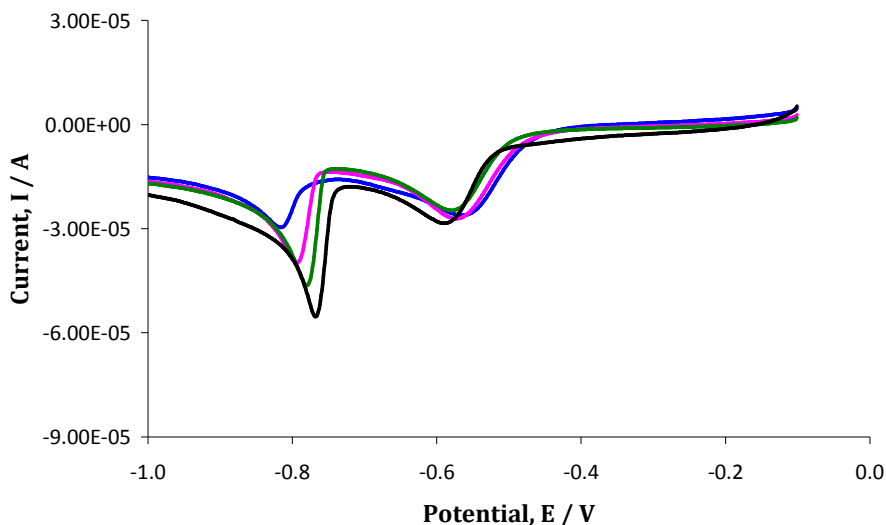


Figure 5.38: CV for the reduction of a 2.50×10^{-3} M solution of BV in 0.10 M NaCl — and of a 2.50×10^{-3} M solution of BV in 0.10 M NaCl and 2.50×10^{-3} M —, 5.00×10^{-3} M — and 1.00×10^{-2} M — β -CD at a bare gold electrode ($d = 3.0$ mm), using a scan rate of 50 mV s^{-1} . Potential referred to SCE scale.

Representative rotating disc voltammograms, illustrating the electrochemistry of BV in two different electrochemical windows, are shown in Figure 5.39. As previously observed for the other two viologens, Figure 5.39 shows the reversibility of the first reduction process, when the fully reduced species is not produced. This confirms that the radical cation of the benzyl viologen, $BV^{+\cdot}$, is a relatively soluble species, at least at the concentrations used here, despite the fact that the substituents are more hydrophobic than those of the methyl and ethyl viologens. The presence of an adsorption peak, which arises from the oxidation of the adsorbed BV^0 species is again clearly evident in Figure 5.39 (b) on the reverse cycle.

In Figure 5.40 RDV voltammograms for the benzyl viologen alone and in the presence of a 10-fold excess of the neutral β -CD are presented. On comparing the reduction waves for the $BV^{•+}$ species, observed at about -0.800 V vs SCE, a large negative potential shift is immediately evident (blue trace), when the neutral β -CD host is added to the electrolyte. This suggests complexation of the radical $BV^{•+}$ species with the neutral β -CD. Furthermore, adsorption phenomena are still visible in the reverse oxidation wave for the sample containing the cyclodextrin. This, in turn, confirms the low affinity of the neutral β -CD for the fully reduced BV^0 species. Again, these observations are very different to those described in Sections 5.2.1 and 5.3.1, where the addition of the neutral β -CD gave rise to the inclusion of MV^0 and EV^0 into the hydrophobic cavity of the neutral cyclodextrin; hence their deposition/adsorption onto the electrode surface was prevented. This is not the case for the benzyl viologen, as shown in Figure 5.40.

The negative potential shift recorded for the reduction of $BV^{•+}$ to give BV^0 on the addition of the neutral β -CD is clearly evident in Figure 5.40 and indicates a relatively strong interaction. Nevertheless, this large potential shift is not accompanied by an equally significant decrease in the limiting current (Figure 5.40). This is somewhat different to that observed in Figure 5.38, where the data were recorded under non-rotating conditions. Using the RDV data, the limiting currents were fit to the Levich equation (Equation 5.7). The linear plots obtained are shown in the inset of Figure 5.40. They exhibit excellent linearity, with correlation coefficients of 0.999 for both sets of data. From these plots the diffusion coefficient for the complexed $BV^{•+}$ species, D_c , was calculated as $8.49 \times 10^{-6} \text{ cm}^2 \text{ s}^{-1}$, while the evaluated D_f was found to be $1.32 \times 10^{-5} \text{ cm}^2 \text{ s}^{-1}$. This gives rise to a D_c/D_f ratio of 0.64, which is somewhat higher than the expected value of 0.4, but is consistent with the relatively small changes in the limiting currents, Figure 5.40. This experimental D_c/D_f ratio and the $\Delta E_{1/2}$ of 57 mV were fit to Equation 5.6 to work out the K_f value for the complex $BV^{•+}/\beta$ -CD. A value of $1048 \pm 41 \text{ M}^{-1}$ was computed, indicating that $BV^{•+}$ is efficiently included within the neutral cyclodextrin cavity.

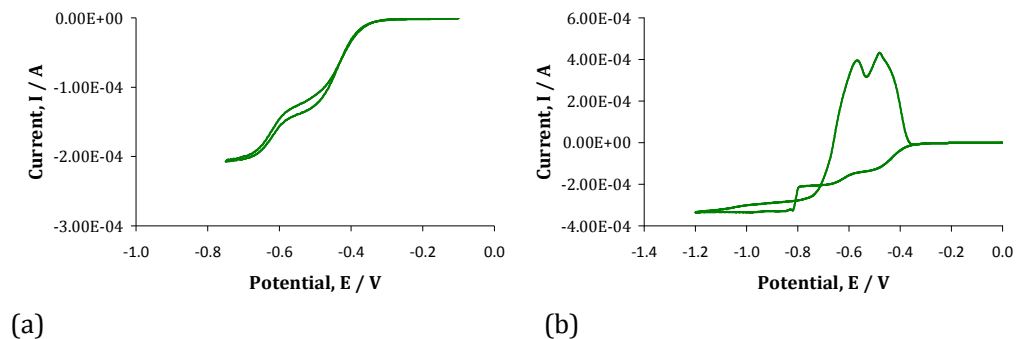


Figure 5.39: RDV voltammograms of 1.00×10^{-3} M BV in 0.10 M NaCl recorded using a GC disc electrode ($d = 4.0$ mm), scan rate 50 mV s^{-1} , rotation frequency 2000 rpm, from 0.0 to -0.9 V vs SCE (a) and from 0.0 to -1.4 V vs SCE (b). Potential referred to SCE reference scale.

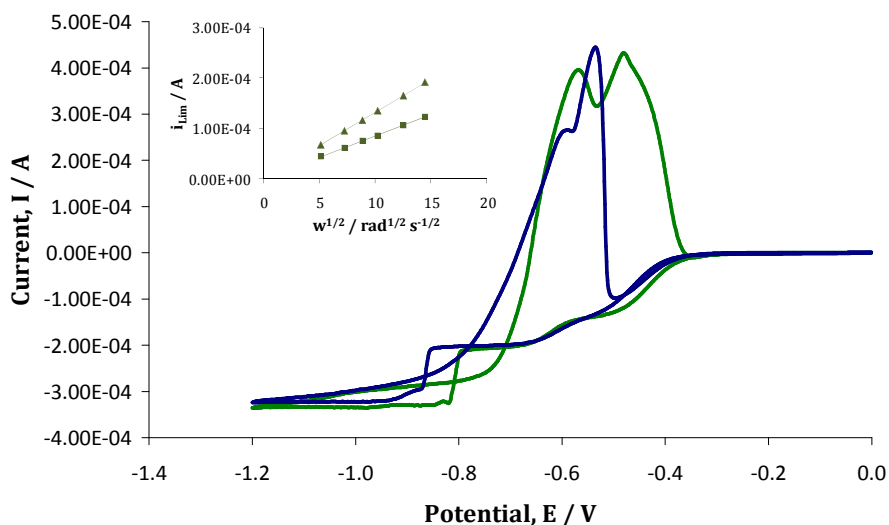


Figure 5.40: RDV voltammograms of 1.00×10^{-3} M BV in 0.10 M NaCl on a GC disc electrode ($d = 4.0$ mm) in the absence (—) and the presence (—) of 1.00×10^{-2} M β -CD, scan rate 50 mV s^{-1} , rotation frequency 2000 rpm. Inset shows limiting currents recorded at -1.0 V vs SCE, which relate to the second reduction of BV in the absence (\blacktriangle) and the presence (\blacksquare) of β -CD, as a function of the square root of the rotation rate. Potential referred to SCE reference scale.

5.4.2 Benzyl viologen and β -CD

The electrochemistry of the benzyl viologen in the presence of β -CD is very different to that observed with the methyl and ethyl viologens, as shown in

Figure 5.41. Firstly, the first reduction, observed at around -0.580 V vs SCE undergoes a slight shift to more positive potentials, in the presence of the s β -CD. An opposite trend was observed for the methyl and ethyl viologens, Figure 5.8 and Figure 5.25, respectively. Furthermore, this reduction peak becomes progressively broader on the addition of the s β -CD, which may indicate a decrease in the rate of the electron transfer and/or a decrease in the rate of diffusion to the electrode surface. On the other hand, the second reduction wave, which occurs at around -0.770 V vs SCE for the free species is dramatically shifted to more cathodic potentials. The potential shift is 0.230 V on addition of 1.0×10^{-2} M s β -CD. There is not a trend between the peak currents and the concentration of the s β -CD (Figure 5.41), as elsewhere observed for the other two compounds. The voltammograms shown in Figure 5.41 represent the tenth cycle. If adsorption phenomena occur as a function of time, this might alter, to some extent, the redox equilibria.

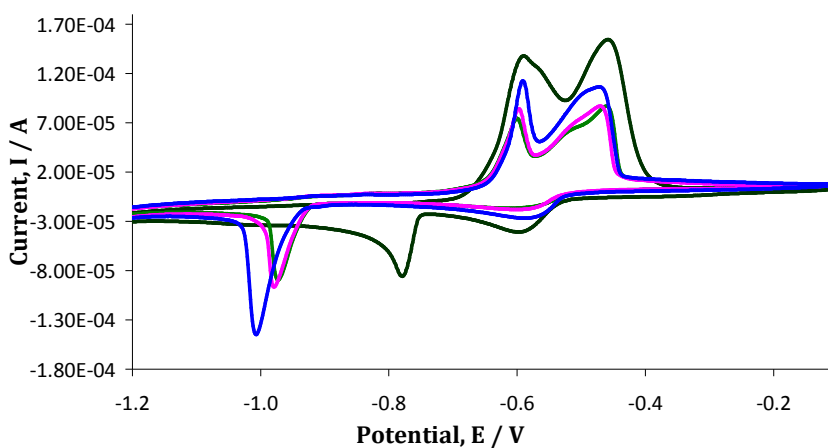


Figure 5.41: CV of a 2.50×10^{-3} M solution of BV in 0.10 M NaCl — and of a 2.50×10^{-3} M solution of BV in 0.10 M NaCl and 2.50×10^{-3} M —, 5.00×10^{-3} M — and 1.00×10^{-2} M — s β -CD at a bare gold electrode ($d = 3.0$ mm), using a scan rate of 50 mV s^{-1} . Potential referred to SCE scale.

The shape of the reverse oxidation waves is not particularly modified by the presence of the s β -CD, except for changes in the peak currents, as depicted in Figure 5.41. This is not surprising as the magnitude of these currents is

influenced by the forward reduction cycle. In particular, the reduction in the peak currents for the conversion of the BV²⁺ species to the radical cations will give rise to lower oxidation currents during the reverse cycle.

RDV experiments were carried out to evaluate the changes in the rate of diffusion of the BV²⁺ species upon addition of the s β -CD to the electrolyte. Figure 5.42 illustrates the voltammograms recorded at different rotation rates for a 1.00×10^{-3} M BV solution. As clearly shown in the figure, the limiting currents increase with increasing the rotation rate.

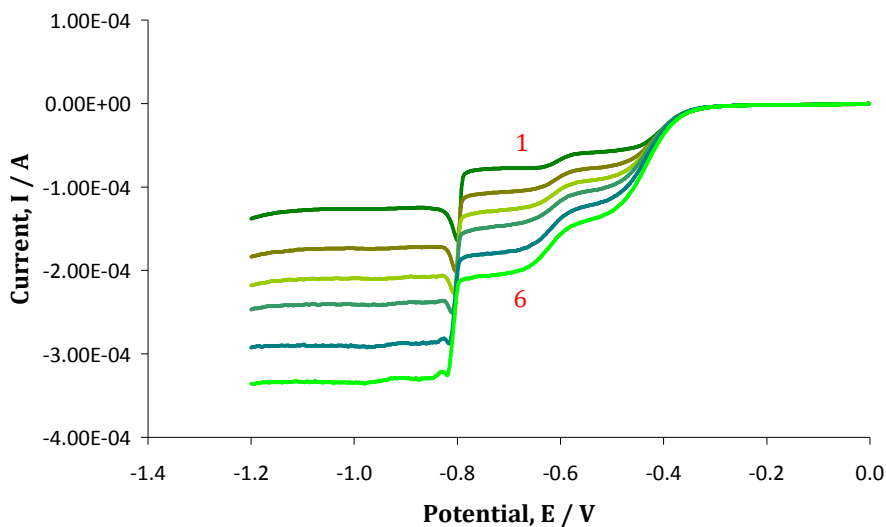


Figure 5.42: RDV voltammograms of 1.00×10^{-3} M BV in 0.10 M NaCl on a GC disc electrode ($d = 4.0$ mm), scan rate 50 mV s^{-1} , rotation frequency varied from 1 to 6: 250, 500, 750, 1000, 1500 and 2000 rpm. Potential referred to SCE reference scale.

A series of similar RDV experiments was performed for BV alone and in solutions with varying concentrations of the s β -CD and the resulting limiting currents measured at -0.700 V vs SCE were fit into the Levich equation (Equation 5.7). The corresponding Levich plots are illustrated in Figure 5.43 (a) and exhibit good linearity, with correlation coefficients ranging from 0.977 to 0.996. The diffusion coefficients were computed from these Levich plots. In Figure 5.43 (b) the diffusion coefficients are plotted as a function of the s β -CD concentration. A clear decrease in the diffusion coefficient is observed as higher

concentrations of the cyclodextrin are present within the solution. This gives evidence of some interaction between the BV analyte in its dication state and the anionic β -CD. This interaction is also confirmed by a reduction in the charge transfer rate constant, as illustrated in Figure 5.44. Here, Koutechy-Levich plots are presented (R^2 exceeding 0.998) as a function of the concentration of β -CD. These data were used with the Koutecky-Levich equation (Equation 5.12) to compute rate constants. The rate constant, k , was computed as $1.27 \times 10^{-1} \text{ cm s}^{-1}$ for the free BV^{2+} species, but this was reduced to $4.90 \times 10^{-2} \text{ cm s}^{-1}$, upon addition of a 40-times excess of the β -CD macrocycle. This suggests that the anionic β -CD reduces both the rate of diffusion of the BV^{2+} species and the rate of the electron transfer.

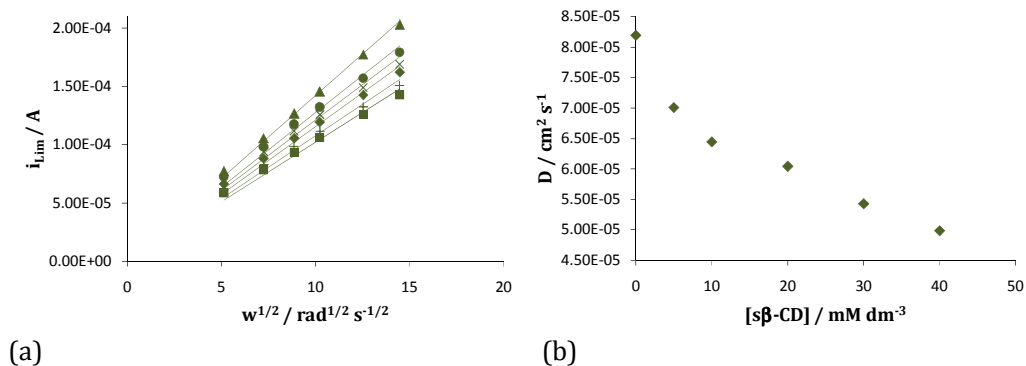


Figure 5.43: Levich plots (a) for the limiting currents relative to the first reduction wave of $1.00 \times 10^{-3} \text{ M}$ BV in 0.10 M NaCl on a GC disc electrode ($d = 4.0 \text{ mm}$), scan rate 50 mV s^{-1} , rotation frequency 250, 500, 750, 1000, 1500 and 2000 rpm, in the presence of different concentration of β -CD: 0.00 M (▲), $5.00 \times 10^{-3} \text{ M}$ (●), $1.00 \times 10^{-2} \text{ M}$ (✕), $2.00 \times 10^{-2} \text{ M}$ (◆), $3.00 \times 10^{-2} \text{ M}$ (+), $4.00 \times 10^{-2} \text{ M}$ (■). Limiting currents were taken at -0.7 V vs SCE. Diffusion coefficients of BV^{2+} plotted as a function of the concentration of β -CD (b).

It proved impossible to quantify the interactions between BV^{++} and β -CD using RDV, as the voltammograms became very complex, in the potential region where BV^{++} is reduced to BV^0 , on addition of β -CD. Figure 5.45 shows typical voltammograms recorded in $1.00 \times 10^{-3} \text{ M}$ BV with varying concentrations of β -CD. The typical limiting currents are not observed. Instead, sharp peaks are

evident. These were attributed to the formation of insoluble species between the BV^{•+} radical species and the s β -CD.

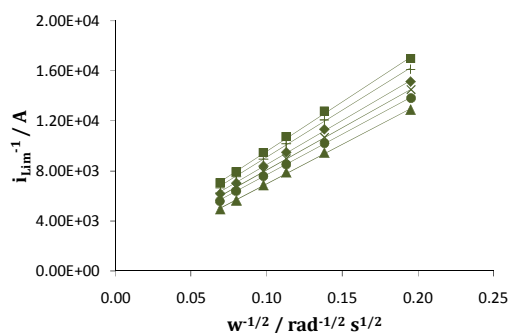


Figure 5.44: Koutechy-Levich plots for the limiting currents relative to the first reduction wave of 1.00×10^{-3} M BV in 0.10 M NaCl on a GC disc electrode ($d = 4.0$ mm), scan rate 50 mV s^{-1} , rotation frequency 250, 500, 750, 1000, 1500 and 2000 rpm, in the presence of different concentrations of s β -CD: 0.00 M (\blacktriangle), 5.00×10^{-3} M (\bullet), 1.00×10^{-2} M (\times), 2.00×10^{-2} M (\blacklozenge), 3.00×10^{-2} M (\oplus), 4.00×10^{-2} M (\blacksquare). Limiting currents were taken at -0.7 V vs SCE.

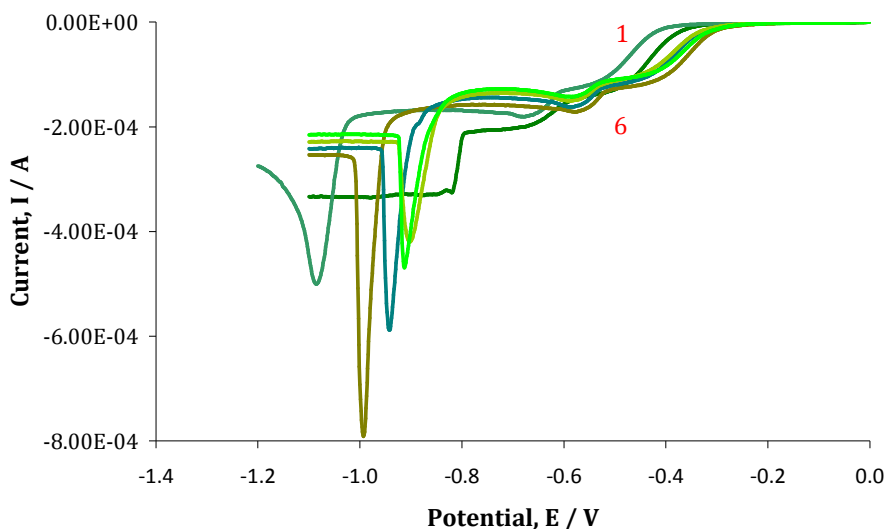


Figure 5.45: RDV voltammograms of 1.00×10^{-3} M BV in 0.10 M NaCl on a GC disc electrode ($d = 4.0$ mm), scan rate 50 mV s^{-1} , rotation frequency 2000 rpm, in the presence of different concentration of s β -CD, from 1 to 6: 0.00, 5.00×10^{-3} , 1.00×10^{-2} , 2.00×10^{-2} , 3.00×10^{-2} , 4.00×10^{-2} M s β -CD. Potential referred to SCE reference scale.

5.4.3 Influence of oxygen

In the attempt to understand the role of oxygen in the benzyl viologen electrochemistry, a set of experiments, similar to those discussed in Section 5.2.3 and 5.3.3, was carried out with the BV solution saturated totally with nitrogen. In Figure 5.46 the signals before and after removal of the oxygen are depicted. After purging of the solution with nitrogen for 60 min, the double wave during the first reduction step is suppressed; thus resulting in an analogous ratio of the limiting currents for the first and second reduction. As discussed earlier for the MV and EV systems, these changes are due to the effects of dissolved oxygen.

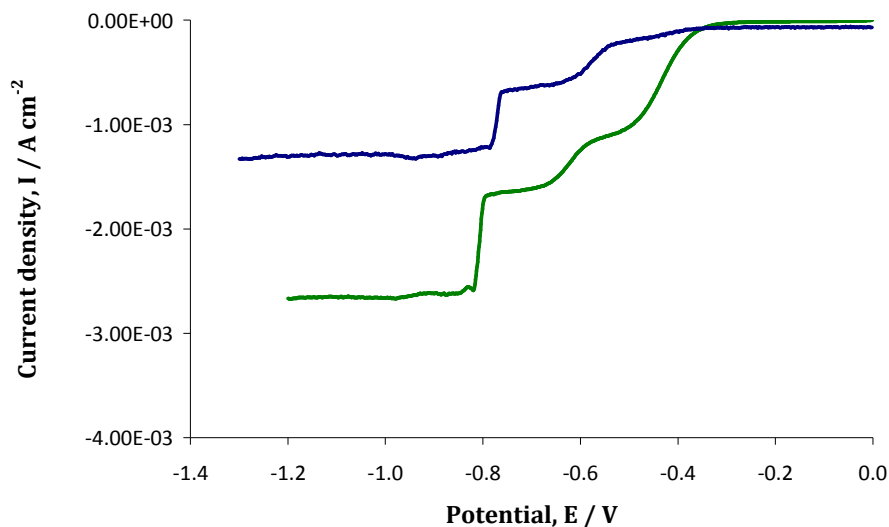


Figure 5.46: RDV voltammograms showing current densities for 1.00×10^{-3} M BV in 0.10 M NaCl, on a GC disc electrode, at a scan rate 50 mV s^{-1} , rotation frequency 2000 rpm, before — and after — saturation of the solution with N_2 .

In Section 5.2.3 and 5.3.3 it was shown that by removing the contribution of the oxygen it was possible to observe a negative potential shift for the first or the second steps of methyl and ethyl viologen reduction. In contrast, it is visible from Figure 5.47 that even after oxygen removal, the presence of a 40-fold excess of β -CD has an almost negligible effect on the reduction of the dication,

BV²⁺. As a matter of fact a $\Delta E_{1/2}$ of only 18 mV was evaluated for the first reduction step upon addition of a 40-times excess of the anionic s β -CD.

Since the Levich plots of Figure 5.48 (a) exhibited very good linearity (R^2 was 0.998) they allowed the calculation of the D_c and D_f values in the absence of oxygen. These values were computed as $1.66 \times 10^{-5} \text{ cm}^2 \text{ s}^{-1}$ and $4.72 \times 10^{-5} \text{ cm}^2 \text{ s}^{-1}$, respectively, giving a D_c/D_f ratio of 0.35. When all the required parameters were fit in Equation 5.6, a very weak formation constant, K_f , of 60 M^{-1} was computed for the BV²⁺/s β -CD system. However, the decrease in the charge transfer rate constant for the benzyl viologen dication in solution with an excess of the s β -CD provides additional evidence of a real interaction between the analyte and the macrocycle. In this case a decrease in the rate constant from $1.31 \times 10^{-1} \text{ cm s}^{-1}$ to $1.20 \times 10^{-2} \text{ cm s}^{-1}$ was observed.

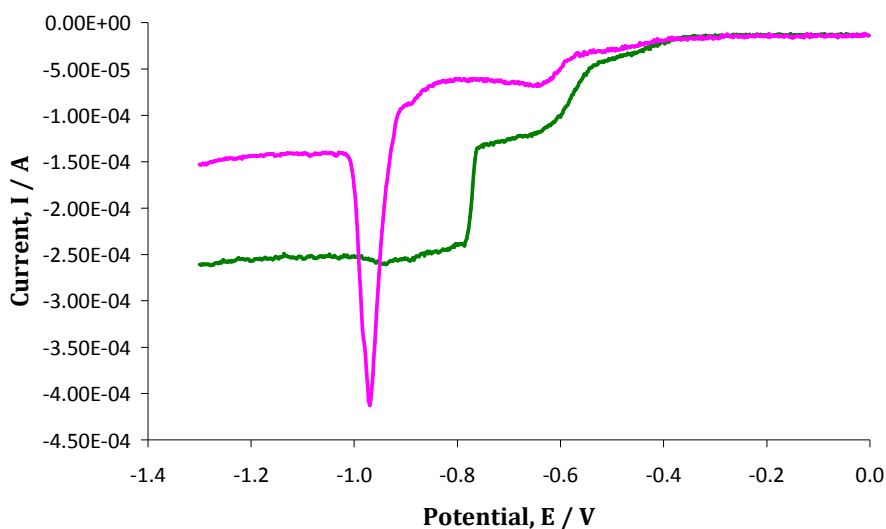


Figure 5.47: RDV voltammogram of $1.00 \times 10^{-3} \text{ M}$ BV in 0.10 M NaCl on a GC disc electrode ($d = 5.0 \text{ mm}$), scan rate 50 mV s^{-1} , rotation frequency 2000 rpm , in the absence — and the presence of $4.00 \times 10^{-2} \text{ M}$ s β -CD —. Potential referred to SCE reference scale. Solutions were purged with nitrogen for 60 min prior to the experiment.

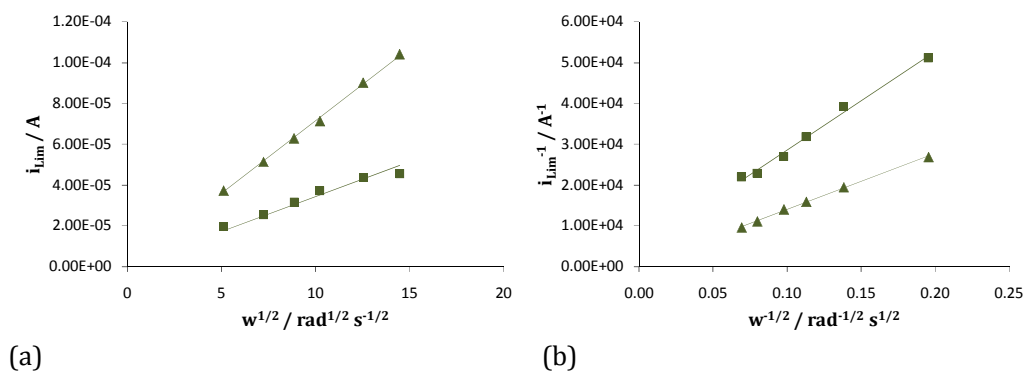


Figure 5.48: Levich plot (a) and Koutechy-Levich plot (b) for the limiting currents relative to the first reduction of 1.00×10^{-3} M BV in 0.1 M NaCl on a GC disc electrode ($d = 5.0$ mm), scan rate 50 mV s^{-1} , rotation frequency 250, 500, 750, 1000, 1500 and 2000 rpm, in the absence (▲) and the presence of 4.00×10^{-2} M s β -CD (■). Limiting currents taken at -0.7 V vs SCE.

5.5 Conclusions and summary of results

In the present chapter, the electrochemistry of three different viologens in solution with the anionic s β -CD, explored by means of CV and RDV, was discussed. Data were compared with analogous experiments recorded in the presence of the neutral β -CD. The results provide clear evidence for an interaction between the s β -CD and the viologens. More precisely, the anionic cyclodextrin interacts preferentially with the positively charged states of the analytes: V^{2+} and $V^{\bullet+}$. On the other hand, the neutral species MV^0 and EV^0 and the radical cation, $BV^{\bullet+}$ exhibited higher affinity for the neutral β -CD. The formation constants, K_f , for the complexation of the relevant species are summarized in Tables 5.10 and 5.11. However, K_f for the radical species $BV^{\bullet+}$ and the s β -CD could not be evaluated, since the $BV^{\bullet+}/s\beta$ -CD complex is insoluble in aqueous solution.

It should be noted that the concentration of s β -CD is used in the calculation of K_f . In all cases nine sulfated groups were used to compute the molecular mass of the macrocycle. The maximum error based on this approximation is 8%. However, this error does not influence the trend observed for the data.

There is some discrepancy between the K_f values computed using RDV measurements and those calculated from CV data. This can be explained in terms of the parameters considered in the analysis. The RDV data were fitted to Equation 5.6, which considers changes in the potential at which the analyte is reduced or oxidized. On the other hand, the analysis of the CV data using Equation 5.8, is dominated by changes in the rate of diffusion of the analyte species, and this in turn depends on the size of the complex formed and it is governed by the size of the cyclodextrins. However, in this case RDV results are considered more accurate; since the small potential shifts evaluated employing this technique are an additional indication that supports the formation of a weak complex between the β -CD and the three viologens.

The K_f values listed in Table 5.11 are in agreement with the formation of an inclusion complex between the neutral β -CD and the reduced species.⁶ The neutral viologen forms a host-guest complex with the hydrophobic cavity of the β -CD. However, there is one exception and that is the apparently high formation constant observed with the radical species of the benzyl viologen. As the BV contains phenyl rings, as shown in Figure 5.2, the inclusion complex may form between the benzyl groups and the cyclodextrin cavity. In this way the electron deficient bipyridilium is not included within the cavity. Cyclodextrins are well known to form strong inclusion complexes with phenyl rings.²⁰

In contrast, the smaller K_f values obtained using RDV for the positively charged species of the three viologens and the β -CD, provide evidence for weaker interactions. The exact nature of this interaction is difficult to establish. It has been reported that the sulfated cyclodextrin is similar in terms of its cavity size and hydrophobicity to the neutral cyclodextrin. Consequently, the formation of a host-guest inclusion complex between the charged viologens and the hydrophobic cavity is unlikely. There is no precedence in the literature for the inclusion of such a highly charged polar molecule within the cavity of a cyclodextrin. Moreover, it was shown that the interaction between the V^{2+} species and the anionic cyclodextrin was in fact higher than that between the $V^{•+}$

and the anionic cyclodextrin. This finding points to an association that is controlled by electrostatic interactions.

The formation of an association complex is instead suggested. This association complex could arise from a charge-transfer type interaction or simply be the result of an ion pairing interaction. The bipyridilium dication is electron deficient and is well known to form charge-transfer complexes with electron donors, such as hexacyanoferrate.^{22,23} If the ionization energy of the electron donor is compatible with the electron affinity of the dicationic viologen, then a charge transfer complex will form. However, the formation of a charge-transfer complex generates a new optical absorption band, due to orbital overlapping between the donor and the acceptor.^{32,33} If there is no orbital overlap then the interaction is electrostatic and an ion pair is formed.

Table 5.10: Summary of the formation constants, K_f , for the complex formation of the different species of the viologen compounds with the s β -CD.

Species	K_f / M^{-1} by RDV
MV^{2+}	171 ± 5
$MV^{\bullet+}$	135 ± 4
EV^{2+}	122 ± 8
$EV^{\bullet+}$	41 ± 3
BV^{2+}	60 ± 3

Table 5.11: Summary of the formation constants, K_f , for the complex formation of the different species of the viologen compounds with the neutral β -CD.

Species	K_f / M^{-1} by RDV
MV^0	681 ± 22
EV^0	336 ± 15
$BV^{\bullet+}$	1048 ± 41

In an attempt to clarify these issues, UV-Vis spectroscopy experiments were carried out (these results are presented in Chapter 6). As will be shown in Chapter 6, the results obtained are consistent with the formation of an ion pair between the charged viologens and the anionic β -CD. The bipyridilium viologen dications are electron deficient systems and can form ion pairs with the negatively charged β -CD anions. This hypothesis is supported by several publications where extensive ion-association between the viologen dications and electron-rich anions is discussed.^{22,23,34} This ion pairing is consistent with the decrease in the diffusion coefficient of the charged viologens when in the presence of the anionic β -CD, as the ion pair is considerably larger in size than the free viologens.

As will be discussed in Chapter 6, UV-Vis and ^1H NMR spectroscopy experiments reveal that the dication of the benzyl viologen forms the strongest ion pair with the anionic β -CD. However, the CV and RDV results discussed in Section 5.4.2 and 5.4.3 show that the electrochemistry of this dication is the least affected by the presence of the anionic β -CD. This can only be explained by considering events at the electrode interface. Various publications report on the adsorption of the viologen dications on different electrode substrates, including gold and GC.³⁵⁻⁴¹ This adsorption occurs at potentials more electropositive than that of the reduction potential.⁴¹ In particular, the benzyl viologen dication can form a very ordered layer on the electrode surface^{42,43} and the reduction of the adsorbed species takes place in the same potential region where the bulk solution species are reduced and so is making it difficult to distinguish.⁴³ These characteristics may influence the electrochemical behaviour of BV^{2+} in the presence of the β -CD anions. The β -CD may alter the adsorption equilibria of methyl and ethyl viologens, due to their weaker interactions with the electrode surface. On the other hand, the highly organized structure of the benzyl viologen layer on the electrode surface gives rise to a stronger adsorption and the presence of the β -CD within the solution may have less influence on the electrochemistry of the BV^{2+} . Therefore, the observed electrochemistry of the dication is of an adsorbed species.

It appears that the β -CD anions exert a significant influence on the BV^{2+} cations in solution, but have less influence on the highly ordered adsorbed layer on the electrode surface. This will be discussed in Chapter 6.

5.6 References

1. Monk P. M. S., Turner C. and Akhtar S. P.; *Electrochimica Acta*, 44, 1999, 4817-4826.
2. Engelman E. E. and Evans D. H.; *Journal of Electroanalytical Chemistry*, 349, 1993, 141-158.
3. Sivagnanam U. and Palaniandavar M.; *Journal of Electroanalytical Chemistry*, 341, 1992, 197-207.
4. Kim J. Y., Lee C. M. and Park J. W.; *Journal of Electroanalytical Chemistry*, 504, 2001, 104-110.
5. Lee C., Kim C. and Park J. W.; *Journal of Electroanalytical Chemistry*, 374, 1994, 115-121.
6. Matsue T., Kato T., Akiba U. and Osa T.; *Chemistry Letters*, 1985, 1825-1828.
7. Bird C. L. and Kuhn A. T.; *Chemical Society Reviews*, 10, 1981, 49-82.
8. Xiao L., Wildgoose G. G. and Compton R. G.; *New Journal of Chemistry*, 32, 2008, 1628-1633.
9. Jeon W. S., Kim H. J., Lee C. and Kim K.; *Chemical Communications*, 2002, 1828-1829.
10. Coutouli-Argyropoulou E., Kelaidopoulou A., Sideris C. and Kokkinidis G.; *Journal of Electroanalytical Chemistry*, 477, 1999, 130-139.
11. Matsue T., Evans D. H., Osa T. and Kobayashi N.; *Journal of the American Chemical Society*, 107, 1985, 3411-3417.
12. Brett C. M. A. and Oliveira A. M.; *Electrochemistry. Principles, Methods and Applications*; Oxford Science Publications, 1993.
13. Singh M., Sharma R. and Banerjee U. C.; *Biotechnology Advances*, 20, 2002, 341-359.
14. Ibrahim M. S., Shehatta I. S. and Al-Nayeli A. A.; *Journal of Pharmaceutical and Biomedical Analysis*, 28, 2002, 217-225.
15. Mendoza S., Castano E., Meas Y., Godinez L. A. and Kaifer A. E.; *Electroanalysis*, 16, 2004, 1469-1477.
16. Dang X. J., Nie M. Y., Tong J. and Li H. L.; *Journal of Electroanalytical Chemistry*, 448, 1998, 61-67.
17. Zhao G. C., Zhu J. J., Zhang J. J. and Chen H. Y.; *Analytica Chimica Acta*, 394, 1999, 337-344.
18. Fini P., Longobardi F., Catucci L., Cosma P. and Agostiano A.; *Bioelectrochemistry*, 63, 2004, 107-110.
19. Oh I., Lee M. Y., Lee Y. B., Shin S. C. and Park I.; *International Journal of Pharmaceutics*, 175, 1998, 215-223.
20. Dodziuk H.; *Cyclodextrins and Their Complexes*; Wiley-VCH, 2006.
21. Ugwu S. O., Alcalá M. J., Bhardwaj R. and Blanchard J.; *Journal of Pharmaceutical and Biomedical Analysis*, 19, 1999, 391-397.
22. Monk P. M. S. and Hodgkinson N. M.; *Electrochimica Acta*, 43, 1998, 245-255.

23. Monk P. M. S., Hodgkinson N. M. and Partridge R. D.; *Dyes and Pigments*, 43, 1999, 241-251.
24. http://www.engineeringtoolbox.com/water-dynamic-kinematic-viscosity-d_596.html.
25. Sweetser P. B.; *Analytical Chemistry*, 39, 1967, 979-&.
26. Van der Leest R. E.; *Journal of Electroanalytical Chemistry and Interfacial Electrochemistry*, 43, 1973, 251.
27. Sun W. L., Xue J., Chen J. S., Mao L. Q., Jin L. T., Yamamoto K., Tao S. G. and Jin J. Y.; *Talanta*, 49, 1999, 345-356.
28. Ding S. J., Chang B. W., Wu C. C., Chen C. J. and Chang H. C.; *Electrochemistry Communications*, 9, 2007, 1206-1211.
29. Yanez C. and Basquinzay R.; *Journal of Electroanalytical Chemistry*, 622, 2008, 242-245.
30. Ling Y. H., Mague J. T. and Kaifer A. E.; *Chemistry-a European Journal*, 13, 2007, 7908-7914.
31. Kostela J., Elmgren M., Hansson P. and Almgren M.; *Journal of Electroanalytical Chemistry*, 536, 2002, 97-107.
32. Harris D. C. and Bertolucci M. D.; *Symmetry and Spectroscopy*; Dover Publications, Inc: New York, 1978.
33. Nakahara H. and Wang J. H.; *Journal of Physical Chemistry*, 67, 1963, 496-&.
34. Monk P. M. S. and Hodgkinson N. M.; *Journal of Electroanalytical Chemistry*, 462, 1999, 43-54.
35. Reipa V., Monbouquette H. G. and Vilker V. L.; *Langmuir*, 14, 1998, 6563-6569.
36. John S. A., Okajima T. and Ohsaka T.; *Journal of Electroanalytical Chemistry*, 466, 1999, 67-74.
37. Pham D. T., Gentz K., Zorlein C., Hai N. T. M., Tsay S. L., Kirchner B., Kossmann S., Wandelt K. and Broekmann P.; *New Journal of Chemistry*, 30, 2006, 1439-1451.
38. Arihara K., Ohsaka T. and Kitamura F.; *Physical Chemistry Chemical Physics*, 4, 2002, 1002-1005.
39. Gomez L., Ruiz J. J. and Rodriguez-Amaro R.; *Journal of the Electrochemical Society*, 152, 2005, E364-E370.
40. Kobayashi K., Fujisaki F., Yoshimine T. and Niki K.; *Bulletin of the Chemical Society of Japan*, 59, 1986, 3715-3722.
41. Kelaidopoulou A., Kokkinidis G. and Coutouli-Argyropoulou E.; *Electrochimica Acta*, 43, 1998, 987-997.
42. Safarowsky C., Rang A., Schalley C. A., Wandelt K. and Broekmann P.; *Electrochimica Acta*, 50, 2005, 4257-4268.
43. Breuer S., Pham D. T., Huemann S., Gentz K., Zorlein C., Hunger R., Wandelt K. and Broekmann P.; *New Journal of Physics*, 10, 2008.

Chapter 6

Interaction of β -CD with viologens: spectroscopic study

6.1 Introduction

In Chapter 5, the interaction between the three viologens (methyl, ethyl and benzyl) and the sulfated cyclodextrin was investigated by means of two electrochemical techniques. Here, the phenomena are regarded from a spectroscopic point of view. Ultraviolet-visible (UV-Vis) and ^1H nuclear magnetic resonance (NMR) spectra were recorded for the three analytes, in the absence and presence of measured amounts of the anionic $s\beta$ -CD.

Firstly, the stoichiometry of the complex was determined by applying the Job's method to the UV-Vis data, as described in Section 2.6.1.1. In the case of benzyl viologen an additional Job's plot was constructed using ^1H NMR spectroscopy. Then, the variation in the absorbance spectrum of the dication species, V^{2+} , upon addition of fixed amounts of $s\beta$ -CD, was monitored and the results compared with the corresponding electrochemical data, Chapter 5.

A spectroelectrochemical study was performed to investigate the interaction of the radical cations of the three viologens with the anionic $s\beta$ -CD, following the procedure described in Section 2.5.3. It was possible to isolate and study the absorbance of the unstable radical species by controlling and fixing the potential applied to the transparent working electrode. By careful selection of the applied potential, the radicals were generated without any further reduction to give the neutral state. Similar experiments were carried out with the neutral β -cyclodextrin as a term of comparison.

Finally, in the last part of this chapter, ^1H NMR spectra of the viologens, alone and in the presence of the anionic cyclodextrin, are presented and a comparison of the complexation ability of the $s\beta$ -CD and the neutral β -CD is given. To conclude, a hypothesis on the form of interaction between the viologens and the $s\beta$ -CD is put forward. This hypothesis is based on an evaluation of the results obtained using the two spectroscopic techniques and the electrochemical data presented in Chapter 5.

6.2 Determination of the stoichiometry of the complex between β -CD and the viologens

The well known Job's plots were constructed to determine the stoichiometry of the complex between the β -CD and the three viologens.^{1,2} The stoichiometry of the complex can be determined by the position of the highest point.^{1,3} This "continuous variation method" can be employed using different techniques *e.g.* UV-Vis⁴, fluorescence⁵ and NMR spectroscopy.^{3,6}

For the UV-Vis data two stock solutions of 2.50×10^{-5} M viologen and 2.50×10^{-5} M β -CD in 0.10 M sodium chloride were prepared. A series of solutions was prepared in which the sum of the number of moles of the viologen (MV, EV or BV) and the β -CD, was kept constant but the relative amount of the two was systematically varied, according to Table 6.1. A constant volume of 3.0 mL was used.

As discussed in Chapter 2, the commercial β -CD contains pyridine as an impurity and pyridine absorbs around 257 nm. This absorption band interferes with the typical absorbance bands of the three viologens. For example paraquat exhibits a band centred at 257 nm. Ethyl and benzyl viologen have bands with λ_{\max} at 259 and 260 nm, respectively. In Chapter 2, a method for the purification of the β -CD was discussed. Despite the fact that it was effective in the significant removal of pyridine, as shown in the UV-Vis plots and ^1H NMR spectra depicted in Section 2.2.1, the residual impurity still present could not be neglected. The spectral intensity at the λ_{\max} of MV^{2+} , EV^{2+} or BV^{2+} , from a viologen/ β -CD mixture would be expected to result from the viologen and the cyclodextrin absorbance (pyridine) and hence in the interest of accuracy all measurements made for viologen/ β -CD solutions were corrected by subtracting the corresponding absorption resulting from the pyridine in β -CD. In practice, a reference solution containing the same amount of cyclodextrin was used for each solution, as summarized in Table 6.1.

Absorption spectra of MV/ β -CD of varying mole fractions are overlaid in Figure 6.1 (a), whereby the paraquat band intensity increases with increasing the MV^{2+}

mole fraction. For example, the absorbance at 257 nm was 3.70×10^{-2} for a mole fraction of 0.1, while it increased to 2.72×10^{-1} when the mole fraction of MV²⁺ was 0.6.

Table 6.1: Composition of the solutions used to generate the UV Job's titrations of each viologen (V) in the presence of s β -CD. The viologen stock concentration was 2.50×10^{-5} M in 0.10 M NaCl as supporting electrolyte. The s β -CD stock concentration was 2.50×10^{-5} M in 0.10 M NaCl. The total volume was 3.0 mL.

Solution	V (mL)	S β -CD (mL)	Mole fraction $n_V/(n_V+n_{S\beta-CD})$	Reference solutions (mL)	
				NaCl	[S β -CD]
1	3.0	0.0	1.0	3.0	0.0
2	2.7	0.3	0.9	2.7	0.3
3	2.4	0.6	0.8	2.4	0.6
4	2.1	0.9	0.7	2.1	0.9
5	1.8	1.2	0.6	1.8	1.2
6	1.5	1.5	0.5	1.5	1.5
7	1.2	1.8	0.4	1.2	1.8
8	0.9	2.1	0.3	0.9	2.1
9	0.6	2.4	0.2	0.6	2.4
10	0.3	2.7	0.1	0.3	2.7
11	0.0	3.0	0.0	0.0	3.0

The Job's plots were generated from the change of the absorbance at a wavelength of 257 nm for methyl viologen, 259 nm for ethyl viologen and 260 nm for benzyl viologen relative to that of an equal concentration of free viologen, using Equation 6.1:

$$\Delta A = A_0 - A$$

6.1

where A_0 and A are the absorbance values for the viologen in the absence and presence of β -CD, respectively. These ΔA numbers were then multiplied by the corresponding mole fraction and the product was plotted as a function of the viologen mole fraction. Figure 6.1 (b) shows the Job's plot of the UV absorbance change at 257 nm of the complex when varying the MV^{2+} mole fraction in the MV/β -CD solutions. The maximum absorbance value was achieved at the 0.5 mole fraction. This result is evidence of a 1:1 $MV^{2+}:\beta$ -CD complex stoichiometry.^{7,8}

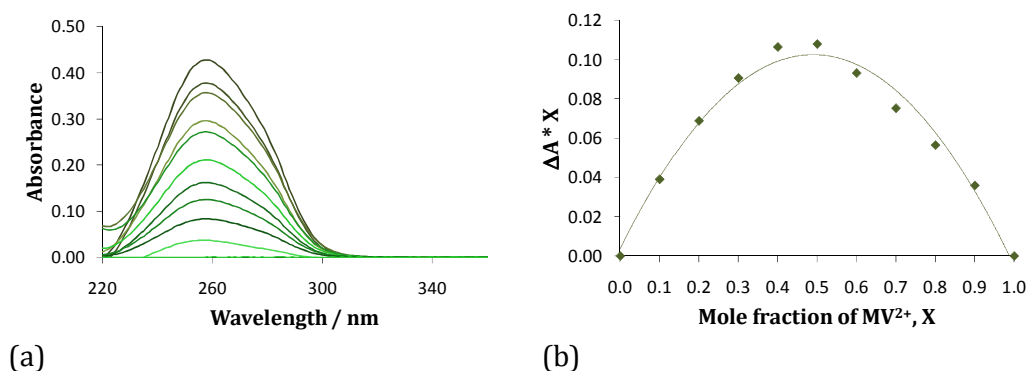


Figure 6.1: (a) UV spectra for the Job's plot titration curve with β -CD and MV^{2+} . From low to high absorbance values, the mole fraction of MV^{2+} increases from 0.0 to 1.0, in increments of 0.1. (b) Job's plot curve of UV absorbance change at 257 nm for MV upon addition of β -CD.

Using a similar procedure and the mole fractions outlined in Table 6.1, UV spectra were recorded for ethyl and benzyl viologens in the absence and presence of β -CD. These data are shown in Figure 6.2 (a) and Figure 6.3 (a), respectively. Figure 6.2 (a) and Figure 6.3 (a) show an increase of the absorbance with increasing the ethyl and benzyl viologen mole fractions. Job's plots for ethyl viologen and benzyl viologen were constructed too and these are illustrated in Figure 6.2 (b) and Figure 6.3 (b), respectively. Again, the bell shaped plots exhibit a clear maximum at 0.5 mole fraction, indicating a stoichiometric ratio of 1:1 for the viologen/ β -CD complex.

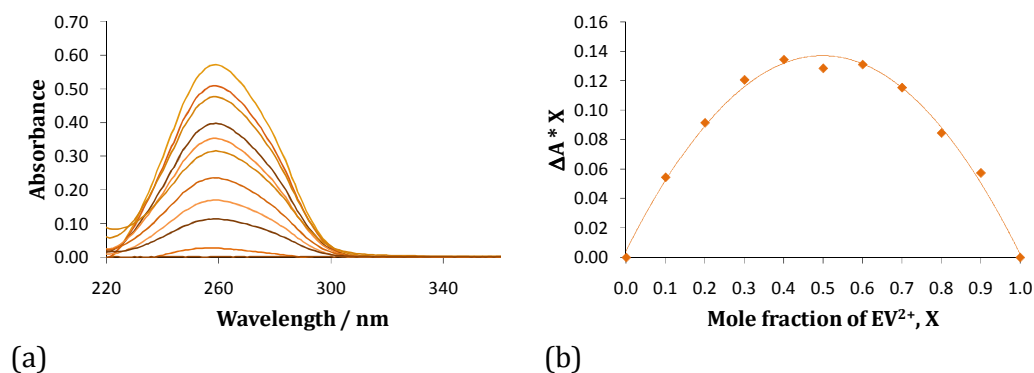


Figure 6.2: (a) UV spectra for the Job's plot titration curve with s β -CD and EV²⁺. From low to high absorbance values, the mole fraction of EV²⁺ increases from 0.0 to 1.0, in increments of 0.1. (b) Job's plot curve of UV absorbance change at 259 nm of EV²⁺ upon addition of s β -CD.

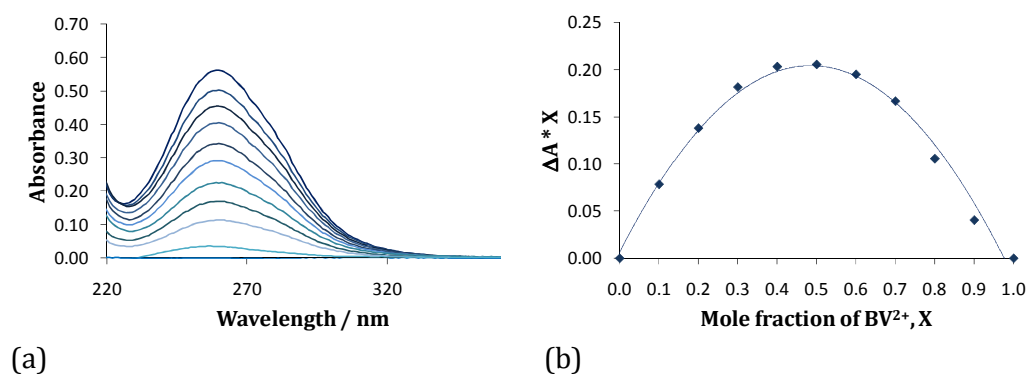


Figure 6.3: (a) UV spectra for the Job's plot titration curve with s β -CD and BV²⁺. From low to high absorbance values, the mole fraction of BV²⁺ increases from 0.0 to 1.0, in increments of 0.1. (b) Job's plot curve of UV absorbance change at 260 nm of BV²⁺ upon addition of s β -CD.

In the case of the benzyl viologen, the stoichiometry of the complex was also evaluated by means of the NMR technique. The Job's method was applied to chemical shift data collected by ¹H NMR spectroscopy. The mole fraction of BV²⁺ was varied from 0.0 to 1.0 in increments of 0.1. Each BV²⁺/s β -CD solution was prepared from 5.00 \times 10⁻³ M BV²⁺ and 5.00 \times 10⁻³ M s β -CD stock solutions in the presence of 0.10 M NaCl/D₂O in order to maintain a constant ionic strength. The

volumes of each stock solution used to give the required mole fraction values are shown in Table 6.2.

Table 6.2: Volumes of stock solutions used for the ^1H NMR Job's plot measurements. Total volume is 0.5 mL in 0.10 M NaCl/D $_2$ O.

Solution	BV 5.00 x 10 ⁻³ M (mL)	Sβ-CD 5.00 x 10 ⁻³ M (mL)	Mole fraction $n_{BV}/(n_{BV}+n_{S\beta\text{-CD}})$
1	3.0	0.0	1.0
2	2.7	0.3	0.9
3	2.4	0.6	0.8
4	2.1	0.9	0.7
5	1.8	1.2	0.6
6	1.5	1.5	0.5
7	1.2	1.8	0.4
8	0.9	2.1	0.3
9	0.6	2.4	0.2
10	0.3	2.7	0.1
11	0.0	3.0	0.0

The NMR spectra of each solution were recorded. The parameters observed experimentally in this case are the chemical shifts of the methylene protons of the benzyl substituents (Hc) and the protons in the β position to the quaternary nitrogen atoms (Hb), as represented in Figure 6.4. The NMR spectroscopy data are presented and discussed later in Section 6.5, where the ^1H NMR spectrum of benzyl viologen is shown in Figure 6.16. The signals considered were shifted to lower field as the mole fraction of the s β -CD was increased. For example, the chemical shift for Hb was 8.43 ppm when the mole fraction of BV $^{2+}$ was 1.0. It changed to 8.58 ppm for a mole fraction of 0.1. To generate the Job's plot and establish the stoichiometry of the complex, the continuous variation method was applied to follow the changes in chemical shifts, $\Delta\delta$, of the Hb and Hc protons. The chemical shift differences, $\Delta\delta$, were computed using Equation 6.2:

$$\Delta\delta = \delta_o - \delta_c \quad 6.2$$

where δ_o and δ_c are the chemical shift values for BV^{2+} in the absence and presence of the β -CD, respectively. As a consequence of the downfield shift, the measured $\Delta\delta$ were negative values. They were then multiplied by the corresponding mole fraction ($\Delta\delta * X$) and the product was plotted as a function of the mole fraction, X , of BV^{2+} , as shown in Figure 6.4. Job's plots exhibiting a maximum at a BV^{2+} mole fraction of 0.5 were obtained for the chemical shift changes of the two protons. These findings confirm the results evaluated by means of UV-Vis spectroscopy and taken together are strong evidence for a 1:1 complex stoichiometry.

These results obtained with the continuous variation method suggest that the methyl, ethyl and benzyl substituents on the bipyridine ring do not affect the stoichiometric ratio of the complex formed between the dicationic species and the sulfated cyclodextrin. Complexes with a 1:1 V^{2+}/β -CD stoichiometric ratio are formed for all three viologens.

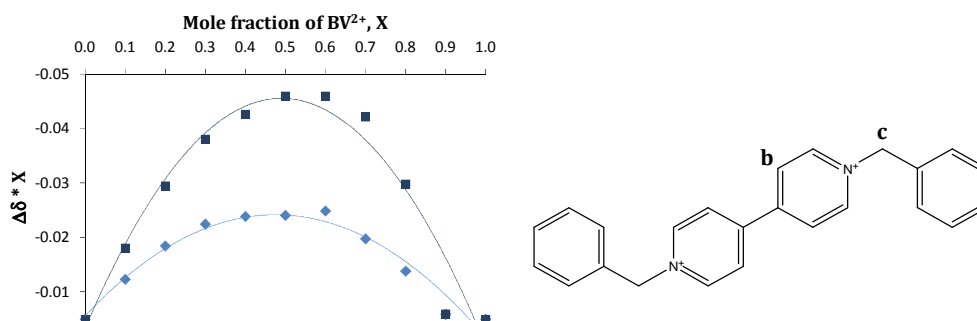


Figure 6.4 Job's plot curve for the determination of the stoichiometry of the BV/β -CD complex; H_b ■ and H_c ◆ protons of BV^{2+} . Also shown are the labeled protons.

6.3 UV-Vis spectroscopic study on the interaction of the viologen dications with β -CD

The viologens, in the dication state (V^{2+}), exhibit an absorption in the UV region. Methyl viologen has a λ_{\max} at 257 nm, while EV and BV have a maximum absorbance at 259 and 260 nm, respectively.

Titration followed using UV-Vis spectroscopy were carried out to explore the interaction of the viologens, in their dication states, with the β -CD. Figure 6.5 (a), (b) and (c) shows that the presence of β -CD at concentrations comparable with the concentration of the viologen has almost no influence on the absorbance and position of the absorbance band. In the case of MV^{2+} and EV^{2+} , even a 20-fold excess of β -CD gives negligible changes in the intensity of absorption. For example, for methyl viologen the absorbance of the free viologen is 0.416 at $\lambda_{\max}=257$ nm and it only decreases to 0.405 upon addition of a 20 times excess of β -CD. In the case of ethyl viologen, the absorbance at $\lambda_{\max}=259$ nm decreases from 0.565 to 0.560, which is within the range of experimental error. In contrast, the absorbance of BV at $\lambda_{\max}=260$ nm decreases from 0.570 to 0.511 when the β -CD reaches a concentration of 5.00×10^{-4} M and the λ_{\max} undergoes a reproducible bathochromic shift of 2 nm.

This negligible variation in the absorbance in Figure 6.5 (a) and (b) is consistent with the weak complexation evaluated between the MV^{2+} and EV^{2+} with the β -CD, by means of electrochemical techniques. In Chapter 5, formation constants, K_f , of 171 ± 5 and 122 ± 8 M^{-1} were computed for the complex of MV^{2+} and EV^{2+} , respectively, with the β -CD. The trend observed with the BV^{2+} is very different, Figure 6.5 (c), indicating a stronger interaction. It has been reported by Lee *et al.*⁹ for viologens with long alkyl chains that the absorption band is red shifted when the viologens associate with counterions. This explanation could be extended to the present case. A strong electrostatic interaction between BV^{2+} and the negative SO_3^- of the CD could be responsible for the lower absorption intensity and the small red shift. However, the small red shift recorded is not consistent with the formation of a charge-transfer complex.¹⁰ For most of the

species forming charge transfer complexes, a new UV-Vis band is recorded for the complex, at a different wavelength with respect to the peak observed for the free species.¹¹ Often, the formation of a charge transfer complex is discerned optically also, by the change in the colour of the solution.¹¹ As outlined in Section 5.5, the complexation of the benzyl viologen with the s β -CD is reasonably explained by the formation of ion pairs between the negative charges of the cyclodextrin and the positive charge of the nitrogen atoms of the two pyridine rings.

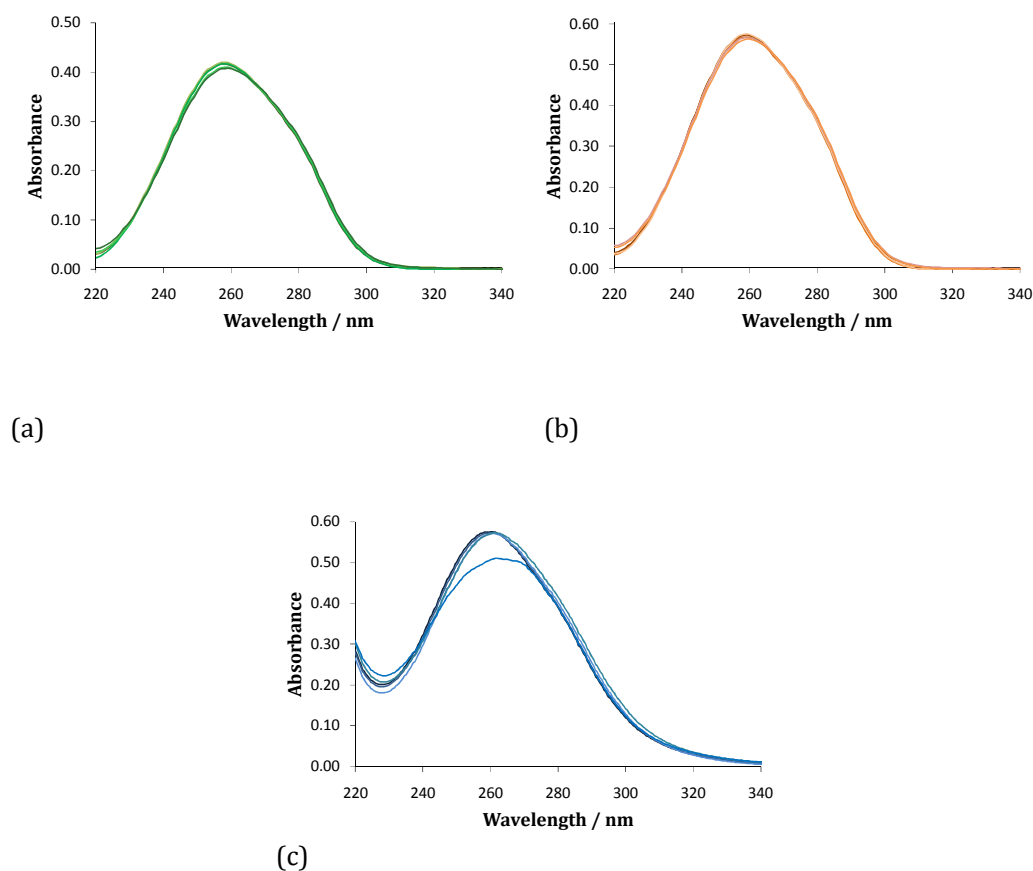


Figure 6.5: UV-Vis spectra of 2.50×10^{-5} M MV (a), 2.50×10^{-5} M EV (b) and 2.50×10^{-5} M BV (c) in 0.10 M NaCl in the absence and presence of varying amounts of s β -CD. The s β -CD concentrations were varied from 2.50×10^{-5} to 5.00×10^{-4} M.

The UV-Vis spectroscopic study of the three dicationic species revealed a substantial difference in the interaction of the smaller viologens (MV²⁺ and EV²⁺) with s β -CD compared to the interactions between BV²⁺ and s β -CD. This

highlights the influence of the benzyl substituents on the strength of the interaction. The very small variation in the absorbance of MV²⁺ and EV²⁺ upon addition of the s β -CD, depicted in Figure 6.5 (a) and (b), suggests that the ion pairing with the s β -CD for these two species is weaker than for the BV/s β -CD system. Alkyl chains are known to possess a weak inductive electron donor effect.¹² The inductive effect of the methyl and ethyl group increases the electron density on the nitrogen atoms. The benzyl group is known to have a minor inductive effect with respect to methyl and ethyl substituents. These statements are supported by the σ parameter of the Taft equation.¹³ As a consequence, the benzyl groups donate less electron density to the nitrogen atoms; hence these nitrogens have more electropositive character and the ion-pairing with the negative sulfate group is stronger.

6.4 UV-Vis spectroscopy study on the interaction of the radical species with s β -CD

To investigate the interaction between the radical species of the three viologen compounds and the s β -CD, spectroelectrochemical experiments were performed, following the procedure described in Section 2.5.3. This method consists of the application of a constant potential which generates the radical cations, while the UV-vis spectra are recorded. Numerous works have been published on the application of the spectroelectrochemical technique to the electrochemistry of viologens.¹⁴⁻¹⁸ In these papers, the well known ability of the viologen monocation radicals to form dimers, which are in equilibrium with the radical monomer, as in Equation 6.3, has been discussed.



Different controversial hypotheses have been made on the possible structure of the dimers. In the mid seventies Mel'nikov and coworkers¹⁹ suggested a quinhydrone structure, as shown in Figure 6.6. Vandam and Ponjee²⁰ proposed a sandwich-type ion pair structure. An alternative pattern was suggested by

Vargalyuk *et al.*²¹ They advanced a hypothesis where association of the cation radicals with counterions takes place on the electrode surface. More recently, it has been proposed that the viologen dimers exist in aqueous solution *via* a face-to-face interaction involving overlapping of the π systems of the two viologen molecules.^{22,23} In addition, electronic paramagnetic resonance (EPR) studies clarified that the radical dimerization produces a diamagnetic species.^{22,24} Hence, dimerization is a coupled chemical reaction, despite the fact that the structure of the dimer has not yet been totally elucidated.

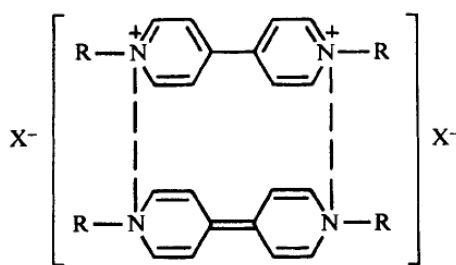


Figure 6.6: Quinhydrone structure proposed for the viologens dimer.

It is well established that water promotes dimerization more than any other solvent. In addition, the tendency to dimerize is parallel with the hydrophobicity of the substituent on the bipyridine ring.^{15,17,23} Park *et al.*²⁵ quantified the dimerization equilibrium constants, K_D , for a series of viologens. They computed a K_D of 500 M^{-1} for the methyl viologen radical cation, in contrast with a value of 850 M^{-1} for $\text{C}_{11}\text{C}_8\text{V}^{\bullet+}$.

In this work, spectroelectrochemical results obtained for methyl, ethyl and benzyl viologen radical cations in the absence and presence of β -CD have been compared with analogous experiments performed in the presence of the neutral β -CD. The spectroelectrochemical pattern of several viologens, in the presence of neutral cyclodextrins has been already investigated.^{14,15,18,25} The free viologens, in their radical state, exhibit an absorption band at longer wavelength with respect to their dication states, as shown in Figure 6.7, Figure 6.8 and Figure 6.9. It is known that reduced hetero-rings shift the absorption band towards longer wavelengths.²⁶ In Figure 6.7 the UV-Vis spectrum for the radical

cation of the benzyl viologen, $BV^{\bullet+}$, generated by electrolysis at -0.70 V vs Ag/Ag⁺ is illustrated, as the dark blue trace. The spectrum exhibits a band centered at 370 nm, which corresponds to the dimer absorption, while the small shoulder around 400 nm has been attributed to the radical as a monomer species. In the visible region, the absorption spectrum of the $BV^{\bullet+}$, as a dimer, has a band around 500 nm, while the monomer has a maximum absorbance around 600 nm. Most papers published agree on the assignments of the bands.^{9,14-17,27} In particular, Lee *et al.*¹⁵ and Evans *et al.*²⁸ recorded the spectroelectrochemical experiments in non-aqueous solution (methanol), where the hydrophobic nature of the environment prevents dimerization. Under these conditions they only observed absorption bands around 400 and 600 nm. As a consequence, they attributed the signals at 370 and 500 nm to the dimer species.

From Figure 6.7 it is clearly evident that an equimolar concentration of the neutral β -CD is sufficient to alter significantly the monomer to dimer ratio. With a 2.5 fold excess of β -CD, the change is even more pronounced. On adding β -CD to the $BV^{\bullet+}$ solution, the spectra of Figure 6.7 show an increase absorbance band of the monomer, accompanied by a decrease in the intensity of the band due to the dimer. As a matter of fact the ratio of the monomer/dimer absorbance increases from 0.40 to 0.68 when a 2.5-fold excess of the β -CD is added. The presence of three clear isosbestic points (390, 420 and 570 nm) is an additional proof of the equilibrium between the two radical states of the benzyl viologen, being altered upon addition of the macrocycle. This feature of the spectra implies that the radical cation, as a monomer is included in the hydrophobic cavity of the β -CD, as depicted in Equation 6.4. Thus, the dimerization reaction, described in Equation 6.3, is prevented because the complexed monomer undergoes dimerization with difficulty. It is reasonable to conclude that the β -CD is an efficient host for the benzyl viologen as a radical cation. This statement is consistent with what Lee and coworkers¹⁵ published on $BV^{\bullet+}$.



Furthermore, these UV-Vis data on the partially reduced BV are in perfect agreement with electrochemical data collected by means of CV and RDV. As a matter of fact, in Section 5.4.1, the negative potential shift and current decrease, recorded upon addition of the β -CD, for the reduction of the radical to give the neutral benzyl viologen (Equation 5.2) were considered evidence for complexation. Using RDV measurements a formation constant, K_f , of $1048 \pm 41 \text{ M}^{-1}$ was evaluated for the host-guest inclusion complex formed between the $\text{BV}^{\bullet+}$ radical and the neutral β -CD.

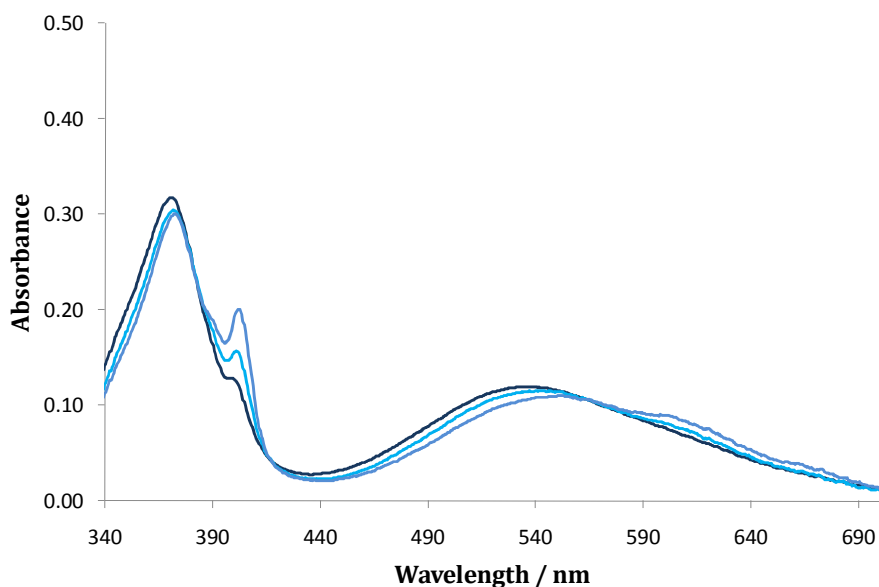


Figure 6.7: Spectroelectrochemical data recorded at -0.7 V vs Ag/Ag^+ for $1.00 \times 10^{-3} \text{ M}$ BV in 0.10 M NaCl, alone (—) and in the presence of $1.00 \times 10^{-3} \text{ M}$ β -CD (—), $2.50 \times 10^{-3} \text{ M}$ β -CD (—).

A different pattern was observed for both MV and EV. First of all, as visible from Figure 6.8 and Figure 6.9, the band corresponding to the absorption of the radical monomer, around 400 nm , is more pronounced with respect to the smaller shoulder, observed at 400 nm , for $\text{BV}^{\bullet+}$. This is due to the fact that the tendency to form a dimer depends on the hydrophobicity of the groups bonded to the pyridine ring. The hydrophobicity of a benzyl group is more pronounced than for a methyl or ethyl group. For this reason, the monomer radical contributes significantly to the absorption spectra of MV and EV, while in the BV spectrum, the dimer is the predominant species.

Another peculiar difference is the presence of an additional absorption band in the UV region, between the signals for the monomer, around 400 nm, and that for the dimer, at 370 nm. The assignment of this band is unknown. However, it seems to be a general characteristic for all the viologens having alkyl substituents, either long chains or small moieties, like MV and EV.^{9,14}

The absorbance for $MV^{•+}$ slightly increases on increasing the concentration of β -CD, without the appearance of any isosbestic point. Such a phenomenon is encountered in the literature as well. For example, Pospisil and coworkers¹⁸ published a spectroscopic study on the interaction of the herbicide, difenzoquat, with β -CD where they highlight the absence of any isosbestic points. The increment in the absorbance of an analyte, upon addition of the CD is usually explained as a consequence of the enhanced solubility, due to complexation of the compound within the cavity of the CD.²⁹⁻³¹ In the present case, the solubility of MV or EV radicals is quite high and hence the moderate increase may be due to the change in the spectral characteristics of the analytes surrounded by β -CD molecules. However, the most interesting parameter to consider is the ratio of the absorbance of the monomer to the dimer, and in turn the influence of β -CD on that ratio. For the free methyl viologen, this ratio is 1.57. Such a value is only slightly affected by the presence of a 10-fold excess of β -CD. As a matter of fact, the ratio of the monomer/dimer absorbance, with 1.00×10^{-2} M β -CD (10-fold excess) is 1.68. In other words, the CD is not very efficient in suppressing dimerization. This suggests the formation of a very weak inclusion complex between the radical of MV and the neutral cyclodextrin. This finding is consistent with the results elucidated by means of electrochemical techniques. In Section 5.2.1 CV and RDV results showed that the neutral β -CD had a higher affinity for the neutral state, MV^0 , rather than for the radical state, $MV^{•+}$.

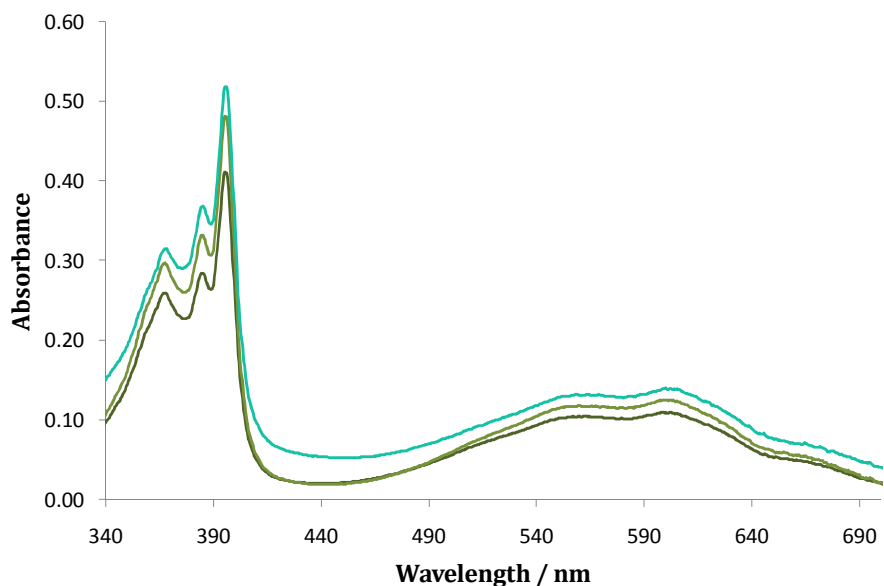


Figure 6.8: Spectroelectrochemical data recorded at -0.9 V vs Ag/Ag^+ for 1.00×10^{-3} M MV in 0.10 M NaCl, alone (—) and in the presence of 1.00×10^{-3} M β -CD (—) and 1.00×10^{-2} M β -CD (—).

Analogous remarks can be made for ethyl viologen. Figure 6.9 illustrates the UV-Vis spectra for $\text{EV}^{•+}$, alone and in presence of different concentration of β -CD. The ratio of the monomer/dimer absorbance varies from 1.45 for the free species to 1.70 for a 1:10 EV: β -CD solution. Again, the properties of ethyl viologen are very similar to those exhibited by methyl viologen. The small enhancement in the monomer absorbance reveals a negligible effect of the CD in suppressing dimerization, which in turn means that complexation does not occur. Again, excellent agreement is seen between the spectrophotometric and electrochemical methods, Section 5.3.1.

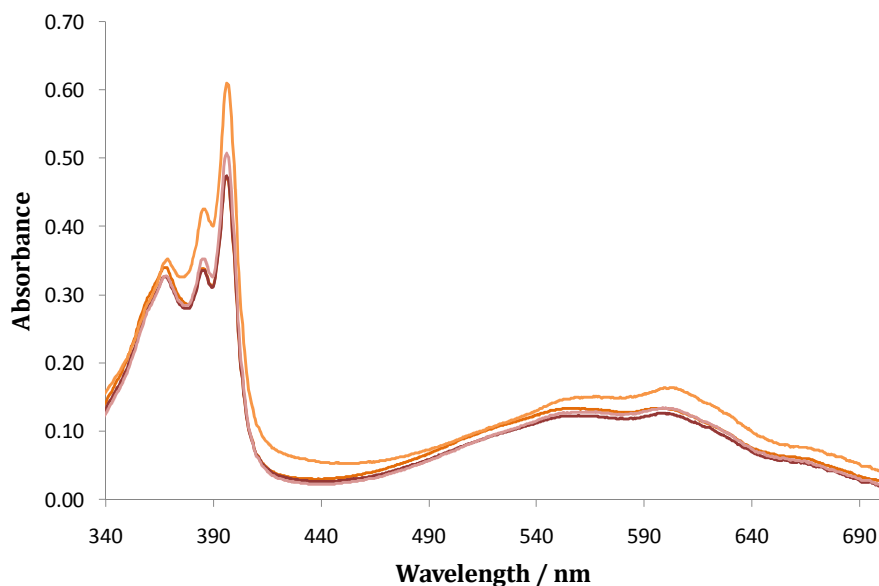


Figure 6.9: Spectroelectrochemical data recorded at -0.9 V vs Ag/Ag^+ for 1.00×10^{-3} M EV in 0.10 M NaCl, alone (—) and in the presence of 1.00×10^{-3} M β -CD (—), 2.50×10^{-3} M β -CD (—), and 1.00×10^{-2} M β -CD (—).

Spectroelectrochemical data collected for the three viologens in the presence of the anionic s β -CD are presented in Figure 6.10, Figure 6.11 and Figure 6.12. Although after purification the pyridine present in the s β -CD batch exhibits a small absorption at the required wavelength, in the interest of accuracy all measurements made for the viologen/s β -CD solutions were corrected by subtracting the absorption (arising from pyridine) from the corresponding s β -CD solution.

By comparing Figure 6.10 with Figure 6.8 the different influence of the s β -CD is immediately evident. An equimolar concentration of s β -CD is sufficiently high to produce a drastic decrease in the absorbance of the MV radical. Furthermore, it affects as well the ratio of the monomer/dimer absorbance, in favour of the dimer species, as listed in Table 6.3. A similar trend is observed in Figure 6.11 for EV^{2+} . A reasonable explanation could involve a slower diffusion of the dicationic species to the ITO electrode surface, upon addition of the anionic s β -CD. As a consequence, a lower amount of radical is generated, which in turn is reflected in a lower absorbance. In Chapter 5, the dramatic decrease in the reduction peak current of the methyl and ethyl viologens dications was

discussed in Section 5.2.2 and 5.3.2. Both CV and RDV revealed a decrease of the diffusion coefficients for the two analytes in solution with the β -CD. In particular, a significant drop in the peak or limiting current was recorded for equimolar concentrations of β -CD and viologen. A further less significant decrease in the peak current was observed as the β -CD concentration was increased, as depicted for MV in Figure 5.8 and Figure 5.14 and for EV in Figure 5.25 and Figure 5.31. In agreement with the electrochemical data, Figure 6.10 and Figure 6.11 illustrate that the largest drop in the absorbance is recorded for equimolar concentrations of the analytes and the β -CD. For larger excesses of the sulfated cyclodextrin, the absorbance bands undergo further decreases in intensity, but these are smaller. This suggests that the interaction between ethyl or methyl viologen dications and the β -CD is mainly driven by electrostatic forces. UV-Vis data are consistent with the proposal that the negative $-\text{SO}_3^-$ of the CD interacts with the positively charged viologen dication, slowing its diffusion to the electrode surface. This is consistent with the classification the viologen/ β -CD interaction as an association complex or ion pairing complex. Indeed, Osella and coworkers³² came to a similar conclusion in their systematic study of ferrocenium derivatives with β -CD.

Another interesting aspect to highlight is the increased ratio of the radical dimer to the radical monomer, Table 6.3. The β -CD seems to stabilize and promote the dimer state over the monomer one. Quintela and Kaifer²⁷ reported an analogous conclusion in a paper investigating the electrochemistry of MV in the presence of sodium decyl sulfate. They stated that small concentrations of the surfactant were found to enhance dimerization of the viologen radical. This may point to the formation of a radical dimer/ β -CD ion pair or association complex.

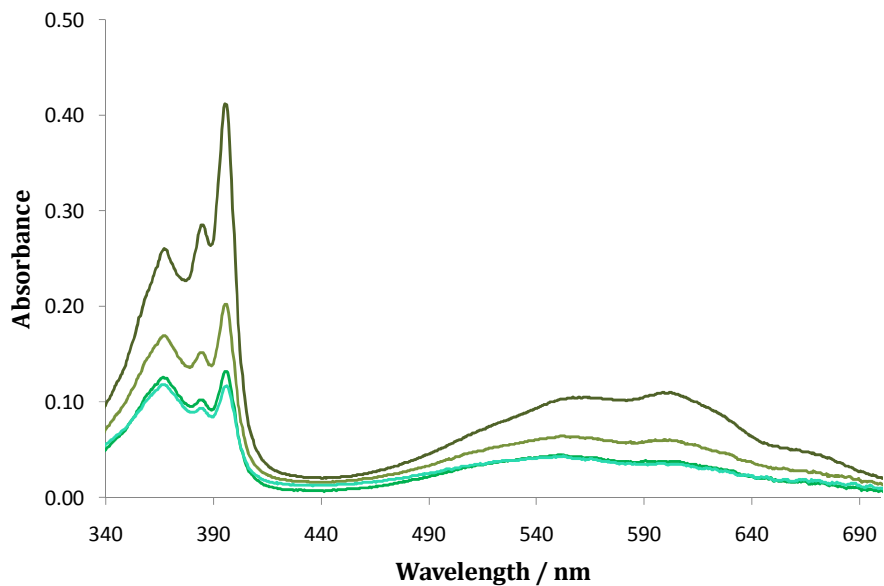


Figure 6.10: Spectroelectrochemical data recorded at -0.9 V vs Ag/Ag^+ for 1.00×10^{-3} M MV in 0.10 M NaCl, alone (—) and in the presence of 1.00×10^{-3} M s β -CD (—), 2.50×10^{-3} M s β -CD (—), and 1.00×10^{-2} M s β -CD (—).

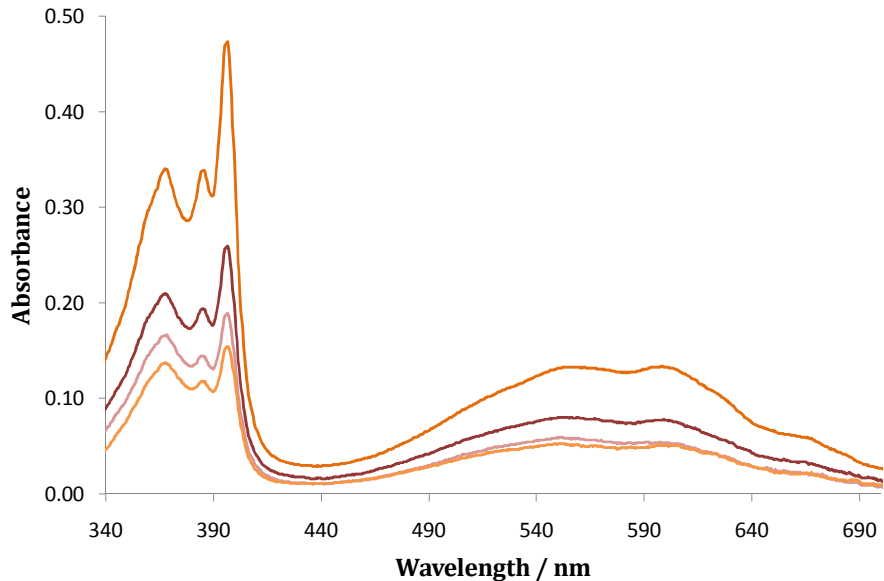


Figure 6.11: Spectroelectrochemical data recorded at -0.9 V vs Ag/Ag^+ for 1.00×10^{-3} M EV in 0.10 M NaCl, alone (—) and in the presence of 1.00×10^{-3} M s β -CD (—), 2.50×10^{-3} M s β -CD (—), and 1.00×10^{-2} M s β -CD (—).

Table 6.3: Absorbance ratio of the radical monomer to the radical dimer for methyl and ethyl viologens, 1.00×10^{-3} M, alone and in the presence of 1.00×10^{-3} M, 2.50×10^{-3} M, and 1.00×10^{-2} M s β -CD. Absorbance values taken at a λ_{\max} of 368 nm and 396 nm for the MV^{•+} dimer and monomer, respectively, and at 370 nm and 394 nm for the EV^{•+} dimer and monomer, respectively.

Mole ratio V : sβ-CD	MV	EV
	Absorbance ratio Monomer/Dimer	Absorbance ratio Monomer/Dimer
1.0 : 0.0	1.54	1.38
1.0 : 1.0	1.21	1.22
1.0 : 2.5	1.05	1.15
1.0 : 10.0	0.95	1.13

The behavior of the benzyl viologen radical cation in the presence of the s β -CD differs substantially from the other two compounds of the same class. As evident from Figure 6.12, there is no decrease in the absorbance, instead there is a slight increase in the absorbance on addition of the s β -CD. Figure 6.12 shows that the intensity of the band centered at 370 nm, and corresponding to the absorption of the dimer, increases upon addition of the anionic s β -CD. On the other hand, the monomer signal around 400 nm is suppressed. Jeon *et al.*³³ published similar results in a study on the interaction between methyl viologen and a macrocycle comprising eight glycoluril units, Cucurbit[8]uril. Similarly to CDs, such a molecule possesses a hydrophobic cavity. To explain the increase of the band associated with the dimer and the disappearance of the monomer band, they postulated the inclusion of the dimer species within the cavity of the host. Such a cavity is, in fact, large enough to accommodate two viologen molecules. To verify if this explanation could be valid for the anionic s β -CD, spectroelectrochemical data were acquired for BV^{•+} in solution with sulfated α -cyclodextrin (s α -CD). This α -derivative, made up from only six glucose moieties does not possess a cavity large enough to host two viologen guests. Also Lee *et al.*¹⁵ reported data where they showed that the bipyridine does not fit the cavity

size of the α -CD. The data recorded for $BV^{•+}$ in solution with $s\alpha$ -CD (data not shown) were very similar to the data collected for the $s\beta$ -CD system. With the sulfated α -cyclodextrin the dimer peak was enhanced and the monomer absorption depressed. Thus, the spectroelectrochemical results collected for the benzyl viologen could not be explained with the hypothesis of the dimer forming an inclusion complex with $s\beta$ -CD.

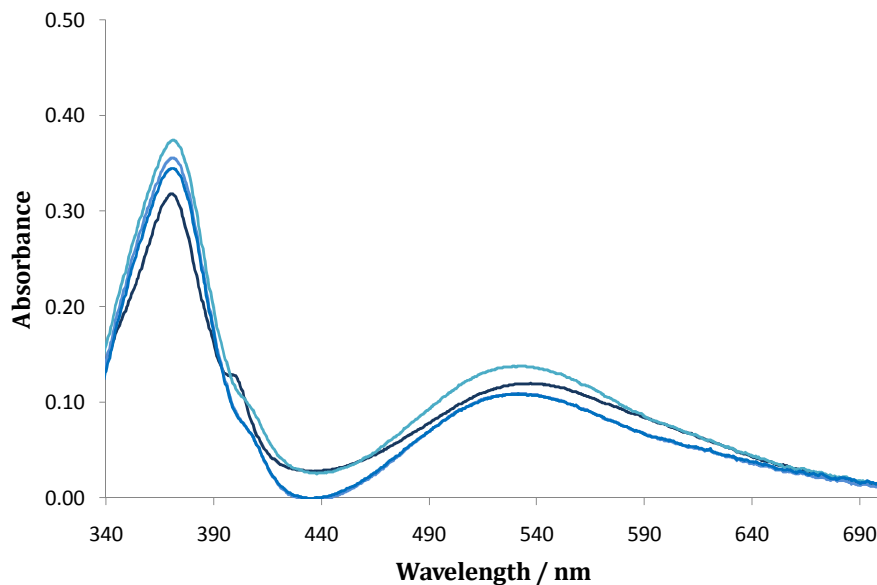


Figure 6.12: Spectroelectrochemical data recorded at -0.9 V vs Ag/Ag^+ for 1.00×10^{-3} M BV in 0.10 M NaCl, alone (—) and in presence of 1.00×10^{-3} M $s\beta$ -CD (—), 2.50×10^{-3} M $s\beta$ -CD (—), and 1.00×10^{-2} M $s\beta$ -CD (—).

Considering the voltammetric plots for the BV in solution with the $s\beta$ -CD as illustrated in Section 5.4.2, the radical cation of the benzyl viologen was observed to form an insoluble aggregate and to deposit on the electrode substrate. Considering that a $BV^{•+}/s\beta$ -CD aggregate deposits on the ITO electrode, this would explain the enhancement of the absorption intensity upon addition of the sulfated CD. This aggregate could well resemble a $BV^{•+}$ dimer, however, the dimer is complexed with the $s\beta$ -CD through the anionic sulfated groups to give a complex ion pair. This is consistent with the data recorded with the $s\alpha$ -CD, where the size of the cavity is no longer important, as it is the charged SO_3^- groups which gives rise to the formation of a complex ion pair.

Moreover, it accounts for the reduction in the concentration of the monomeric radical species. Interestingly, as shown in Figure 5.41, there is a considerable shift, approximately 200 mV, in the reduction potential for the conversion of BV^{•+} to BV⁰. This significant potential shift is difficult to explain. However, given the results presented in Figure 6.12 one possible explanation involves the formation of an insoluble complex ion pair between the dimer, (BV^{•+})₂ and the s β -CD.

6.5 ¹H NMR spectroscopic study on the interaction of the viologen dications with s β -CD

¹H NMR was previously employed to gather information on the stoichiometry of the interaction between benzyl viologen and the s β -CD. It can be also applied to study the geometry of the complex formed. Verification of the interaction between the s β -CD and the viologens was explored by adding a 20-fold excess of s β -CD to 0.5 mL volumes of a 1.00 x 10⁻³ M viologen solution. The solutions of the analytes were made up in 0.10 M NaCl/D₂O. The samples were allowed to equilibrate for 60 min before acquiring their ¹H NMR spectra. Spectra recorded were compared to data collected in the presence of the neutral β -CD. In order to analyze the spectral data, it was important to identify and assign the ¹H peaks for the three viologens and for the s β -CD. The signals for the s β -CD, Figure 6.13, are quite broad and confined to the range from 3.50 to 5.50 ppm on the ¹H NMR spectrum. Such a broad spectrum is a consequence of the varying degree of substitution of the cyclodextrin. Due to the complexity of the s β -CD spectra, the spectral region of the viologens was used to monitor chemical shift variations. The large singlet, around 4.7 ppm, is attributed to H₂O present in the D₂O sample due to its hygroscopy.

In Figure 6.14, a spectrum for MV is depicted. At 8.45 ppm and 8.95 ppm the aromatic protons, labeled as H_a and H_b, α and β to the quaternary nitrogen, appear, while the protons of the methyl group, labeled as H_c, are found at 4.40 ppm.

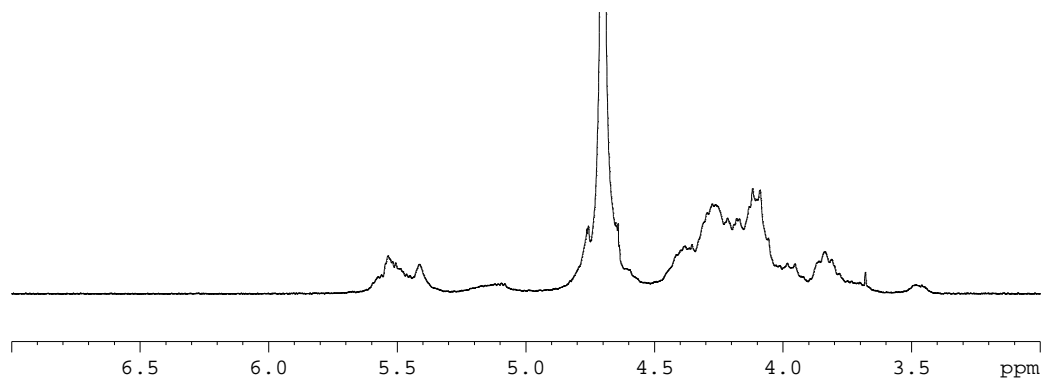


Figure 6.13: ^1H NMR spectrum of 2.00×10^{-2} M s β -CD in 0.10 M NaCl in D_2O .

The spectrum of the ethyl viologen, illustrated in Figure 6.15, shows doublets at 9.04 ppm and 8.45 ppm for the protons in position α and β to the nitrogen, respectively. Again, these are labeled as Ha and Hb in the figure. The triplet at 1.61 ppm has been assigned to the protons of the methyl group, coupling with the methylene protons. The methylene protons have a chemical shift close to the water signal. For this reason they cannot be identified. Finally, in Figure 6.16, the ^1H NMR of the benzyl viologen is presented. The doublets at 9.06 ppm and 8.43 ppm represent the resonance of the protons in position α and β to the nitrogen of the pyridine rings. The aromatic protons of the phenyl ring appear as a singlet at 7.45 ppm, while the singlet at 5.84 ppm is the signal for the methylene protons of the benzyl groups.

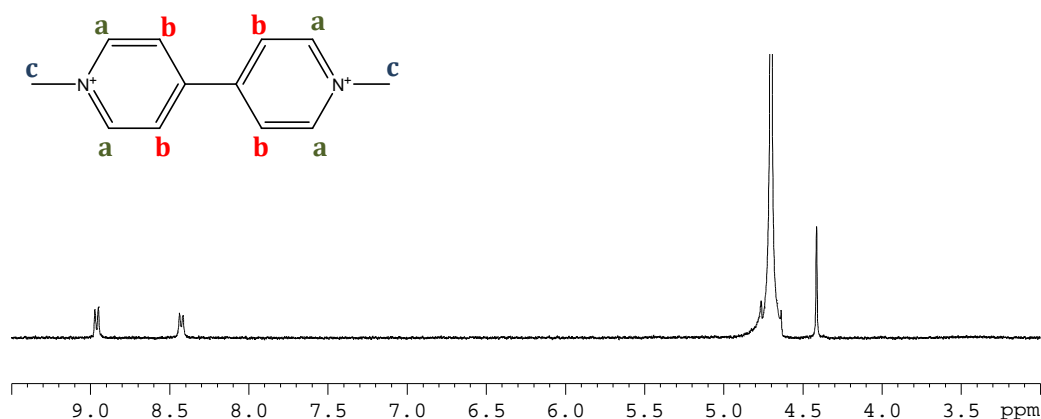


Figure 6.14: ^1H NMR spectrum of 1.00×10^{-3} M MV^{2+} dichloride in 0.10 M NaCl in D_2O .

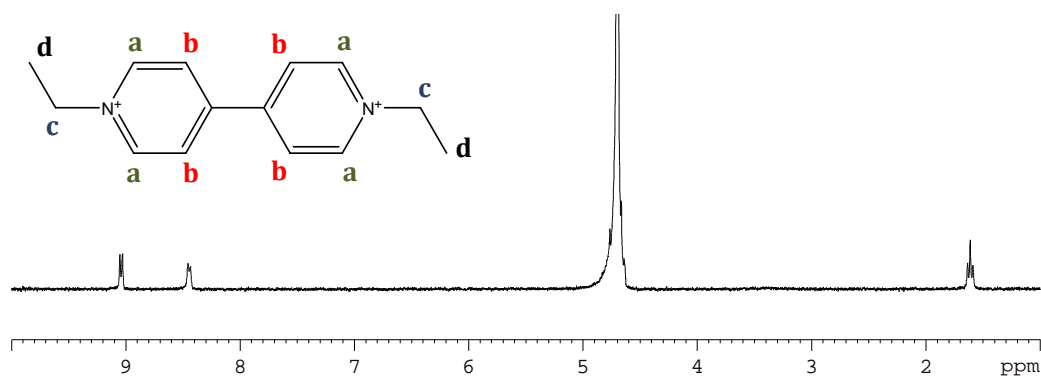


Figure 6.15: ^1H NMR spectrum of 1.00×10^{-3} M EV^{2+} diperchlorate in 0.10 M NaCl in D_2O .

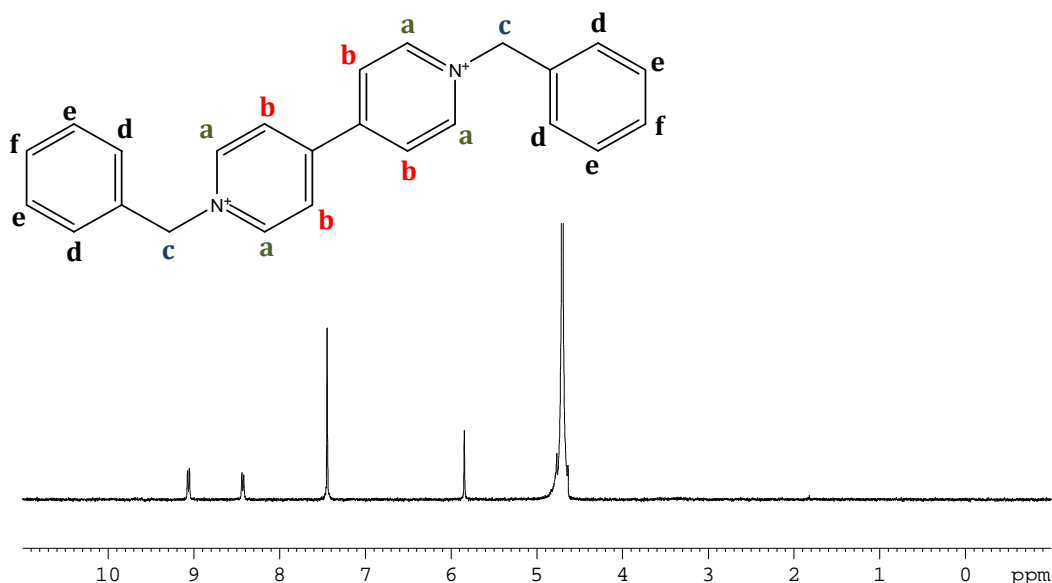


Figure 6.16: ^1H NMR spectrum of 1.00×10^{-3} M BV^{2+} dichloride in 0.10 M NaCl in D_2O .

A 20-fold excess of β -CD induces a downfield shift for the aromatic protons of the three viologens, as visible in Figure 6.17, Figure 6.18 and Figure 6.19. However, the down field shift, $\Delta\delta$, was very small, ranging from 0.03 to 0.07 ppm for the MV and EV dications. It is important to highlight that such small $\Delta\delta$ values were not due to experimental errors because they were very reproducible, and all experiments were repeated three times. Furthermore when the experiments were repeated in the presence of the neutral β -CD no

shift was observed for any of the protons, as shown by the blue traces in Figure 6.17 and in Figure 6.18.

The protons of the benzyl viologen in solution with a 20 times excess of the β -CD gave a slightly larger $\Delta\delta$. As a matter of fact, a $\Delta\delta$ of 0.17 ppm was calculated for Hb and 0.10 ppm for Hc. In addition, the singlet for the aromatic protons at 7.45 ppm was split into a multiplet, highlighting a change in the environment of the benzyl group.

The inclusion of a molecule in the hydrophobic cavity of a cyclodextrin is well documented to shield the proton signals of the guest, thus resulting in an upfield shift of the protons within the CD cavity.^{3,34-36} In the literature interactions between electron rich and electron deficient species, like ion pairing interactions are often associated with de-shielding phenomena of the protons in the vicinity of the cationic species involved in the formation of the pair.³⁷⁻⁴¹ However in this work the most probable explanation for the downfield shift of the protons of the viologens in the presence of the β -CD is a relative effect due to the displacement of chloride anions by the sulfate groups of the β -CD. The commercial viologens used are available as chloride (MV, BV) and perchlorate (EV) salts. In addition the NMR studies were carried out in a 0.10 M solution of NaCl in D₂O. When they are dissolved in the presence of the β -CD, the chloride (or perchlorate) anions forming ion pairs with the viologens are displaced by the sulfate groups of the cyclodextrin, since the macrocycle is in a large excess to the viologens. Chloride anions are well known to be more electron donating species in comparison to sulfate anions¹⁰ and this characteristic would explain the shift to lower field. Furthermore, it was demonstrated in Section 6.2 that the viologen/ β -CD complex originates from a 1:1 interaction hence the two quaternary atoms of nitrogen of the viologen form ion pairs with two of the sulfate groups on the same β -CD molecule. This interaction is entropically favoured compared to the 1:2 interaction between the viologen and chloride or perchlorate anions. Results presented in this section are consistent with the hypothesis of ion pairing interactions, between the quaternary nitrogens of the viologens and the negatively charged sulfate groups of the β -CD, as formulated

in Chapter 5 and confirmed by UV-Vis spectroscopy investigations. UV-Vis experiments presented in Section 6.4 also revealed that among the three compounds examined, the benzyl viologen forms the strongest ion pair. This conclusion is in agreement with ^1H NMR data, where a larger $\Delta\delta$ was evaluated for the chemical shift of the benzyl viologen protons.

To clarify if the viologens are affected by the presence of negatively charged species or if they have a unique and specific interaction with the s β -CD, ^1H NMR spectra were recorded for the benzyl viologen in the presence of a 0.10 M solution of sodium sulfate (Figure 6. 20). The presence of sulfate anions also induced a small shift towards higher ppm (downfield) but to a lower extent in comparison to the s β -CD. Again, this is consistent with the displacement of chloride anions and with the formation of an ion pair between the anionic sulfate and the charged viologen.^{10,11} Puchta and coworkers⁴² discussed the complexation between a calixarene-phenolate and *t*-butylamine. They stated that the nature of the complex can be an ion pair interaction because the main forces driving the process are Coulombic attraction between the calixarene-phenolate and the ammonium ion of the amine compounds. They postulated the amine does not have any close contact with the upper rim of the calixarene. Moreover, their conclusion is supported by Nachtigall *et al.*³⁹ who investigated the interactions of calixarenes with aliphatic amines, by means of NMR, spectrophotometric and conductimetric methods. They demonstrated the electrostatic interaction between the macrocycles and the amines. Most importantly, they affirmed that the absence of shielding effects on the aliphatic chain of the amine is a clear proof that no intracavity inclusion is taking place. All these studies corroborate the hypothesis formulated in this thesis: the viologens are not included in the hydrophobic cavity of the s β -CD. The interaction involves electrostatic forces, more specifically the formation of ion pairs.

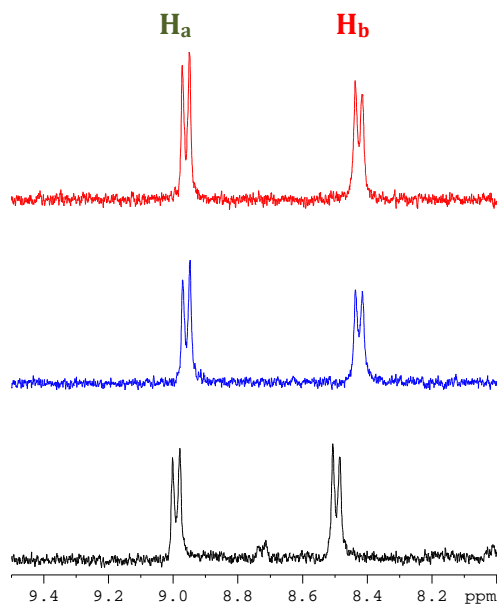


Figure 6.17: Magnification of the ^1H NMR spectra for 1.00×10^{-3} M MV^{2+} in 0.10 M NaCl, alone (red), in the presence of β -CD 1.50×10^{-2} M (blue) and in the presence of 2.00×10^{-2} M $s\beta$ -CD (black).

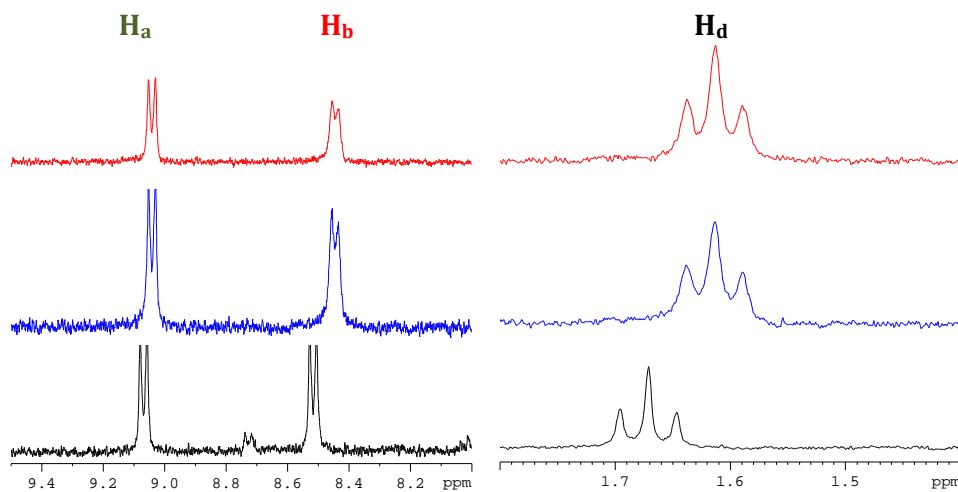


Figure 6.18: Magnification of the ^1H NMR spectra for 1.00×10^{-3} M EV^{2+} in 0.10 M NaCl, alone (red), in the presence of β -CD 1.50×10^{-2} M (blue) and in the presence of 2.00×10^{-2} M $s\beta$ -CD (black).

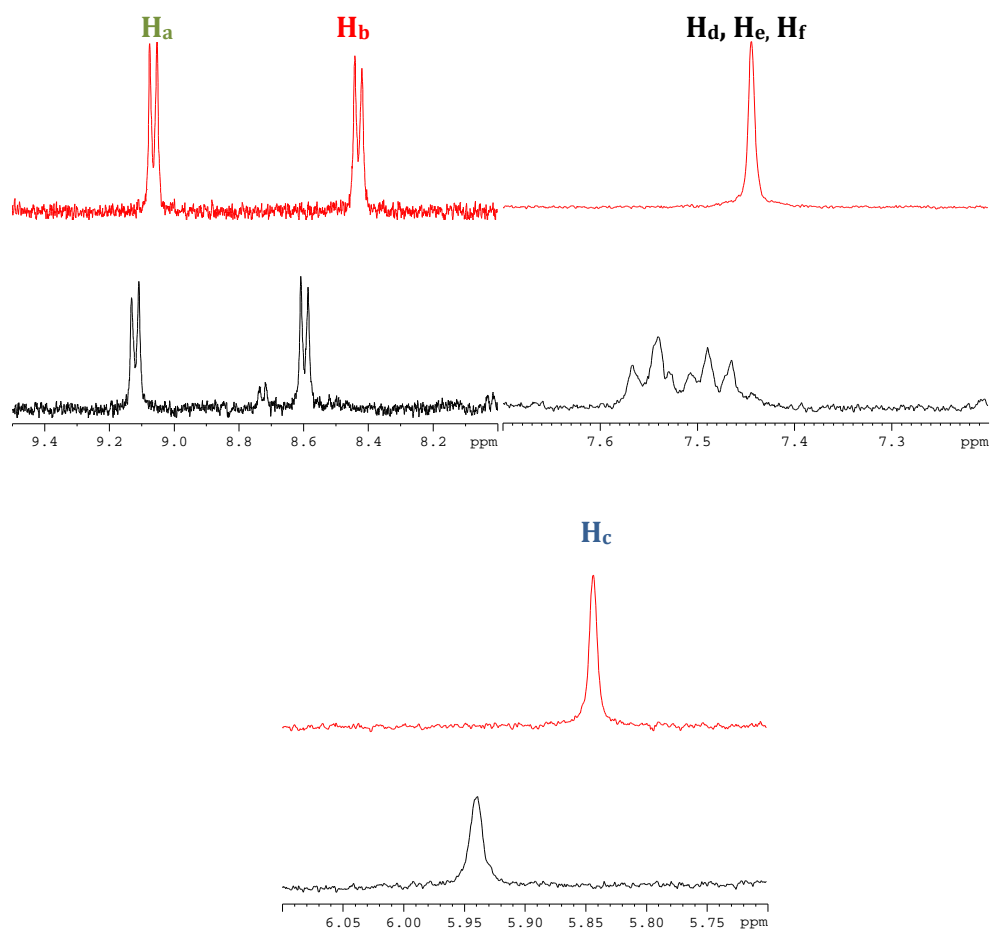


Figure 6.19: Magnification of the ^1H NMR spectra for 1.00×10^{-3} M BV^{2+} in 0.10 M NaCl, alone (red), in the presence of β -CD 1.50×10^{-2} M (blue) and in the presence of 2.00×10^{-2} M $s\beta$ -CD (black).

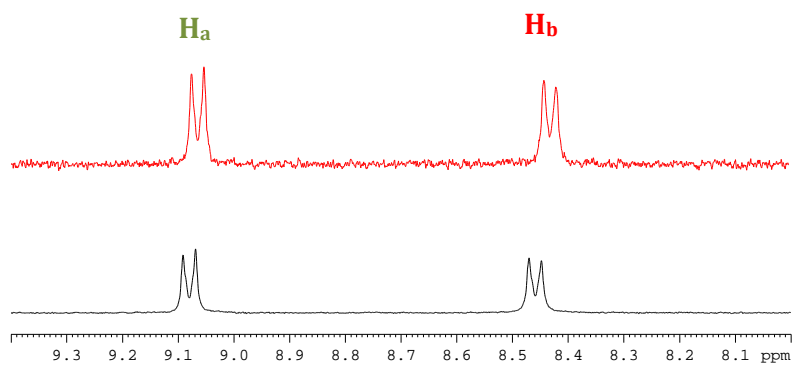


Figure 6.20: Magnification of a ^1H NMR spectra for 5.00×10^{-3} M BV^{2+} alone (red) and in 0.10 M Na_2SO_4 (black).

6.6 Summary of results

In the present chapter the interaction between methyl, ethyl and benzyl viologen with the s β -CD have been investigated by means of two spectroscopic techniques: UV-Vis and ^1H NMR. The stoichiometry of the complex between each viologen, in the dicationic state, and the s β -CD was determined by UV-Vis analysis. The stoichiometric analyte/s β -CD ratio resulted to be 1:1 for all the three viologens.

Furthermore, UV-Vis titrations were performed to investigate the nature of the complex, which is formed between the three viologens in their dication state, MV^{2+} , EV^{2+} and BV^{2+} and the s β -CD. Results showed the strongest interaction to be between BV^{2+} and the negatively charged cyclodextrin. Weaker interactions were observed between the anionic cyclodextrin and the MV^{2+} and EV^{2+} species. The nature of the complex was established to be driven by electrostatic forces and it was concluded that the V^{2+} /s β -CD system was an association or ion pair complex.

^1H NMR experiments showed a downfield shift for the protons of the viologens upon addition of the s β -CD. This downfield shift is in agreement with the formation of an ion pair constituted by the positively charged bipyridilium molecule and the negatively charged s β -CD. ^1H NMR investigation of the dicationic species confirmed the existence of electrostatic phenomena governing the complexation process. ^1H NMR spectra were also in agreement with UV-Vis data in elucidating a stronger interaction between BV^{2+} and the s β -CD. The fact that ^1H NMR signals for the protons of the viologens were not shifted upon addition of the neutral β -CD is an additional indication to support the hypothesis of ion pairing formation, between the charged s β -CD and the viologens.

The radical cation species of the three compounds were explored by employing the spectroelectrochemical technique. Results were compared with corresponding data collected in the presence of the neutral β -CD. The β -CD seemed to have a more significant impact on the $\text{BV}^{\bullet+}$ signal. As a matter of fact,

in Chapter 5, the benzyl viologen radical was established to form an inclusion complex with the neutral β -CD.

The UV-Vis spectra recorded for the MV^{•+} and EV^{•+} species in the presence of the s β -CD, were explained in terms of an ion pair complex involving the dication and s β -CD. This bulkier species has a slower rate of diffusion to the ITO surface; hence less radical is generated and this was used to explain the lower absorbance values recorded in the presence of the s β -CD. This interpretation is in good agreement with CV and RDV results, discussed in Chapter 5, where lower diffusion coefficients were computed for the V²⁺/s β -CD system. The benzyl viologen (BV^{•+}) spectroelectrochemical signal was harder to analyze, since the radical generated at the electrode substrate was deposited on the electrode surface in the presence of the s β -CD. This characteristic was consistent with the increase in the absorbance of the radical on addition of s β -CD. The higher ratio of the dimeric to the monomeric BV^{•+} species was explained in terms of a dimer/s β -CD ion pair.

The UV-Vis and ¹H NMR results presented in this chapter confirm and support what was elucidated by analysing the CV and RDV data. The K_f values computed in Chapter 5, both for the dication and the radical species of the viologens, the small variation of the dication absorbance, combined with the small ¹H NMR downfield shift suggest the formation of an ion pair complex for the V²⁺/s β -CD and V^{•+}/s β -CD systems.

6.7 References

1. Job P.; *Annales des Chimie*, 9, 1928, 113-203.
2. Huang C. Y.; *Methods in Enzymology*, 87, 1982, 509-525.
3. Fielding L.; *Tetrahedron*, 56, 2000, 6151-6170.
4. Gao H., Wang Y. N., Fan Y. G. and Ma H. B.; *Bioorganic & Medicinal Chemistry*, 14, 2006, 131-137.
5. Landy D., Tetart F., Truant E., Blach P., Fourmentin S. and Surpateanu G.; *Journal of Inclusion Phenomena and Macrocyclic Chemistry*, 57, 2007, 409-413.
6. Terekhova I. V., Kumeev R. S. and Alper G. A.; *Journal of Inclusion Phenomena and Macrocyclic Chemistry*, 59, 2007, 301-306.

7. Connors K. A.; *Binding Constants. The Measurement of Molecular Complex Stability*; Wiley: New York, 1987.
8. Masson M., Sigurjonsdottir J. F., Jonsdottir S. and Loftsson T.; *Drug Development and Industrial Pharmacy*, 29, 2003, 107-112.
9. Lee Y. and Lee C.; *Bulletin of the Korean Chemical Society*, 20, 1999, 187-194.
10. Monk P. M. S. and Hodgkinson N. M.; *Electrochimica Acta*, 43, 1998, 245-255.
11. Monk P. M. S., Hodgkinson N. M. and Partridge R. D.; *Dyes and Pigments*, 43, 1999, 241-251.
12. Peter K., C. V. and Schore N. E.; *Organic chemistry*; Freeman: USA, 1987.
13. Eric Anslyn E. and Dougherty D. A.; *Modern Physical Organic Chemistry* University Science Books, 2006.
14. Lee C., Sung Y. W. and Park J. W.; *Journal of Electroanalytical Chemistry*, 431, 1997, 133-139.
15. Lee C., Kim C. and Park J. W.; *Journal of Electroanalytical Chemistry*, 374, 1994, 115-121.
16. Lee C., Lee Y. K., Lee Y. and Jeon I. C.; *Journal of Electroanalytical Chemistry*, 463, 1999, 224-231.
17. Monk P. M. S., Hodgkinson N. M. and Ramzan S. A.; *Dyes and Pigments*, 43, 1999, 207-217.
18. Pospisil L., Hanzlik J., Fuoco R. and Colombini M. P.; *Journal of Electroanalytical Chemistry*, 368, 1994, 149-154.
19. Mel'nikov N. N., Novikov E. G. and Khaskin B. I.; *Chemistry and biological activity of bipyridyls and their derivatives*; Gosimdat: Moscow, 1975.
20. Vandam H. T. and Ponjee J. J.; *Journal of the Electrochemical Society*, 121, 1974, 1555-1558.
21. Vargalyuk V. F., Starokozheva T. I. and Loshkarev Y. M.; *Soviet Electrochemistry*, 15, 1979, 1337-1339.
22. Vuckovic M., Mentus S. V., Janata E. and Milosavljevic B. H.; *Physical Chemistry Chemical Physics*, 3, 2001, 4310-4315.
23. Lee C., Lee Y. M., Moon M. S., Sang S. H., Park J. W., Kim K. G. and Jeon S. J.; *Journal of Electroanalytical Chemistry*, 416, 1996, 139-144.
24. Webster R. D., Dryfe R. A. W., Eklund J. C., Lee C. W. and Compton R. G.; *Journal of Electroanalytical Chemistry*, 402, 1996, 167-174.
25. Park J. W., Choi N. H. and Kim J. H.; *Journal of Physical Chemistry*, 100, 1996, 769-774.
26. Armarego W. L. P. and Katritzky A. R.; *Physical methods in heterocyclic chemistry*; Academic Press: New York, 1971; Vol. 3.
27. Quintela P. A. and Kaifer A. E.; *Langmuir*, 3, 1987, 769-773.
28. Evans A. G., Dodson N. K. and Rees N. H.; *Journal of the Chemical Society-Perkin Transactions 2*, 1976, 859-863.
29. Archontaki H. A., Vertzoni M. V. and Athanassiou-Malaki M. H.; *Journal of Pharmaceutical and Biomedical Analysis*, 28, 2002, 761-769.
30. Al-Marzouqi A. H., Shehatta I., Jobe B. and Dowaidar A.; *Journal of Pharmaceutical Sciences*, 95, 2006, 292-304.
31. Woodberry R., Ransom S. and Chen F. M.; *Analytical Chemistry*, 60, 1988, 2621-2625.

32. Osella D., Carretta A., Nervi C., Ravera M. and Gobetto R.; *Organometallics*, 19, 2000, 2791-2797.
33. Jeon W. S., Kim H. J., Lee C. and Kim K.; *Chemical Communications*, 2002, 1828-1829.
34. Hao Y. Q., Wu Y. Q., Liu J. Q., Lao G. M. and Yang G. D.; *Journal of Inclusion Phenomena and Macrocyclic Chemistry*, 54, 2006, 171-175.
35. Ling Y. H., Mague J. T. and Kaifer A. E.; *Chemistry-a European Journal*, 13, 2007, 7908-7914.
36. Schneider H. J., Hacket F., Rudiger V. and Ikeda H.; *Chemical Reviews*, 98, 1998, 1755-1785.
37. Higashiyama M., Inada K., Ohtori A. and Kakehi K.; *Journal of Pharmaceutical and Biomedical Analysis*, 43, 2007, 1335-1342.
38. Tatikolov A. S., Ishchenko A. A., Ghelli S. and Ponterini G.; *Journal of Molecular Structure*, 471, 1998, 145-159.
39. Nachtigall F. F., Lazzarotto M. and Nome F.; *Journal of the Brazilian Chemical Society*, 13, 2002, 295-299.
40. Bertolasi V., Gilli P., Ferretti V. and Gilli G.; *Journal of the American Chemical Society*, 113, 1991, 4917-4925.
41. Liu J. S., Jiang N., Ma J. and Du X. Z.; *European Journal of Organic Chemistry*, 2009, 4931-4938.
42. Puchta R., Clark T. and Bauer W.; *Journal of Molecular Modeling*, 12, 2006, 739-747.

Chapter 7

Conclusions

7.1 Conclusions

In the research work for this thesis, a modified sensor composed of conducting polypyrrole (ppy) doped with sulfated β -cyclodextrin (s β -CD) was electrosynthesized and characterized. A corresponding polymer doped with chloride anions, ppyCl, was used for comparison purposes.

When the required potential is applied to a conducting ppy film the polymer can be switched between a conducting and insulating states. Cyclodextrin molecules possess the unique ability to include compounds with certain characteristics in their hydrophobic cavity. The idea behind the project of this thesis was to combine the properties of conducting polymers with the characteristic of cyclodextrins to form inclusion complexes in order to construct a new sensor for viologens. For this purpose an anionic cyclodextrin, the s β -CD, was employed. The anionic sulfated groups were necessary so that the s β -CD could be incorporated in the polymer matrix as a common dopant.

In the literature there are no papers published on the inclusion of highly charged polar molecules, such as the viologen compounds, within the cavity of a cyclodextrin. However, Guo *et al.*¹ investigated the interaction of methyl viologen with *p*-sulfonatocalix[4,5]arenes (C4AS, C5AS) which are anionic macrocyclic cages, as the s β -CD. They proved the partial inclusion of the methyl viologen within the hydrophobic cavity of the *p*-sulfonatocalixarenes. By means of ¹H NMR spectroscopy and isothermal titration calorimetry (ITC) they postulated that methyl viologen is immersed into the cavity of C4AS in its axial orientation, with the methyl group being included, while the quaternary nitrogens interact with the sulfated groups. Analogous hypothesis could be formulated on the interaction of the viologens with the s β -CD. In addition, ethyl and benzyl viologen, with larger hydrophobic substituents would be expected to form even stronger inclusion complexes with the s β -CD with respect to methyl viologen. However, this was not the case, since it was demonstrated that the s β -CD does not include the three viologens but the interaction is due to electrostatic phenomena.

Furthermore, previous studies in Professor Breslin's group demonstrated the great ability of ppys β -CD in the sensing of the neurotransmitter dopamine.² Additional works developed a controllable device, based on ppys β -CD, for the controlled release of dopamine.³ The interesting results obtained outlined the need of a deep understanding of the polymer properties. For this reason the characterization of the ppys β -CD films has been a salient part of the research work presented in this thesis.

The efficient immobilization of the large macrocyclic polyanion s β -CD within the ppy matrix was proven and confirmed by means of various techniques, including QCM, CV and DSC. The polymer of interest, ppys β -CD was found to behave as a cations exchanger. The influx of cations and water molecules of their solvation shell, was discovered to depend on the applied potential.

A redox active probe species, the ferri/ferrocyanide couple, was employed to investigate the behavior of ppys β -CD and ppyCl towards diffusion and charge transfer, i.e., the electron transfer rate constant, k . Both polymers exhibited similar results, indicating that the large dopant, s β -CD, does not have a negative effect on the diffusion of electroactive species or on the rate of the electron transfer at the polymer interface.

Moreover, higher capacitance values were computed for the ppys β -CD films and this was attributed to the higher number of anionic charges within the polymer matrix. Electrochemical impedance spectroscopy was used to study the properties of oxidized and reduced ppys β -CD films. When applied potentials higher than 0.5 V vs SCE were not used, the polymer could be reversibly switched from one state to another giving identical impedance profiles. On the application of higher applied potentials over-oxidation of the film occurred, giving rise to a considerable reduction in the charging capacitance. A similar decrease in the capacitance of the film was observed on reduction of the film. The capacitance measured at -0.7 V vs SCE was consistent with the formation of a more insulating film. However, the conducting and high charging capacitance of the film was restored on oxidation of the film. Similar behavior was observed

for the ppyCl film. Overoxidation of the ppyCl film was clearly observed on applying potentials higher than 0.6 V vs SCE, indicating that the ppyCl film is more resistant to the onset of overoxidation compared to the ppys β -CD film. The charging capacitance was somewhat lower for the ppyCl film, consistent with the CV data.

Then, the potential application of ppys β -CD in the sensing of viologen compounds was explored. The aim was to develop a new sensor for the pollutant methyl viologen (paraquat) and possibly for other molecules of the same class, able to detect and remove the pollutant from solutions.

The ppys β -CD films have a high affinity for Na⁺. Using this unique property the ppys β -CD films, they were investigated in the sensing and uptake of three different cationic species, methyl, ethyl and benzyl viologens. Methyl viologen is the well-known pollutant paraquat. The viologens were accumulated on the polymer surface utilizing the well characterized ability of ppys β -CD to exchange cations. Then a suitable reduction potential was applied, and the current recorded by DPV (differential pulse voltammetry) for the reduction of the adsorbed species was plotted as a function of the viologen concentration.

To elucidate how the anionic β -CD interacts with the three analytes, the electrochemistry of the three different viologens in solution with the anionic β -CD was explored by means of CV (cyclic voltammetry) and RDV (rotating disc voltammetry). Data were compared with analogous experiments recorded in the presence of the neutral β -CD. The results provide clear evidence for an interaction between the $s\beta$ -CD and the viologens. In particular, the anionic cyclodextrin interacts preferentially with the positively charged states of the analytes: V²⁺ and V^{•+}. On the other hand, the neutral β -CD exhibited higher affinity for the neutral species, MV⁰ and EV⁰, and for the radical cation, BV^{•+}. The K_f values computed were in agreement with the formation of an inclusion complex between the neutral β -CD and MV⁰, EV⁰ and BV^{•+}. In contrast, the smaller K_f values obtained using RDV for the positively charged species of the three viologens and the $s\beta$ -CD, provide evidence for weaker interactions.

Moreover, it was shown that the interaction between the V^{2+} species and the anionic cyclodextrin was higher than that between the V^{+} and the anionic cyclodextrin. This finding points to an association that is controlled by electrostatic interactions. The formation of an association complex arising from ion pair interactions was suggested. A charge transfer complex was excluded, since no new optical absorption bands were generated when UV-Vis spectra of the complexed species were performed. The formation of ion pairs is consistent with the decrease in the diffusion coefficient of the charged viologens when in the presence of the anionic $s\beta$ -CD, as the ion pair is considerably larger in size than the free viologens.

UV-Vis titrations were performed to investigate the nature of the complex, which is formed between the three viologens in their dication state, MV^{2+} , EV^{2+} and BV^{2+} and the $s\beta$ -CD. Results showed the strongest interaction to be between BV^{2+} and the negatively charged cyclodextrin. Weaker interactions were observed between the anionic cyclodextrin and the MV^{2+} and EV^{2+} species. The nature of the complex was established to be driven by electrostatic forces and it was concluded that the $V^{2+}/s\beta$ -CD system was an association or ion pair complex. Furthermore, the stoichiometry of the complexes between the $s\beta$ -CD and the three viologen was determined also by UV-Vis titrations and a 1:1 $V^{2+}/s\beta$ -CD molar ratio was found for all the three compounds with the anionic cyclodextrin.

Furthermore, ^1H NMR experiments showed a downfield shift for the protons of the viologens upon addition of the $s\beta$ -CD. This downfield shift is in agreement with the displacement of the counterions of the commercial viologens and with the formation of an ion pair constituted by the positively charged bipyridilium molecule and the negatively charged $s\beta$ -CD. ^1H NMR spectroscopic investigation of the dicationic species confirmed the existence of electrostatic phenomena governing the complexation process. ^1H NMR spectra were also in agreement with UV-Vis data in elucidating a stronger interaction between BV^{2+} and the $s\beta$ -CD. The fact that ^1H NMR signals for the protons of the viologens were not shifted upon addition of the neutral β -CD is an additional indication to support

the hypothesis of ion pairing formation, between the charged s β -CD and the viologens.

The radical cation species of the three compounds were also explored by employing the spectroelectrochemical technique. Results were compared with corresponding data collected in the presence of the neutral β -CD. The β -CD seemed to have a more significant impact on the BV^{•+} signal. As a matter of fact, in Chapter 5, the benzyl viologen radical was established to form an inclusion complex with the neutral β -CD. The UV-Vis spectra recorded for the MV^{•+} and EV^{•+} species in the presence of the s β -CD, were explained in terms of an ion pair complex involving the dication and s β -CD. This bulkier species has a slower rate of diffusion to the ITO surface; as a consequence, less radical is generated and this was used to explain the lower absorbance values recorded in the presence of the s β -CD. This interpretation is in good agreement with RDV results discussed in Chapter 5, where lower diffusion coefficients were computed for the V²⁺/s β -CD system. The benzyl viologen (BV^{•+}) spectroelectrochemical signal was harder to analyze, since the radical generated at the electrode substrate was deposited on the electrode surface in the presence of the s β -CD. This characteristic was consistent with the increase in the absorbance of the radical on addition of s β -CD. The higher ratio of the dimeric to the monomeric BV^{•+} species was explained in terms of a dimer/s β -CD ion pair.

Experimental results clarified that methyl, ethyl and benzyl viologen are not included in the hydrophobic cavity of the s β -CD. Interactions between the s β -CD and the viologens are mainly driven by electrostatic forces and the formation of ion pairs was postulated. In Chapter 4 it was shown that the viologens can be accumulated within the polymer matrix by cycling the polymer in a specific potential window. Using this method, the smallest concentrations detected were 1.00×10^{-4} M for the ethyl viologen, 5.00×10^{-5} M for the methyl viologen and 2.50×10^{-5} M for the benzyl viologen. In addition a CPA study was performed for the methyl viologen, since this molecule is one of the most commonly used herbicides. In this case the reduction of the dication to give the radical was followed ($MV^{2+} + 1 e^- \rightarrow MV^{\bullet+}$). With CPA a further increase in the detection was

reached since the detection limit evaluated was 1.56×10^{-5} M. However, the detection limit evaluated for methyl viologen at the ppys β -CD was significantly higher than the minimum concentration tolerated by the European Union regulations.⁴ Varying the experimental parameters used to accumulate the analyte on the polymer surface might lead to an improvement in the detection limit and to the design of a strategy to remove the pollutant from solution.

7.2 Conference presentations

7.2.1 *Poster presentations*

59th Irish Universities Chemistry Research Colloquium, Dublin City University 2007.

“Conducting Polypyrrole Matrix modified with sulfated β -Cyclodextrin: Electrochemical Synthesis and Characterization”, [Valeria Annibaldi](#), Carmel B. Breslin and Denise A. Rooney; National University of Ireland, Maynooth.

6th Spring Meeting of the International Society of Electrochemistry, Foz do Iguaçu, Brazil, March 16-19, 2008.

“Conducting Polypyrrole Matrix modified with sulfated β -Cyclodextrin and its ability to sense Viologens”, [Valeria Annibaldi](#), Carmel B. Breslin and Denise A. Rooney; National University of Ireland, Maynooth.

1st Regional Symposium on Electrochemistry of South- East Europe, Crveni Otok, Rovinj, Istria, Croatia, May 4-8, 2008.

“A Novel Cyclodextrin modified Polypyrrole Sensor for Benzyl Viologen: Investigations into its Supramolecular Chemistry”, [Valeria Annibaldi](#), Carmel B. Breslin and Denise A. Rooney; National University of Ireland, Maynooth.

214th Electrochemical Society Meeting, Honolulu, USA, October 12-17, 2008.

“A Novel Cyclodextrin Modified Polypyrrole Sensor and its Interaction with Benzyl Viologen”, [Valeria Annibaldi](#), Carmel B. Breslin and Denise A. Rooney; National University of Ireland, Maynooth.

7.2.2 Oral presentations:

212th Electrochemical Society Meeting, Washington DC, USA, October 7-12, 2007.

“Polypyrrole Modified with Supramolecular cages: Higly Selective Sensor for the Detection of Dopamine”, Claire C. Harley, Gillian M. Hendy, Valeria Annibaldi, Denise A. Rooney and Carmel B. Breslin; National University of Ireland, Maynooth.

6th Spring Meeting of the International Society of Electrochemistry, Foz do Iguaçu, Brazil, March 16-19, 2008.

“Polypyrrole modified with Supramolecular Cages: Applications in the Electrochemical Sensing of Herbicides”, Carmel B. Breslin, Valeria Annibaldi, Sinead MC Dermott, Denise A. Rooney; National University of Ireland, Maynooth.

214th Electrochemical Society Meeting, Honolulu, USA, October 12-17, 2008.

Polypyrrole Modified with Cyclodextrins: Characterization and Applications in the Electrochemical Sensing of Viologens, Valeria Annibaldi, Carmel B. Breslin and Denise A. Rooney; National University of Ireland, Maynooth.

7.3 References

1. Guo D. S., Wang L. H. and Liu Y.; *Journal of Organic Chemistry*, 72, 2007, 7775-7778.
2. Harley C. C.; The Formation of an Electrochemical Sensor for the Selective Detection of Dopamine, Ph.D, NUIM, Department of Chemistry, 2009.
3. Hendy G. M.; Polypyrrole modified with sulfonated Beta-cyclodextrin: Controlled release of DA and host-guest complexation properties, Ph.D, NUIM, Department of Chemistry, 2009.
4. de Oliveira U. M. F., Lichtig J. and Masini J. C.; *Journal of the Brazilian Chemical Society*, 15, 2004, 735-741.